1-1-2015

Platination Kinetics: Insight Into Rna-Cisplatin Interactions As A Probe For Rna Microenvironments

Gayani Dedduwa-Mudalige
Wayne State University,

PLATINATION KINETICS: INSIGHT INTO RNA-CISPLATIN INTERACTIONS AS A PROBE FOR RNA MICROENVIRONMENTS

by

GAYANI N P DEDDUWA-MUDALIGE

DISSERTATION

Submitted to the Graduate School

of Wayne State University,

Detroit, Michigan

in partial fulfillment of the requirements

for the degree of

DOCTOR OF PHILOSOPHY

2015

MAJOR: CHEMISTRY (Biochemistry)

Approved by:

_____

Advisor Date

_____

_____

_____

DEDICATION

To my mother K. Pearl De Silva, father D. M. Raymond Perera, my husband Lasantha Wenura Perera, parents-in-law; Indrajith Perera and Soma Wijesiri, and brother-in-law Rajive Lakmal Perera for their endless love and support.

ACKNOWLEDGEMENTS

First, I would like to convey my sincere gratitude to my thesis advisor Prof. Christine S. Chow for her invaluable guidance, support, and encouragement throughout my Ph.D. work. I would like to thank her for the opportunity to join her lab and be involved in interesting research projects. I'm really grateful for her mentorship and insightful scientific criticism that trained me to become a better scientist. I greatly appreciate her time, dedication, and patience on reading and editing all of my documents. I am thankful for her encouragement and guidance to choose a career path that I want to follow, and for all the research as well as cultural exposures that I experienced while working in her lab.

Next, I'm thankful to my committee members, Profs. Andrew L. Feig, Stephanie L. Brock, and Timothy L. Stemmler for the invaluable insight that they gave on my research. I'm thankful to Dr. Feig for allowing me to use his lab equipment to do my research. I would like to thank Dr. Brock for being supportive to my husband during the toughest times that he faced in his life. Also, I would like to thank her for the opportunity and training that I had working with the Go-Girls program. I really appreciate Dr. Stemmler for the great discussions we had during my research presentations.

I am greatly thankful to Prof. Sofi K. C. Elmroth from Lund University, Sweden for her time and effort to read, edit, and comment on my manuscripts. I'm grateful to Prof. Philip R. Cunningham and the Cunningham lab members for their help and support for the ribosome preparations.

I feel really lucky to be a part of a wonderful and enjoyable group during my Ph.D. studies. Here, I thank all past and present Chow lab members; Keshab, Asare, Moninder, Daya, Sakina, Yogo, Xun, Supuni, Nisansala, Jun, Danielle, Prabuddha, Hyosuk, Bett, and other colleagues; Ashley, May, and Amanda for their help and support. I really enjoyed working with many talented undergrads; Rana, Brianne, Aya, Kareem, and John.

In addition to research, there are many department staff members who helped me with the administrative work. I thank all main office, business office, science stores, and CIF staff members, including Melissa, Mary Wood, and Nestor for their help and support. I also want to thank the radiation safety office staff members, Maha and Diane, for their help with all my radiation-related work. I really enjoyed talking about movies with Diane!

My heartiest gratitude goes to Prof. Amy Prieto and Prof. Brian McNaughton, and the Prieto and McNaughton lab members from Colorado State University for their understanding, help, and support during the time I was writing my thesis in Colorado.

I would like to thank all my professors from University of Kelaniya, and all teachers who paved the path to earn this Ph.D. To all my friends from Sri Lanka, Iowa, Colorado, and Detroit – thank you very much for being there for me and my husband. Finally, I would like to thank the three most impactful people in my life; my mother, my father, and my husband, without whose love, care, support, and sacrifices this Ph.D. would never have been possible.

TABLE OF CONTENTS

LIST OF TABLES

LIST OF FIGURES

LIST OF SCHEMES

LIST OF ABBREVIATIONS

3-HPA	3-hydroxypicolinic acid
CD	circular dichroism
CMCT	1-cyclohexyl-3-(2-morpholinoethyl) carbodiimide metho-*p*-toluene sulfonate
DC	decoding center
DMF	dimethylformamide
DMS	dimethyl sulfate
EF	elongation factor
h24	helix 24
h44	helix 44
H69	helix 69
IF	initiation factor
$k_{2,app}$	apparent second-order rate constant
k_{obs}	observed pseudo-first-order rate constant
MALDI MS	matrix assisted laser desorption ionization mass spectrometry
mRNA	messenger RNA
$n\,\Psi'$	fraction of counterions condensed or displaced according to the polyelectrolyte theory
PTC	peptidyl transferase center
RF	release factor
RNase T1	Ribonuclease T1

RRF	ribosome recycling factor
RRE	Rev responsive element
rRNA	ribosomal RNA
SHAPE	selective 2'-hydroxyl acylation analyzed by primer extension
tRNA	transfer RNA
$Z_A Z_B$	charge of species A and B interacting in a reaction according to Brønsted-Debye-Hückel theory
Ψ	pseudouridine

CHAPTER 1

INTRODUCTION

1.1 Significance of RNA Research and Historic Landmarks

Nucleic acids are important biomolecules for all living organisms [1]. Deoxyribonucleic acid, or DNA, carries the genetic code for cellular functions. Although earlier considered only as information transporters, ribonucleic acids, or RNAs, are now proven to play major roles in many diverse biological processes. RNA brings the genetic information stored in DNA to make proteins, catalyzes biological reactions, and regulates gene expressions in cells. The versatile roles played by RNAs make them ideal therapeutics, as well as therapeutic targets. Some historical landmarks in the field of RNA research will be discussed.

François Jacob, André Lowff, and Jacques Monod were awarded the Nobel Price in 1965 for their discoveries on genetic control of enzyme and virus synthesis [2]. Their findings were valuable for understanding the nature and function of messenger RNAs [3,4]. In 1968, Robert W. Holley, Har Gobind Khorana, and Marshall W. Nirenberg won the Nobel Prize for their interpretation of the genetic code and its function in protein synthesis. Their contributions to the RNA field included determination of the first sequence of a nucleic acid (yeast alanine-$tRNA^{Ala}$), determining the genetic code, and showing that proteins can be synthesized in a cell-free system using synthetic RNA [5-7]. One interesting idea put forward after discovery of the catalytic properties of RNA was the RNA-world hypothesis. The capability of RNA to carry out self-splicing reactions was suggested to provide recombined molecules that have functional diversity. These

findings showed that RNA plays a dual role, which includes storage of information and performance of chemical reactions [8]. Another major breakthrough in RNA research was the discovery of introns and RNA splicing in 1977 by Phillip Sharp and Richard Roberts, who were awarded the Nobel Prize in 1993 [9]. Until the early 1980s when Thomas Cech and Sidney Altman first discovered RNA's catalytic properties, it was considered merely as a messenger of DNA. They won the Nobel Prize in 1989 for this finding [10,11]. The discovery of RNA-interference gene silencing by double-stranded RNA was another major breakthrough in RNA research [12]. The contribution from Andrew Fire and Craig Mello was acknowledged by the Nobel Price in 2006. A very recent Nobel award in the area of RNA research went to Venkatraman Ramakrishnan, Thomas A. Steiz, and Ada E. Yonath in 2009 for their invaluable contributions to determining the structure and function of ribosomes [13-15]. With these many exciting discoveries and a greater appreciation from the scientific community, the RNA research field is growing with still much to be learned about these fascinating molecules.

1.2 Introduction to Ribonucleic Acids

RNA is a polymer of ribonucleotides. These RNA oligonucleotides are formed either biologically by polymerization of ribonucleotides, through RNA polymerases, or synthetically through phosphoramidite chemistry. An RNA strand containing four standard ribonucleotides is shown in Figure 1.1. One of the main features that distinguishes RNA from DNA is the presence of the 2'-OH group in the sugar ring. This functional group plays a major role in RNA structure and

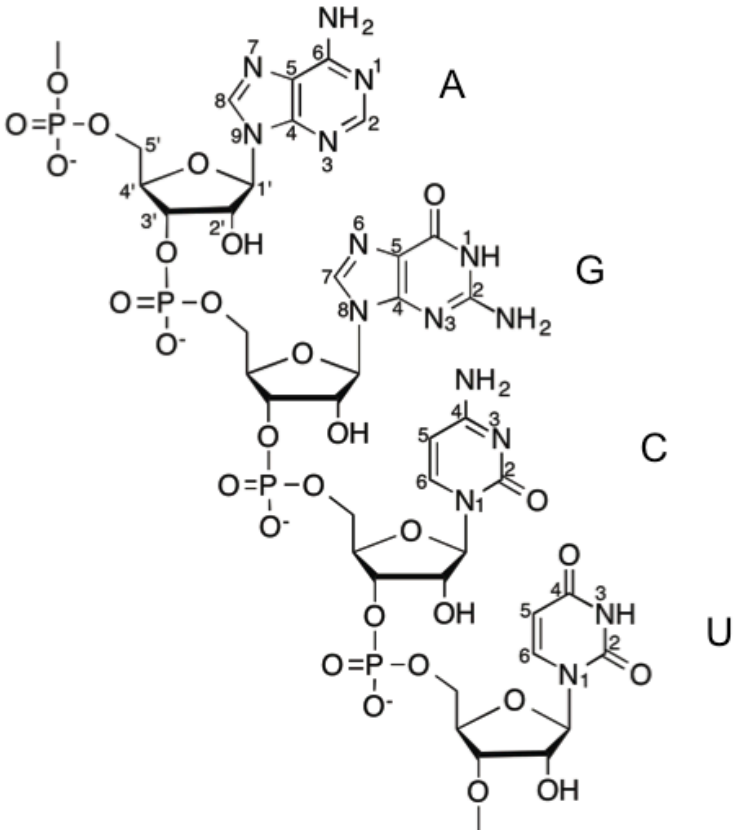

Figure 1.1. An RNA fragment with the four standard ribonucleotides is shown. The bases adenine (A), guanine (G), cytosine (C), and uracil (U) are indicated. The sugar ring is numbered on the adenosine nucleoside.

function [16]. The 2'-OH functionality makes RNA more susceptible to hydrolysis than DNA; however, the 2'-OH group also provides RNA with extra H-bonding capabilities and allows for specific interactions and catalysis [17].

Each ribonucleotide contains a base, ribose sugar, and phosphate group. The base and sugar components together are called nucleosides, and combined with phosphate groups make nucleotides. The four most common bases found in RNA are adenine, guanine, uracil, and cytosine (Figure 1.1). Adenine and guanine are purine bases. Purines connect to the sugar rings through the N9 position of the imidazole ring. Cytosine and uracil are pyrimidines with

connections to the sugar ring through the N1 position. The bases are connected to the sugar ring through a glycosidic bond. The orientation of the base around the glycosidic bond can be either *syn* or *anti* (Figure 1.2). The *anti* conformation is most commonly found in RNA. The base in the *syn* conformation is more sterically hindered, yet not uncommon. The *syn* conformation is favored when a bulky group is present at the 8 position of purines (*e.g.*, 8-bromoguanosine), or the 6 position of pyrimidines (*e.g.*, 6-methyluridine) [17].

The sugar conformation in RNA is typically 3'-*endo* (Figure 1.3) particularly in double-helical regions [16]. In contrast, B-type nucleic acids (generally DNA) have a 2'-*endo* sugar pucker. The 3'-*endo* configuration in A DNA or RNA brings the adjacent phosphate groups closer (about 5.9 Å) compared to B DNA (7.0 Å). Another important feature in RNA is the presence of an open cylinder along the helix axis because of the dislocation of the base pairs to the periphery. This results in a very deep and narrow major groove, and a shallow and wide minor groove in A-type nucleic acids such as RNA. The major groove in A-type helices is more electronegative than the minor groove [18]. It is observed that metal cations tend to bind to these electronegative regions in RNA [19,20]. Such interactions between cationic ligands and electronegative regions are critical for the structure, dynamics, and function of RNA [17].

RNA performs versatile functions in cells. A diverse array of RNA structures are involved in these functions. After folding of the polynucleotide backbone, the bases in single-standard regions of RNA interact to form various secondary and

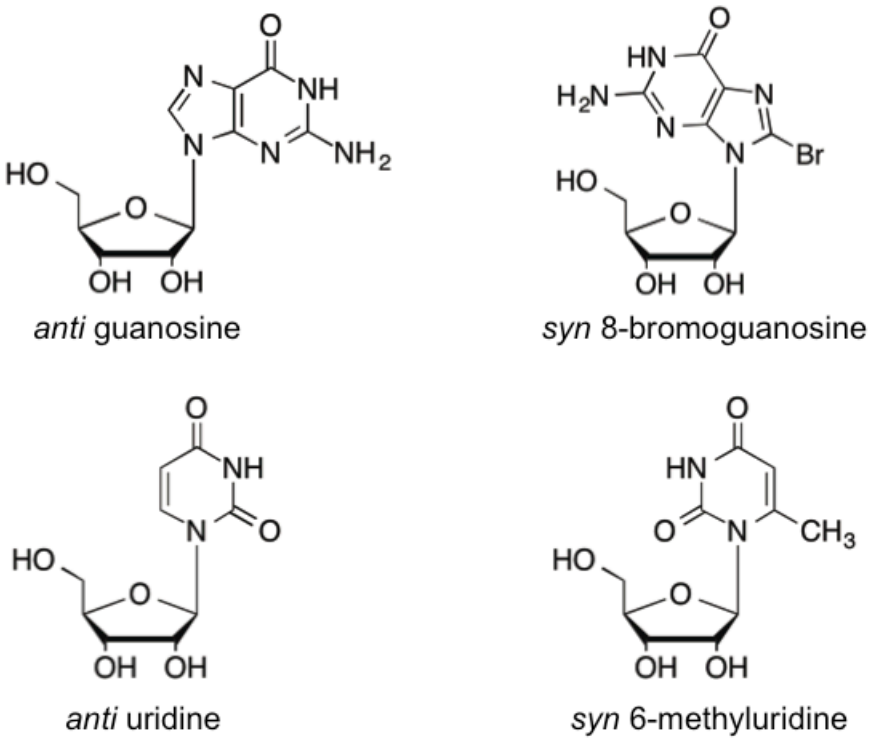

Figure 1.2. Ribonucleosides in the *anti* and *syn* conformations are shown. The *anti* conformation is more favored and common. Although steric interference between the base and sugar can occur, the presence of bulky groups on base rings can still favor the *syn* conformation.

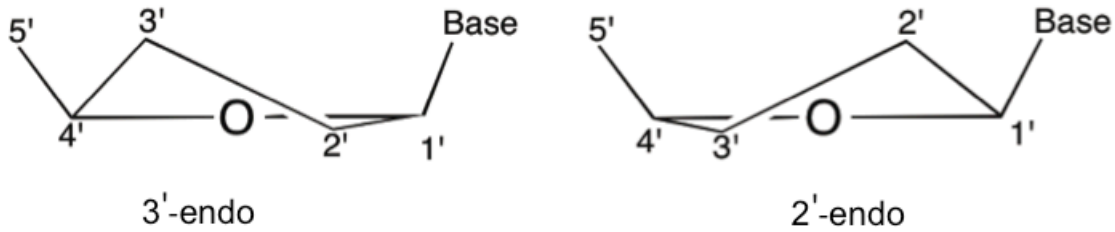

Figure 1.3. The different sugar pucker conformations are shown. The A-type nucleic acids have a 3'-*endo* conformation, while B types have a 2'-*endo* conformation.

tertiary structure elements [21,22]. Some of the RNA secondary and tertiary structural motifs are shown in Figure 1.4. The hairpins or stem-loop structures have unpaired nucleotides at the top of a double-stranded stem. Bulges have one or more unpaired nucleotides on one strand, which are either stacked into or

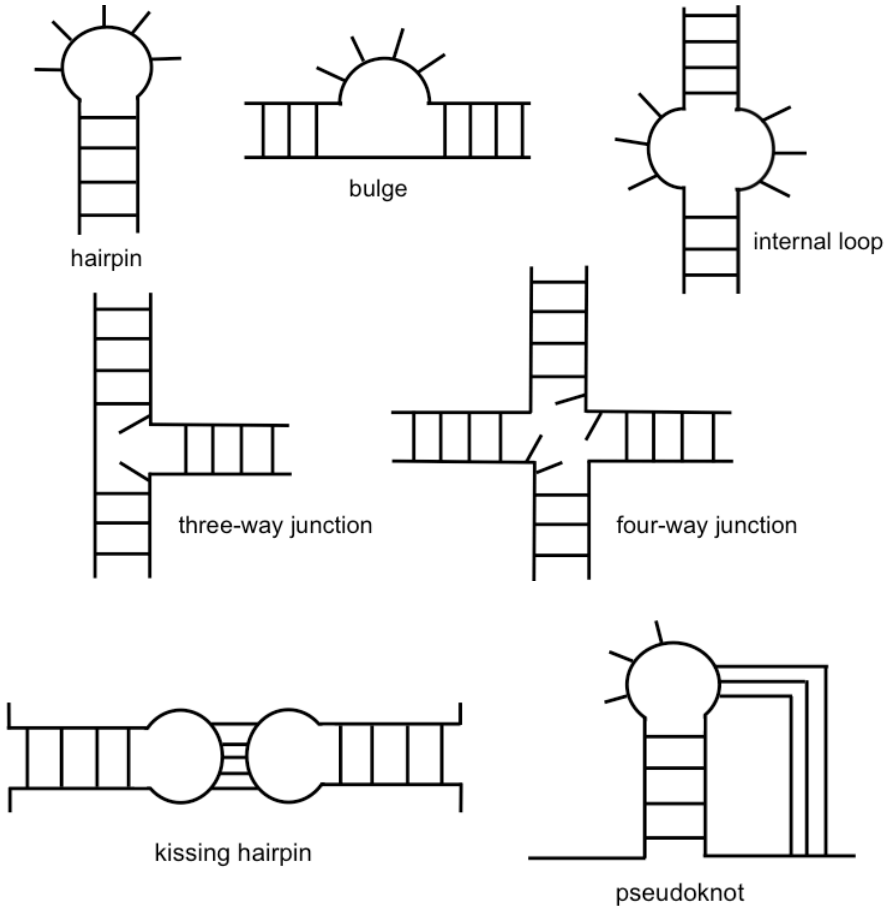

Figure 1.4. Common examples of RNA secondary and tertiary structural motifs are shown.

out of the strand. In internal loops, one or more unpaired nucleotides are present on both strands. If the number of unpaired nucleotides on the two strands are equal, the loop is symmetrical; otherwise it is asymmetrical. The unpaired nucleotides in internal loops are often involved in non-Watson-Crick base pairing [23]. A branch point or junction in a nucleic acid is a connection point between multiple helical segments [24]. The three- and four-way junctions are common elements in RNA and important for the global architecture and long-range interactions of large, complex systems [25,26].

The production of higher-order structures in RNA is hierarchical. A tertiary structure in RNA is formed by the association of pre-formed secondary structures with specific geometrical and topological arrangements [22]. A kissing hairpin is made by base pairing between two hairpin loops (Figure 1.4) [27]. The "kissing" interactions between RNA molecules are implicated in human immunodeficiency virus replication [27]. The minimal structure for an RNA pseudoknot is two helical segments that are connected by single-stranded regions [28]. Pseudoknots can form complex and stable structures, and therefore are found in many catalytic cores of ribozymes, self-splicing introns, and telomeres [28].

Cellular functions are complex and highly regulated. RNA is a component in many of these biological reactions. A variety of RNAs are dedicated to different functions in a cell. Transfer RNA (tRNA), messenger RNA (mRNA), and ribosomal RNA (rRNA) are well-known RNA molecules, all of which participate in protein biosynthesis. The tRNAs carry the correct amino acids corresponding to the anticodons. The codons of mRNA indicate the order of amino acid assembly after correct pairing with the tRNA anticodons. The peptidyl transferase center of the ribosome catalyzes peptide-bond formation between amino acids. The structure and function of ribosomes will be discussed later in this chapter. With the realization that only 1.5-2% of the genome accounts for protein-coding sequences, examination of the function of non-protein-coding regions revealed the presence of non-coding RNAs [29]. Some of these RNAs include microRNA (miRNA), small nucleolar RNA (snoRNA), PIWI-interacting RNA (piRNA), and long non-coding RNA (lncRNA). These RNAs are involved in regulation of gene

expression and post-transcriptional modifications [30-32]. In addition, other RNAs such as ribozymes (*e.g.*, hammerhead, Hepatitis Delta Virus (HDV) hairpin, group I intron, and group II intron) carry out catalytic reactions, and riboswitches that bind to adenosylcobalamin, thiamin pyrophosphate (TPP), lysine, glysine, flavin mononucleotide (FMN), guanine, adenine, and S-adenosylmethionine (SAM) are involved in regulatory functions [33].

1.3 The Ribosome

A cell depends on many biological functions for survival. The central dogma of molecular biology states that DNA is transcribed into mRNA, which is then translated to proteins [34]. The ribosomes that carry out protein synthesis are therefore crucial for a cell. The RNA component of ribosomes is essential for many steps in translation, including catalysis of peptide-bond formation. A detailed view of the structure, dynamics, and function of bacterial ribosome is discussed below.

1.3.1 The Structure of Bacterial Ribosomes

The ribosome is the protein synthesis machinery in a cell [35]. Its primary function is translation of the genetic code into functional proteins in all living organisms. The ribosome is a ribonucleoprotein complex composed of both RNA and proteins. The bacterial ribosome is about 25 nm in diameter with a molecular mass of 2.4 x 10^6 Da and sedimentation coefficient of 70S [36-38]. The size of archaeal ribosomes is similar to bacterial ribosomes, whereas eukaryotic ribosomes are larger.

The 70S bacterial ribosome contains two subunits (Figure 1.5). The interface between the subunits mainly contains RNA [35]. The basic architecture of the 30S subunit (also called the small subunit) is shown in Figure 1.6. The molecular mass of the 30S subunit is 0.8 x 10^6 Da. This subunit contains 20 ribosomal polypeptides and a single 16S rRNA composed of 1541 ribonucleotides [37]. About one third of the mass of 30S is in the so-called "head region". The "body" contains the remaining two thirds [35]. The broad shelf-like protrusion in the upper body is called the "platform". The mRNA binds to the cleft between the head and platform. Generally, the small subunit ribosomal proteins are concentrated in the head, shoulder, and platform regions [39]. The secondary

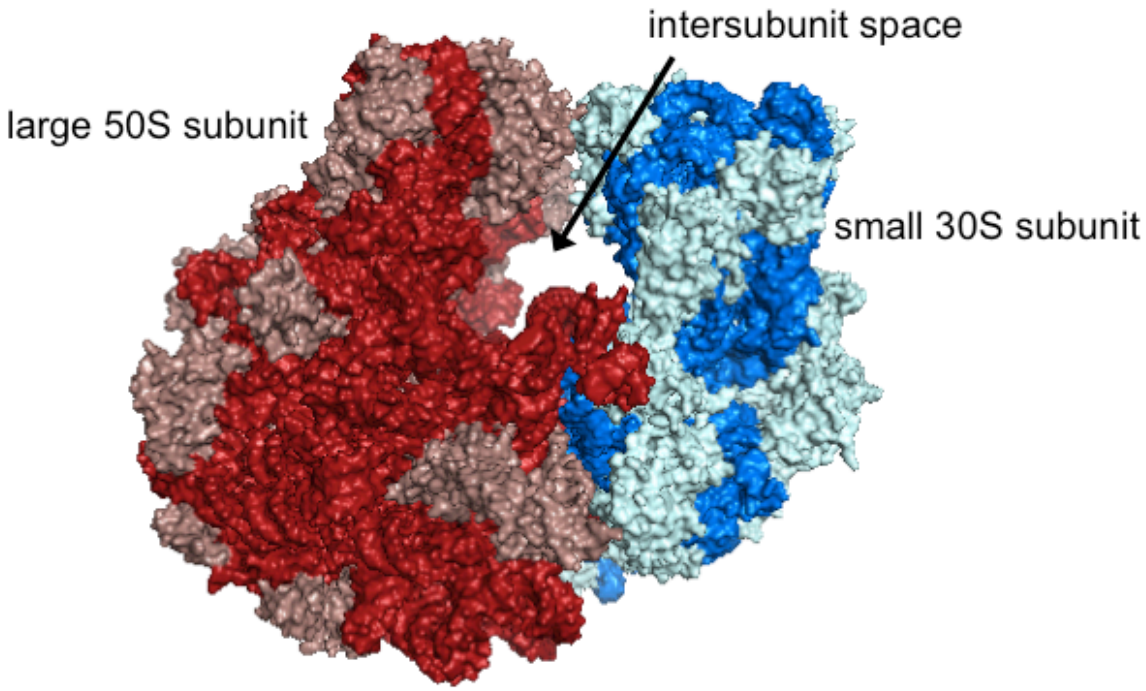

Figure 1.5. A crystal structure of the *E. coli* 70S ribosome is shown (PDB 2AVY, 2AW4) [40]. RNA and proteins in the subunits are indicated as follows: large subunit rRNA (red) and proteins (brown); small subunit rRNA (blue) and proteins (cyan).

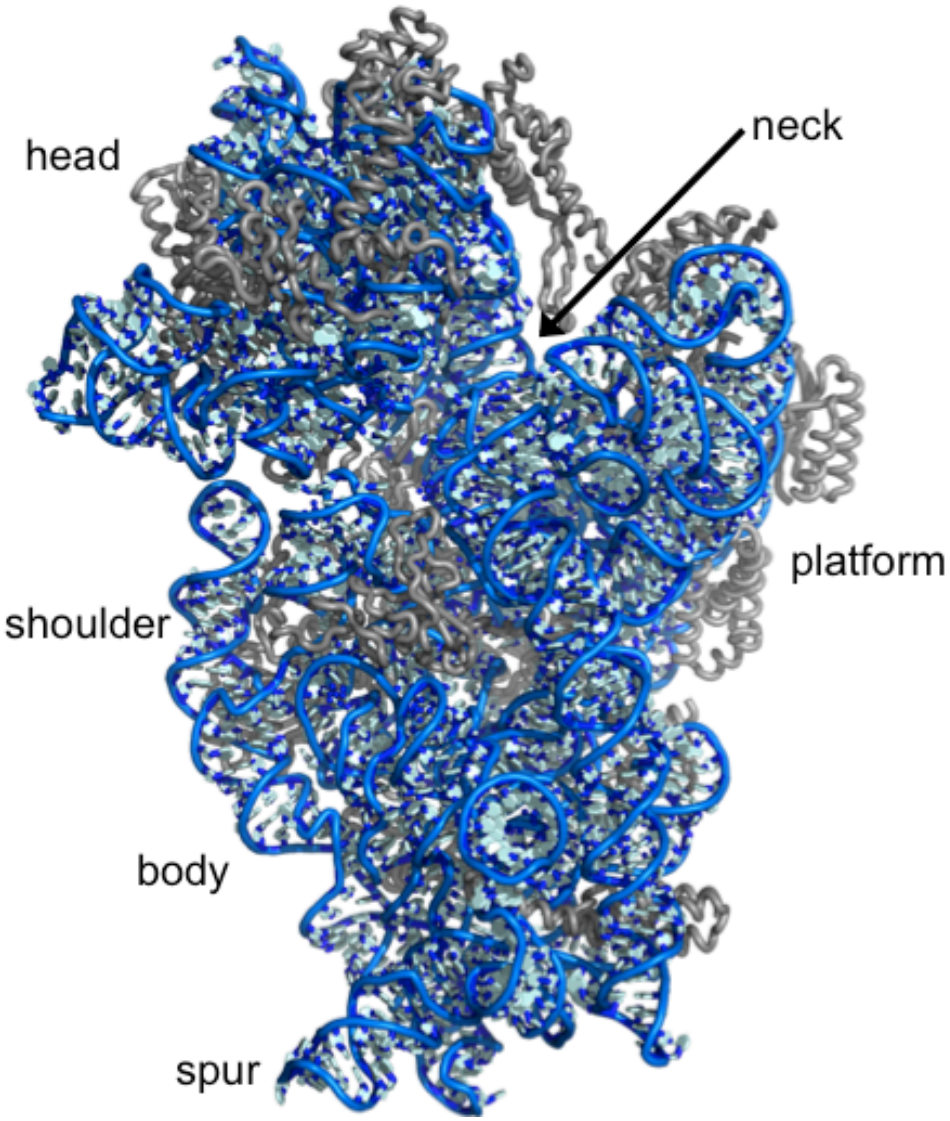

Figure 1.6. The small ribosomal subunit (*E. coli*) is shown from the interface side. The small 30S subunit (PDB 2AVY) rRNA (16S) is shown in blue. The ribosomal proteins are shown in gray. Distinct landmarks on the subunit are indicated [40].

structure of 16S rRNA is shown in Figure 1.7 [41]. The 16S rRNA can be divided into four domains. The 5' domain forms the 30S body, the central domain forms the platform, the 3' major domain forms the head, and the 3' minor domain runs

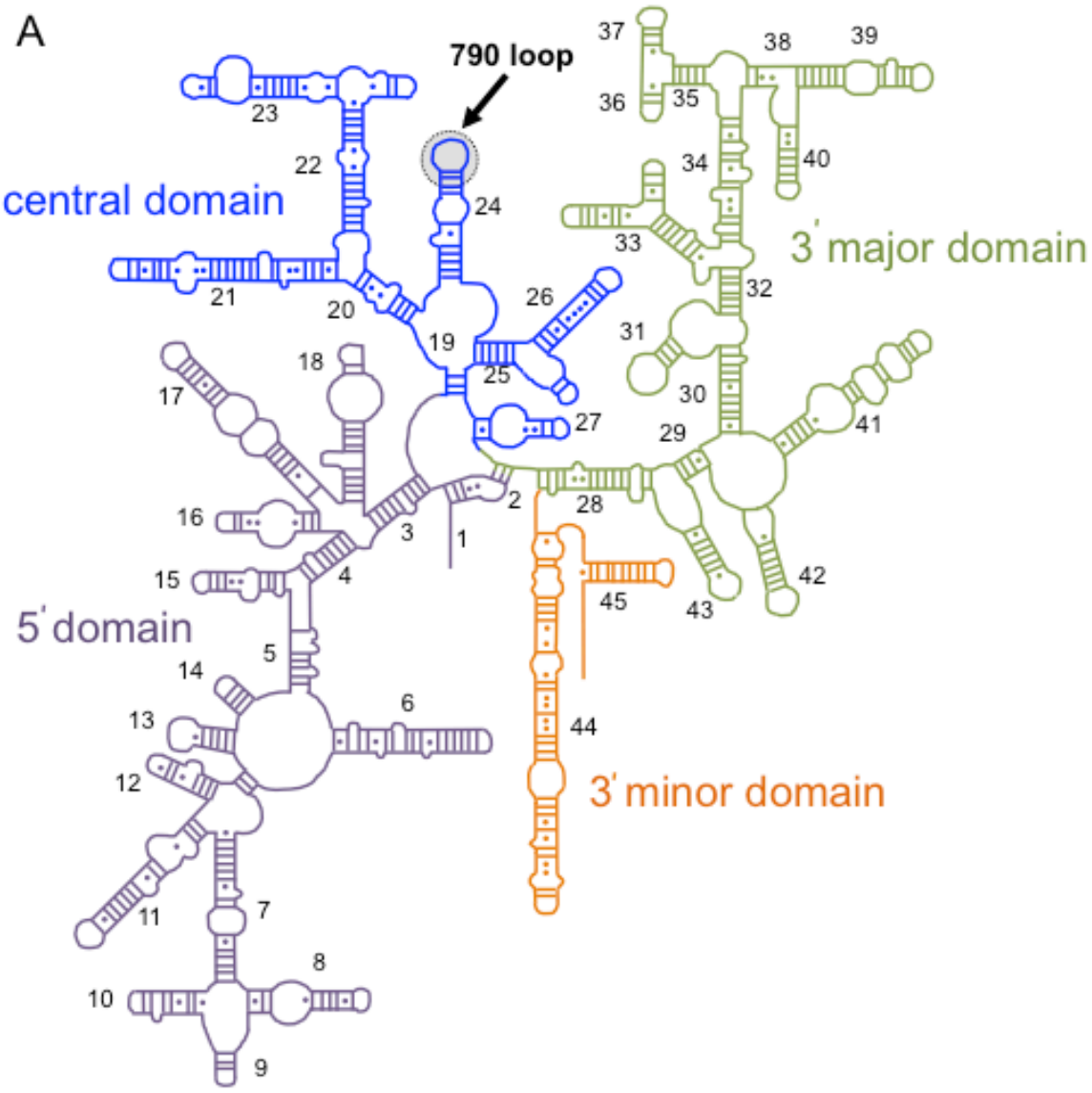

Figure 1.7. The secondary structure of *E. coli* 16S rRNA is shown. The domains in each rRNA are color coded and the helix numbers are also indicated. The 790 loop (h24) studied in this thesis work is highlighted [42-44].

along the intersubunit face [35]. The 790 loop studied in this dissertation work is located in helix 24 (h24) of the central domain.

The large 50S subunit has a molecular mass of 1.6 x 10^6 Da. It contains 23S rRNA with 2904 nucleotides, 5S rRNA with 120 nucleotides, and 34 polypeptides [37]. When viewed from the interface side, the 50S subunit has three

protuberances, which gives it a crown-like shape (Figure 1.8). The L1 stalk is on the left protuberance, 5S rRNA is on the central protuberance, and the flexible L7/L12 stalk protuberance is on the right. The interface canyon is a deep groove that runs across the entire flat side of the 50S subunit [45]. The tRNA molecules fit into this space of the 50S subunit [43]. The large ribosomal proteins are evenly scattered on the solvent surface [46]. The secondary structures of the 23S and 5S rRNAs of *E. coli* ribosomes are shown in Figure 1.9. The 23S rRNA contains six domains. Helix 69 (H69) studied in this thesis work is located in domain IV.

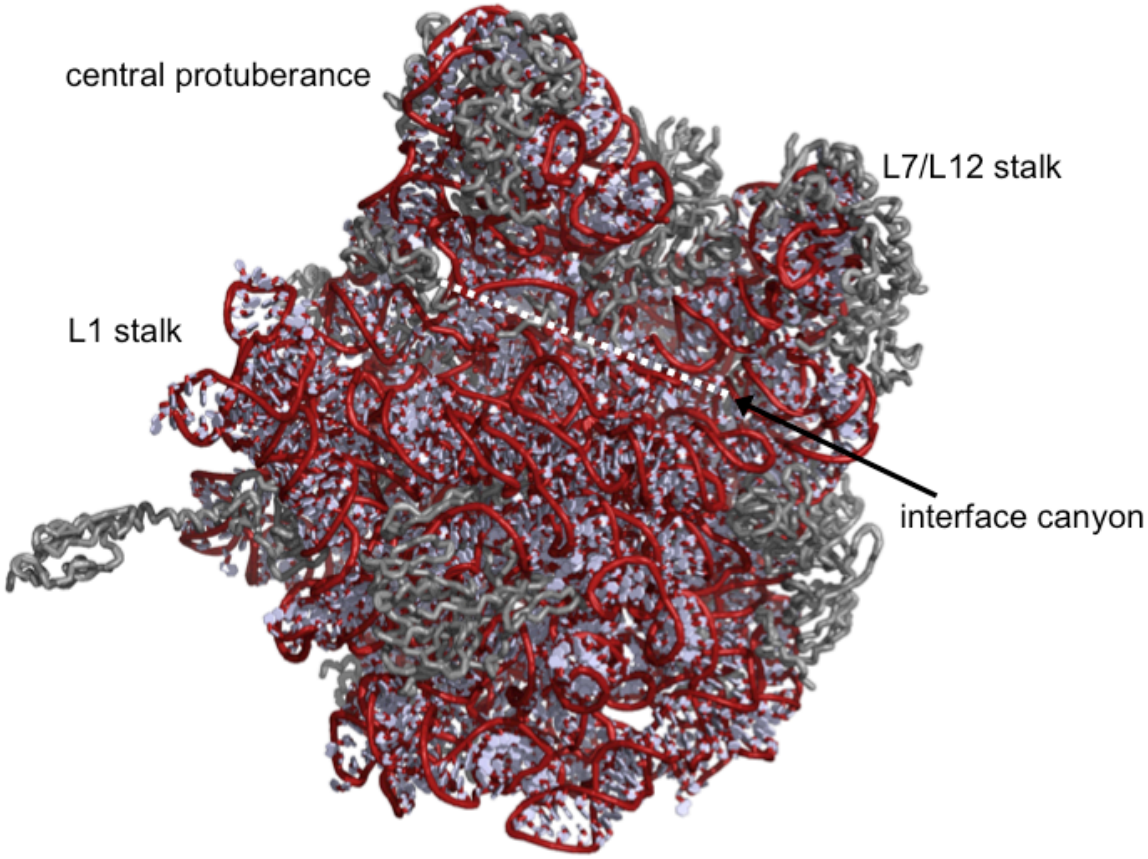

Figure 1.8. The large ribosomal subunit (*E. coli*) is shown from the interface side. The large 50S subunit (2AW4) rRNA (23S) is shown in red. The ribosomal proteins are shown in gray. Distinct landmarks on each subunit are indicated [40].

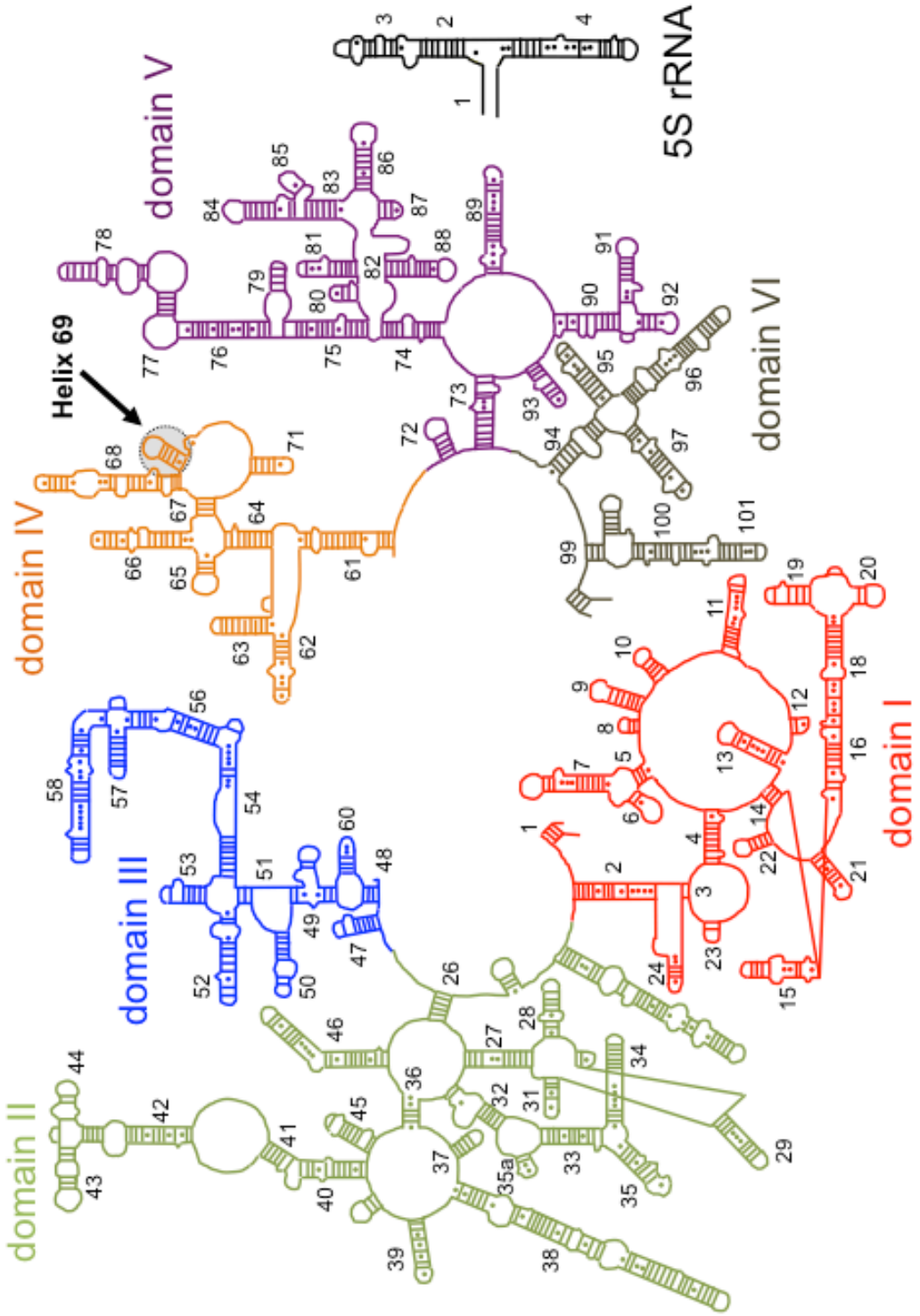

Figure 1.9. The secondary structure of *E. coli* 23S and 5S rRNA are shown. The domains in each rRNA are color coded and the helix numbers are also indicated. Helix 69 (H69), studied in this thesis work, is indicated [42-44].

1.3.2 Protein Synthesis

The biosynthesis of proteins is an essential process for all living organisms. The ribosome is the molecular machinery that catalyzes peptide-bond formation between amino acids to produce proteins. Perhaps not surprisingly, translation is a complex process that uses many factors during the catalytic cycle (Figure 1.10) [47]. The peptidyl transferase center (PTC) in the large subunit is the catalytic core of the ribosome. The decoding center (DC) located in the small subunit

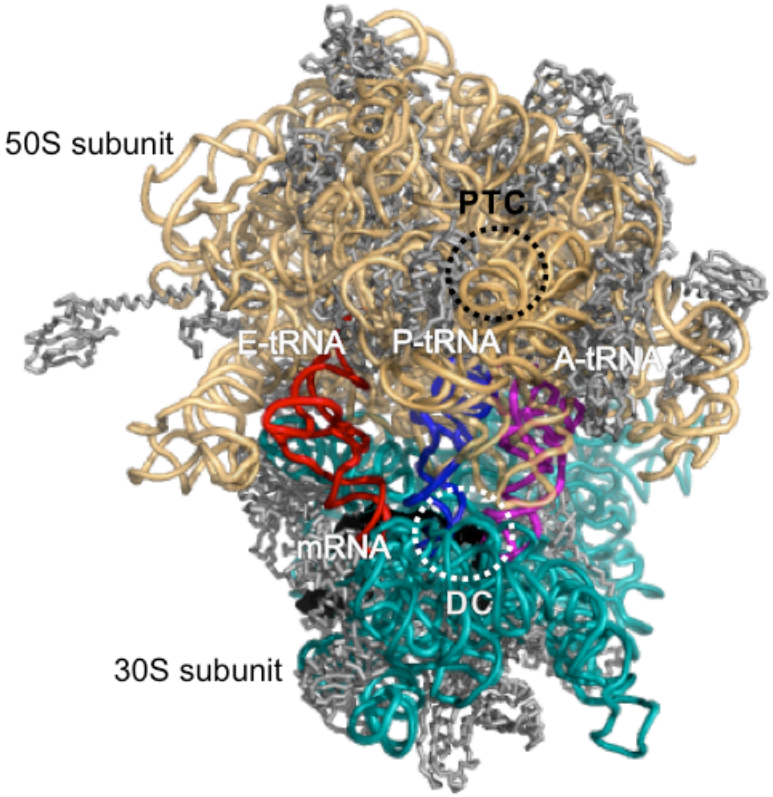

Figure 1.10. The basic components involved in protein synthesis are highlighted. The tRNA molecules occupying the A, P, and E sites in the ribosome are shown. The A-site tRNA (purple), P-site tRNA (blue), and E-site tRNA (red) are indicated. The mRNA (black) is shown in the 30S subunit. The peptidyl transferase center (PTC) and decoding center (DC) are indicated. This figure represents the *Thermus thermophilus* ribosome made from PDB files 3I8F and 3I8G [48].

checks for correct base pairing between the mRNA codon and tRNA anticodon, and is responsible for accurate translation [47]. The tRNA molecules that bring amino acids to the translational machinery occupy three regions in the ribosome. The A site binds the aminoacyl tRNA (aa tRNA), whereas the growing nascent peptide chain is attached to the peptidyl tRNA in the P site, and the E site is occupied by the deacylated tRNA before it leaves the ribosome. Motifs in the 50S subunit also play a role in decoding. Residue A1913 in H69 projects into the codon-anticodon minihelix and hydrogen bonds to the 2'-OH of A37 of the A-site tRNA [13]. A Mg^{2+} ion also connects A1913 to residue 38 of the A-site tRNA [13]. All of these contacts between H69 and the A-site tRNA are suggested to signal 50S for correct decoding. In addition to these basic molecules, many protein factors also participate in translation. A detailed discussion of the translation mechanism is given below (Figure 1.11).

Bacterial translation can be roughly categorized into three main steps: initiation, elongation, and termination. In translation initiation, the initiator Met-$tRNA^{fMet}$ is positioned over the start codon of mRNA in the P site. Correct placement of the start codon on the ribosome is accomplished by base pairing between the Shine-Dalgarno sequence upstream of the start codon and the anti-Shine-Dalgarno sequence at the 3' end of the 16S rRNA [47]. The binding of Met-$tRNA^{fMet}$ and initiation factors 1-3 precisely position the start codon in the P site [47]. The first step in initiation is recycling of the 30S subunit, which dissociates from the 50S in the previous translation cycle [47]. Initiation factor 3

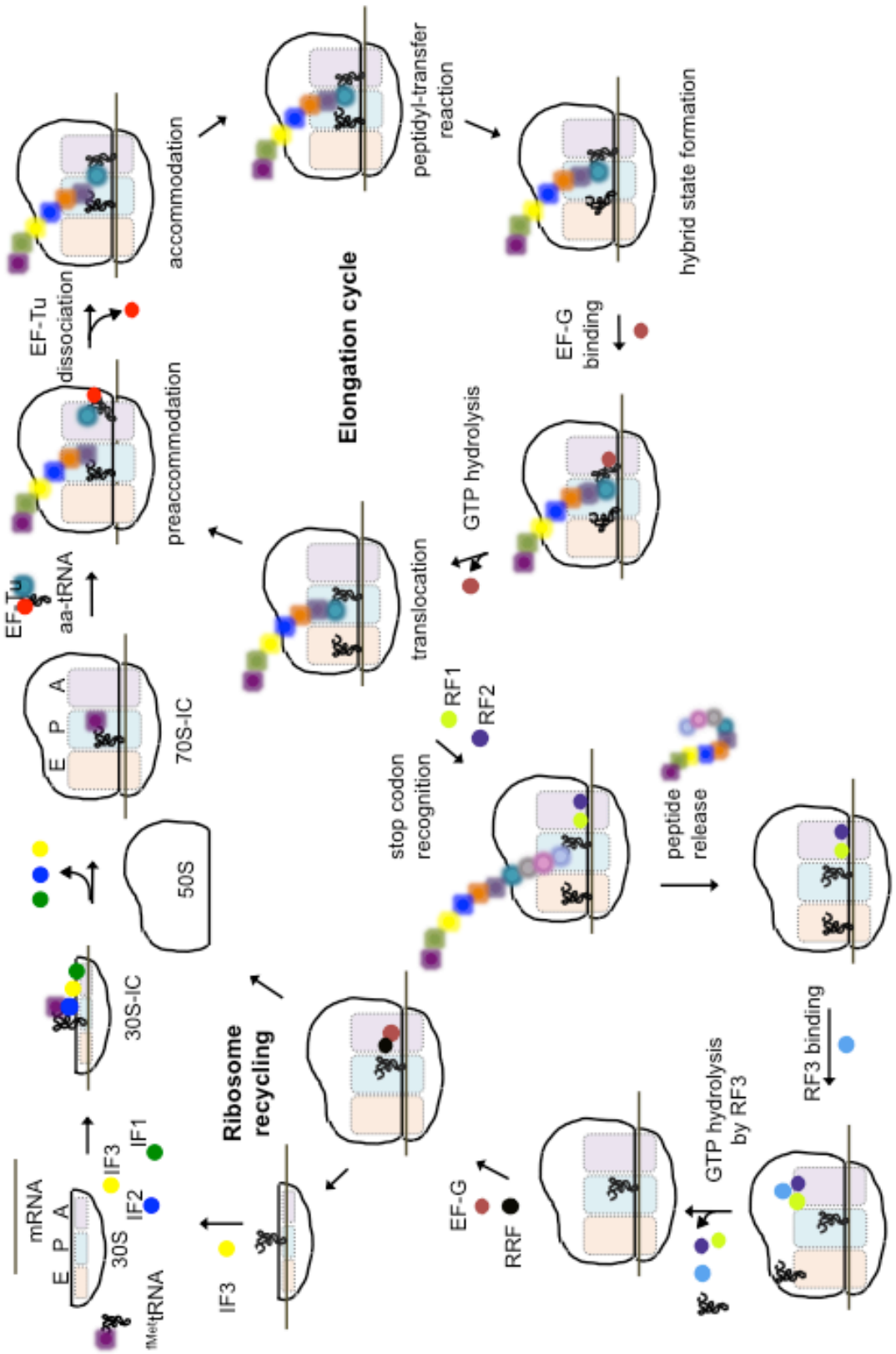

Figure 1.11. The basic steps of protein translation are shown. This figure is adapted from ref. [47].

(IF3) binding releases the mRNA and deacylated tRNA on 30S remaining from the previous translation cycle. The 30S-IF3 complex binds to mRNA, IF1, IF2, and initiator tRNA to form the 30S initiation complex (30S-IC). Initiation factor 2 promotes binding of the 50S subunit to 30S-IC to form the 70S initiation complex (70S-IC) accompanied by IF3 release [49-51]. After GTP hydrolysis of IF2, Met-tRNA^{fMet} moves to the PTC and the ribosome is ready for elongation.

In the elongation cycle of protein synthesis, the polypeptide chain is extended from the N to the C terminus by sequential addition of amino acids. This process is facilitated by two elongation factors. Elongation factor Tu (EF-Tu) delivers the aminoacyl-tRNA to the ribosomal A site, and elongation factor G (EF-G) catalyzes translocation of the tRNA and mRNA with respect to the ribosome [37]. Delivery of the correct aminoacyl-tRNA by EF-Tu to the A site involves two steps. The first step is the anticodon/codon interaction, which is followed by GTP hydrolysis. Three bases on 16S rRNA, A1493, A1492, and G530, are involved in determining the specificity of the anticodon-codon interaction [52]. In the absence of a correct mRNA codon and tRNA anticodon interaction, these residues are flipped out and point away from the ribosomal A site [52]. When Watson-Crick base pairs are formed between the cognate anticodon and codon bases, the A-site residues re-orient towards the major groove and interact with the minor groove of the codon-anticodon helix [13,52].

During translation, residue A1492 interacts with the first of the triple codon-anticodon base pairs, which occurs for all four Watson-Crick base pairs, but not for any non-cognate base pairs [53]. Residues A1942 and G530 interact with the

second position of the anticodon-codon helix. The interaction of 16S rRNA with the third anticodon-codon paired site is not as specific, consistent with the occurrence of wobble base pairs at this position [52].

The complete accommodation of tRNA in the A site requires GTP hydrolysis on EF-Tu. This step takes place at the GTPase center on the 50S subunit. Studies have shown that tRNA plays an active role in this process [54]. The elbow region of tRNA appears in contact with the GTPase center of the 50S subunit. After transmitting information regarding the correct anticodon-codon interaction, GTP hydrolysis leads to dissociation of EF-Tu from the ribosome. The tRNA aminoacyl end orients itself into the PTC. The P-site tRNA is buried in ribosomal proteins and RNA for tight and stable binding [55].

The next step in protein synthesis is peptide-bond formation. In the peptidyl-transfer reaction, the α-amino group of the aminoacyl tRNA attacks the carbon atom of the ester linkage of the peptidyl tRNA (Figure 1.12). Protein synthesis is an efficient process. The rate of translation *in vivo* is about 22 amino acid additions per second, coupled with $>10^6$ accuracy [56].

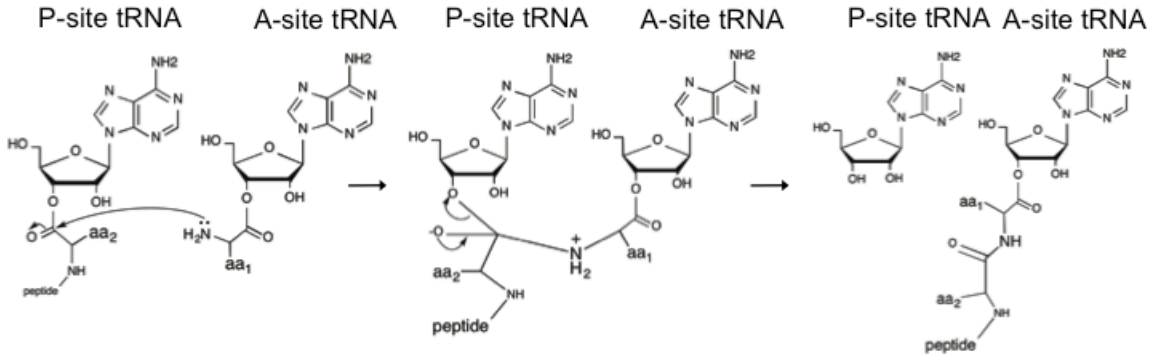

Figure 1.12. A schematic of peptide-bond formation is shown. The aminoacyl tRNA α-amino group attacks the carbonyl carbon of the peptidyl tRNA. Finally, the extended peptide chain is hydrolyzed from the P-site tRNA [47].

The step that follows peptidyl transfer is translocation. After peptide-bond formation, the P-site tRNA becomes deacylated and the peptide chain is transferred to the A-site tRNA. Translocation shifts the mRNA exactly by one codon, and tRNAs from the P to E site and A to P site. This movement forms the tRNA hybrid states, P/E and A/P, for deacylated tRNA and peptidyl tRNA, respectively [57]. During this process, the ribosome undergoes a ratcheted-like rotation in which the subunits rotate ~6° relative to each other [58]. EF-G assists with the passage of tRNA anticodon ends and mRNA on the small subunit [57]. The E site traps the hybrid P/E tRNA efficiently and facilitates translocation.

Another feature of the ribosomes is the polypeptide exit tunnel, which starts from the PTC and extends through to the center of the 50S subunit, with the exit on the back. The tunnel is about 80 Å long and 12-20 Å in diameter [14,59]. The addition of amino acids to the polypeptide chain continues until a stop codon reaches the A site. In bacteria, release factors RF1, RF2, and RF3 hydrolyze the nascent polypeptide chain from the P-site tRNA. Ribosome recycling factor (RRF) and EF-G cause subunit dissociation [60]. IF3 binding then removes mRNA and tRNA from the 30S subunit and prepares the ribosome for the next protein synthesis cycle.

1.3.3 The Helix 69 and 790 Loop Motifs of *Escherichia coli* Ribosomes

As explained in the previous section, protein synthesis is a complex process. Many rRNA motifs play crucial roles during translation and have therefore become drug targets [36]. This thesis work focused on two such rRNA regions,

namely, helix 69 (H69) and the 790 loop (h24). The following section discusses the structure and function of these regions in detail.

The H69 RNA is a 19-nucleotide hairpin located in domain IV of 23S rRNA (Figure 1.9). The secondary structure, location on the 50S subunit, and the tertiary structure of H69 in bacterial ribosomes are shown in Figure 1.13. Many nucleotides in the loop region of H69 are conserved, indicating their significance for ribosome structure and function [41]. Three post-transcriptionally modified nucleotides, namely pseudouridine (Ψ) at positions 1911, 1915, and 1917 (*E. coli* numbering), are found in the loop region of H69. In bacteria, the conversion of uridine to Ψ in H69 is carried out by a single pseudouridine synthase RluD [61]. Pseudouridylation is an isomerization reaction that involves conversion of an N1-C1' glycosidic bond to a C5-C1' glycosidic bond (Figure 1.13) [62]. In addition, the Ψ at residue 1917 is methylated at the N3 position. The H69 RNA also contains a G•U mismatch in the stem region. The G•U wobble pairs have been reported to have strong electronegative potentials in the major groove to which divalent ion binding occurs [63].

Helix 69 is located in the subunit interface along with helix 44 (h44) of the small subunit to form bridge B2a [43]. The A1919 and A1912 residues of H69 project towards h44 of the small subunit. These H69–h44 interactions are stabilized by reverse-Hoogsteen base pairs formed with the H69 loop residues [40]. As a structural element connecting the two subunits, it is not surprising that H69 is a dynamic motif in the ribosome. It is involved in many steps during

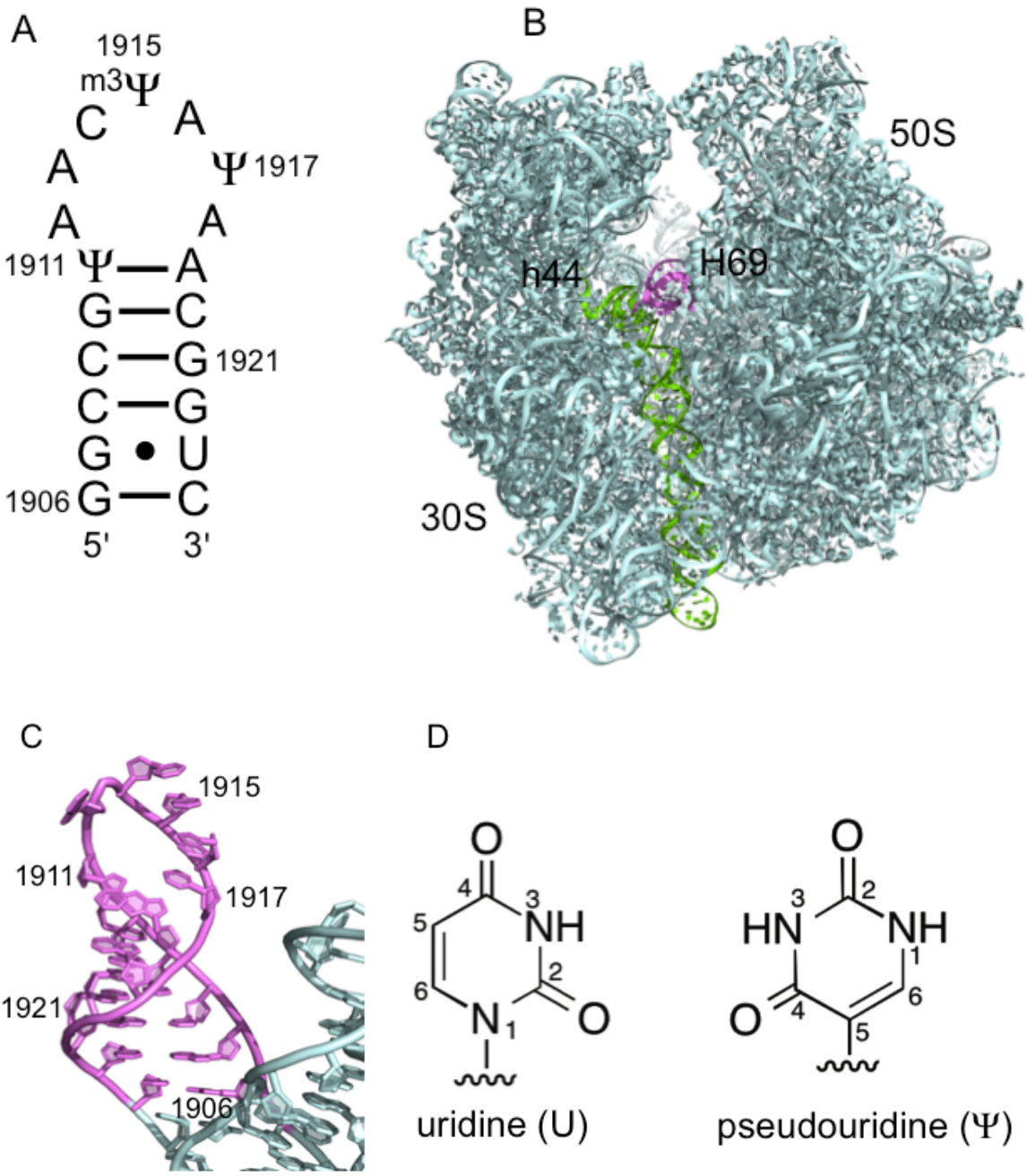

Figure 1.13. Bacterial H69 and structures of uridine and pseudouridine are shown. A) The secondary structure of H69 is given with the residues numbered according to *E. coli* 23S rRNA. B) H69 (purple) is displayed from a side view of the 50S subunit. H69 interacts with h44 (green) of the 30S subunit to form bridge B2a. C) A closer view of the tertiary structure of H69 is given [64]. The figures were created using PDB files 2AVY and 2AW4. D) The base structures of uridine and pseudouridine are shown.

translation, including subunit association, initiation, elongation, termination, and recycling [65]. Helix 69 interacts with both aminoacyl and peptidyl tRNAs [43,48]. The deletion of H69 has been shown to cause defects in subunit association [66]. During the translocation step, residues 1914 and 1915 in H69 interact with hybrid tRNA complexed with EF-Tu.

During the last steps of protein synthesis, H69 interacts with the release factors and the ribosome recycling factor [67-69]. In stop codon recognition, nucleotides 1914 and 1915 of H69 interact with RF1 and contribute to its conformational changes [68]. Crystallographic studies revealed that H69 is the only 23S rRNA component that interacts with RRF, and this motif undergoes significant conformational changes in the loop region. As such an integral part of the ribosome, mutations or deletions of residues or the complete H69 show deleterious effects to bacteria [65]. Deletion of H69 residues lead to defects in peptide synthesis, translational processivity, internal-codon frame shifting, and stop-codon read-through [70,71].

Nucleotide modifications in rRNA mostly occur in the functionally important regions, highlighting their significance in ribosome function [72]. Pseudouridine is the most commonly found nucleotide modification in the ribosome and is a key component in H69 [73]. It is important for the rigidity of the loop region [74], and slow-growing phenotypes result from the absence of pseudouridine [61]. Biophysical studies carried out using truncated models have shown Ψ's impact on H69 structure. The pH-dependent CD experiments revealed that Ψ-containing H69 undergoes a structural change with an apparent pK_a of 6.3 ± 0.2 [75]. The

same study suggested that at low pH, a protonation may be occurring near 1911 or causing a structural change at the loop-closing base pair in Ψ–modified H69. Biochemical studies performed on ribosomes revealed that pseudouridylated H69 undergoes a base-stacked ("closed") to a base-flipped ("open") conformation in response to increased pH, temperature, and Mg^{2+} [76]. Biological studies revealed that Ψ-deficient H69 could affect subunit association [77].

The 790 loop (h24) is a hairpin structure located in the central domain of 16S rRNA (Figure 1.7) [78]. In the secondary structure of 16S rRNA, the 790 loop resides on the tip of h24. The loop motif comprises nine nucleotides, in which six of them are universally conserved and two are highly conserved (Figure 1.14) [78]. The 790 loop is a functionally important region of the ribosome that has been implicated in initiation factor binding, subunit association, and tRNA binding [79-82]. Chemical probing experiments carried out using 1-cyclohexyl-3-(2-morpholinoethyl) carbodiimide metho-*p*-toluene sulfonate, or CMCT, showed that initiation factor 3 binding protects U793 [79]. Site-directed mutagenesis of the universally conserved G791 to A showed reduced cell growth, IF3 binding, and subunit association [83]. Kethoxal modification experiments revealed that G790 is protected after tight coupling of the subunits [81]. Other studies showed that residues 787-795 are protected by cDNA probes after subunit association [80]. Perhaps the 790-loop connection to subunit association is not surprising, since it is involved in an intersubunit bridge confirmed by crystallographic studies (Figure 1.14B) [43]. The 790-loop residues 784-785 and 794 form the bridge B2b through interactions with H67 and H69 of the large subunit [43].

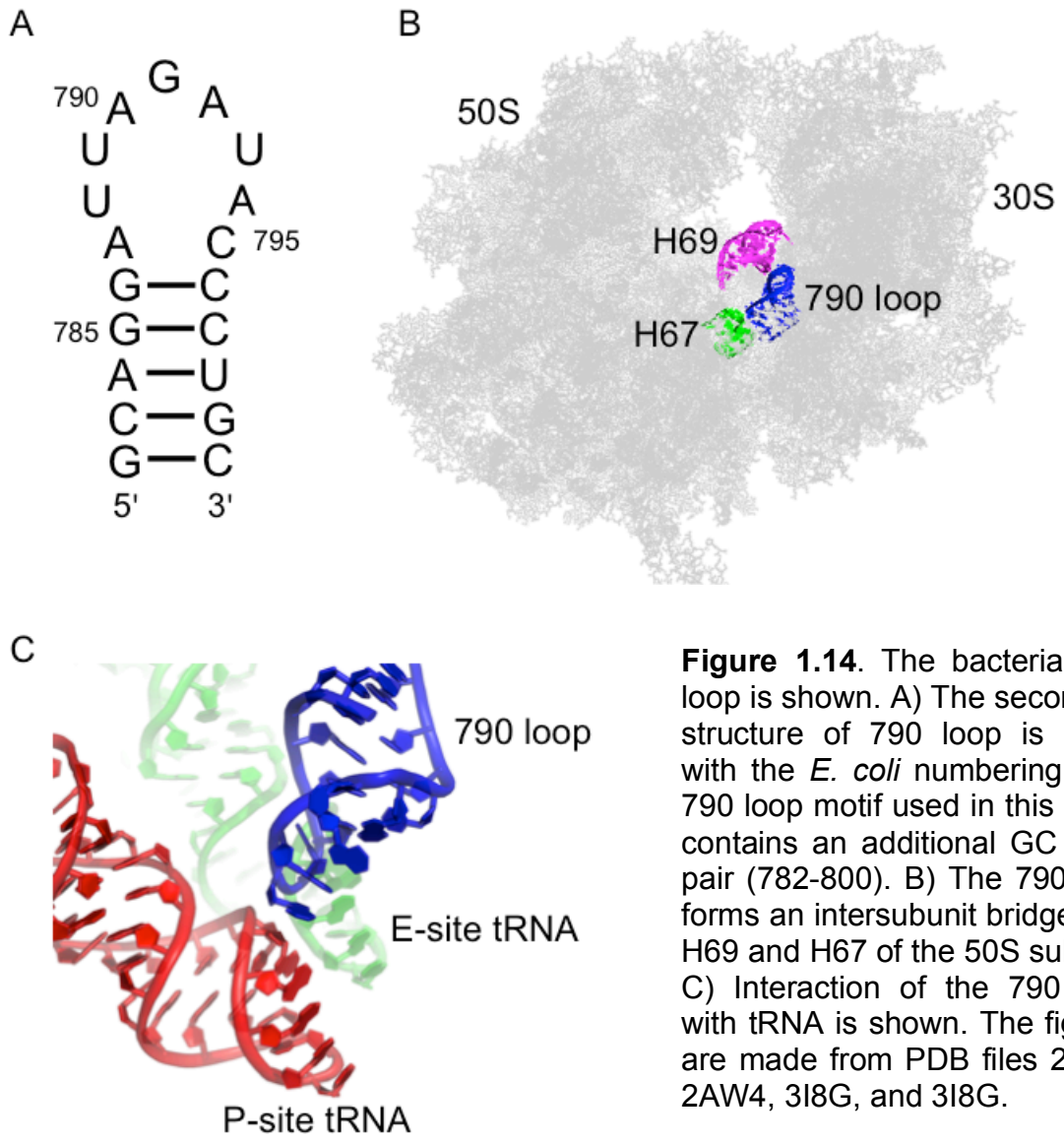

Figure 1.14. The bacterial 790 loop is shown. A) The secondary structure of 790 loop is given with the *E. coli* numbering. The 790 loop motif used in this study contains an additional GC base pair (782-800). B) The 790 loop forms an intersubunit bridge with H69 and H67 of the 50S subunit. C) Interaction of the 790 loop with tRNA is shown. The figures are made from PDB files 2AVY, 2AW4, 3I8G, and 3I8G.

Another important involvement of the 790 loop in protein synthesis is its interaction with tRNAs (Figure 1.14C) [82]. Residue A790 contacts the anticodon stem loop of the P-site tRNA. The *E. coli* ribosome structure at 3.5 Å resolution also shows the importance of the 790 loop in translocation [40]. Together with G1338 and U1314, A790 forms a 12-13 Å gap that prevents tRNA from passing through. This feature allows for formation of the P/E tRNA hybrid state [40].

Random mutagenesis and selection of functional ribosomes also revealed that positions 787 and 795 are important for the 790-loop structure and strongly affect subunit association [84]. Of note, the 790 loop has an identical size and nucleotide composition, but altered sequence, compared to unmodified H69, and was therefore used to examine the effect of nucleotide arrangement on cisplatin reactions in this thesis work.

Collectively, these two chosen regions of rRNA, H69 and the 790 loop, are integral for the translation process. Ligand binding to these regions may be a promising approach for antibacterial therapies. Although less is known about the roles of H69 and the 790 loop in eukaryotic ribosome systems, these essential components might also serve as target sites for anticancer drugs. Therefore, studying the local environments of these assemblies and how such atmospheres control ligand interactions is important.

1.4 RNA Microenvironments

RNAs are essential biomolecules. The complex three-dimensional RNA scaffolds are necessary for their activity. RNA microenvironments and their interactions with other ligands such as cations are important for producing functional molecules. Computational studies have revealed the significance of the RNA microenvironments in molecular recognition and ligand binding [18,85]. Understanding the local environments of these biomolecules and their changes in response to the bulk medium is therefore important for recognition of unique RNA regions by small molecules and for future drug development. Further, identification of probes that can interpret these microenvironments, especially

when currently applied methods are mostly based on computational work, will be invaluable for RNA biochemists.

1.4.1 Electrostatic Interactions with RNA

RNA is a highly charged anionic biopolymer. Therefore, electrostatics play a major role in RNA biology. Many RNAs have been identified that possess regions with characteristic electrostatic potentials where biological reactions take place. Some examples include yeast $tRNA^{Phe}$, mouse mammary tumor virus (MMTV) pseudoknot, 5S rRNA, and G•U tandem basepairs (Figure 1.15) [18]. Computational analyses applied to yeast $tRNA^{Phe}$ have shown distinct electrostatic patches on the aminoacyl end and anticodon loop (Figure 1.15) [18]. These regions are suggested to facilitate the association of other negatively-charged molecules such as mRNA [86]. The potential hole on MMTV occurs over residue G7 where the structure is bent [18]. This region is implicated in playing a role in ribosome recognition, and further supports the concept of minimizing electrostatic repulsions. Moreover, the study on MMTV suggested that the connection between potential hole location and molecular shape may indicate evolution of RNAs to modulate electrostatic potentials. Computational calculations further showed an unusually large electronegative region on 5S rRNA. This region corresponds to a site referred as the "metal ion zipper" [18]. The presence of several magnesium ions in this region cause a narrowing of the major groove [87]. In the last example, wobble pairs have also been implicated

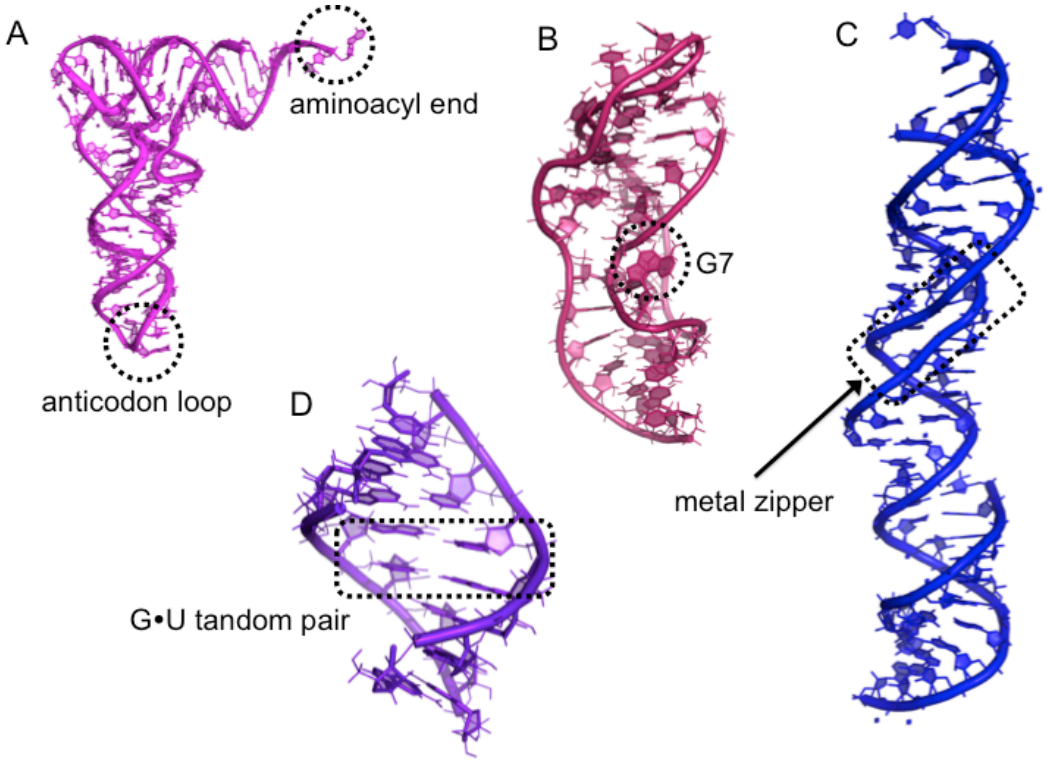

Figure 1.15. Examples of RNAs with varying electrostatic potentials on their surfaces are given. A) Yeast $tRNA^{Phe}$, B) mouse mammary tumor virus (MMTV) pseudoknot, C) 5S rRNA with the metal zipper region, and D) RNA with tandem G•U base pairs are shown. The regions with either potential holes or high electronegative surfaces are indicated with dotted circles or boxes, respectively. The figures are made from PDB files 1TRA, 1RNK, 364D, and 1QES and adapted from ref. [18].

in RNA function. The most common non-Watson-Crick pair in RNA is G•U [63]. Analysis of the surface potential of an RNA with tandem G•U pairs also revealed a major groove with increased negative potential where metal binding occurs [63].

The electrostatic characteristics of the major and minor grooves of nucleic acids are important. These regions are implicated in drug binding and cation accumulation. Analysis of the electrostatic potential on A-form nucleic acids (typically RNA) has revealed that the major groove is more negative than the

minor groove [18]. This result is supported by the observation that cations tend to bind to the major groove of RNA [20]. In contrast, the minor groove of B-form nucleic acids was found to be more electronegative, but also supporting cationic drug binding [18].

Calculation of the electrostatic potentials on rRNA revealed that the codon-binding region is surrounded by positive potentials, which suggested a stabilizing effect on mRNA and tRNA binding [88]. Electrostatics are important for many RNA-protein interactions. An arginine-rich motif in the Rev peptide has been suggested to play a role in stabilizing unfavorable electrostatic interactions in a bulge region of the Rev response element (RRE) RNA of HIV [89]. Similarly, the specific binding of transcription activating (Tat) protein to the trans-acting responsive element (TAR) RNA was shown to require an arginine residue that participated in electrostatic interactions [90]. Other examples of electrostatics in protein-RNA interactions include tRNA-EF-Tu and tRNA-tRNA synthetase binding [91].

1.4.2. The Influence of Salts and Divalent Ions on RNA Structure and Electrostatics

Biomolecules in cellular environments are immersed in a mixture of ions. Concentrations of different cations found in a variety of cellular environments are listed in Table 1.1. The most common ions *in vivo* are K^+ and Mg^{2+}. The most abundant cation in the extracellular fluid is Na^+; however, an increase in *E. coli* cytoplasm Na^+ concentrations in response to external conditions has also been reported [92]. Therefore, cations are in constant contact with biomolecules and can play important roles in ligand interactions [93,94].

Table 1.1. Concentrations of cations in biological fluids are shown [92,95,96].

Ionic species	Mammalian cells (mM)	Mammalian extracellular fluid (mM)	Blood plasma (mM)	*E. coli* cytoplasm (mM)
Na^+	10	145	138	42
K^+	140	5	4	230-930
Mg^{2+}	30	1	1	23
Ca^{2+}	1	4	3	
Fe^{2+}			$2x10^{-2}$	

The high negative charge of RNA acts against its folding. Many different cations including Na^+, K^+, NH_4^+, and Mg^{2+} have been identified to bind to various types of RNA [97]. Cations neutralize the negative charge of RNA and assist in folding and stabilization. There are different types of cation-RNA interactions (Figure 1.16). The diffusely bound ions, classically described by Manning and Record, screen electrostatic repulsions between RNA backbone charges [98,99]. The behavior of diffuse ions or the "ion atmosphere" is determined by the long-range electrostatic interactions with RNA [93]. The concentration of diffuse ions is proportional to the magnitude of the local RNA electrostatic potential. The ionic cloud comprises group I monovalent ions such as Na^+ and K^+, which often remain well hydrated. Diffusely bound divalent cations such as Mg^{2+} are reported to play a dominant role in RNA tertiary structure stabilization [100,101]. The Mg^{2+} ion is small with an ionic radius of ~0.60 Å. Given the higher charge compared to the larger K^+ (~1.3 Å) and Na^+ (~1.0 Å) ions, Mg^{2+} carries a higher charge density. These differences in monovalent versus divalent cations lead to a strong RNA-Mg^{2+} electrostatic interaction [93]. Therefore, the entropic effects in which one Mg^{2+} ion releases RNA electrostatic stress in a similar manner as two K^+ ions explains the dominant role of Mg^{2+} in RNA stabilization [93].

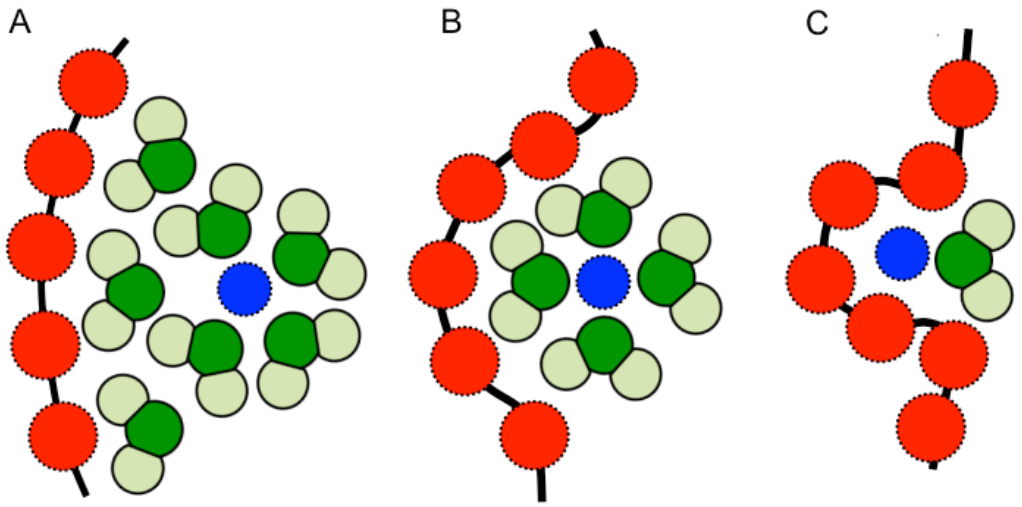

Figure 1.16. Different modes of ion-RNA interactions are shown. A) Diffuse binding, B) outer-sphere site binding, and C) inner-sphere site binding are represented with cations in blue, RNA in red, and water in green. The figure is adapted from refs. [93,94].

The evaluation of salt-dependent platination rates by electrostatic models in this thesis work also emphasizes the significant impact of such ionic atmospheres for RNA-ligand interactions.

In addition to diffuse binding, metal ions interact with RNA through outer-sphere and inner-sphere complexes [93,94]. In outer-sphere binding, metal ions often interact with RNA through water molecules [94]. One example of this binding occurs in the *Tetrahymena* pre-ribosomal RNA intron [102]. In the crystal structure, docking of the tetraloop to the receptor motif is facilitated by binding of $Mg(II)(H_2O)_6^{2+}$ to tandem G•U pairs [103]. One of the studied RNAs in this thesis work, H69, contains a G•U mismatch (Figure 1.13). Therefore, similar Mg^{2+} ion binding near this pair is likely and could impact ligand-binding reactions. In contrast, the formation of inner-sphere complexes occurs through direct contacts between the metal and nucleic acid ligands [93,94,102].

One of the bacterial rRNA motifs that was studied in this thesis work is H69. Crystal structures revealed Mg^{2+} ions binding to the stem, loop, and stem-loop junction of H69 [65]. Figure 1.17 shows Mg^{2+} ions bound to these regions of H69 [104]. A 2-aminopurine-substituted H69 construct revealed high exposure of residue 1913 in the presence of >0.8 mM Mg^{2+} [105]. Chemical- probing studies carried out on *E. coli* 50S subunits and complete ribosomes further supported Mg^{2+}-induced A1913 conformational changes in H69 [76,77]. The binding of cationic antibiotics such as neomycin and Mg^{2+} to the G1921 and G1922 residues have also been observed [104,106]. Collectively, these observations suggest that H69 in bacterial ribosomes should possess electronegative surfaces to which cationic ligands prefer to bind.

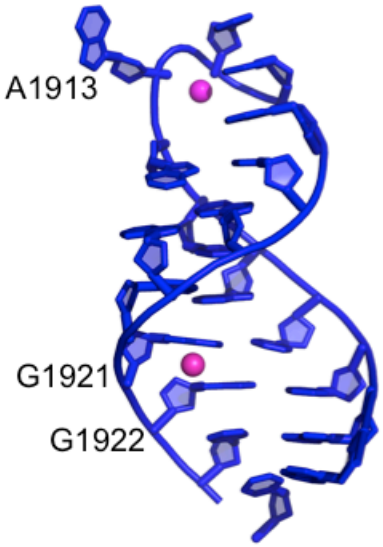

Figure 1.17. The Mg^{2+} ions (magenta) bound to the loop and stem regions of *Thermus thermophilus* H69 are highlighted [104]. PDB entry 3HUX.

High Mg^{2+} concentrations (>6 mM) and low NH_4Cl (30 mM) are necessary for the isolation of complete ribosomes with proteins *in vitro* [107].

1.4.3. The Impact of pH on Structure and Dynamics of RNA

Local environments impact biochemical reactions. The concentrations of reactants, temperature, ionic strength, cofactors (*e.g.*, Mg^{2+}), and pH influence bimolecular interactions as well as chemical reactions and rates. The oxygen and nitrogen atoms in nucleobases act as H-bond acceptors, and hydrogens are donors (Figure 1.18). Complementary donors and acceptors interact to form Watson-Crick base pairs [108]. The pK_a values of nucleotide bases are well outside of the neutral pH range, and therefore are not charged at physiological pH [16]. The pK_a values of nucleosides and their ionizations are shown in Figure 1.19 [109,110].

The pK_a values of nucleotides increase by 0.3-0.5 units due to the addition of a phosphate group [110]. In a polynucleotide where the electrostatic field is

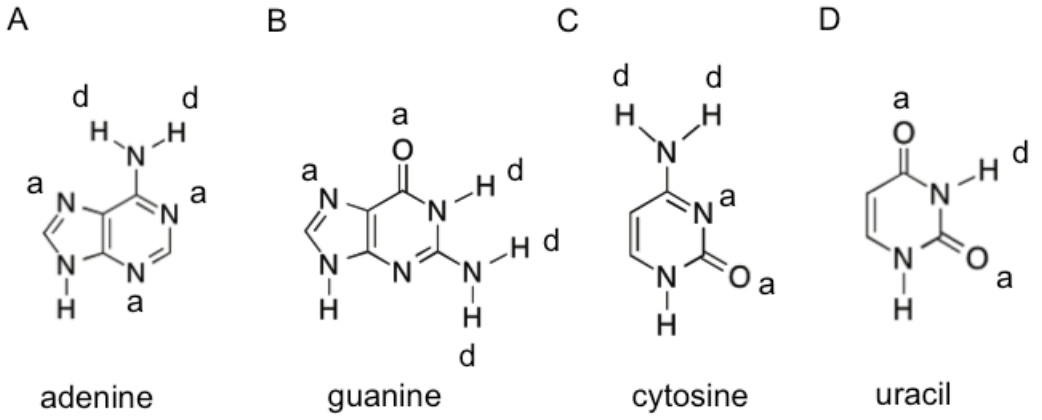

Figure 1.18. The H-bonding donors (d) and acceptors (a) of the nucleobases found in RNA are shown.

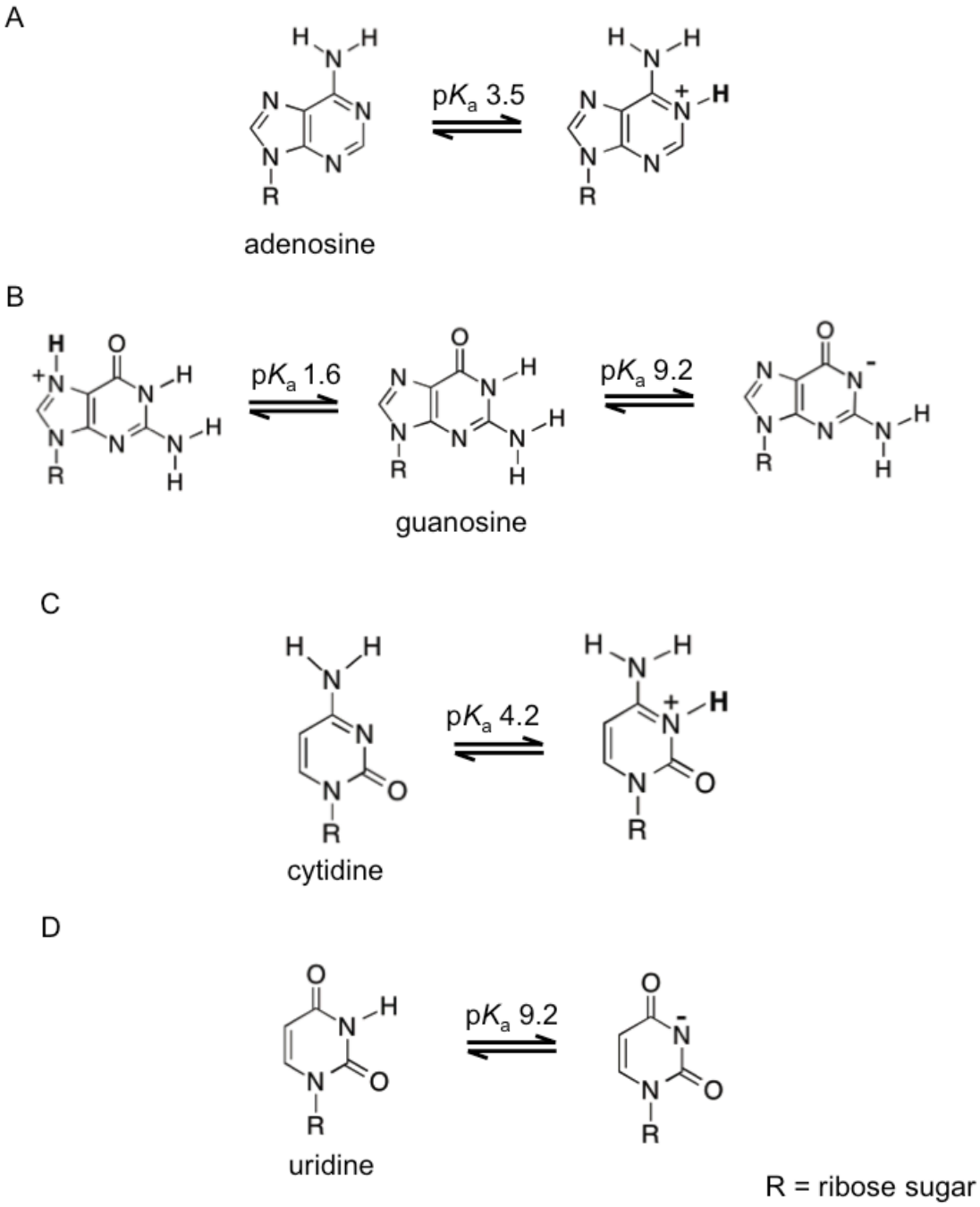

Figure 1.19. The pK_a values and sites of ionization of ribonucleosides are shown. The figure is adapted from ref. [17].

higher, the pK_a values further increase [17]. Other ionizable groups present in the RNA include phosphates and 2'-OH of the ribose ring [110]. The phosphate

groups on the ends of oligonucleotides have two ionizable groups; the second ionization has a pK_a close to physiological pH. The phosphodiester ionizable group is very acidic with a pK_a value of ~1. In contrast, the sugar 2'-OH has a pK_a of ≥ 12.5 [110]. The apparent pK_a values are dependent on the temperature and the ionic strength [17].

As discussed previously, counterion condensations are crucial for nucleic acid-ligand interactions. However, little is known about H^+ ion condensations and their concomitant release upon ligand binding to nucleic acids [111]. Computational calculations carried out on poly(dG)•poly(dC) revealed that high concentrations of H^+ are localized in the major groove near the N7 of deoxyguanosine in the G•C pairs [111]. The pH near the van der Waals surface was about 1.9-3.5 units lower than the bulk pH [111,112]. The authors suggested that this increase in H^+ concentration results from an effective increase in the pK_as of water molecules near high negative electrostatic potentials of nucleic acids. Moreover, the study revealed an interesting contrast between counterion condensation and H^+ condensation. In counterion condensation, the number of counterions bound to the polyelectrolyte does not depend on bulk salt concentration. In contrast, the H^+ ions on nucleic acid surfaces are proportional to the bulk pH. Overall, these studies showed that the high electrostatic potential surfaces of nucleic acid polyelectrolytes could generate acidic microenvironments. Such environments can therefore impact pH-dependent nucleic acid interactions.

1.5 Small Molecule Binding to Ribosomal RNA

Finding solutions to medical challenges, drug-resistant bacteria, lethal and life-threatening infections (*e.g.*, Ebola, HIV), cancers, and genetic disorders are some major interests in scientific research. The imperative function, structural complexity, and little-known repair mechanisms of RNA make ribosomes a versatile target for drug development [36,113-115]. Not surprisingly, there are many drugs that target ribosomes; more than half of the clinically used antibiotics target this macromolecule [114,116]. Some examples of compounds used in clinical treatments include macrolides, ketolides, lincosamides, oxazolidines, aminoglycosides, and tetracyclines [113].

Many clinically used drugs such as aminoglycosides, tetracyclines, and cyclic peptides target the small ribosomal subunit (Figure 1.20A) [36]. The chemical structures of some of these drugs are shown in Figure 1.20B. Aminoglycosides, *e.g.*, paromomycin and neomycin, target the decoding site and lead to amino acid misincorporation, and also impact EF-G-catalyzed translocation [52,117-119]. The pK_a values of the amino groups on aminoglycosides are approximately 5.7-9.5, hence they are charged at physiological pH [120,121]. Electrostatic interactions between cationic amino groups and anionic RNA are important for aminoglycoside binding [122-126]. Helix 69, one of the rRNA motifs studied in this thesis work, has shown interactions with aminoglycosides [127]. Edeine is a peptide-like antibiotic that has been identified to bind near the E site of 16S rRNA and interfere with translation initiation [128,129]. The 790 loop studied in this thesis work has shown interactions with edeine [129].

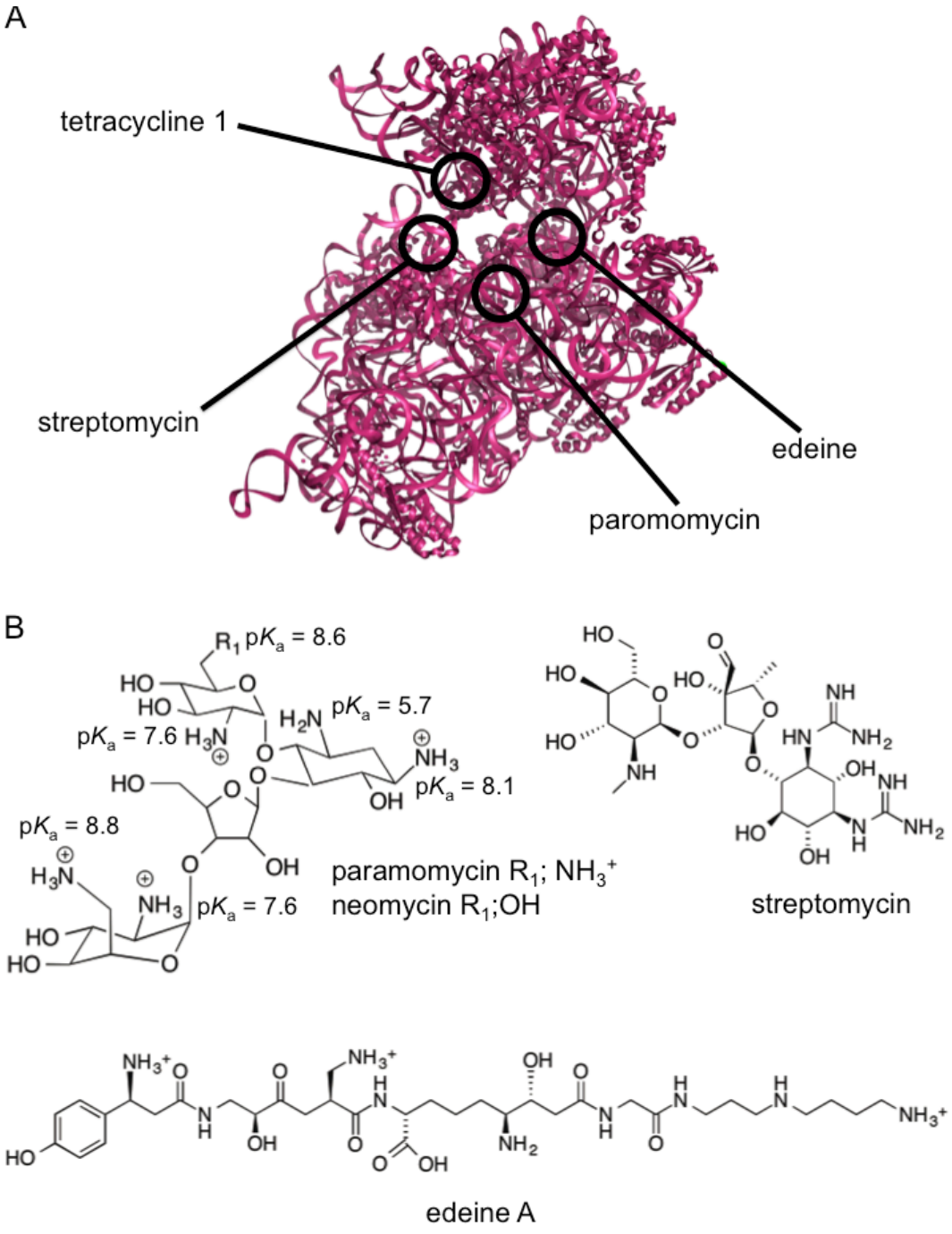

Figure 1.20. Antibiotic binding to the small subunit of the ribosome is shown. A) The locations of some 30S subunit targeting compounds are indicated. The figure was created from PDB file 1FJG and adapted from ref. [36]. B) The chemical structures of some of the small subunit binding drugs are shown. The amino groups of neomycin and paromomycin are shown at pH 7, with their pK_a values listed [130,131].

The large 50S subunit catalyzes peptide-bond formation and not surprisingly many antibiotics, including chloramphenicol, puromycin, macrolides, streptogramin A and B, and lincosamides, target 23S rRNA (Figure 1.21) [36]. Most of these compounds bind to the PTC of the ribosome. The large subunit targeting drugs interfere with A-site tRNA binding and elongation, or block nascent peptide chain growth [36,132,133].

The ribosomal RNAs that were investigated in this thesis work, H69 and the 790 loop, are also targets of antibiotics. Although well known to bind to h44 of the small subunit, aminoglycosides were revealed by crystallographic studies to also interact with H69 (Figure 1.22) [127]. In this binding, neomycin bridges the subunit interface and substantially alters subunit rotation [127]. The H69-neomycin interactions have also been shown to interfere with the ribosome-recycling process [106]. Neomycin makes specific interactions with G1921, G1922, U1923, and also the RNA backbone [127]. Biochemical footprinting assays on complete ribosomes also revealed aminoglycoside binding to H69 [134]. Another region that was of interest in this study, the 790 loop, is a target of the antibiotic edeine (Figure 1.23) [129]. Edeine is a peptide-like compound (Figure 1.23B) that interacts with RNA residues 790-792 in the loop of h24 and affects translation initiation [135].

The chemical structures of RNA-binding molecules shown in Figures 1.20 and 1.21 reveal polar, H-bonding, and possibly protonating functional groups. Some of the examples are hydroxyl, carbonyl, amine and guanidinium groups. These moieties can form electrostatic interactions with their targets. Kinetic studies

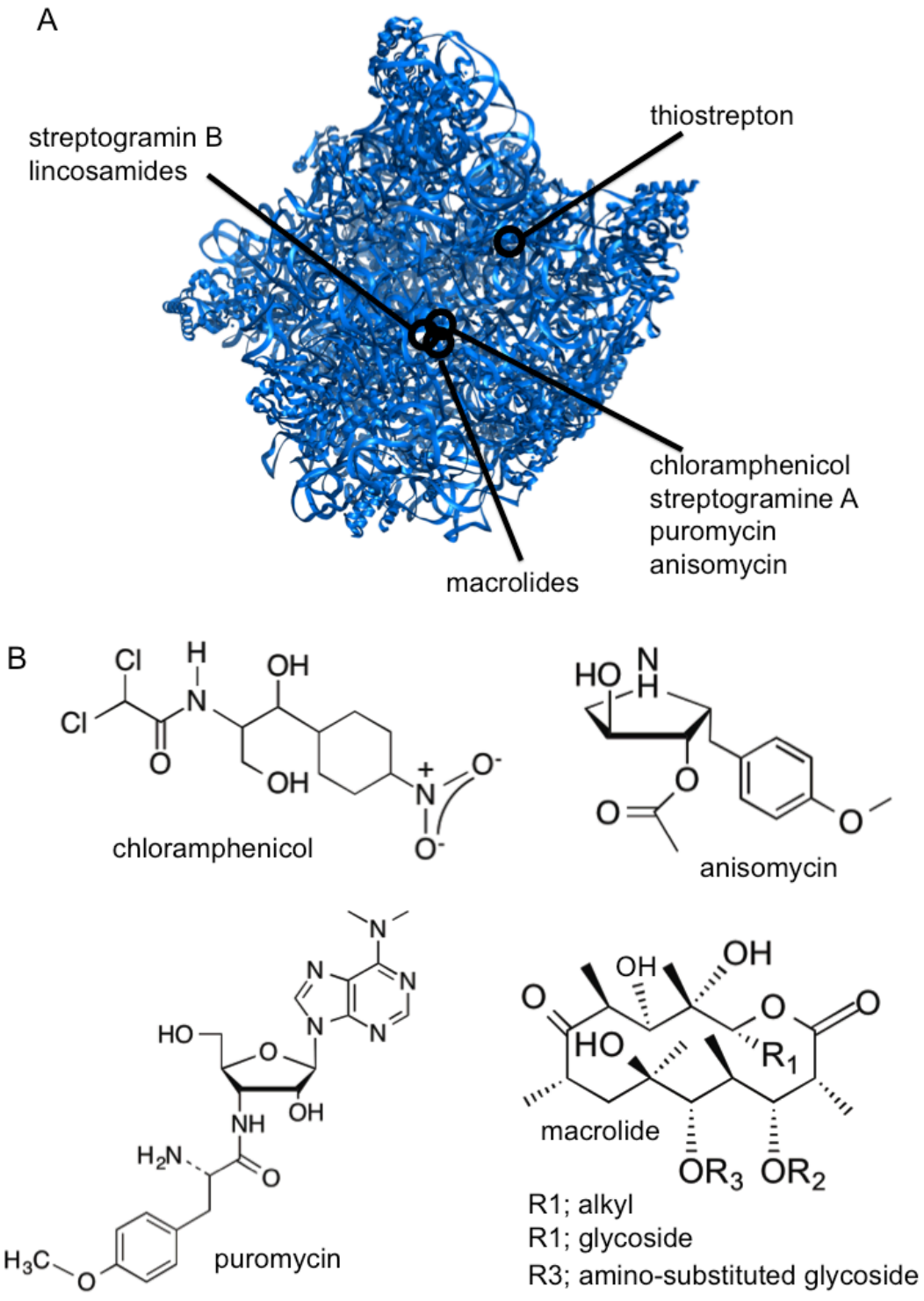

Figure 1.21. The antibiotics targeting the large ribosomal subunit are shown. A) The regions where 50S targeting antibiotics bind are indicated. The figure was created from PDB file 3CC4 and adapted from ref. [36]. B) The chemical structures of some 50S binding compounds are shown [130].

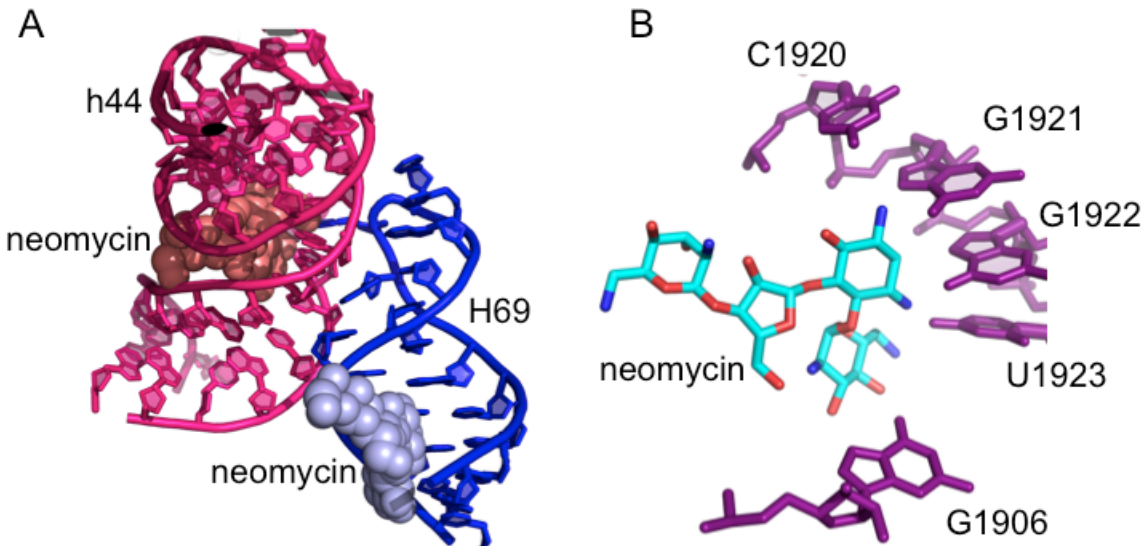

Figure 1.22. Neomycin binding to the bacterial ribosome is shown. A) Neomycin binding sites in h44 and H69 are indicated. B) A closer view of neomycin interactions with H69 residues is shown. The figures are generated from PDB files 4GAQ and 4GAR [127].

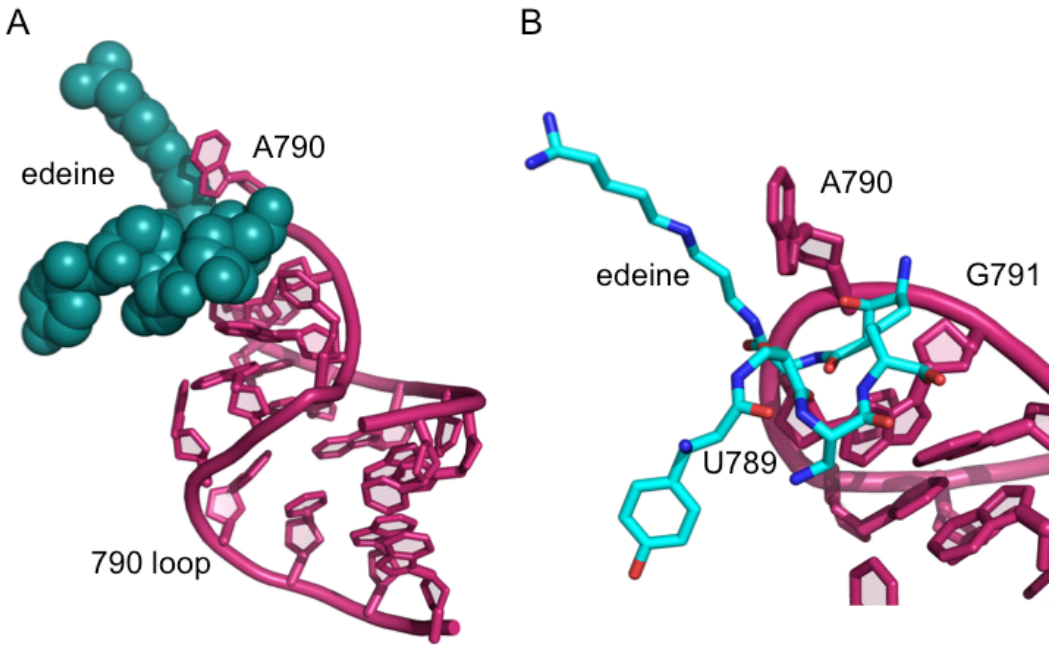

Figure 1.23. The edeine-790 loop interaction is shown. A) The binding of edeine to the 790 loop is shown. B) Specific interactions of edeine with the 790 loop residues are indicated. The figure was created using PDB file 1I95 from ref. [129].

showed the importance of amino groups on aminoglycosides on the inhibition of hammerhead ribozyme catalytic rates [124]. Computational docking experiments provided further evidence for aminoglycoside-hammerhead ribozyme recognition through electrostatic interactions [136]. An array of interactions, including electrostatic forces, was shown to govern tobramycin-RNA recognition [137]. Mapping 30S electrostatic potential onto the paromomycin surface revealed good agreement between the placement of charged functional groups and the rRNA environment [125]. These electrostatic correlations between drug-target interactions have also been applied to design RNA inhibitors by stabilizing electrostatic "hot spots" [138]. In the aggregate, these reports provide evidence for an imperative role played by electrostatics in drug-inhibition kinetics, drug-target affinities, binding modes, recognition, and docking.

1.6 Cisplatin

1.6.1 Introduction to Cisplatin

Cisplatin, initially known as “Peyrone salt” was first synthesized by Michel Peyrone in 1845 [139]. In 1913, Alfred Werner proposed the square-planar configuration for the compound, and distinguished between *cis* and *trans* isomers, cisplatin and transplatin, respectively [140]. For this finding Alfred Werner won the Nobel Prize in Chemistry [140]. However, not until the 1960s was the anticancer property of cisplatin discovered. In 1965, Barnett Rosenberg carried out an experiment designed to monitor the effects of electromagnetic fields on bacterial growth [141]. The observation that bacteria grew filamentous, but had not divided, hinted that a compound produced during the experiment

could be a potential tumor-cell-growth inhibitor. The agent responsible for this effect was eventually identified as *cis*-diamminedichloridoplatinum(II) [142]. After successful demonstration of its anticancer activity, the FDA approved cisplatin in 1979 [143]. Since then, cisplatin and related platinum compounds (Figure 1.24) have been used to treat many carcinomas, including testicular, ovarian, bladder, colorectal, head and neck cancers, and lung cancers [144].

The cytotoxicity of cisplatin, the platinum compound used in this thesis work, is believed to originate from coordination to the nucleobases in DNA [145]. A general pathway for binding is shown in Figure 1.25 [146]. Once given as an intravenous drug, the labile chlorido ligands in cisplatin stay intact due to the high chloride concentration in blood plasma. Experimental results suggest that cisplatin is up taken by cells by both active transport and passive diffusion [147]. Once inside a cell, the chlorido ligands on cisplatin are displaced and the aquated, positively charged, activated form of cisplatin is generated. This active species then reacts with nucleic acids, and the resulting platinated adducts then lead to cell death [148].

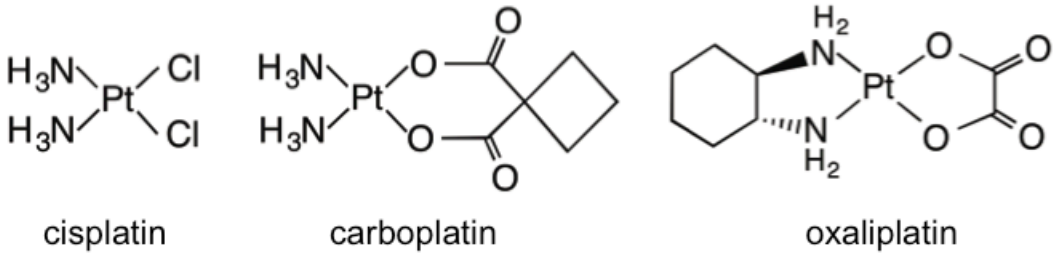

cisplatin carboplatin oxaliplatin

Figure 1.24. Structures of cisplatin and related platinum compounds are shown.

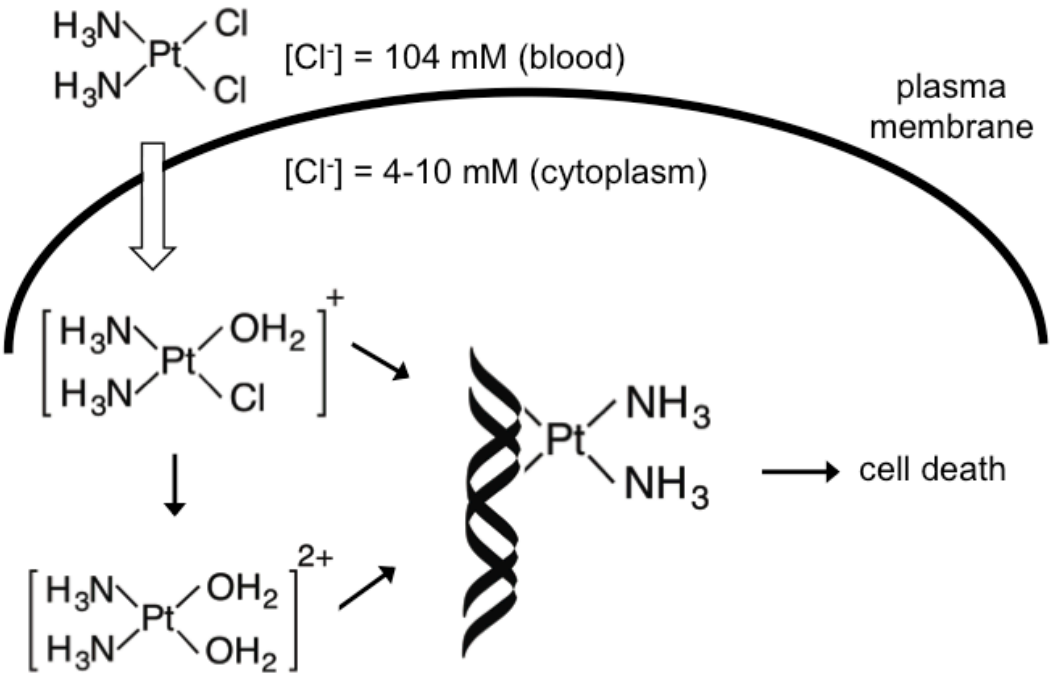

Figure 1.25. A general pathway of cisplatin mechanism of action is shown [146].

Cisplatin forms different adducts with DNA (Figure 1.26A). It coordinates to the N7 position of purine bases, which is exposed in the major groove of DNA, to generate stable adducts (Figure 1.26B) [149]. In early studies, platination and characterization of cisplatin-treated salmon sperm DNA revealed 1,2-intrastrand cross-links as the major adducts, followed by 1,3-intrastrand and interstrand cross-links as the minor adducts [150]. The major 1,2-intrastrand cross-links are *cis*-[Pt(NH_3)$_2${d(GpG)}] (or *cis*-GpG; 47-50%) and *cis*-[Pt(NH_3)$_2${d(ApG)}] (or *cis*-ApG; 23-28%) [150]. The 1,3-intrastrand and interstrand cross-links are 8-10% percent of all adducts and monofunctional guanine comprises 2-3% of the damaged sites.

Cisplatin binding to DNA leads to significant structural effects. Crystallographic studies have shown that cisplatin binding bends the duplex

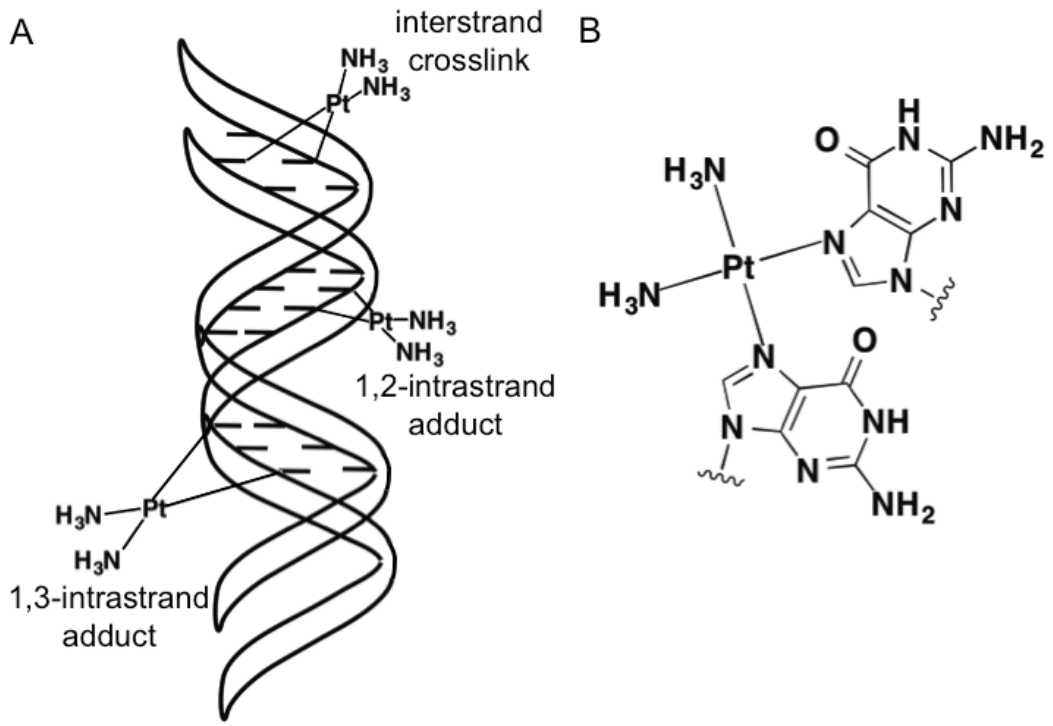

Figure 1.26. Cisplatin binding to nucleic acids is shown. A) Some of the cisplatin binding modes to a double helix are illustrated. B) The coordination of cisplatin to the N7 position of nucleobases is shown [151,152].

toward the major groove by about 35° [152]. The change in supercoiling of circular DNA suggests unwinding of the double helix [153]. NMR studies on a 1,3-intrastrand cross-linked adduct on DNA further supports the idea that the platination site is locally unwound and kinked [154]. Studies revealed that cisplatin adduct formation results in duplex destabilization and loss of helix stability [155,156]. Crystallographic studies revealed that the ammine ligands on cisplatin hydrogen bond to the oxygen atoms on the 5'-phosphate group, potentially stabilizing the adduct [152]. Collectively, these studies show that stable cisplatin adduct formation can induce structural changes to nucleic acids.

1.6.2. Kinetic Studies of Cisplatin-Nucleic Acid Interactions

Cisplatin can react with many targets such as nucleic acids, proteins, and small S-containing molecules in a cell [151]. Formation of different cisplatin adducts would depend on the reaction kinetics. The ligand-exchange reactions of square-planer compounds are slow [157]. This leads to kinetically controlled platination reactions of cisplatin binding to nucleic acids [158,159]. The proposed mechanism of cisplatin binding to double-stranded DNA is shown in Figure 1.27. The rate-limiting step for initial binding is hydrolysis of the first chlorido ligand. [160,161]. The aquated species then rapidly coordinates to DNA specifically at the N7 of purine bases. Loss of the second chlorido is the rate-determining step in the closure of the monoadduct [158].

Kinetic studies have given detailed insight to the primary reactive species, sequence-dependent reactivities, and the mechanism of cisplatin binding to nucleic acids [162]. Determination of reaction rates of phosphorothioate-substituted oligomers using ^{31}P NMR showed that increased local concentrations of Pt(II) complexes, combined with higher mobility along the polymer backbone increases the platination rate [163,164]. Kinetic studies also demonstrated that target sites located at the ends of an oligomer platinate more slowly compared to the ones in the middle, indicating the importance of target location in platination reactions [165,166]. Flanking bases at the target site and nucleotide sequence also impact the platination rate [167,168]. Some of these observations were explained by a combined effect from electrostatic potential and N7 accessibility

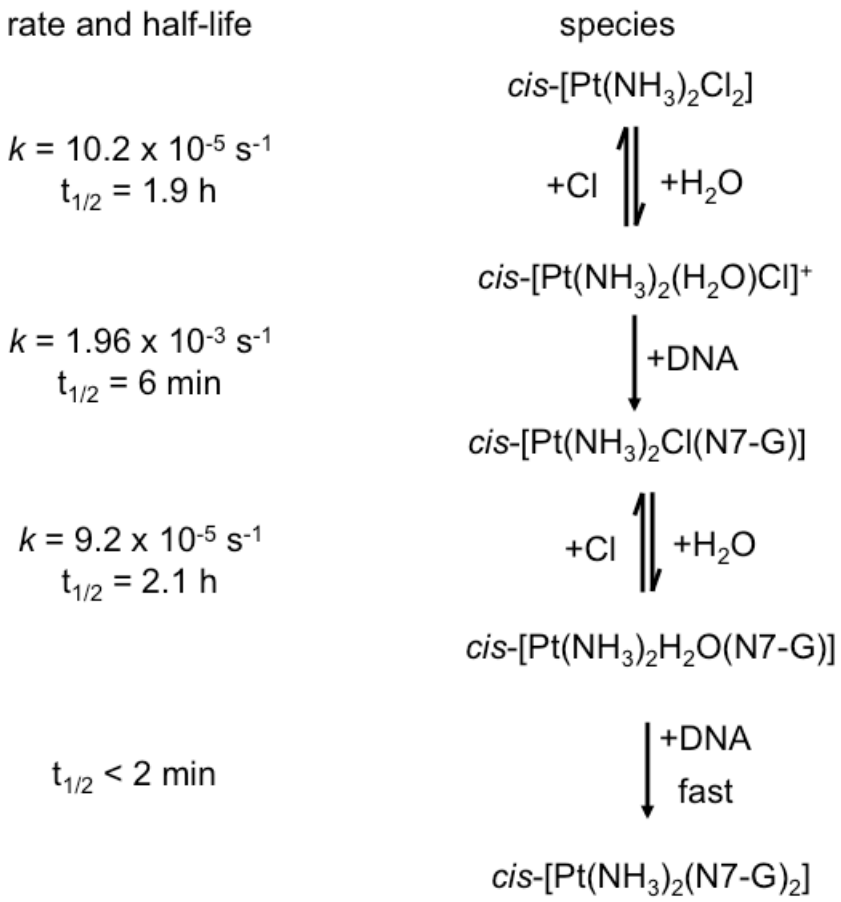

Figure 1.27. Proposed mechanism of cisplatin binding to double helical DNA is shown [158].

of the target [169]. Kinetic studies have also shown that cisplatin discriminates between the 5' and 3' dGs in a dGG sequence for platination [170]. While the first platination is faster on 5' dG than on 3' dG, the chelation rates are opposite for the two Gs. The cisplatin preference for dAG adduct formation over dGA has also been explained by kinetic studies [171]. The higher rates of monoadduct formation, hydrolysis of the second chlorido ligand, and closure to form chelates on dAG compared to those of dGA have contributed to the increased platination of the former sequence. The platination kinetics also revealed that adduct

formation is dependent on whether the target sequence (dGG) is in a single- or double-stranded region [172].

Solution ionic strength and the type of cations present also determine the platination rates. Increasing pH, concentrations of salt, or divalent ions compared to monovalent ions reduce the platination rates [166,173,174]. Evaluation of salt-dependent kinetic data revealed that metal-complex binding releases cations from the nucleic-acid surface [173,175]. Interestingly, comparison of DNA and RNA reactions showed a more pronounced salt dependence in the platination rate of the latter [176]. Kinetic studies using full-length tRNA also showed a preference for G-C–rich and wobble base-pair regions in the platination reactions [177].

Platination kinetic studies can reveal much insight into nucleic acid-platinum complexes reactions. In addition, platination kinetics can be used to investigate the impact of RNA microenvironments on ligand interactions, which was a major focus of this thesis work. RNAs with natural nucleotide modifications (pseudouridine, Ψ, in H69) or altered sequences (the 790 loop) were selected to examine the impact of local environments on platination reactions. The evaluation of salt-dependent platination rates by the Brønsted-Debye-Hückel and polyelectrolyte theories allowed determination of the impact of global electrostatics on RNA-ligand interactions. The role of bulk solutions containing different monovalent and divalent cation concentrations or varying and pH values on selected RNA platination rates was determined. Platination kinetics were also applied to evaluate aminoglycoside-RNA interactions.

1.7 Specific Aims of the Research and Thesis Overview

Many studies have examined the characteristics of RNA molecular interactions. RNAs are central for various cellular functions; therefore, their interactions with small drug molecules can have a significant impact on cell biology. Characterization of RNA-drug interactions and investigation of their dynamics in response to changes in local environments are important. These studies are useful to identify unique RNA targets and to develop effective small molecule-based therapeutics.

This dissertation work was designed to investigate the kinetics of ribosomal RNA interactions with a platinum(II) complex, cisplatin. Many structural, biological, computational, and kinetic studies on DNA-cisplatin interactions have been reported to date [148,151,162,178]. Specifically, kinetic studies have provided valuable insight on the mechanism of drug binding [158,163-168,173,175,176,179,180]. Many RNAs are also targeted by cisplatin [181-187]; however, kinetic studies on RNA-cisplatin interactions are largely unexplored and the binding mechanisms with RNA are largely unknown. Furthermore, salts, divalent ions, and pH play significant roles in biological interactions in a cell. Therefore, one of the main objectives of this thesis work was to carry out a broad kinetic study on cisplatin coordination to RNA. Analysis of the kinetic data with two different electrostatic models was done to reveal the impact of RNA microenvironments on drug binding. These findings are significant for expanding our knowledge on the mechanisms of platinum drug-RNA interactions. Importantly, this study reveals the impact of bulk conditions on RNA

electrostatics, which govern the platinum complexation reactions. Findings from the current study are valuable for identifying distinctive "druggable" RNA targets on bacterial ribosomes and their interactions with metal-based compounds. This knowledge could be further expanded to understand general cationic interactions with RNA.

The cationic cloud plays a significant role in RNA electrostatics, hence could impact structure, function, and ligand interactions [93,188-190]. The primary methods for studying these local environments are often based on computational approaches [85,191]. However, such theoretical methods may not reflect the true biological environments of molecules. Applications of some solution-based methods such as small-angle x-ray scattering and spectroscopic techniques to investigate the ionic cloud around DNA and RNA have been reported [192-195]. However, specific details on the RNA charge density and counterion displacement by ligand binding cannot be obtained from these studies. The use of chemical tools to interrogate RNA electrostatics is even rarer. Therefore, a gap in the field with respect to the development of chemical tools that can provide detailed information on microenvironments of structured RNA still exists. Another objective of this thesis work was to show the use of platination kinetics as an experimental tool to examine local environments of RNA, as it is sensitive to electrostatics illustrated by the binding mechanism. Platination kinetics was further applied as a tool to probe a known aminoglycoside-RNA interaction.

An overview of the dissertation work is as follows. Chapter 1 has introduced RNA and discussed its functions with respect to a key cellular activity, namely

protein synthesis. An introduction to ribosomes, RNA constructs studied in this thesis work, H69 and the 790 loop, RNA electrostatics, salt and pH influence on RNA, RNA-ligand interactions, and cisplatin was also provided in this chapter. The various techniques used in this thesis work and a description of the data analyses are provided in Chapter 2. Chapter 3 reports on cisplatin targeting of rRNA hairpins and site determination. The remaining chapters then focus on kinetic studies between cisplatin and the rRNA hairpins. The impact of monovalent cations on reaction rates (Chapter 4), the influence of monovalent and divalent cations on kinetics (Chapter 5), the sensitivity of cisplatin-ribosomal RNA binding rates to pH (Chapter 6), and probing aminoglycoside-ribosomal RNA interactions using cisplatin kinetics (Chapter 7) are reported. Finally, Chapter 8 gives some overall conclusions of the study and future directions.

CHAPTER 2

BIOCHEMICAL METHODS, KINETIC MEASURMENTS, AND DATA ANAYSIS

A variety of biochemical methods and analytical/biophysical approaches are used in RNA research. This chapter provides a detailed background on the biochemical and biophysical techniques used to study cisplatin binding to ribosomal RNA. Data analysis methods used to determine platination rates and electrostatics of rRNA will be discussed in this chapter; whereas, specific experimental details will be given at the end of each section.

2.1 Matrix Assisted Laser Desorption Ionization Mass Spectrometry (MALDI MS)

Matrix assisted laser desorption ionization mass spectrometry (MALDI MS) is a technique used to analyze biomolecules such as peptides, proteins, oligonucleotides, and carbohydrates [196,197]. In a typical MALDI experiment, the analyte is first dissolved in a suitable solvent and mixed with an appropriate matrix. The sample is then spotted onto a MALDI plate and solidified by air drying. The analyte is then irradiated with a laser beam to bring the molecules into the gas phase. The most commonly used wavelength is 337 nm from a nitrogen laser [198]. The analyte ions are then separated and directed to a detector. The mass analyzer is a part of the mass instrument, in which ions are separated based on their m/z values [199]. The mass analyzer in a TOF instrument is the time-of-flight tube. A schematic of a MALDI-TOF instrument is shown in Figure 2.1. The three main components, ionization source, mass analyzer, and detector, are illustrated.

The matrix used to co-crystallize the sample in MALDI plays an important role. The ideal matrix absorbs energy from the laser and relays it to the analyte in a controlled manner to produce gas-phase ions. Some commonly used matrices for nucleic acids and proteins are shown in Figure 2.2. The most effective matrix for nucleic acids is 3-hydroxypicolinic acid (3-HPA) [200]. The 3-HPA matrix, discovered in the early 1900s, causes minimal ion fragmentation and has a suitable signal-to-noise ratio for nucleic acid detection [201,202]. Unlike other matrices, in which poor signals are obtained in the positive-ion mode, 3-HPA shows comparable results for positive- or negative-ion modes [201]. The absorption of laser energy by the matrix results in ionization of both matrix and analyte molecules [200]. In this desorption step, rapid heating of the matrix follows a phase change of the matrix-analyte mixture from a solid to a gas [200].

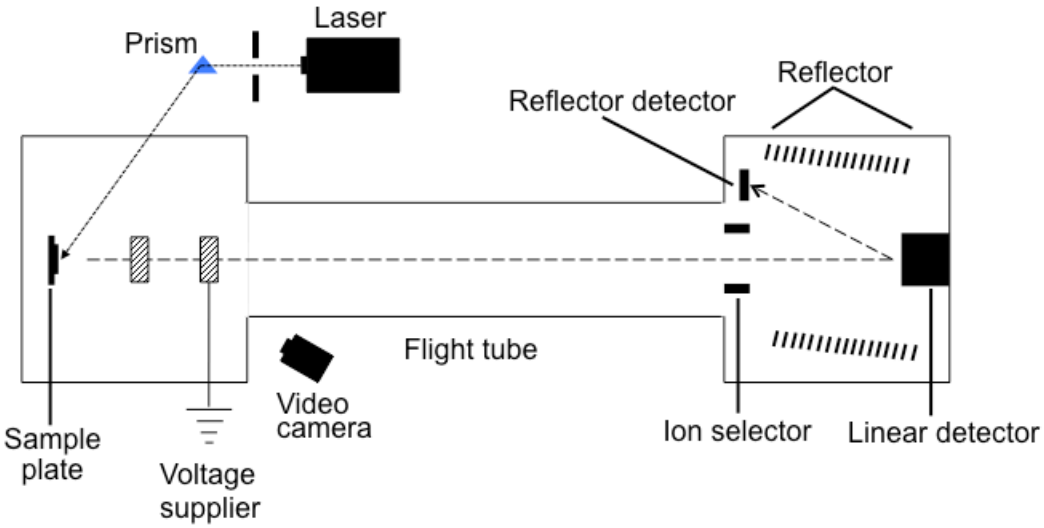

Figure 2.1. A schematic diagram of MALDI-TOF instrumentation with the basic components is shown [203].

.

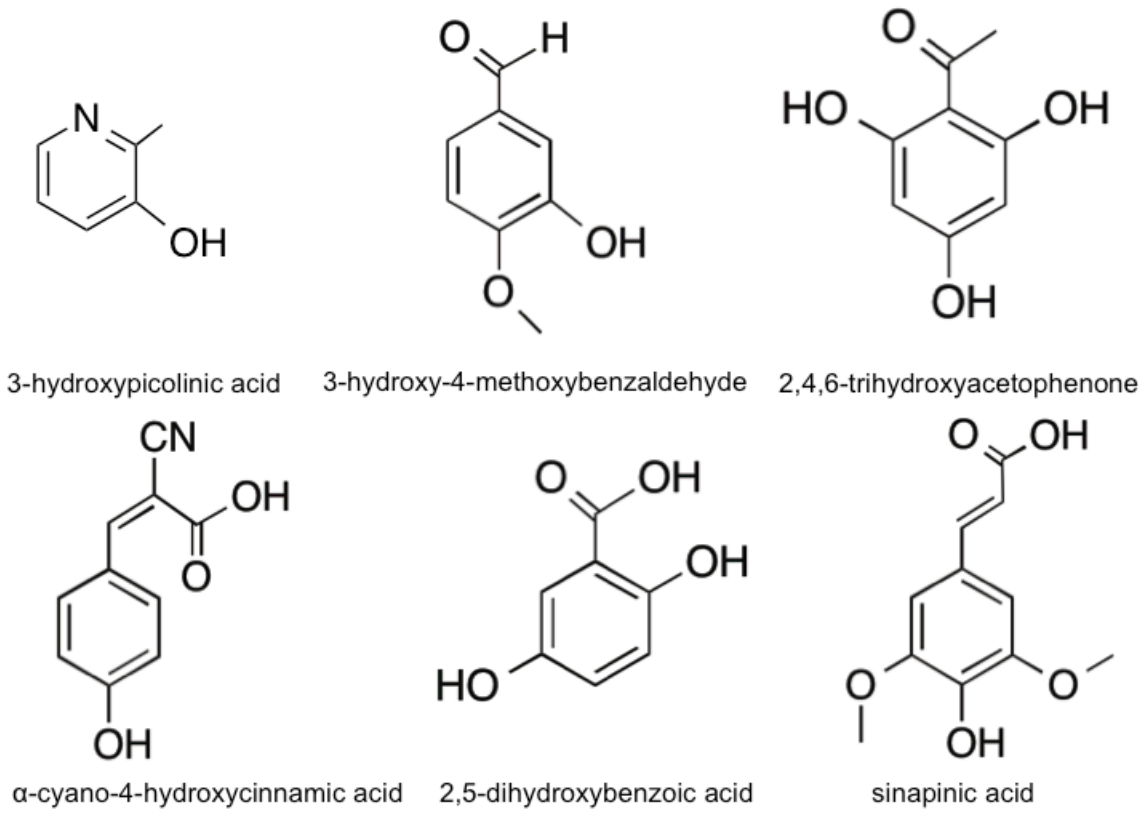

Figure 2.2. Chemical structures of commonly used matrices in MALDI are shown. The top half shows the matrices typically used in nucleic acid analysis and the bottom half shows the matrices commonly used in protein analysis.

The next ion formation step is assumed to occur promptly after the desorption step [200]. The gas-phase interactions between matrix and analyte molecules are suggested to produce ions [200]. The dominant species in MALDI are singly charged ions, but doubly and triply charged ions may also be present [200]. The sensitivity of the peaks can be lower and the mass range is restricted to lower (<10,000) *m/z* values [204,205]. Typically the mass accuracy of MALDI-TOF instruments is on the order of 0.2 to 0.005% with an internal calibrant [205].

For nucleic acids, the ion-detection mode in MALDI can be negative or positive. The mechanisms of positive- or negative-ion formation in MALDI are not yet well understood [200]; however, many pathways have been proposed for ion formation in MALDI, which involve excited and radical matrix intermediates that form charged analyte molecules [198]. For a negative-ion mode MALDI DNA mass spectrum, the authors explained that the observed negatively charged ions most likely resulted from the loss of hydrogens, presumably from the phosphate backbone [200]. In contrast, the positive ions are generated through protonation of the nucleobases [200].

In the case of nucleic acids, the high preference of phosphate charges for alkali cations such as sodium and potassium can limit the quality of the mass spectrum. The peaks are broadened as a result of unresolved multiple salt adducts. The removal of salt peaks in MALDI spectra is primarily achieved by using ammonium salts. High concentrations (~100 mM) of ammonium citrate or tartrate are mixed with the analyte [201]. The ammonium salts transfer protons to the phosphate groups giving off neutral ammonia, and thus preventing alkali metal binding to the oligonucleotides. Substitution of metal cations with ammonium salts by cation-exchange resins, or by addition of ammonium salts in sample preparations, have helped to produce high quality MALDI results. The low ionization efficiency, poor incorporation of analyte into matrix crystals, and fragmentation are some other problems associated with nucleic acid MALDI experiments [200]. Fragmentation of nucleic acids can also result due to base

loss and subsequent backbone cleavage or removal of nucleotides from the 3′ and 5′ ends [200,201].

The predominant singly charged mass peaks have made MALDI MS an effective tool in nucleic acid analysis. Many RNA molecules such as tRNA, RNA transcripts, and ribosomal RNA have been detected by MALDI [206-208]. Similarly, MALDI has been utilized to characterize oligonucleotide sequences after exonuclease digestions. In these studies, the oligonucleotide ladders generated after treating the nucleic acids with bovine spleen phosphodiesterase, a 5′ to 3′ exonuclease, and snake venom phosphodiesterase, a 3′ to 5′ exonuclease, were subjected to MALDI analysis. RNase T1 digestions combined with MALDI MS have also been used to quantify RNA [209]. Similar approaches are applied for identification of tRNAs from a total tRNA pool based on unique or "signature" digestion product(s) [210]. Nucleotide modifications such as pseudouridine have been mapped using MALDI MS combined with chemical modification and RNase T1 digestion [211]. Nucleic acids modified by platinum complexes have also been detected by MALDI MS [184,212].

2.2 Structure Probing of RNA

RNAs adopt highly structured biologically active scaffolds to carry out their functions. Therefore, identifying key RNA structural features at the nucleotide level is crucial for understanding their biological roles and to develop RNA-targeting therapeutics.

2.2.1 Basic Approaches of RNA Structure Probing

Two basic tools, chemical and enzymatic, can be used to interrogate RNA structures (Figure 2.3) [213,214]. Ideally, chemical and enzyme treatments should lead to less than one cleavage or modification per RNA molecule, with a statistical distribution such that the added chemicals don't cause structural alterations [213]. In chemical probing, reagents react with compatible nucleotide functional groups such as nitrogens on bases or 2'-OH groups, and either introduce modifications or lead to strand scission at the modified residue. In enzymatic probing, RNases that are specific for nucleobases (or non-specifically digest RNA at all positions) are used to produce RNA fragments.

Both chemical and enzymatic modifications can be applied to small or large RNA molecules. The detection methods used in such techniques are dependent on the length of the RNA molecule and the nature of the probe used. The first method detects modified or cleaved nucleotide stops during cDNA synthesis [214]. Modifications on the Watson-Crick face that interfere with reverse transcriptase produce stops in primer extension. The primers are radiolabeled, allowing for the determination of electrophoretically separated cDNA fragments by autoradiography. Identity of the modified nucleotides is determined by running dideoxy sequencing reactions in parallel. Analysis of RNA modifications via chemical probing and nucleotides by primer extensions can be applied to larger RNA molecules such as ribosomal RNA. The number of nucleotides that can be read depends on the gel resolution, which is typically about 150-200 nucleotides [215]. Read-throughs of up to 650-1000 nucleotides per experiment are feasible

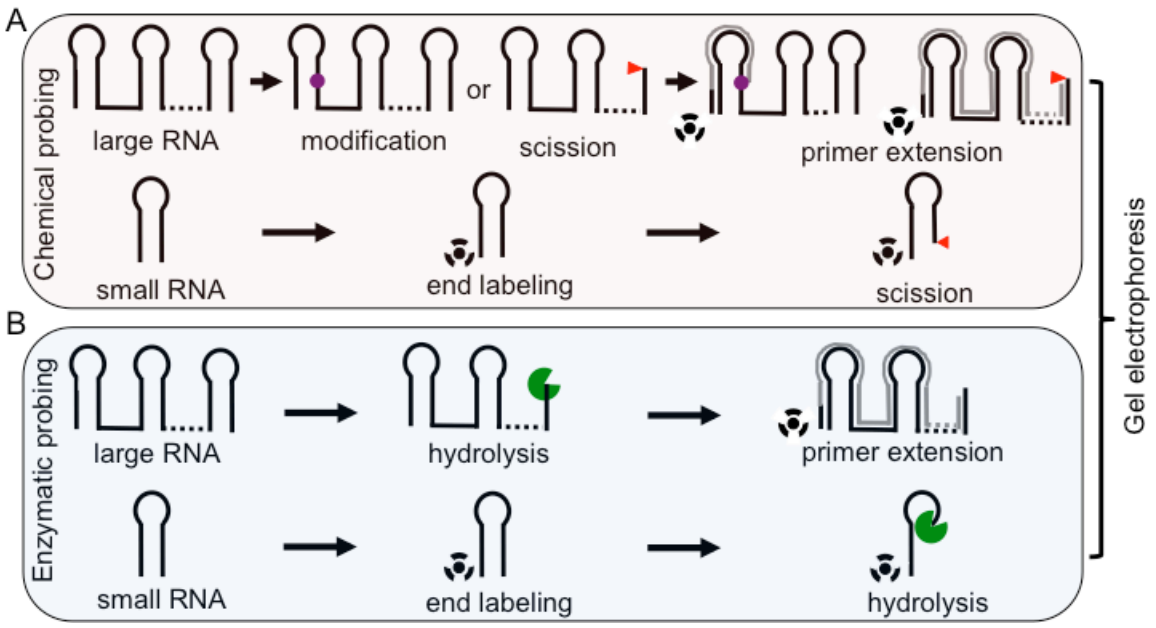

Figure 2.3. A general overview of RNA probing methods is shown. A) An outline of chemical probing and detection of large and small RNA molecules is illustrated. Chemical treatments on large RNA molecules can either lead to nucleotide modifications or RNA strand scission at locations that can be determined by using primer extension. Chemical modifications of end-labeled small RNA molecules are detected by gel electrophoresis after strand scission. B) The enzymatic hydrolysis in large RNA molecules is detected by primer extension. The enzyme target sites in small RNA are determined by the separation of end-labeled oligonucleotides by gel electrophoresis.

with capillary electrophoresis and fluorescently labeled cDNAs [215].

The second approach in chemical probing uses end-labeled RNA, in which strand scissions are directly identified on sequencing gels, and is limited to about 200 nucleotides [214]. Strand cleavage resulting from enzymatic digestion or RNase hydrolysis can also be detected using end-labeled RNA. RNA labeling can be done at either the 5' or 3' end. Labeling at the 5' end is carried out by transferring a γ-^{32}P phosphate group from [γ-^{32}P]-ATP to the 5'-OH end of RNA using T4 polynucleotide kinase [216]. Labeling of RNA at the 3' terminus is

achieved by adding a [5'-^{32}P]-pCp to the 3'-OH using T4 RNA ligase and ATP [217].

Chemical and enzymatic probing provide valuable information about RNA. These methods have been used extensively to map binding sites of RNA ligands such as antibiotics or proteins [215]. The folding of RNA molecules into tertiary structures has also been monitored by these techniques [215]. Advances in the field such as time-resolved chemical probing have lead to a greater understanding of RNA-folding processes [218,219]. Compounds that can penetrate the cell wall have been useful in determining *in vivo* RNA structure [220]. These probes are useful for providing RNA structural changes depending on growth conditions. Overall, both chemical and enzymatic probing of RNA have been invaluable to the research field.

2.2.2 Chemical Tools Used in RNA Probing

RNA creates complex folded tertiary structures, thus determining the solvent accessible residues at equilibrium and under a variety of ionic conditions is important. Chemicals can be applied to analyze these RNA structures. A summary of the different chemical probes used for RNA structure analysis is given in Table 2.1. Dimethyl sulfate (DMS) has been widely used in DNA and RNA sequencing and RNA conformational analysis [221,222]. DMS primarily reacts with G N7, A N1, and to lesser extent C N3. Further chemical treatment is necessary for the detection of G N7 methylation using either end-labeled RNA or by primer extension. The general reaction scheme for strand scission involves

Table 2.1. Commonly used chemical probes for RNA structural analysis are given [214,215,223].

Probe	Target	Detection		
		direct	**RT**	***in vivo***
DMS	G N7	s	s	+
	A N1	-	+	+
	C N3	s	+	+
DEPC	A N7	s	+	?
kethoxal	G N1 N2	-	+	-
CMCT	G N7	-	+	-
	U N3	-	+	-
Pb(II) acetate	cleaves phosphodiester bonds in unpaired nucleotides and unstable helices	+	+	+
ENU	phosphates	s	s	+
NMIA	2'-OH of flexible nucleotides, half life 8.5 min	-	+	+
1M7	2'-OH of flexible nucleotides, half life 14 s	-	+	+
BzCN	2'-OH of flexible nucleotides, half life ~1 s	-	+	?
Fe-EDTA (•OH radicals)	cleaves at ribose C1' and C4'	+	+	?
in-line	cleaves phosphodiester bonds	+	+	?
NAIM	cleaves at phosphorothioate substitutions	+	-	+

DMS; dimethyl sulfate, DEPC; diethylpyrocarbonate, CMCT; 1-cyclohexyl-3-(2-morpholinoethyl) carbodiimide metho-*p*-toluene sulfonate, ENU; *N*-ethyl-N-nitrosourea, NMIA; *N*-methylisatoic anhydride, 1M7; 1-methyl-7-nitroisatoic anhydride, BzCN; benzoyl cyanide. NAIM; nucleotide analog interference mapping. Detection methods; (direct) modification can be detected by using end-labeled RNA and (RT) modification is detected by primer extension. (+) the specified detection method can be used. (S) chemical treatment is required to split the polynucleotide chain. *In vivo* mapping; (+) probes diffuse through the cell wall and membrane, (-) probes can only be used after permeabilization of the cell. (?) probes might be adaptable for *in vivo* applications, BzCN half life is too short to be used *in vivo*. Caution should be taken with DEPC as it can strongly modify proteins and effect to their activity.

sodium borohydride and aniline treatment following N7 methylation (Figure 2.4A). The methylation adds a positive charge on the N7 position of a guanosine nucleotide. Sodium borohydride treatment reduces the 7,8-double bond, and the resulting dihydro-7-methyl guanosine is hydrolyzed to produce a hemiacetal. The unstable hemiacetal then proceeds to ribose ring opening. Aniline treatment then causes a β-elimination reaction to take place, thus cleaving the 3'-phosphodiester bond. Dimethyl sulfate also methylates the N1 position of adenosine (Figure 2.4B). Primer extension can be used to monitor this modification directly, since the reverse transcriptase is blocked in the major groove. DMS reacts with the N3 position of unpaired cytidines (Figure 2.4C). The N3-methyl cytidine can also be detected directly by primer extension, while further treatment with hydrazine and aniline is required when end-labeled RNA is used. Dimethyl sulfate is the primary chemical probe used in this thesis work.

All of the chemical probes mentioned are limited to providing information about solvent accessibility and/or flexibility of specific functional groups in RNA. These chemicals fail to provide information about electrostatics of RNA, as they are neutral in their active forms. Up to date, very few chemical probes have been used to interrogate electrostatics of RNA [224]. The application of 2'-aminoguanosine as an electrostatic probe revealed rigidity in the *Tetrahymena* group I ribozyme active site [224]. One of the major goals in this thesis work was to use platination kinetics as a probe to investigate electrostatic microenvironments of RNA.

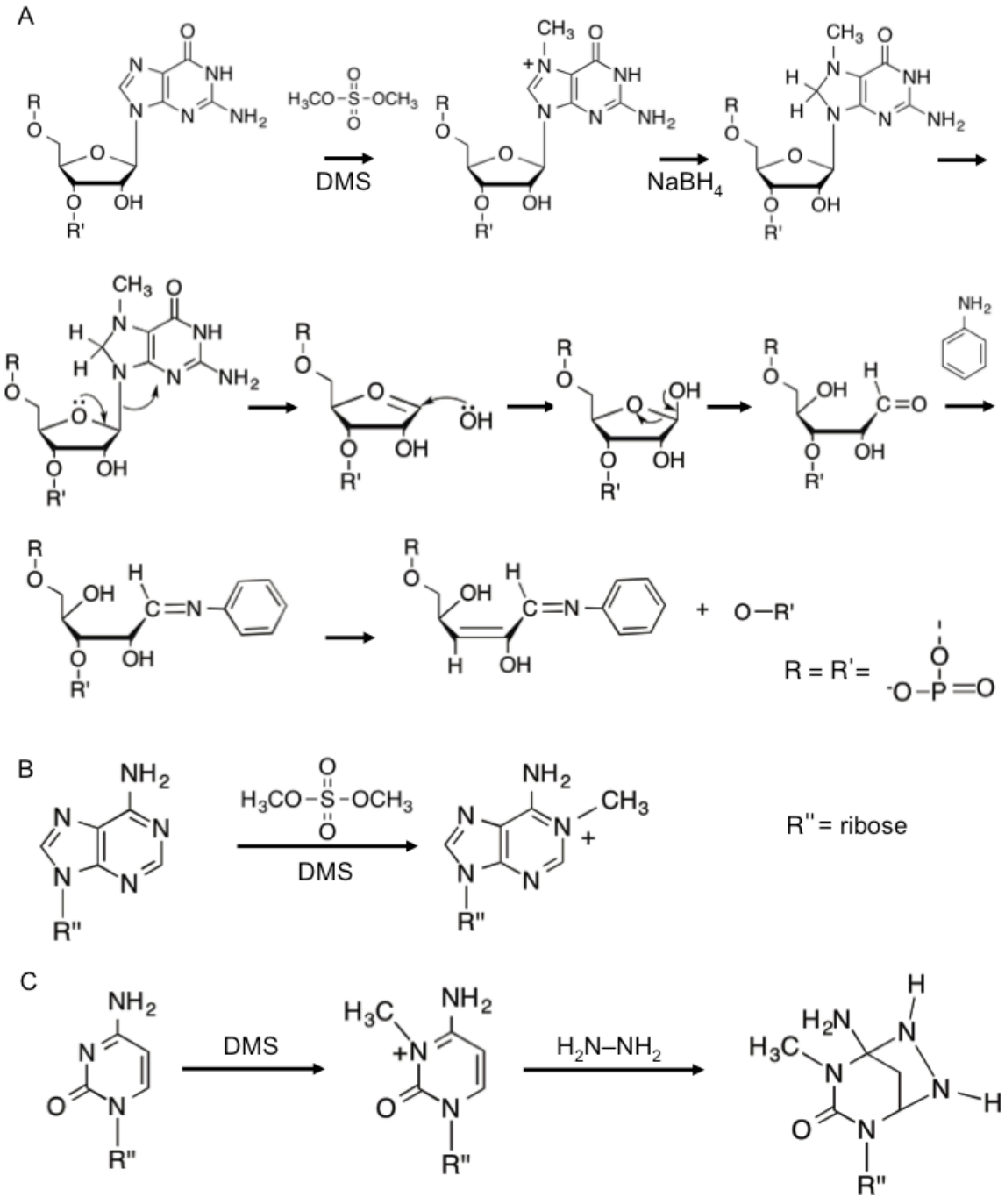

Figure 2.4. The use of dimethyl sulfate as a chemical probe is shown. A) The general reaction scheme involves strand scission following DMS modification at G N7. B) Methylation of adenosine N1 by DMS and C) methylation of cytidine N3 by DMS and subsequent hydrazine treatment are illustrated [214].

2.2.3 *In vivo* Probing of RNA

RNA folding and ligand interactions are significantly affected by the surrounding conditions, which could be considerably different *in vivo* compared to *in vitro* conditions. In cellular environments, the speed of transcription and translation, the presence of protein factors, small ligands, and other RNA molecules, as well as cellular crowding, influence the RNA structure and function. Therefore, determining RNA structures *in vivo* is important to identify characteristics specific to their natural environment. It is also helpful to determine structural adaptations in different cell types. Several different chemical probes have been applied to *in vivo* studies. These include DMS, lead(II), and nucleotide analog interference mapping (NAIM) reagents [220,225,226]. A variety of cell types from bacteria, protozoa, yeast, and plants have been used for *in vivo* chemical probing. The probes must penetrate the cell wall and membrane or be introduced by microinjection techniques. Many chemical probes used to date have limited uses *in vivo*. Therefore, high demand exists for developing or introducing novel tools for *in vivo* RNA interrogation.

2.2.4 Enzymatic Probes for RNA

RNA structural information can be obtained by using different RNA-targeting enzymes. RNases that cut strands at specific nucleobases (*e.g.*, RNase T1, RNase A) and non-specific enzymes like nuclease P1 have been employed to acquire RNA structural information. Probing RNA with large enzymes reveals less-structured regions of RNA. Some examples of commonly used RNases for probing are discussed below.

Ribonuclease T1 (RNase T1) is a small enzyme with a single polypeptide chain of 104 amino-acid residues [227]. It contains two disulfide bonds that are important for its structure [227]. The enzyme degrades single-stranded RNA at guanosine residues to yield oligonucleotides with terminal 3'-phosphate groups [228]. This nucleobase-specific RNA strand scission by RNase T1 has been a valuable tool in RNA sequencing and mapping studies.

Generally, RNase T1 shows specificity towards guanosines in RNA. The rate of GpC cleavage by RNase T1 is 150,000 times faster than an ApC fragment [228]. However, RNase T1 is not completely specific for RNA-strand hydrolysis at Gs. Kinetic studies carried out using dinucleotide monophosphates have shown that RNase T1 catalyzes the hydrolysis of ApN dinucleotides [229]. A crystallographic study using 2'-AMP has shown the adenine and ribose moieties binding to a subsite in RNase T1 with the phosphate group located at the T1 catalytic site [230]. Therefore, RNase T1 probing is likely to generate non-specific strand scissions as well. It is valuable in determining the binding of G-specific ligands to RNA [176]. The G-specific ligand binding prior to enzyme treatment can block the enzyme from cleaving the RNA. Therefore, the disappearance of RNase T1 bands after cisplatin treatment was used to identify the drug binding sites in the current dissertation work.

Ribonuclease A, or RNase A, is a small 124 amino-acid enzyme. RNase A is specific for cleaving RNA strands on the 3' side of pyrimidine residues. Among pyrimidines, RNase A has been reported to catalyze poly(C) cleavage faster than poly(U) and can also degrade poly(A) [231]. Preference to bases other than

pyrimidines has also been reported for RNase A due to the presence of subsites as in the case of RNase T1 [232].

Table 2.2 lists available RNase structure probes. RNase VI is specific for double-stranded regions and is the only probe that can provide evidence for helical regions. RNase T2 has preference for unpaired adenosines.

Table 2.2. Enzymatic probes used for RNA structure analysis are listed [213].

Probe	Target
RNase VI	Paired or stacked N
Nuclease S1	Unpaired N
N. crassa nuclease	Unpaired N
RNase U2	Unpaired A>G>>C>U
RNase T2	Unpaired A>C,U,G
RNase T1	Unpaired G
RNase A	Unpaired pyrimidines (C>U)

2.3 Materials and Methods Used in Probing Studies of this Thesis Work

The following sections give detailed experimental protocols for generation of buffers, metal complexes, and nucleic acid constructs used in this thesis work, as well as experimental details of RNA 3'- and 5'-end radiolabeling. The large-scale RNA platinations used in RNase T1 mapping with MALDI MS analysis, and chemical probing will be discussed. Lastly, experimental details of dimethyl

sulfate probing, alkaline hydrolysis, and RNase T1 digestion of radiolabeled RNA will be given.

2.3.1 Buffers

Standard aqueous buffer solutions were prepared from KH_2PO_4 and K_2HPO_4 (Fisher Scientific, Fair Lawn, NJ) and Millipore water (ddH_2O). The following buffers were employed: buffer A (10 mM KH_2PO_4/K_2HPO_4, pH 6.2 [233], 20 mM NaCl), buffer B (10 mM KH_2PO_4/K_2HPO_4, pH 6.2), 10× TBE (89 mM Tris-HCl, 89 mM boric acid, 2.5 mM EDTA, pH 8.3), and denaturing loading buffer (0.1% bromophenol blue, 0.1% xylene cyanol, 1× TBE, 8 M urea).

2.3.2 Metal Complexes

Cisplatin, *cis*-$[PtCl_2(NH_3)_2]$, was obtained from Alfa Aesar (Ward Hill, MA). Silver nitrate was purchased from Fisher Scientific (Fair Lawn, NJ). Dimethylformamide (DMF) was obtained from Acros Organics (Gibbstown, NJ). The activated complex *cis*-$[PtCl(NH_3)_2X]^{+/0}$, in which X is DMF or NO_3^-, was prepared by mixing 1:1 eq. of cisplatin and $AgNO_3$ dissolved in DMF and agitating in the dark overnight at 37 °C. The resulting AgCl precipitate was removed by repeated centrifugation. For all studies, the activated (monoaquated) complex **1** was freshly prepared by dilution of *cis*-$[PtCl(NH_3)_2X]^{+/0}$ to intermediate stock concentrations with Millipore water just prior to the experiments (Figure 2.5).

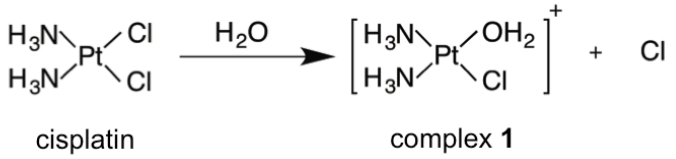

Figure 2.5. The activation of cisplatin is shown. Cisplatin or *cis*-diamminedichloridoplatinum(II) forms *cis*-diammine(aqua)chloridoplatinum(II), complex **1**, in water by displacement of a chlorido ligand.

2.3.3 Nucleic Acids

The following RNA constructs were used in this thesis work. Unmodified H69; 5'GGCCGUAACUAUAACGGUC3', modified H69; 5'GGCCGΨAACΨAΨAACGG UC3', 790 loop; 5'GCAGGAUUAGAUACCCUGC3'. All RNA constructs were obtained from Thermo Scientific Dharmacon (Lafayette, CO). Concentrations of RNA solutions were calculated using the absorbance at 260 nm and single-stranded extinction coefficients obtained by the nearest-neighbor approach (H69 modified or unmodified, ε_{260nm} = 189,400 $M^{-1}cm^{-1}$; 790 loop, ε_{260nm} = 188,800 $M^{-1}cm^{-1}$) [75,84].

2.3.4 3'-End Labeling of RNA Constructs

RNA constructs were radiolabeled at the 3' end with T4 RNA ligase (New England Biolabs, Ipswich, MA) and [5'-^{32}P]-pCp (Perkin-Elmer Life Sciences, Inc. Boston, MA). The labeling was performed in T4 RNA ligase buffer (50 mM Tris-HCl, pH 7.5, 10 mM $MgCl_2$, 1 mM dithiothreitol) with 50 pmol RNA, 10 μCi of [5'-^{32}P]-pCp, 12 units of T4 RNA ligase, and 1 mM ATP in a 30 μL reaction at 4 °C overnight. Labeled RNAs were ethanol precipitated and purified on 20% denaturing (8 M urea) polyacrylamide gels. The labeled products were visualized by autoradiography, then excised and eluted by the "crush and soak" method in 350 mM NaOAc, pH 5.3, 0.1 mM EDTA buffer overnight at 4 °C. The extracted RNAs were desalted over C18 Sep-Pak cartridges (Waters, Milford, MA).

2.3.5 5'-End Labeling of RNA Constructs

RNA constructs were 5'-end labeled in T4 polynucleotide kinase buffer (70 mM Tris-HCl, pH 7.6, 10 mM $MgCl_2$, 5 mM dithiothreitol, New England Biolabs)

with 10 μCi of [γ-^{32}P]-ATP (Perkin-Elmer Life Sciences, Inc.) and 3 units of T4 polynucleotide kinase (New England Biolabs, Ipswich, MA) in a total volume of 30 μL. After incubation at 37 °C for 30 min, the RNAs were ethanol precipitated and purified as described for 3'-end labeling.

2.3.6 Large-Scale Platination and RNase T1 Mapping

The platination reactions of all RNA constructs for RNase T1 mapping studies were performed in buffer A. Prior to platination, the RNAs were renatured by boiling for 2 min followed by placement on ice. Platination was carried out in the dark at 37 °C for 5 h with a 1:2 ratio of RNA:complex **1** and 3 nmol RNA. The RNA products were separated on 20% denaturing polyacrylamide gels. The RNA bands were visualized by UV shadowing and excised from the gel. Bands with slower mobility than the unmodified RNAs were assigned as the platinated products. The platinated RNA products were eluted in 550 mM NH_4OAc, pH 5.5, 0.1 mM EDTA buffer and desalted with C18 Sep-Pak cartridges. RNase T1 digestion of platinated and unplatinated RNAs was performed in water for 20 min at 37 °C using 1 unit of enzyme (Sigma, St. Louis, MO). Digested samples were dried and resuspended in deionized water, mixed with saturated 3-hydroxy picolinic acid (Sigma, St. Louis, MO) in 50% acetonitrile, and spotted on a MALDI plate. MALDI MS analysis was performed on a Bruker Daltonics TOF-300 MALDI Ultraflex instrument equipped with a nitrogen laser (λ 337 nm). The mass spectra of all RNAs were acquired in the positive-ion reflector mode. Peak masses were assigned using Flex Analysis version 2.0 software [210].

2.3.7 Large-Scale Platination Reactions for Chemical Probing

Gel purified, radiolabeled RNAs (8×10^5 – 10×10^5 cpm) and unlabeled RNAs (0.7 μM) were combined and renatured in buffer B containing 20 mM $NaClO_4$. Platination reactions were initiated by adding complex **1** (final concentration 94 μM) to RNA in a final reaction volume of 60 μL. The reactions were incubated in the dark at 37 °C for 3 h. Control RNA samples did not contain platinum complex. Platinated RNA products and unreactive RNAs were separated on 20% polyacrylamide gels, followed by elution with the "crush and soak" method.

2.3.8 Chemical Probing of Platinated RNAs

Guanosine-specific reactions [222] on the platinated RNAs were performed in dimethyl sulfate (DMS) buffer (50 mM sodium cacodylate, pH 5, 1 mM EDTA) in the presence of 5 μg of carrier tRNA. The reactions were initiated by addition of 1 μL of 50% (v/v) DMS (Sigma, St. Louis, MO) in water and incubating for 60 s at 90 °C, followed by immediate quenching with stop solution (1.5 mM sodium acetate, pH 7, 1 M β-mercaptoethanol). The RNAs were ethanol precipitated, redissolved in 10 μL of 1 M Tris-HCl, pH 8.2, and then treated with 10 μL of freshly prepared 0.2 M $NaBH_4$ (Sigma, St. Louis, MO) and incubated on ice for 30 min in the dark. The RNAs were ethanol precipitated again and treated with 10 μL of 1 M aniline acetate, pH 4.5, at 60 °C for 30 min in the dark. The samples were dried, lyophilized twice in water, and resuspended in denaturing loading buffer. Samples (approximately 2×10^4 cpm) were run on high-resolution

sequencing gels (20% denaturing polyacrylamide gels, 0.4 mm thickness, 1× TBE, 8 M urea) and visualized by autoradiography.

2.3.9 Alkaline Hydrolysis of the Labeled RNA

RNA constructs labeled at the 3' or 5' ends (1×10^4 cpm) were mixed with alkaline hydrolysis buffer (30 mM NaOH, 0.3 mM EDTA) and boiled for 90 sec followed by quick freezing on dry ice. The samples were thawed and mixed with denaturing loading buffer just prior to electrophoresis.

2.3.10 RNase T1 Mapping of Labeled RNA

End-labeled RNA (1×10^4 cpm) was mixed in RNase T1 buffer (20 mM sodium citrate, pH 5.0, 7 mM urea, 1 mM EDTA). Hydrolysis was initiated by adding 0.5 units of RNase T1 followed by incubation at 55 °C for 20 min. The reaction products were mixed with denaturing loading buffer and loaded directly onto 20% denaturing gels.

2.4 Determination of Cisplatin Coordination Rates to Nucleic Acids

There are many methods that have been used to determine the kinetics of platinum binding to nucleic acids. These include HPLC, NMR, LC, and UV spectroscopy [162]. HPLC is a widely used technique to determine the kinetics of platination of nucleosides, nucleotides, nucleobases, and oligomers [164,234]. HPLC can be used to separate adduct isomers, and also allows for the determination of platination rates of individual species [168]. However, the analysis of all quenched samples by HPLC can be time consuming. Separation of the reactants from products may not always be possible for certain sized oligomers.

NMR has also been widely used to study platination kinetics. NMR is a non-invasive method that allows monitoring of several species at the same time, therefore providing details on reaction pathways. Proton, ^{31}P, ^{195}Pt, and two-dimensional [^{1}H,^{15}N]-HSQC NMR have been used in platinum kinetic studies with small oligonucleotides [158,163,172,235]. Pre-requisites for the application of NMR methods include well-resolved peaks for reactants, products, and intermediates, and slow reaction rates compared to the acquisition time.

UV absorbance has also been used to measure the kinetics of platination reactions with 5'-GMP, DNA fragments, and RNA [235-237]. Absorbance measurements have been shown to be valuable for monitoring RNA reactivity differences due to subtle structural changes [237]. However, the number of base pairs in the vicinity of the platination site as well as the overall stability of the oligonucleotide is likely critical for a clear absorbance change to occur during the reaction. Thus, the technique may not be applied to a variety of RNA secondary structures that possess single-stranded regions. The other methods used to determine platination kinetics include circular dichroism spectroscopy and fluorescence spectroscopy with ethidium bromide [238,239].

Determination of platination rate constants in kinetic experiments can also be accomplished by using an electrophoretic mobility shift assay (EMSA), or gel-shift assay. It is a simple, convenient, and efficient method used to separate and quantify starting materials from products. The separation depends on the size, shape, and charge of the biopolymers [240]. In this work, the platinated RNA

migrates more slowly compared to the unreacted starting material on a denaturing polyacrylamide gel.

A general overview of the experimental procedure carried out to determine the rate constants in this work using EMSA is given in Figure 2.6. Experimental details are given at the end of Section 2.4.

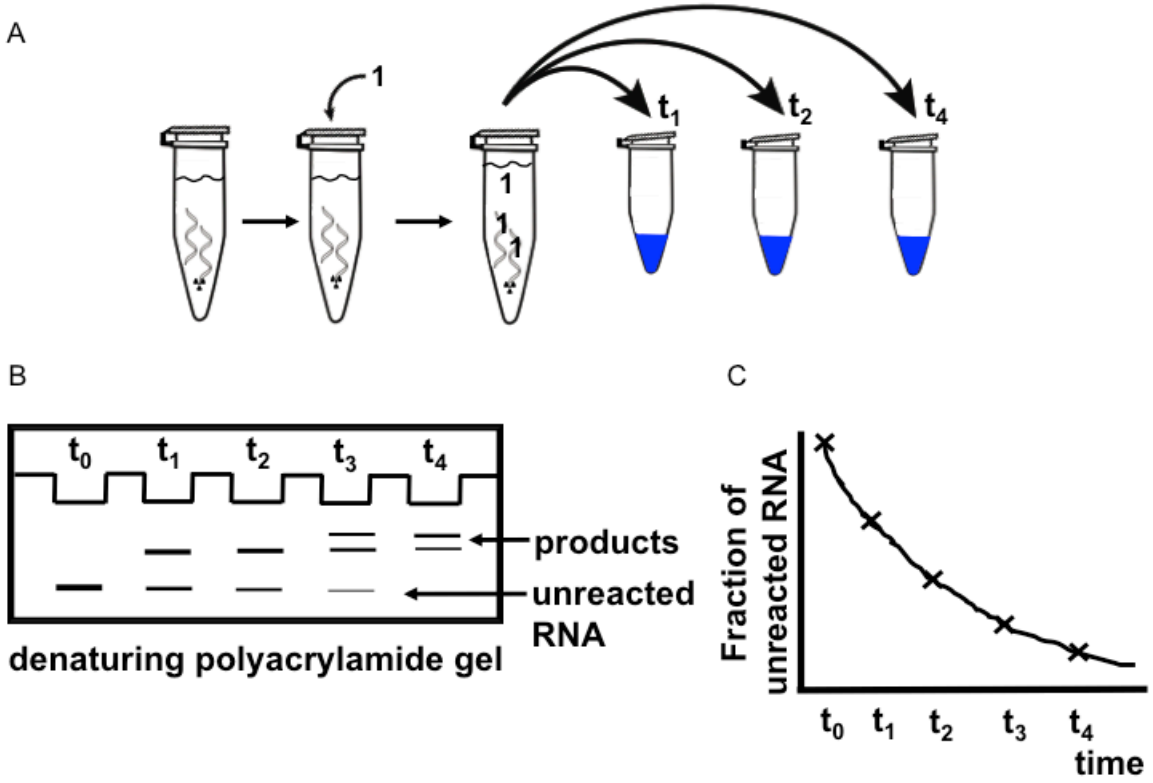

Figure 2.6. Determination of platination rate constants by gel-shift assays is illustrated. A) A schematic of the experimental procedure used to monitor the platination of RNA is shown. After renaturing a mixture of radiolabeled and unlabeled RNA in buffer, complex **1** is added to initiate the reaction. Aliquots of the reaction are then quenched in a mixture of loading dye and NaCl at different time intervals. B) A representative denaturing polyacrylamide gel shows the separated reactants and products, and disappearance of unreacted RNA band intensity with simultaneous appearance of products with time. C) A representative kinetic graph shows the decrease of unreacted RNA fraction with time well described by mathematical models.

2.5 Experimental Procedures for the Determination of Platination Rates

All kinetic experiments were carried out using 3'-labeled RNA (50,000-60,000 cpm) mixed with 40 pmol of cold RNA in buffer B (10 mM K_2HPO_4/KH_2PO_4 pH 6.2) and varying $NaClO_4$ concentrations in a 60 μL reaction. The unlabeled RNA was used to maintain the RNA concentration and desired Pt ratio, whereas the radiolabeled RNA acted as a probe to visualize the consumption of starting material. The RNA in buffer was boiled for 2 min, quickly placed on ice, and incubated for 5 min. The reaction was spun down and allowed to reach to room temperature. Reactions were initiated by adding freshly prepared complex **1** to the tube wall. The final concentration of complex **1** was 94 μM, unless stated otherwise. The reaction was mixed, spun down, and then incubated at 37 °C in dark [176]. A control reaction was carried out similar to the platination reaction, but using ddH_2O instead of complex **1**. Three μL aliquots from the reaction mixture were taken out and added to a mixture of 200 mM NaCl and denaturing loading dye, then quickly frozen on dry ice. The aliquots were thawed just prior to loading onto a 20% denaturing polyacrylamide gel to minimize experimental errors arise from longer thawed samples.

The platinated products were separated from the unreacted RNA by running a polyacrylamide gel at 1300 V for about 3 h. The gels were developed for 24-48 h and visualized by autoradiography, and quantified using ImageQuant software (GE Healthcare Life Sciences) [124,177]. The bands of unreacted RNA and products were quantified in each lane. The unreacted RNA fraction at any given time, t, was calculated by using the following equation;

$$\text{Fraction of unreacted RNA} = \frac{[\text{unreacted RNA counts}_t - \text{bkg counts}]}{[\text{unreacted RNA counts}_t - \text{bkg counts}]+[\text{product counts}_t - \text{bkg counts}]}$$

Therefore, at t = 0 the unreacted RNA fraction was equal to 1. The gel counts were determined by adding a rectangle around each band. The size of the rectangle used to determine the counts was the same for either unreacted RNA or products throughout the lanes. When smeared products were seen at longer incubation times, larger rectangles were used to obtain the product counts, and again, the size was consistent for each lane. A region where no bands were found from the experiment was selected as the background (bkg counts) and was subtracted from the reactant and product counts. The size of rectangles used to obtain the background counts was identical to the corresponding unreacted RNA or product bands. The fraction of unreacted RNA was then graphed versus time using KaleidaGraph 4.1 software (Synergy Software). The observed pseudo-first-order rate constant (k_{obs}) was then determined by a single-exponential decay fit.

The equation used to fit the data is: fraction of unreacted RNA=A*(exp-k_{obs}*t)+C, in which A, k_{obs}, t, and C represent the amplitude of the reaction, the pseudo-first-order rate constant in min^{-1}, time in minutes, and the extent of the reaction, respectively. When fraction of unreacted RNA versus time was fitted to the above equation, the software provided the values for A, k_{obs} and C. The apparent second-order rate constant $k_{2,app}$ was then determined by dividing the observed pseudo-first-order rate constant by the complex **1** concentration ($k_{2,app}$ = k_{obs}/[**1**]). This is the basic platination rate constant determination procedure carried out in this thesis work (Chapter 4), and modified accordingly for Mg^{2+} or

pH dependence, and neomycin-RNA interaction kinetic studies. The platination reactions were carried out as mentioned in the previous section in buffer B either in the absence or presence of 20 mM $NaClO_4$ together with corresponding $Mg(ClO_4)_2$ concentrations of 1, 3, 6, and 12 mM (Chapter 5). Kinetic experiments between complex **1** and H69 RNA were carried out in buffer B made at either pH 5.8 or 6.8 and mixed with varying amounts of $NaClO_4$ (Chapter 6) [233]. The pH was adjusted by adding either dilute $HClO_4$ or NaOH. Reactions were initiated by adding freshly prepared ddH_2O-diluted cisplatin complex **1** to a final concentration of 6.6 μM. Following pseudo-first-order reactions at higher ratios was limited by the fast kinetics at pH 5.8.

Prior to performing kinetic experiments, RNA and neomycin were incubated as follows. After renaturing RNA in buffer B with 20 mM $NaClO_4$, freshly prepared neomycin was added to final concentrations of 1, 3, and 6 μM and incubated for 30 min at 37 °C. Platination was initiated by adding fresh complex **1** to a final concentration of 188 μM. As the cationic neomycin may compete with positively charged complex **1,** the pseudo-first-order reaction was carried out at a higher complex **1** concentration compared to the rest of the kinetic studies.

2.6 Determination of RNA Electrostatics Using Platination Kinetics Analyzed by Brønsted-Debye-Hückel and Polyelectrolyte Theories

Nucleic acids are highly charged biopolymers. They show polyelectrolyte behavior in solutions. Specifically, the approach and binding of charged molecules like aminoglycosides, cations, and cationic platinum drugs can be affected by RNA electrostatics. Currently, computational approaches are

primarily applied to investigate RNA electrostatics [18,241]. Application of platination kinetics as an experimental tool to monitor RNA electrostatics was one of the objectives of this thesis work. Among different models available for evaluating nucleic acid electrostatics, Brønsted-Debye-Hückel and polyelectrolyte theories have been applied extensively to analyze platination reactions [176].

In ionic solutions, electrostatic interactions between oppositely charged ions lower the number of "free" or available ions to react. Therefore, solution ionic strength is important for reactions between charged species. When a reaction takes place mediated by an electrostatic attraction between two ions in dilute solutions, the Debye-Hückel theory together with the transition-state theory predict a qualitative influence of ionic strength on the reaction rate [242-244]. The Debye-Hückel limiting law (for conditions at infinite dilution) is applicable to solutions with ionic strengths 0.01 M or less. For solutions with ionic strengths greater than 0.01 M, modified Debye-Hückel equations have been derived [243]. The Brønsted-Debye-Hückel theory that is applicable to solutions with up to 0.1 M ionic strength was used in this thesis work. The electrolyte solutions with 0.5 M and greater ionic strengths behave strikingly different from dilute solutions and deviate from the Debye-Hückel law [243].

Nucleic acids are polyelectrolytes and interact strongly with positively charged cations. Some ions interact at specific sites in a polyelectrolyte, while some of them show Debye-Hückel-type interactions forming a diffuse ion atmosphere. Unique to highly charged biopolymers such as nucleic acids, a third group of ions

show a territorial binding and form a layer of *condensed counterions* (Figure 2.7) [17].

In the 1970s, Manning developed a method to quantitatively interpret interactions of polyanions and counterions with the *counterion condensation theory* [188,245]. The basic assumption in counterion condensation theory is that when a biopolymer carries a linear charge density greater than unity, counterions will "condense" on the polyanion to lower the linear charge density to unity. Hence, the counterion condensation does not depend on the solution ionic strength. The residual polyion charge is screened by an additional layer of diffusely bound counterions. Further theoretical developments to counterion condensation theory have been reported by Record [246]. For short oligomers, the *end effects* dominate the counterion condensation [247]. The end effect describes that the average concentration of condensed counterions is a linear function of 1/N for N>24, in which N is the number of nucleotides. Until N>>100, the end effect does not become negligible [246].

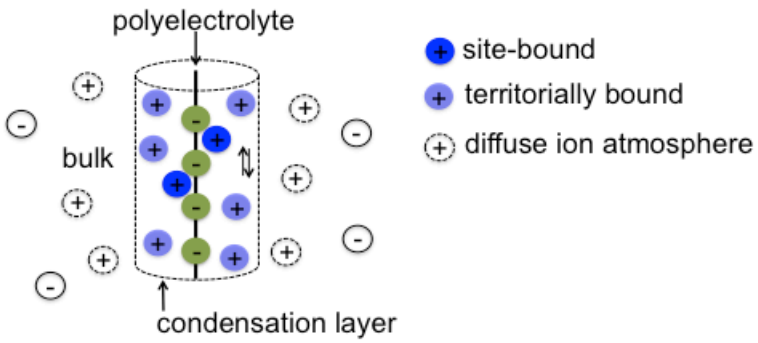

Figure 2.7. Different types of nucleic acid-cationic interactions are shown. The formation of counterion condensation layer by territorially bound cations is indicated.

When a reaction changes the linear charge density of a nucleic acid, a fraction of condensed counterions should either be released or bound. This uptake or release of cations is the predominant source of the salt dependence in nucleic acid reactions. The polyelectrolyte theory provides a relationship to quantify these salt-dependent reaction rates. In the case of platination reactions, association of the Pt^{+} center displaces a fraction of counter-cations from the RNA surface (Figure 2.8). Therefore, the basic application of polyelectrolyte theory is the quantification of this fraction of counterions, which also depends on the linear charge density of RNA in a particular medium, displaced by platinum coordination.

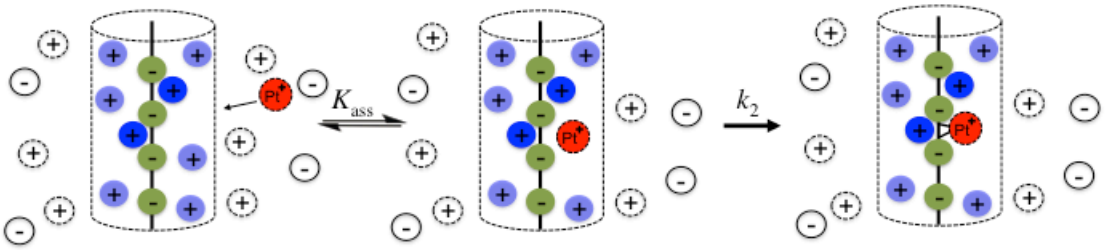

Figure 2.8. The reaction mechanism of platinum complexes binding to nucleic acids in accordance to the polyelectrolyte theory is shown. The association of Pt^{+} compounds on the nucleic acid surface displaces a fraction of surface condensed cations (K_{ass}). Then, the platinum compound coordinates to the nucleic acid (k_2).

The ionic strength I was calculated using Equation 1, in which c_i is the concentration of each ion in $molL^{-1}$ and Z_i is the charge of the ion,

$$I = 1/2\Sigma c_i Z_i^2 \qquad (1)$$

The K^+ concentration coming from 10 mM K_2HPO_4/KH_2PO_4 buffer was calculated according to the pH. The Brønsted-Debye-Hückel theory used in this thesis work is shown in Equation 2.

$$\log k_2 = \log k_0 + 2AZ_AZ_B \frac{I^{1/2}}{(1+I^{1/2})} \quad (2)$$

The k_2 is the reaction rate constant, k_0 is the limiting rate constant, and A is a constant that depends on the temperature [248]. The Brønsted-Debye-Hückel equation predicts that the rate of a reaction between like-charged ions will increase linearly with $I^{1/2}/(1+I^{1/2})$, while a reaction between unlike-charged ions will decrease (Figure 2.9). For oppositely charged ions, the increasing ionic strength poorly stabilizes the less-charged state and increases the activation energy, therefore reducing the reaction rate [17]. This is the case for complex **1** and RNA platination reactions studied in this thesis work.

The slopes of linear fittings correspond to $2AZ_AZ_B$, in which the product of the charge of the reactants (Z_AZ_B) can be determined. In platination reactions, the activated platinum complex, **1**, which carries a +1 charge, interacts with nucleic acids. Hence, the Z_AZ_B, should simply represent the charge density/effective charge of the interacting RNA. This provides a method to evaluate the charge density of RNA by using platination kinetics.

The intercept of the Brønsted-Debye-Hückel plot provides the platination rate at limiting conditions or infinite dilutions (k_0). Under such situations, the platination reaction can be assumed to take place in the absence of electrostatic influences from solution ions. Therefore, comparisons of k_0 values determined by platination kinetics under different solution conditions can provide an idea of the

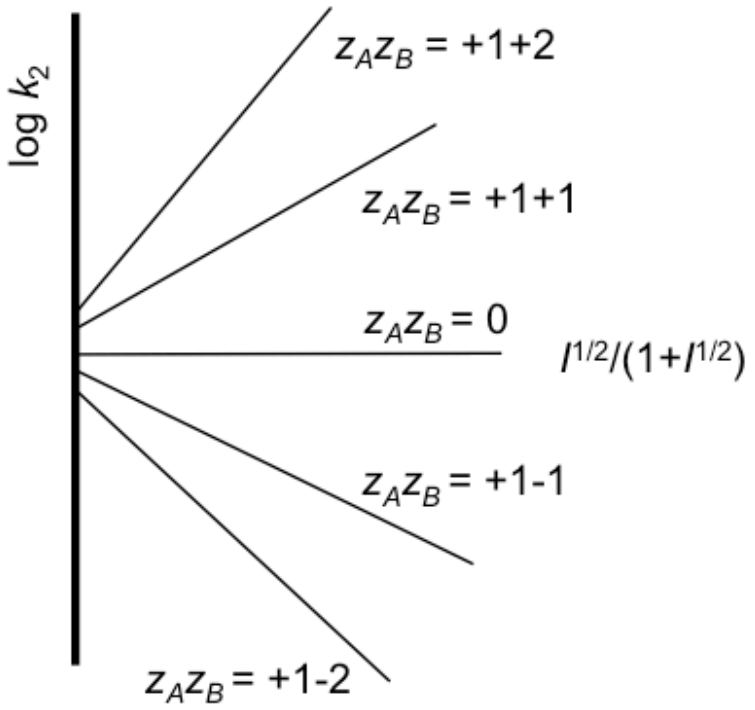

Figure 2.9. The Brønsted-Debye-Hückel plots for reactions between ions with different charges are indicated.

electrostatic impact from salts on RNA-ligand interactions.

Equation 3 shows the relationship used to analyze platination kinetics according to polyelectrolyte theory.

$$\log k_2 = \log k'_0 - n\Psi \log[M^{+/2+}] \qquad (3)$$

The k_2 is the rate constant and $[M^{+/2+}]$ is the total cation concentration in the reaction medium. When calculating $M^{+/2+}$ concentrations, all monovalent and divalent cations were included. The slope ($n\Psi$) of the polyelectrolyte fitting (Figure 2.10) gives the fraction of cations that platinum compound **1** displaces when associating on the RNA surface.

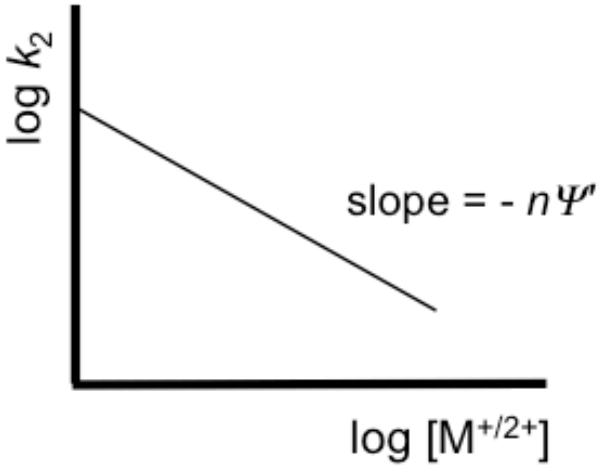

Figure 2.10. The dependence of reaction rate on the cation concentration [$M^{+/2+}$] according to polyelectrolyte theory is shown.

CHAPTER 3

IDENTIFICATION OF CISPLATIN TARGETS ON RIBOSOMAL RNA HAIRPINS

3.1 Abstract

Cisplatin is a clinically important chemotherapeutic agent known to target purine bases in nucleic acids. Cisplatin forms stable adducts with many types of RNA including siRNA, spliceosomal RNAs, tRNA, and rRNA. All of these RNAs play vital roles in the cell such as catalysis of protein synthesis by rRNA, and therefore serve as potential drug targets. Identifying target preferences and implications of drug binding are crucial to recognize novel drug targets as well as design molecules with better efficacies. This chapter focuses on platination of three rRNA constructs, pseudouridine-modified and unmodified helix 69, and the 790 loop of helix 24 from *E. coli* ribosomes. RNase T1 probing, MALDI MS, and DMS mapping confirmed platination at GpG sites. Chemical probing studies also revealed structural changes followed by cisplatin coordination. These findings suggest that functionally significant regions of the ribosome are viable targets for cisplatin, as well as similar compound classes, due to solvent accessibility and a high level of sequence conservation. Collectively, the work reported in this chapter shows that cisplatin binding to functionally significant rRNA regions induces structural changes that could potentially be lethal to bacterial cells.

3.2 Introduction

Since its discovery as an anticancer agent in the 1960s, *cis*-diamminedichloridoplatinum(II), or cisplatin, has been used to treat a variety of human carcinomas [141,148]. The cytotoxic activity of this platinum-based

compound is believed to be associated with DNA lesions that influence key cellular functions [148]. Cisplatin is a neutral molecule that becomes positively charged upon displacement of a chlorido ligand with water to form the active monoaquated complex (**1**) (Figure 2.5) [158,249]. The positive charge on **1** directs it to negatively charged nucleic acids. The active species coordinates to the N7 of purine bases and forms stable adducts [250-252]. Although DNA is considered to be the major target of cisplatin, RNA and proteins are also susceptible to platinum-adduct formation [253-257]. Studies directed towards understanding RNA-cisplatin interactions have revealed that different cellular RNAs are targets of cisplatin and cisplatin analogues [176,177,181-184,258].

In this chapter, reactions of complex **1** with three rRNA constructs representing H69 and the 790 loop of *E. coli* ribosomes were examined. The influence from pseudouridine (Ψ) modifications and sequence alterations on platination of rRNA was investigated by using these rRNA constructs. The platination of unmodified H69, which contains uridines at positions 1911, 1915, and 1917 (*E. coli* numbering), was compared to that of modified H69 possessing Ψs at the same positions [75,259]. The impact of nucleotide sequences on cisplatin coordination was evaluated using the 790 loop, which contained an identical type and number of nucleotides ($A_5G_5U_4C_5$) to the unmodified H69. Complex **1** formed two adducts with H69 RNAs and one adduct with the 790 loop. Mass spectrometry, RNase T1 digestion, and chemical-probing analysis revealed consecutive Gs as platination sites in all rRNA hairpins. The DMS-probing experiments revealed structural changes induced by cisplatin

coordination to H69 rRNA hairpins. Work reported in this chapter showed that H69 and the 790 loop are potential cisplatin targets in *E. coli* ribosomes and possibly interfere with ribosome function and contribute to drug cytotoxicity.

3.3 Results and Discussion

3.3.1 MALDI Mass Spectrometry and RNase T1 Mapping Studies

The ribosome comprises the key protein synthesis machinery of the cell. A number of studies revealed RNA as a target for platinum-based drugs, as well as other drug classes [36,176,177,181-184,258]. In this chapter, the interaction of cisplatin with three model rRNAs hairpins from *E. coli*, namely, unmodified H69, modified H69, and the 790 loop, was investigated. Comparisons were made with unmodified H69 to determine whether Ψs (modified H69) or altered nucleotide sequences (790 loop) would influence platination. The data indicate minimal influence of Ψs and sequence for platination target selectivity. However, structural and/or stability effects on residues distant to the target sites were observed, and a possible sequence influence to this effect was identified.

Platination was carried out between complex **1** and rRNA hairpins as described in Section 2.3.6, and the products were isolated and characterized by MALDI MS to first determine the number of adducts. The platination sites were then determined through RNase T1 digestion. Mass increases for the fragments obtained from enzyme digestion of platinated RNAs revealed the locations of the adduct sites. Mass data were collected in the positive-ion mode, and analysis of the H69 and 790 RNAs produced $[M+H]^+$ and $[M+2H]^{2+}$ peaks. The experimental and expected masses of full-length RNA molecules and RNase T1 fragments are

listed in Table 3.1 and Figures 3.1-3.3. Following the reaction with complex **1**, two molecular ion peaks ($[M+Pt-H]^+$ or $[M+2Pt-3H]^+$) were observed for both unmodified and modified H69. Platination of the 790 loop produced a single molecular ion peak ($[M+Pt-H]^+$). The experimental masses obtained correspond well to the predicted masses. An increase in mass by 229 or 458 Da corresponds to coordination of one or two $Pt(NH_3)_2$ moieties to the RNA, respectively, with loss of the aqua and chlorido ligands, indicating one or two platination sites for each RNA [186,260]. This observation is supported by the addition of a $Pt(NH_3)_2$ group to DNA platinations detected by MALDI MS [212,261].

RNase T1 digestion occurs via a 2',3'–cyclic phosphate intermediate [228]. Therefore, under partial digestion conditions, RNase T1 treatment led to RNA fragments containing either a 2', 3', or 2',3'–cyclic phosphate (indicated as >p in Table 3.1). The digestion of H69 RNA produced mass peaks corresponding to fragments CCG>p, (U/Ψ)AAC(U/Ψ)A(U/Ψ)AACG>p, and CCGΨAACΨAΨAACG->p (in modified H69 only). RNase T1 digestion of the 790 loop generated mass peaks assigned as fragments CAG>p, AUUAG>p, and AUACCCUG>p. In contrast, the mass spectrum obtained after treatment of platinated H69 RNAs revealed two new peaks corresponding to GGCCG>p+$Pt(NH_3)_2$ and (U/Ψ)AAC(U/Ψ)A(U/Ψ)AACGGUC+$Pt(NH_3)_2$. RNase T1 digestion of the platinated 790 loop produced a new peak corresponding to CAGGAUUAG>p+$Pt(NH_3)_2$.The production of RNase T1 fragments CCG>p, (U/Ψ)AAC(U/Ψ)A(U/Ψ)AACG>p, and CCGΨAACΨAΨAACG>p (modified H69

Table 3.1. Predicted and experimental masses of unmodified H69, modified H69, and 790 loop RNAs parent strands, platinated products, and RNase T1 digestion fragments are given.

Construct	[RNA]$^+$	Predicted mass[a] *m/z*	Experimental mass *m/z*
unmodified H69	Parent strand + H^+	6061.7	6061.3
	Parent strand + $[Pt(NH_3)_2]^{2+}$ - H^+	6288.7	6287.9
	Parent strand + 2$[Pt(NH_3)_2]^{2+}$ - 3H^+	6515.7	6514.9
	5'CCG>p3' + H^+	956.6	957.2/956.9[b]
	5'UAACUAUAACG>p3' + H^+	3521.1	3521.8
	5'GGCCG>p3' + $[Pt(NH_3)_2]^{2+}$ - H^+	1873.9	1874.7
	5'UAACUAUAACGGUC3' + $[Pt(NH_3)_2]^{2+}$ -H^+	4642.7	4642.5
modified H69	Parent strand + H^+	6061.7	6061.1
	Parent strand + $[Pt(NH_3)_2]^{2+}$ - H^+	6288.7	6288.1
	Parent strand + 2$[Pt(NH_3)_2]^{2+}$ - 3H^+	6515.7	6515.0
	5'CCG>p3' + H^+	956.6	957.0/957.0[b]
	5'ΨAACΨAΨAACG>p3' + H^+	3521.1	3521.9
	5'CCGΨAACΨAΨAACG>p3' + H^+	4476.7	4476.8
	5'GGCCG>p3' + $[Pt(NH_3)_2]^{2+}$ - H^+	1874.0	1874.6
	5'ΨAACΨAΨAACGGUC3' + $[Pt(NH_3)_2]^{2+}$ - H^+	4642.7	4642.7
790 loop	Parent strand + H^+	6061.7	6061.5
	Parent strand + $[Pt(NH_3)_2]^{2+}$ - H^+	6288.7	6287.4
	5'CAG>p3' + H^+	980.6	981.0
	5'AUUAG>p3' + H^+	1616.9	1617.4/1617.7[b]
	5'AUACCCUG>p3' + H^+	2532.5	2532.9/2533.4[b]
	5'CAGGAUUAG>p3' + $[Pt(NH_3)_2]^{2+}$ - H^+	3168.7	3169.9

[a] The expected mass values for the parent RNA constructs and the digestion fragments were obtained from Mongo Oligo Calculator v2.06 (http://mods.rna.albany.edu/masspec/Mongo-Oligo) [210].

[b] m/z values correspond to fragments derived from unplatinated/platinated RNA. The production of cyclic phosphates at the 3' ends (or 2' or 3' phosphates) from RNase T1 digestion is denoted as >p.

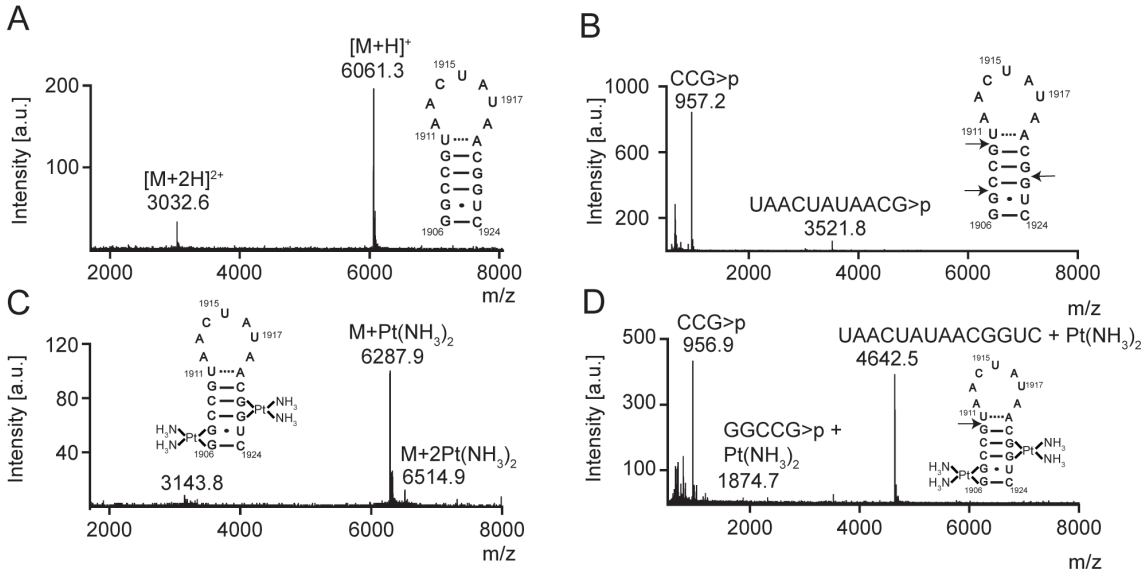

Figure 3.1. Mass analysis of platinated unmodified H69 is shown. Mass spectra of A) unmodified H69 parent RNA (unplatinated H69), B**)** RNase T1 digestion of unplatinated H69, C) platinated unmodified H69, and D) RNase T1 digestion of platinated unmodified H69 are given. Arrows indicate RNase T1 cleavage sites.

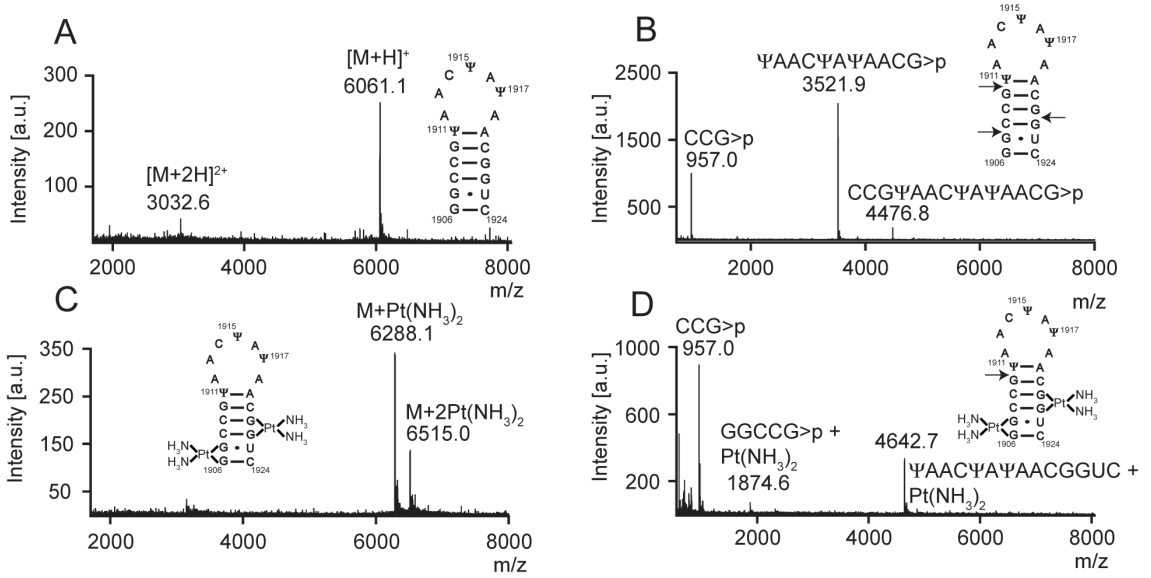

Figure 3.2. Mass analysis of platinated modified H69 is shown. Mass spectra of A) modified H69 parent RNA (unplatinated RNA), B) RNase T1 digestion of unplatinated H69, C) platinated modified H69, and D) RNase T1 digestion of platinated modified H69 are given. Arrows indicate RNase T1 cleavage sites.

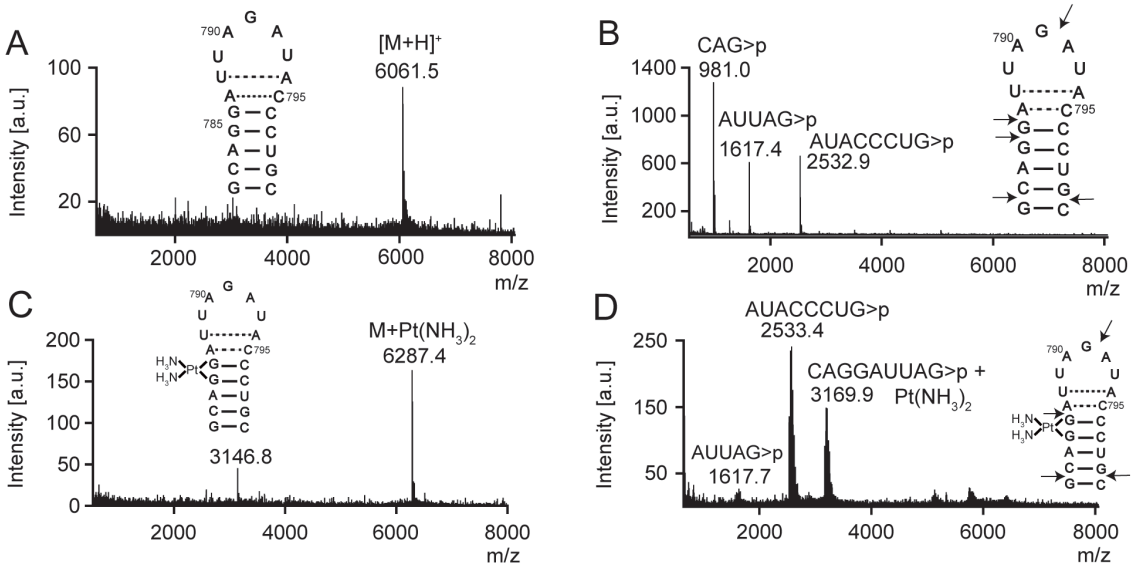

Figure 3.3. Mass analysis of platinated 790 loop is shown. Mass spectra of A) 790 loop parent strand (unplatinated 790 loop), B) RNase T1 digestion of unplatinated 790 loop, C) platinated 790 loop, and D) RNase T1 digestion of platinated 790 loop are shown. Arrows indicate RNase T1 cleavage sites.

only) of H69 RNAs indicated G1907, G1910 and G1921 as the enzyme cleavage sites (Figure 3.4). In contrast, the absence of fragments resulting from cleavage between G1906-07 or G1921-22, as well as production of GGCCG>p and (U/Ψ)AAC(U/Ψ)A(U/Ψ)AACGGUC fragments with a 229 Da mass increase, indicated G1906-07 and G1921-22 as the platinum target sites on H69 RNAs. The production of GGCCG>p with $Pt(NH_3)_2$ indicated that G1910 was still available for RNase T1 cleavage and not a likely platination site. Combined, these results demonstrate that the presence of Ψ does not alter the site preference of **1** for H69 RNAs, and GpG sites are preferentially platinated in these rRNA hairpins.

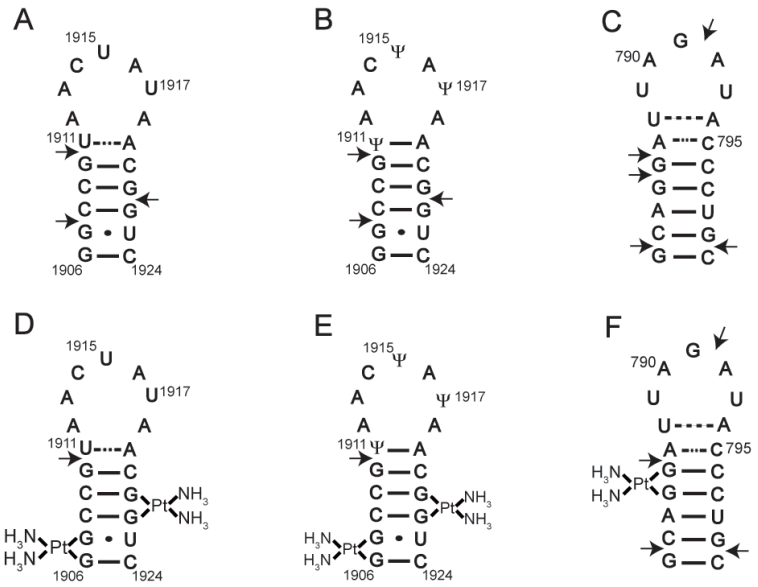

Figure 3.4. Platination sites identified by mass analysis of RNase T1 digestions are shown. The observed RNase T1 cleavage sites on A) unmodified H69, B) modified H69, and C) the 790 loop are indicated by arrows. The RNase T1 digestion products of platinated D) unmodified H69, E) modified H69 and F) 790 loop are shown along with the platinum coordination sites.

The production of CAG>p, AUUAG>p and AUACCCUG>p fragments by RNase T1 digestion on the 790 loop indicated G782, G785, G786, G791, and G799 as the enzyme cleavage sites (Figure 3.4). Following platination and digestion of the 790 loop, the AUACCCUG>p fragment was observed, indicating cleavage at G791 and G799. In contrast, the intensity of the AUUAG>p fragment peak diminished, suggesting blockage of RNase T1 cleavage at G786. Production of the CAGGAUUAG>p fragment with an increased mass of 229 Da, and blocked RNase T1 cleavage with concomitant loss of the CAG>p fragment suggested platination at G785-86. The reaction at G782 was not blocked, thus platination at this site is not likely. All of the RNase T1 fragments resulting from platinated RNA digestion contain consecutive G residues (G1906-G1907 and G1921-G1922 on H69, and G785-G786 on the 790 loop (Figure 3.4)), revealing

that GpG sites are preferred for complex **1** coordination to the studied rRNA constructs.

3.3.2 Dimethyl Sulfate Probing of Platination Sites

Guanine-specific chemical reactions were carried to provide further evidence of platination of the H69 and 790 loop RNAs at nucleotide resolution. The RNAs were treated with DMS, as indicated in Section 2.3.8, to methylate the accessible G N7 positions, followed by sodium borohydride and aniline treatments to initiate strand scission and allow identification of the modified sites [222]. In cisplatin reactions with DNA, platination occurs at G N7 [250]. Therefore, similar adduct formation on H69 or the 790 loop was expected to prevent DMS methylation and cause a disappearance of cleavage bands in sequencing gels [174,176].

DMS probing was carried out on unplatinated and platinated versions of H69 and the 790 loop. Autoradiograms of 20% denaturing polyacrylamide gels containing DMS-treated, 3'-end-labeled RNA constructs are shown in Figure 3.5. Bands corresponding to G1921 and G1922 of H69 and G785 and G786 of the 790 loop were diminished in the DMS-treated platinated RNA samples. Due to poor band resolution at the 5' end of the 3'-labeled RNA, DMS probing was also carried out using 5'-labeled RNA, which revealed platination at G1906 and G1907 (Figure 3.6). DMS treatment led to methylation and cleavage at G1910 for both platinated and unplatinated H69 (Figures 3.5A and 3.5B, lanes 3 and 4), indicating that G1910 is not a platination site, although its cleavage product shifts due to presence of the platinum adduct at the 5' end. Similarly, DMS treatment of the 790 loop produced a cleavage band at G791 (Figure 3.5C, lanes

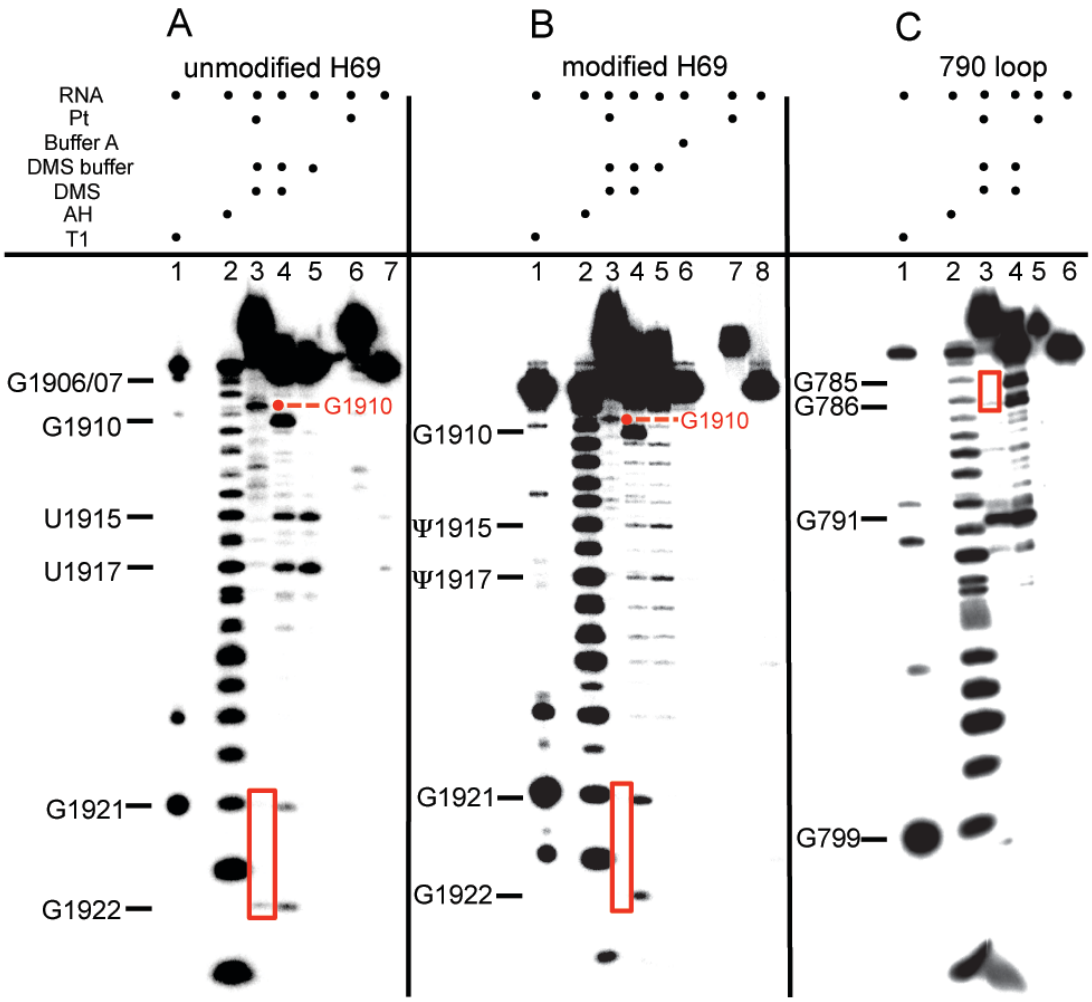

Figure 3.5. DMS probing of H69 and the 790 loop is shown. Autoradiograms show the results for 3'-end-labeled A) unmodified H69, B) modified H69, and C) 790 loop (T1: RNase T1 reaction on unplatinated RNA; AH: alkaline hydrolysis ladder on unplatinated RNA). Note that T1 and AH fragments migrate slower than the DMS products due to different chemical composition of the ends (5' OH vs. 5' phosphate, respectively). In panels a and b, the fragments corresponding to DMS reaction and cleavage at G1910 migrate more slowly in lane 3 compared to lane 4 because of the presence of the platinum adduct. Guanine residues that show slower mobility (dots) or decreased DMS reactivity (boxes) due to platination are indicated in red.

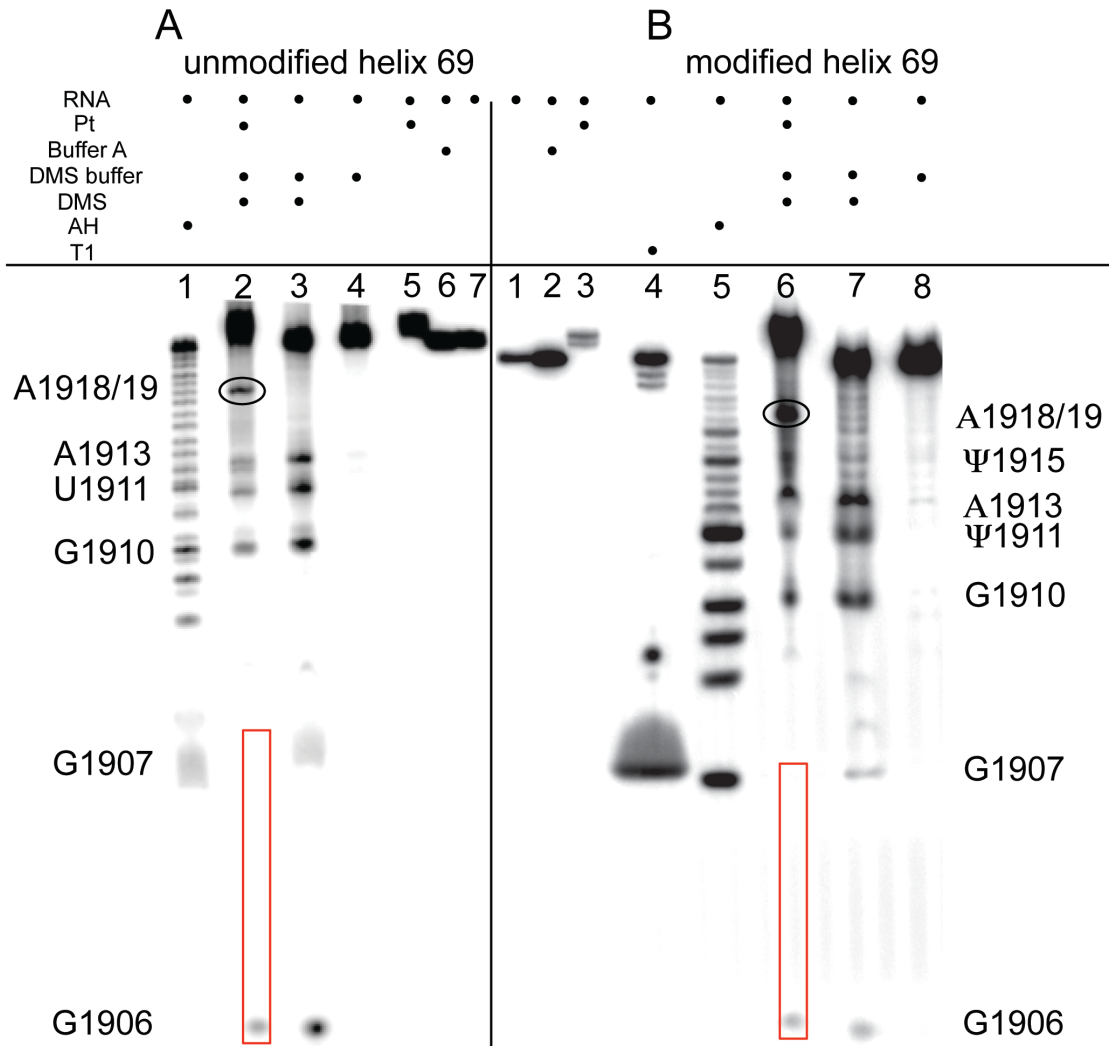

Figure 3.6. Dimethyl sulfate (DMS) probing of H69 using 5'-labeled RNA is shown. Autoradiograms show the DMS-probing results on 5'-end-labeled A) unmodified H69 and B) modified H69 (T1: RNase T1 reaction on unplatinated RNA; AH: alkaline hydrolysis ladder on unplatinated RNA). Guanine residues that show differences due to platination are indicated with red boxes. Residue A1918/19 (circled) is sensitive to DMS reactivity following platination.

3 and 4), indicating the absence of a platinum adduct at this site. In this case, the DMS-cleavage products of both platinum-treated and non-treated samples were observed to co-migrate, since these RNA fragments did not contain any platinum adducts. Together, these results support a model in which complex **1** reacts preferentially at consecutive Gs in RNA (G1906-G1907 and G1921-G1922 for

H69 and G785-G786 for the 790 loop) and forms stable bis-adducts (intrastrand adduct type 1,2-GpG), as observed with DNA (1,2-d(GpG)) [150].

In the determination of platinum coordination sites on 3'-labeled H69 through DMS reactions, hydrolysis was observed at U/Ψ1915 and U/Ψ1917 (Figures 3.5A and 3.5B, lanes 4 and 5). Hydrolysis at these sites did not occur on the platinated H69 (Figures 3.5A and 3.5B, lane 3), suggesting that platination alters the structure and/or chemical stability of H69 at or near these residues. In contrast, reactivity at U/Ψ1911 and A1913 was observed in DMS probing of 5'-labeled H69 for both platinated and unplatinated RNAs (Figure 3.6A, lanes 2 and 3; Figure 3.6B, lanes 6 and 7), indicating a minimal influence of platination on DMS-sensitivities of these nucleotides. However, a new fragment band corresponding to either A1918 or A1919 appeared in the DMS-treated, platinated H69 RNA samples (Figure 3.6A, lane 2; Figure 3.6B, lane 6). Collectively, these observations show that H69 residues become either DMS unreactive, insensitive, or sensitive after platination, indicating different responses of the RNA nucleotides to drug binding.

These observations further suggest that platination of H69 in the stem region induces a structural change in the loop region that leads to DMS sensitivity. The effect on the loop residues upon cisplatin coordination at stem GpG sites is not surprising. Aminoglycoside binding to a 2-aminopurine-modified H69 was shown to affect the loop nucleotides, in which residue A1913 became more solvent exposed [105]. These results were consistent with x-ray crystal structures of bacterial 70S ribosomes with neomycin bound to the stem region of H69 near

residues G1906, 1921, and 1922 and base exposure of A1913 (Figure 3.7A) [106]. Therefore, complex **1** coordination to the same residues as shown by this study could induce structural changes to H69 (Figure 3.7B). However, in the 2-aminopurine modified H69 studies, changes at loop residues were prominent only for modified H69, whereas in the current work, platination of both H69 RNAs caused similar effects on loop reactivity. This result reveals that effects on RNA structure likely depend on the drug types and their binding modes, as well as the RNA composition.

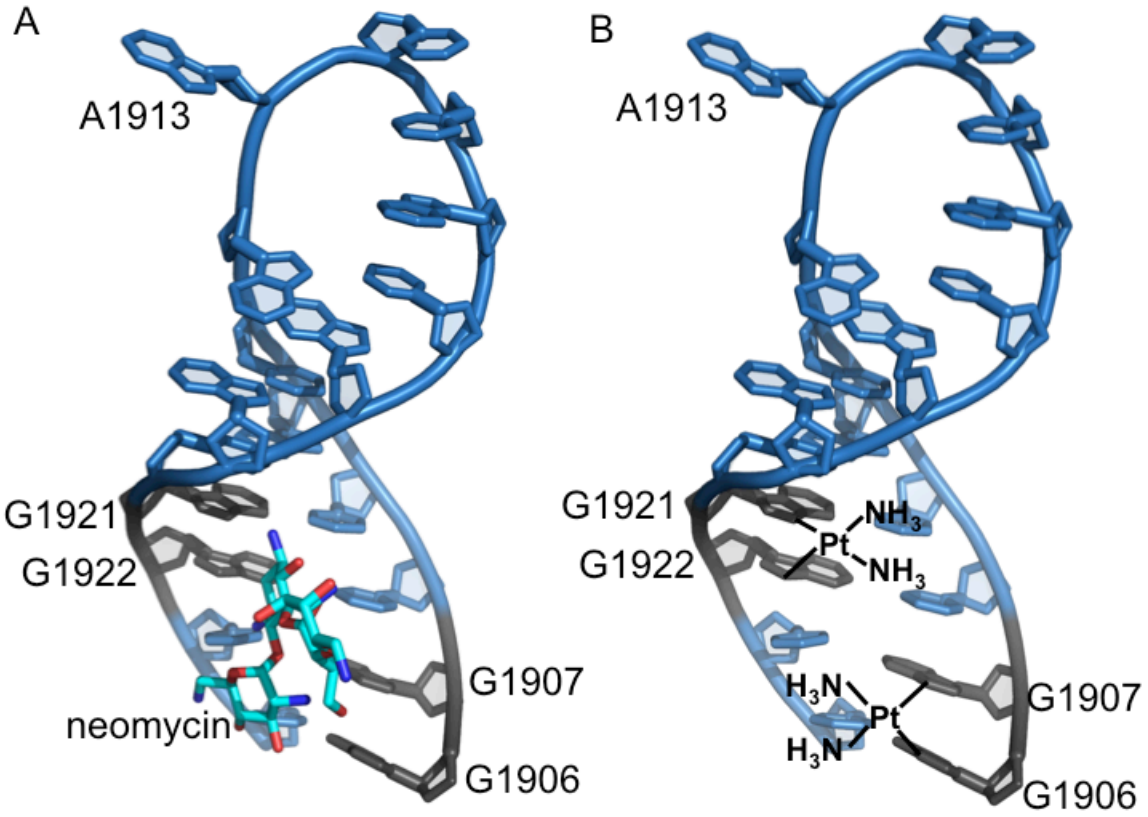

Figure 3.7. The H69-drug interactions and structural changes are shown. A) The interaction of neomycin with H69 residues G1906, G1921, and G1922 as seen by x-ray crystal structures is illustrated together with A1913 flipped out from the loop. B) The binding of cisplatin to similar residues, which could induce structural changes to H69 is indicated. The figures were created by using PDB file 4GAQ [127].

Many structural effects such as bending, unwinding, helix destabilization, and base destacking have been shown to result from cisplatin binding to DNA [151]. Likewise, the current study showed structural changes due to cisplatin coordination to the three rRNA hairpins. The structural effects of platination on DNA have been suggested to interfere with replication, transcription, and repair. Similarly, the structural effects of platination on rRNA could interfere with protein synthesis and recruit proteins that prevent repair, therefore contributing to drug cytotoxicity.

The modified and unmodified H69 RNAs gave similar results for reactions with **1**, whereas differences in reactivity with the 790 loop were observed. Although unmodified H69 and the 790 loop have identical types and numbers of nucleotides ($A_5G_5U_4C_5$), these RNAs have different sequences, with the 790 loop containing one and H69 having two GG sites. Chemical probing of both H69 RNAs showed platination-induced DMS sensitivity in the loop region, whereas no significant differences in reactivity were observed for the platinated and unplatinated 790 loop. Probing of modified and unmodified H69 revealed that these two constructs have similar reactivities with **1** and DMS, suggesting similar solvent accessibilities and chemical properties. A minimal influence from pseudouridines on structural changes induced by cisplatin coordination was seen. Collectively, these data indicate a greater impact of nucleotide sequences than the modified nucleotides on RNA structure following small-molecule binding in the studied RNAs.

The DMS-probing experiments on the three RNA constructs confirmed the RNase T1 mapping data, in which all GpG sites were platinated, whereas ApG and single Gs remained unplatinated for all three RNAs. In a previously published study, the 790 loop in free 16S rRNA, 30S, and 70S ribosomes was found to have a different platination profile with complex **1** [181]. In subunits and ribosomes, a minor reactivity at residue G786 was seen, whereas a likely bis-adduct was formed in the present work. However, in free 16S rRNA, the same residue showed stronger reactivity compared to complete ribosomes [181,262]. The G791 nucleotide in the ApG site was found to platinate in the full-length rRNA, whereas no platination was observed on the short hairpin. Neither of the single Gs was found to platinate on either full-length 16S rRNA or the model RNA construct. These comparisons generally indicate that complex **1** interaction is dependent on the rRNA context, thus microenvironments, bulk salts, and availability of the drug.

3.4 Summary and Conclusions

The rRNA motifs investigated in this study are highly conserved throughout phylogeny and important for proper ribosome function [41,43,73]. The loop Ψs in H69 regulate RNA structure, dynamics, and stability [74-77,105]. In this chapter, platination of modified H69, unmodified H69, and the 790 loop was probed by using RNase T1 mapping and DMS reactions. Activated cisplatin **1** reacted with the three 19-nucleotide rRNA motifs in a similar manner. Platination occurred at consecutive Gs, namely G1921-G1922 and G1906-G1907 in the stem region of H69 (unmodified and pseudouridylated), and at G785-G786 of the 790 loop, most

likely as bis-adducts, in which the chlorido ligands are displaced by two G residues. Previous studies with truncated tRNA molecules showed a kinetic preference for platination at neighboring Gs within a G–C-rich wobble-base-pair region [177]. Therefore, consistent with prior RNA studies, this work shows preferential recognition of G residues by complex **1** [148].

Chemical probing studies also revealed structural alterations in the RNA constructs following drug coordination, and the influence of nucleotide sequence on such changes. Comparisons to previous reports on rRNA-cisplatin interactions indicate that drug availability and electrostatics likely play a role in *in vivo* drug binding. Overall, the data provided here show many similarities of cisplatin coordination to DNA and RNA, such as target preference (*e.g.*, GpG) and impact on structure. The next set of studies focused on understanding the influence from solution conditions and electrostatics on the platination reaction.

CHAPTER 4

ELECTROSTATIC MICROENVIRONMENTS OF RIBOSOMAL RNA HAIRPINS WITH MODIFIED NUCLEOTIDES DETERMINED BY PLATINATION REACTIONS

4.1 Abstract

Electrostatic microenvironments are important for RNA biology. Each nucleotide carries a negative charge, therefore interacting cations assist in folding RNAs into their active states. Understanding RNA electrostatics and salt-dependent ligand interactions is useful for identifying unique drug targets. In this chapter, cisplatin coordination rates with bacterial ribosomal RNA (rRNA) hairpins were examined. Salt-dependent platination profiles were affected by changes in the rRNA sequence as well as modified nucleotide status, providing information about the electrostatic microenvironments. This knowledge gives insight on cationic drug interactions with RNA, and also reveals important factors governing the mechanism of cisplatin coordination to RNA.

4.2 Introduction

RNA is a highly charged biopolymer with many unique biologically active structures. Local electrostatic environments created by RNA folding are important for ligand interactions, stability, and function [18]; however, few methods exist to determine RNA electrostatic environments experimentally. Computational studies on RNA molecules can predict electrostatic potentials on their surfaces where intermolecular interactions take place [18,86]. The importance of electrostatics is also revealed through examination of RNA-protein contacts such as Rev-RRE in HIV or cationic drug binding [89,138]. Varying electrostatic potentials on

ribosomes may influence key interactions with tRNA and mRNA, or impact the recognition of antibiotics on bacteria rRNAs [88]. Therefore, the ability to monitor electrostatic microenvironments within folded RNAs is important for a complete understanding of their functions, as well as improving drug-RNA interactions.

Monovalent or divalent cations play important chemical and biological roles by associating with RNA to screen negative phosphate groups, and by forming a delocalized condensation layer, or ionic cloud, around the RNA [93]. Salts neutralize polyion charge to an extent identified by the Debye-Hückel length [98]. For short oligomers, counterion condensation is dominated by end effects, in which the local concentration of cations increases linearly from the oligomer end to the interior [246]. The influence of added salts in nucleic acid structure and function has been reported for many cases [263], revealing salt-dependent binding and rate constants for DNA interactions with ligands such as *lac* repressor, cationic peptides, and antibiotics [264-266]. Salt-dependent global RNA structural changes and ligand interactions also occur [267-269].

Analogous to the impact of electrostatics and salts on charged RNA-ligand interactions, a similar influence can be expected for coordination of metal complexes such as *cis*-diamminedichloridoplatinum(II) (cisplatin). Cisplatin is well known for DNA adduct formation [148], but an emerging number of studies have also revealed RNA as a potential target [181,183]. Kinetic studies on cisplatin binding to DNA have provided deeper insight on its mechanism [158,163,164,169,239], whereas reports on RNA interactions are still limited. Given the importance of microenvironments in RNA-ligand interactions, this

chapter focuses on platination rates for rRNAs containing modified nucleotides and varying sequences. The impact of electrostatics on drug binding was evaluated by using salt-dependent coordination rates. These results are valuable for understanding cation interactions with RNA and developing tools to investigate microenvironments of various RNA motifs.

4.3 Results and Discussion

Three bacterial (*E. coli*) model hairpin rRNAs were chosen for comparison of platination rates and electrostatics because of their important biological roles and known antibiotic or ligand interactions. Helix 69 (H69) from 23S rRNA plays a key role in protein synthesis [69,70,270], and aminoglycoside binding [105,106]. H69 has three pseudouridine (Ψ) residues that impact structure, stability, and function [75,77,259]. The contribution of Ψ to RNA electrostatic environments has been examined previously by computational methods [241]. In that study, a high electronegative potential localized to the major groove of a branch site in pseudouridylated RNA was determined. Therefore, such electrostatic environments in modified RNA might be expected to influence the initial interaction and approach of platinum compounds on the studied RNAs. Therefore, two H69 constructs containing either uridine (unmodified) or Ψ (modified) were used to determine experimentally the influence of nucleotide modifications on electrostatics and salt-dependent drug binding to rRNA. The 790 loop from 16S rRNA is also important for ribosome function [83,271]. It has an identical size and nucleotide composition but altered sequence compared to H69, and therefore provides a means to examine the effect of nucleotide arrangement on salt-

dependent characteristics of rRNA. The RNAs were platinated by reacting with activated cisplatin, complex **1** (Figure 2.5), under pseudo-first-order conditions, and the products were quantified with gel assays, as described in Section 2.5. The salt influence on platination kinetics was determined by changing Na^+ concentrations in the bulk medium. Electrostatic properties of model rRNAs were then determined by evaluating the kinetic data according to Brønsted-Debye-Hückel and polyelectrolyte theories [173,176].

4.3.1 Kinetics of Cisplatin Binding to Ribosomal RNA Hairpins

Addition of complex **1** to RNA resulted in a decrease of unplatinated RNA in a time-dependent manner, with a concomitant increase in intensity of slower-migrating product bands (platinated RNA) on denaturing polyacrylamide gels (Figure 4.1A-C). In a generally accepted mechanism, the reaction of complex **1** with RNA proceeds in two steps [163-168,173,175,176,179,180]. In the first step, complex **1** displaces a fraction of surface-bound cations ($n\Psi'$) and associates with RNA (Scheme 4.1, Equation 4), followed by the next rate-determining step of direct reaction between **1** and the nucleic acid (Equation 5). Under these conditions, the rate of conversion of unplatinated RNA to platinated RNA should obey first-order dependence of the concentration of **1** and RNA with the rate law according to Equation 6. Under conditions of excess platinum ([**1**] >> [RNA]), the observed pseudo-first-order rate constant, k_{obs}, can be obtained by Equation 7, and the rate law can be rewritten as Equation 8, in which $k_{obs} = k_{2,app}[\mathbf{1}]_{t=0}$. Thus,

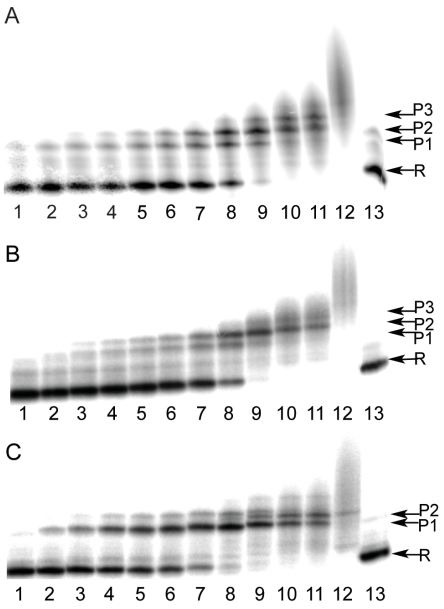

Figure 4.1. Reaction kinetics of **1** and RNA constructs are shown. Autoradiograms for A) unmodified H69, B) modified H69, and C) 790 loop are shown (R: unreacted RNA; P1, P2, and P3: slower migrating Pt products; [RNA] = 0.7 μM, [**1**] = 94 μM; 10 mM K_2HPO_4/KH_2PO_4, pH 6.2, with 20 mM $NaClO_4$; 32 mM total monovalent cation concentration, [M^+], 37 °C). Lanes 1–8; 0, 2, 4, 6, 8, 10, 15, and 30 min, respectively; lanes 9–12; 1, 2, 3, and 22 h, respectively; lane 13; 22 h control (no Pt) are indicated.

$$\mathbf{1} + \mathrm{RNA}\cdots n\Psi'\mathrm{M}^{+/2+} \underset{}{\overset{K_{ass}}{\rightleftharpoons}} \mathrm{RNA}\cdots\mathbf{1} + n\Psi'\mathrm{M}^{+/2+} \qquad (4)$$

$$\mathrm{RNA}\cdots\mathbf{1} \xrightarrow{k_2} \mathrm{RNA}\text{–}\mathbf{1} \qquad (5)$$

$$-\frac{\mathrm{d}[\mathrm{RNA}\cdots n\Psi'\mathrm{M}^+]}{\mathrm{dt}} = k_2 K_{\mathrm{ass}} \frac{[\mathbf{1}][\mathrm{RNA}\cdots n\Psi'\mathrm{M}^+]}{[\mathrm{M}^{+/2+}]^{n\Psi'}} \qquad (6)$$

$$k_{\mathrm{obs}} = k_2 K_{\mathrm{ass}} \frac{[\mathbf{1}]_{\mathrm{tot}}}{[\mathrm{M}^+]^{n\Psi'}} \qquad (7)$$

$$-\frac{\mathrm{d}[\mathrm{RNA}\cdots n\Psi'\mathrm{M}^+]}{\mathrm{dt}} = k_{\mathrm{obs}}\,[\mathrm{RNA}\cdots n\Psi'\mathrm{M}^+] \qquad (8)$$

$$\frac{[\mathrm{RNA}\cdots n\Psi'\mathrm{M}^+]_t}{[\mathrm{RNA}\cdots n\Psi'\mathrm{M}^+]_0} = \mathrm{A}e^{-k_{\mathrm{obs}}t} \qquad (9)$$

Scheme 4.1. The reaction and kinetic model for complex **1** coordination to RNA is given.

the observed rate constant k_{obs} can be obtained by a fit of a single-exponential function to the time dependence of unreacted RNA.

The decrease of unreacted RNA over time fit well to a single-exponential decay for all cation concentrations studied (Figure 4.2). Under pseudo-first-order conditions ([**1**]>>[RNA]), the observed rate constant, k_{obs}, was determined. For all three RNA constructs, a linear relationship exists between k_{obs} and initial complex **1** concentration (Figure 4.3). Therefore, the apparent second-order rate constant, $k_{2,app}$, was determined by the relationship $k_{2,app} = k_{obs}/[\mathbf{1}]_{t=0}$. Standard errors were calculated from three independent experiments.

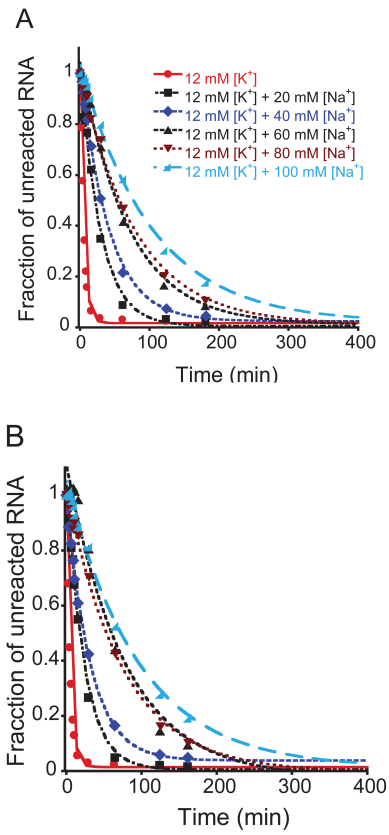

Figure 4.2. Single-exponential-decay fits show disappearance of unreacted RNA A) unmodified H69, B) modified H69, and C) 790 loop as a function of time (min) in 10 mM K_2HPO_4/KH_2PO_4, pH 6.2, and 0–100 mM $NaClO_4$; 12–112 mM total monovalent cation concentration.

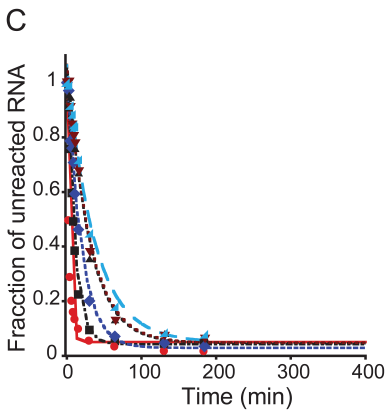

Figure 4.2.continued.

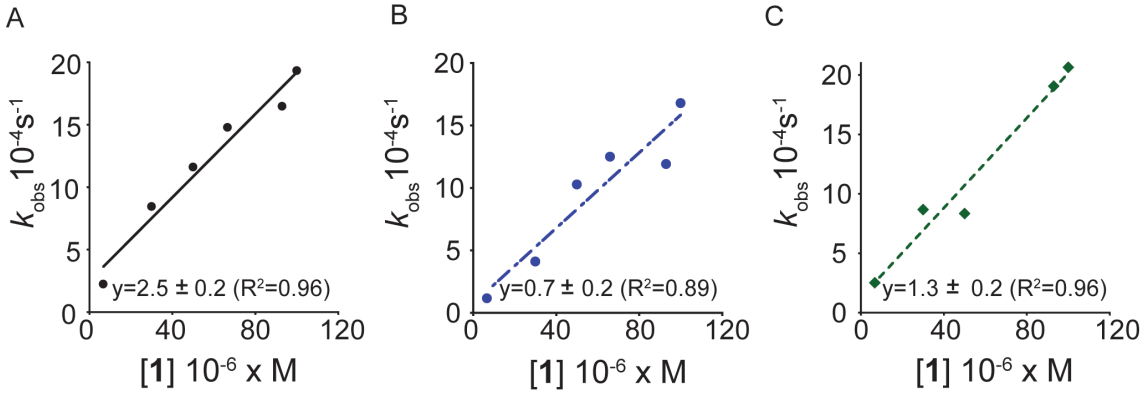

Figure 4.3. Determination of second-order rate constants for reactions of **1** with RNA is shown. The observed pseudo-first-order rate constant, k_{obs}, is plotted as a function of increasing platinum concentration, [**1**], for the reaction of A) unmodified H69, B) modified H69, or C) the 790 loop with complex **1** in 10 mM KH_2PO_4/K_2HPO_4, 20 mM $NaClO_4$, pH 6.2, 37 °C; 6.7 μM < [**1**] < 100 μM (9.5–143 times excess).

4.3.2 Salt-Dependent Platination Reactivities of rRNA

All three RNAs showed a decrease in **1** reactivity as total monovalent cation concentration ($[M^+]$) in the bulk medium increases (Figure 4.4, Table 4.1). Specifically, a ca. one-order-of-magnitude decrease in reactivity was observed

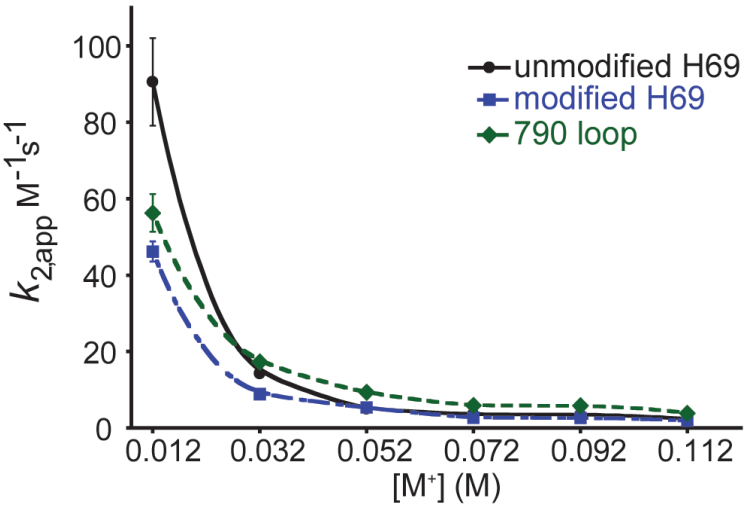

Figure 4.4. The apparent second-order rate constant, $k_{2,app}$, versus total monovalent cation concentration ([M^+]), 12–112 mM, plot shows the salt-dependent platination kinetics for unmodified H69 (black circles), modified H69 (blue squares), and the 790 loop (green diamonds).

Table 4.1. Observed pseudo-first-order rate constants, k_{obs}, and second-order rate constants, $k_{2,app}$ for the reactions between rRNA constructs and activated cisplatin as a function of monovalent cation concentration.

Oligonucleotide	K^+ (mM)[a]	Na^+ (mM)[b]	k_{obs} (10^{-4} s^{-1})	$k_{2,app}$ ($M^{-1}s^{-1}$)
unmodified H69	12	0	85.0 ± 10.7	90.5 ± 11.4
	12	20	13.3 ± 0.9	14.2 ± 0.9
	12	40	4.7 ± 0.5	5.0 ± 0.6
	12	60	3.4 ± 0.4	3.6 ± 0.5
	12	80	3.3 ± 0.2	3.5 ± 0.3
	12	100	2.2 ± 0.2	2.4 ± 0.3
modified H69	12	0	42.6 ± 3.1	45.4 ± 3.3
	12	20	7.9 ± 0.9	8.4 ± 0.9
	12	40	4.6 ± 0.4	4.9 ± 0.4
	12	60	2.6 ± 0.3	2.8 ± 0.3
	12	80	2.4 ± 0.2	2.6 ± 0.3
	12	100	1.8 ± 0.2	1.9 ± 0.2
790 loop	12	0	52.8 ± 4.6	56.2 ± 4.9
	12	20	16.2 ± 1.1	17.2 ± 1.2
	12	40	8.7 ± 0.7	9.3 ± 0.7
	12	60	5.6 ± 0.5	5.9 ± 0.5
	12	80	5.5 ± 0.4	5.8 ± 0.5
	12	100	3.6 ± 0.5	3.8 ± 0.5

[a]10 mM K_2HPO_4/KH_2PO_4 buffer, pH 6.2; [b]0–100 mM $NaClO_4$, 37 °C

with increase of bulk monovalent cation concentration from 12 to 112 mM. Unmodified H69 was more sensitive to salt (38-fold decrease in $k_{2,app}$) than modified H69 (24-fold decrease) and 790 loop (15-fold decrease). A particularly prominent salt dependence for all RNAs was seen between 12 and 32 mM total monovalent cations. Modified H69 showed a ca. two- and 1.7-fold lower reactivity than unmodified H69 at 12 and 32 mM monovalent cation concentrations, respectively, whereas reactivity of the 790 loop was below that of unmodified H69 only at the lower cation concentration. These results indicate that Ψ and the nucleotide sequence (unmodified H69 vs. 790 loop) influenced the rate of cationic complex coordination to RNA. The mechanism of cisplatin adduct formation can be described by a two-step reaction (Scheme 4.1). In the first step, positively charged **1** associates with RNA, replacing a fraction of surface-bound cations ($n\Psi'$) (Equation 4; the symbol Ψ' is used to avoid confusion with pseudouridine, represented as Ψ), which is followed by direct coordination of **1** to RNA as the rate-determining step (Equation 5). The salt-dependent interactions of nucleic acids originate from counterion release upon ligand binding [264,265,272,273]. The entropic contribution from this displacement is a significant driving force for complex formation [264,265,272,273].

4.3.3 Determination of Electrostatics in Cisplatin-rRNA Reactions

Salt-dependent platination kinetics were assessed by two electrostatic models. The Brønsted-Debye-Hückel relationship is well suited for reactants described as point charges [247], such as **1** interacting with a limited number of phosphodiester linkages at the platination site. To analyze the kinetic data

according to this theory (Chapter 2, Equation 2 and Section 2.6.1), the apparent second-order rate constant ($k_{2,app}$) was plotted as a function of ionic strength in the medium (I) (Figure 4.5). When A is 0.5220 at 38 °C [248], the slope provides Z_AZ_B, which indicates the overall charge of each species interacting in the product-formation reaction. The x intercept provides the rate constant at zero ionic strength, k_0 (Table 4.2).

The product of Z_AZ_B was negative, as expected for a reaction between a positively charged platinum complex and negatively charged RNA surface. Although consistent with previously studied systems [173,175,176], the Z_AZ_B values, ranging from -6.6 (790 loop) to -9.5 (unmodified H69), were higher than expected for interaction of +1 charged Pt center and single -1 charged phosphodiester bond. This result suggests increased negative charge density of

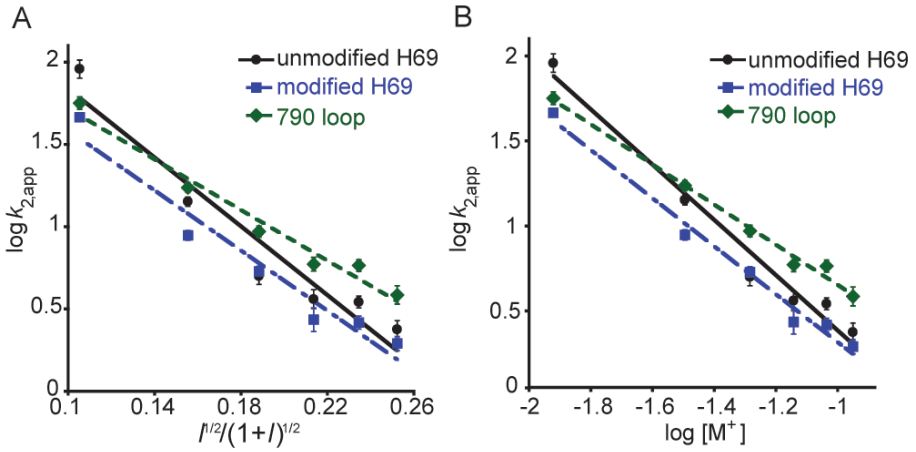

Figure 4.5. Evaluation of salt dependence of RNA platination rates according to electrostatic models is shown. A) A plot of log $k_{2,app}$ versus $I^{1/2}/(1+I^{1/2})$ assuming the salt dependence according to the Brønsted-Debye-Hückel relationship. B) A graph of log $k_{2,app}$ versus log monovalent cation concentrations, [M^+], assuming the polyelectrolyte behavior of RNA constructs, unmodified H69 (black circles), modified H69 (blue squares), and 790 loop (green diamonds).

the folded hairpin structures, which attracts the cationic metal complexes for binding and coordination. The overall negative charge density in these rRNA motifs could play a critical role in initial recognition and recruitment of other charged molecules onto their surfaces.

Electrostatic interactions between charged ligands and polynucleotides can also be described by the polyelectrolyte theory [98,246,247,265,274-276]. Salt-dependent platination of RNA by **1** was evaluated by Equation 3 (Chapter 2 and Section 2.6.1). The theory predicts a linear relationship between log $k_{2,app}$ and log [M^+] (Figure 4.5B), providing log k'_0 and the fraction of surface-condensed cations, $n\Psi'$ (Table 4.2), displaced by complex **1.** Interactions of **1** with all three RNAs were well described by this theory; however, higher $n\Psi'$ values were obtained compared to previously investigated RNAs and DNAs (Table 4.3), indicating higher electrostatic potentials and greater displacement of counterions from the RNA surface following **1** binding. Increased displacement of condensed ions in cationic peptide/protein-nucleic acid interactions has been attributed to formation of thermodynamically stable complexes driven by entropic effects [264,265,272,273]. Therefore, a higher fraction of counterions released by **1**

Table 4.2. Evaluation of the salt dependence of RNA reactivity with **1** using the Brønsted-Debye-Hückel relationship and polyelectrolyte theory.

RNA	Z_AZ_B	log k_0	$n\Psi'$	log k'_0
unmodified H69	-9.5 ± 1.5	2.7 ± 0.5	1.5 ± 0.2	-1.2 ± 0.1
modified H69	-8.7 ± 0.5	2.5 ± 0.2	1.4 ± 0.1	-1.1 ± 0.1
790 loop	-6.6 ± 1.1	2.3 ± 0.3	1.0 ± 0.1	-0.4 ± 0.1

Table 4.3. Comparison of $n\Psi'$ values of different oligonucleotides.

Oligonucleotide	Pt cmpd	Cation conditions	$n\Psi'$	ref.
r(GGCCGUAACUAUAACGGUC)	**1**	12 mM K^+, 0 – 100 mM Na^+	1.5	
r(GGCCGΨAACΨAΨAACGGUC)	**1**	12 mM K^+, 0 – 100 mM Na^+	1.4	
r(GCAGGAUUAGAUACCCUGC)	**1**	12 mM K^+, 0 – 100 mM Na^+	1.0	
r(CGCGUUGUUCGCG)	**2**	19 – 500 mM Na^+	0.69	[176]
r(CGCGTTGTTCGCG)	**3**	19 – 500 mM Na^+	0.62	[176]
d(CGCGTTGTTCGCG)	**2**	19 – 500 mM Na^+	0.44	[176]
d(CGCGTTGTTCGCG)	**3**	19 – 500 mM Na^+	0.41	[176]
d($T_8{}^{s6}IT_8$)	**2**	0.5 mM K^+, 4.3 – 300 mM Na^+	0.80	[175]
d($T_8{}^{s4}UT_8$)	**2**	0.5 mM K^+, 4.3 – 300 mM Na^+	0.74	[175]
d($^{s6}IT_{16}$)	**2**	0.5 mM K^+, 4.3 – 300 mM Na^+	0.60	[175]
d($^{s4}UT^{16}$)	**2**	0.5 mM K^+, 4.3 – 300 mM Na^+	0.60	[175]
d($T_8p(S)T_8$)	**2**	0.5 mM K^+, 4.3 – 300 mM Na^+	0.60	[175]
Native B-DNA	–	–	0.88	[98]
Single-stranded DNA	–	–	0.70	[98]
A-DNA	–	–	0.91	[96]
Poly(U)	–	–	0.68	[96]

1 = *cis*-$[PtCl(NH_3)_2(OH_2)]^+$; **2** = *cis*-$[PtCl(NH_3)(c\text{-}C_6H_{11}NH_2)(OH_2)]^+$;

3 = *trans*-$[PtCl(NH_3)$ (quinoline)$(OH_2)]^+$

interaction may also produce stable and favorable platination adducts with these rRNA hairpins under *in cellulo* conditions. Analysis of platination kinetics by the two electrostatic models revealed that both nucleotide modifications and sequence influence the rate by which a common nucleophile (*e.g.*, G-N7) is targeted. This result is in line with the mechanism shown in Scheme 4.1, in which the observed platination rate is affected by electrostatics during the initial association step (Equation 4) and by other intrinsic RNA characteristics in the rate-determining substitution step (Equation 5). Electrostatic comparisons showed no significant differences in the Z_AZ_B or $n\Psi'$ values for unmodified and modified H69s, indicating that approach, association, and accumulation of **1**

should be similar for the two RNAs. However, different platination rates were seen for the two H69 constructs (Figure 4.4 and Table 4.1), particularly in low salt. Therefore, other factors such as target accessibility and inherent reactivity are likely to influence direct coordination in the substitution step. Structure studies revealed more pronounced stacking interactions from Ψ1915 to A1918 in modified H69 compared to unmodified H69 [74,75], and probing analyses showed that residues in unmodified H69 within complete ribosomes are less constrained and more reactive to chemical modifying agents than pseudouridylated H69 [76,77]. Hence, the less restricted structure, allowing for increased target site access in the substitution step, would account for higher platination rates of unmodified H69 compared to modified H69.

Since platination GpG sites [148,150] are located in the stem, whereas U/Ψ are found in the loop, the differential H69 platination rates indicate crosstalk between the stem and loop motifs. Previous fluorescence studies with 2-aminopurine-substituted H69 also support the idea of crosstalk between the stem and loop upon aminoglycoside binding [105], and ribosome crystal studies show localization of these cationic drugs near the GpG sites of H69 [106]. Differences in the H69 loop due to U/Ψ could be conveyed to the stem platination site, thereby affecting coordination rates. With increasing salts, these structural differences may be screened, leading to comparable reactivities for the two RNAs. These findings indicate that Ψ, although located away from the target site and not contributing to global electrostatics, can still influence the platination mechanisms in rRNA through varying structure and dynamics. Since cellular

RNA contains many modified nucleotides, those residues could also influence cationic interactions *in vivo*.

The kinetics of **1** binding to the 790 loop showed an intermediate reactivity profile compared to unmodified and modified H69 in low salt, combined with a less pronounced salt dependence, providing further support that the local structure is a determinant of cisplatin reactivity. We therefore conclude that sequence effects may be more impactful than pseudouridylation with respect to modulating the RNA electrostatic environments. Lower electrostatics (Z_AZ_B or $n\Psi'$ values in Table 4.2) of the 790 loop indicate reduced attraction and accumulation of **1** during the association step, leading to lower platination rates. However, the altered sequence of the 790 loop may also give rise to a structure in which platinum target sites are more reactive and accessible, therefore restoring the electrostatically lowered drug coordination rates to an intermediate platination profile compared to H69 RNAs.

The k_0 values, which indicate inherent reactivity of the target site in the absence of counterion screening, were similar for all three RNAs. However, the dissimilar kinetic profiles ($k_{2,app}$ in Figure 4.4) exhibited by the three RNAs as a function of increasing salt indicated a significant contribution of target-specific electrostatics to the kinetics during binding of charged compounds to RNA. Overall, these findings strongly support the influence of electrostatics and structure to the mechanism of platinum drugs binding to rRNA hairpins. The data provided herein also show the impact of additional factors such as modified

nucleotides and dynamics to the mechanism of platinum drug coordination to rRNA hairpins.

4.4 Summary and Conclusions

Electrostatic interactions and salt-dependent properties play crucial roles in RNA biochemistry. This work shows the utility of coordination complexes such as cisplatin to probe RNA microenvironments and potential binding interactions. While this thesis work focuses on metallo-drug interactions with RNA, these results may be useful to understand the binding of non-metallic, cationic compounds to the same RNA sites. Platination kinetics revealed how sequence and nucleotide composition control drug binding through different mechanisms. For example, sequence variations lead to global electrostatic changes that impact cationic ligand binding, whereas modifications such as pseudouridylation influence RNA reactivity through structural changes. The higher electrostatics of H69 and 790 loop rRNAs suggest that they would be attractive targets for cationic drug molecules. Although it is important to first understand the reactivity at a basic secondary structure level with smaller RNA motifs, platination of larger RNA constructs and complete ribosomes will be able to shed light on the roles of the surrounding RNA tertiary structure on these processes [181,183].

CHAPTER 5

THE IMPACT OF CATIONS ON KINETICS OF rRNA PLATINATIONS

5.1 Abstract

Metal cations play an indispensable role for RNA. Dynamic cation interactions can influence the global electrostatics of RNA. Consequently, the attraction and binding of cationic drugs like cisplatin depend on the ionic conditions surrounding the targets. In this chapter, complex **1** coordination rates to H69 RNAs were studied under different salt media. The presence of divalent ions reduced the cisplatin binding rate to RNA. Furthermore, platination rates were found to decrease with increasing ionic strength. The analysis of kinetic data according to electrostatic models showed increased RNA global charge and enhanced counterion condensations under high salt conditions. However, nucleotide modifications did not alter the platination rate or the electrostatic properties of RNA. Overall, this kinetic study showed the effect from surrounding ionic conditions, especially the presence of divalent cations, on cationic drug binding rates, RNA microenvironments, and the application of platination kinetics to probe such correlations.

5.2 Introduction

Cations play key roles in RNA [93,97,268,277,278]. Many different monovalent and divalent cations such as K^+, Na^+, NH_4^+, and Mg^{2+} have been identified as playing roles in electrostatics and ligand interactions of RNA [94,95]. The most common monovalent ion present in the *E. coli* cytoplasm, K^+, serves important roles for many RNAs [96,279-282]. Although Na^+ is mainly found in

extracellular fluids, many studies have revealed Na^+ association with nucleic acids within the cell [97,283-285]. The most common divalent ion found in the bacterial cytoplasm is Mg^{2+} [96]. Due to its high charge density and low entropic cost for charge neutralization compared to monovalent ions, Mg^{2+} is suggested to play an important role in screening electrostatics of RNA [93,97,101]. The Mg^{2+} associations on RNA molecules have been identified either with local functional groups or on surface electronegative patches [18,100,286-292].

In addition to roles in attenuating electrostatics, cations also impact nucleic acid-ligand interactions. The effects of mono- and divalent cations on *lac* repressor-operator, peptide-RNA, endonuclease-DNA, and antibiotic-DNA interactions have been documented [266,269,273,293]. The displacement of functionally important Mg^{2+} ions that complement the electrostatic potentials on RNA has been attributed to inhibition of the hammerhead ribozyme by aminoglycosides [126,136]. Although the site-specific binding of cations has been identified to serve important roles such as regulating RNA conformation, the contribution to the ionic cloud that surrounds and stabilizes RNA tertiary structures is considered to be the dominant role of cations [294-298]. Similarly, work reported in this chapter emphasizes the significance of non-specific ionic interactions on RNA microenvironments, cationic ligand binding rates, and application of platination kinetics to probe cation-dependent RNA dynamics.

In this chapter, the influence of Mg^{2+} on complex **1** binding rate to H69 RNAs (modified and unmodified) was determined under two different monovalent cation conditions. The Mg^{2+} dependence of platination rates was evaluated according to

the two electrostatic theories. Platination was carried out under pseudo-first-order conditions with excess complex **1**. The reaction rate was determined by fitting the fraction of unreacted RNA, determined by gel assays, to single-exponential decay plots as described in Chapters 2 and 4. The addition of Mg^{2+} to the reaction medium resulted in a decrease of the platination rates. Interestingly, the analysis of platination kinetics according to the Brønsted-Debye-Hückel theory revealed an increase of RNA charge density under the higher cationic conditions. Under higher salt conditions, higher counterion condensation was observed, which lowered the platination rates. The electrostatic effect on drug-RNA binding rate was dependent on the salt conditions used. Taken together, the results show that RNA electrostatics can be modulated by the surrounding ionic strength, and thus target-ligand interactions can be heavily dependent on cellular cationic levels.

5.3 Results and Discussion

5.3.1 The Impact of Mg^{2+} Ions on the Platination Kinetics of Ribosomal RNA Hairpins

Salts are important for the activity of biomolecules. Specifically for highly-charged biopolymers such as RNA, cations are required to neutralize electronegative potential. In turn, these cationic associations can alter the electrostatic properties of RNA and their interaction with ligands. In this chapter, the influence of Mg^{2+} on complex **1** coordination rate to rRNA was monitored under two different monovalent cation conditions, K^+ only and K^+ + Na^+, as described in Chapter 2, Section 2.5. Evaluation of kinetic data according to the

Brønsted-Debye-Hückel and polyelectrolyte theories allowed for the determination of ionic influence on the electrostatic properties of rRNA.

The platination reaction was initiated by adding an excess amount of complex **1** ([**1**] >> [RNA]) to achieve pseudo-first-order conditions. The progress of complex **1** binding to rRNA hairpins was monitored by gel electrophoresis. Coordination of the platinum complex decreased the amount of unreacted RNA with time and produced slow migrating product bands (Figure 5.1). The decrease of unreacted

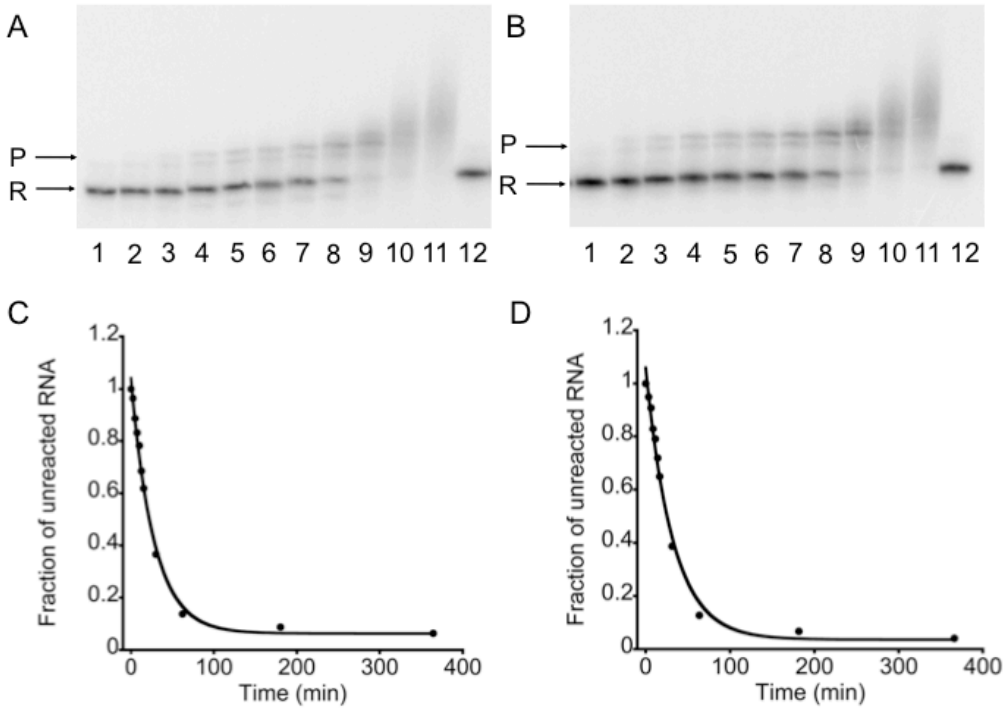

Figure 5.1. The kinetic plots of H69 RNA platination in the presence of Mg^{2+} are shown. Autoradiograms of A) unmodified H69 and B) modified H69 in 10 mM K_2HPO_4/KH_2PO_4 pH 6.2, (buffer B), $[K^+]$ = 12 mM, with 20 mM $NaClO_4$ and 1 mM $Mg(ClO_4)_2$ are shown (R: unreacted RNA, P: slower migrating platinated products, lanes 1-8; 0, 2, 4, 6, 8, 10, 15, 30 min, respectively, lanes 9-11; 1 h, 3 h, 6 h, respectively, and lane 12; 6 h con, no Pt). The corresponding single-exponential decay fits of the autoradiograms for C) unmodified H69 and D) modified H69 are shown.

RNA fraction with time was well described according to single-exponential decay fits (Figure 5.1). The observed pseudo-first-order rate constants (k_{obs}) and apparent second-order rate constants ($k_{2,app}$) were determined by single-exponential decay plots and the $k_{2,app} = k_{obs}/[\mathbf{1}]$ relationship, respectively. Standard errors were calculated from two or three independent trials.

The influence of Mg^{2+} on platination of the H69 rRNA hairpins was determined under two monovalent ion conditions. In one condition, the medium contained only K^+ ions added from a 10 mM K_2HPO_4/KH_2PO_4, pH 6.2 (buffer B), and the second buffer contained 20 mM $NaClO_4$ in addition to 10 mM K_2HPO_4/KH_2PO_4 (buffer B + Na^+). The platination rate deceased with the addition of Mg^{2+} for both H69 RNAs. The decreasing platination rate with increasing Mg^{2+} was observed for both monovalent conditions (Figure 5.2). The platination rate ($k_{2,app}$) was decreased by a ca. one-order-of magnitude in buffer B, and 1.5–2-fold in buffer B + Na^+ by addition of 1 mM Mg^{2+} (Table 5.1). In buffer B, both

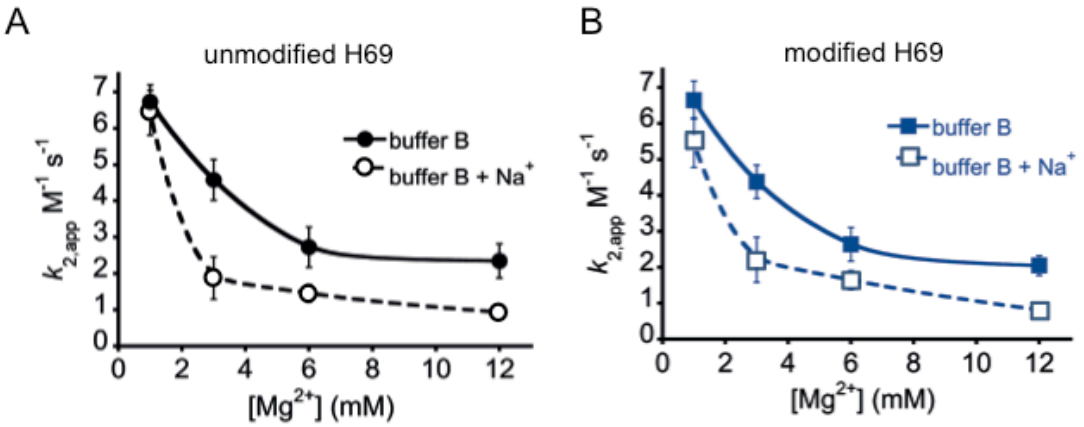

Figure 5.2. The Mg^{2+}-dependent platination kinetic plots are shown. Variation of the apparent second-order rate constant, $k_{2,app}$, with respect to Mg^{2+} concentration for A) unmodified H69 and B) modified H69 is shown. The filled symbols with solid fittings represent data for buffer B (buffer B titrated with Mg^{2+}) and open symbols with dashed fittings represent buffer B with 20 mM $NaClO_4$ (buffer B + Na^+ titrated with Mg^{2+}).

Table 5.1. The observed pseudo-first-order rate constants, k_{obs}, and apparent second-order rate constants, $k_{2,app}$, for the reactions between H69 rRNA constructs and complex **1** as a function of Mg^{2+} concentrations studied under different monovalent ion conditions.

Oligonucleotide	K^+ (mM)[a]	Na^+ (mM)	Mg^{2+} (mM)	k_{obs} (10^{-4} s^{-1})	$k_{2,app}$ ($M^{-1}s^{-1}$)
unmodified H69	12	0	0	85.0 ± 10.7[b]	90.5 ± 11.4[b]
	12	0	1	6.3 ± 0.4	6.7 ± 0.5
	12	0	3	4.3 ± 0.5	4.6 ± 0.6
	12	0	6	2.6 ± 0.5	2.7 ± 0.5
	12	0	12	2.2 ± 0.4	2.3 ± 0.5
	12	20	0	13.3 ± 0.9[b]	14.1 ± 0.9[b]
	12	20	1	6.0 ± 0.6	6.4 ± 0.6
	12	20	3	1.8 ± 0.6	1.9 ± 0.6
	12	20	6	1.4 ± 0.2	1.4 ± 0.2
	12	20	12	0.9 ± 0.1	0.9 ± 0.1
modified H69	12	0	0	42.6 ± 3.1[b]	45.4 ± 3.3[b]
	12	0	1	6.2 ± 0.5	6.6 ± 0.5
	12	0	3	4.1 ± 0.4	4.4 ± 0.5
	12	0	6	2.5 ± 0.4	2.6 ± 0.5
	12	0	12	1.9 ± 0.2	2.0 ± 0.3
	12	20	0	7.9 ± 0.9 [b]	8.4 ± 0.9[b]
	12	20	1	5.1 ± 0.6	5.5 ± 0.7
	12	20	3	2.1 ± 0.6	2.2 ± 0.6
	12	20	6	1.5 ± 0.2	1.6 ± 0.2
	12	20	12	0.8 ± 0.1	0.8 ± 0.1

[a]10 mM K_2HPO_4/KH_2PO_4 buffer, pH 6.2 (buffer B), 37 °C, [b]Data from Chapter 4.

RNAs showed ca. 3-fold decrease in platination ($k_{2,app}$) going from 1 to 12 mM Mg^{2+} and ca. 7-fold reduction in buffer B + Na^+. Except for 1 mM Mg^{2+}, the platination rate in buffer B + Na^+ was always lower compared to buffer B. No significant differences in platination rates were observed for the two H69 RNAs under all Mg^{2+} concentrations studied. The decrease of platination rate with the addition of Mg^{2+} is supported by similar trends reported for other oligomer systems [166,173,185].

In the mechanism of platinum complexes binding to nucleic acids (Chapter 4),

complex **1** first associates with RNA by displacing the surface-bound cations (Equation 4), and then coordinates to the target site in a rate-determining second step (Equation 5) [163,164,168,179]. According to this pathway, the platination rate should depend on the bulk salts, K_{ass}, and k_2. The K_{ass} depends on the electrostatic interaction between complex **1** and RNA, whereas intrinsic RNA characteristics impact k_2. As the cationic Mg^{2+} can electrostatically compete with the positively charged complex **1**, the decrease of platination rate in the presence of Mg^{2+} should therefore arise due to decreased K_{ass} and reduced drug accumulation on RNA.

Ribosome crystal structures identified Mg^{2+} ions near G1921-22 of H69 (Figure 5.3), where complex **1** coordination was also observed (Chapter 3) [104,299,300]. The G•U wobble base pairs in RNA have strong electronegative potentials in the major groove to which Mg^{2+} ion binding has been reported [63]. Studies using small H69 RNA constructs suggested Mg^{2+} ion association at the G1907•U1923 wobble pair [65,301]. Results from Chapter 3 also suggested complex **1** coordination at G1906-07.

In general, Mg^{2+} ions tend to associate on the electronegative deep major groove of RNA [302,303]. Based on results with DNA, cisplatin is believed to access the base N7 position and coordinate in the major groove of RNA [145,304]. Crystallographic studies have further suggested that diffusely bound Mg^{2+} ions could interact with the solvent-exposed regions of ribosomes [284]. The direct associations of Mg^{2+} ions at or near the platinum target sites, as well as accumulating in ionic clouds along the RNA backbone, are likely to pose steric

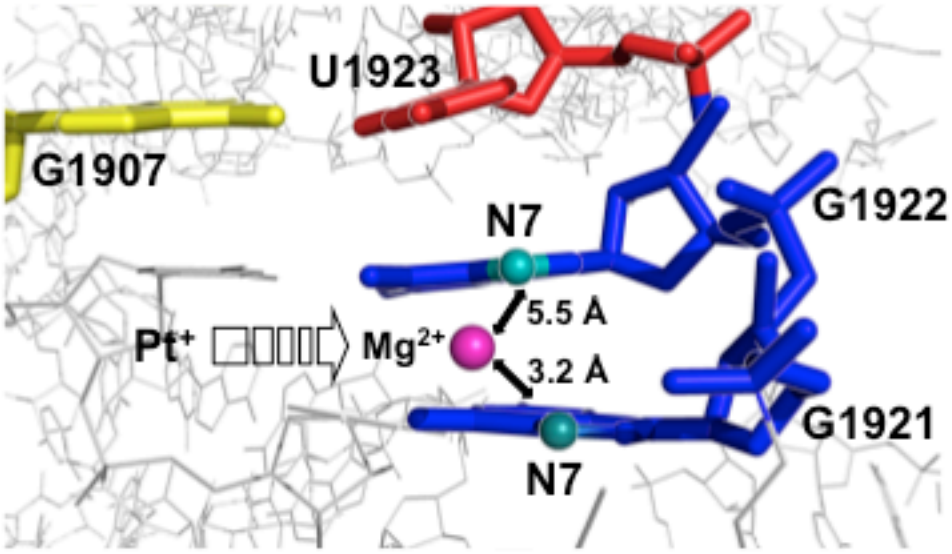

Figure 5.3. The crystal structure of *T. thermophilus* 23S rRNA shows a Mg^{2+} ion (shown in purple) located in between residues G1921 and G1922 (blue) of H69 (PDB: 3HUX) [104]. The distances from the Mg^{2+} metal center to N7 atoms of Gs are indicated. Potential electrostatic and steric hindrance for approach of the Pt^{+} complex by the Mg^{2+} ion near the N7 positions of the 1921-22 Gs is indicated by the open arrow.

and electrostatic barriers for complex **1** coordination, and therefore decrease the platination rate (*i.e.*, lowering K_{ass}).

As mentioned previously, the Mg^{2+}-dependent platination rates were determined for two monovalent ion conditions. One monovalent ion condition had only K^{+} ions present from the 10 mM K_2HPO_4/KH_2PO_4, pH 6.2, buffer (buffer B) and the other solution contained 20 mM $NaClO_4$ in addition to buffer B (buffer B + Na^{+}). Figure 5.2 shows that the platination rates in K^{+} + Na^{+} medium are approximately two-fold lower compared to K^{+}-only medium for all Mg^{2+} concentrations studied except at 1 mM. This result further supports an electrostatic competition between solution cations and complex **1** interacting with RNA, which reduces the overall platination rate.

The addition of 20 mM Na^+ to buffer B decreased the platination rate ($k_{2,app}$) by 6.4-fold for unmodified H69 (compare rows 1 and 6 in Table 5.1, data from Chapter 4). In comparison, the addition of 1 mM Mg^{2+} to buffer B decreased the reaction rate by 13.5-fold for the same H69 RNA (compare rows 1 and 2 in Table 5.1). Similarly, for the modified H69 addition of 20 mM Na^+ to buffer B (compare rows 11 and 16 in Table 5.1, data from Chapter 4) decreased the platination rate ($k_{2,app}$) by 5.4-fold, whereas the rate drop in 1 mM Mg^{2+} (compare rows 11 and 12 in Table 5.1) was 6.8-fold. These data showed that both Na^+ and Mg^{2+} decreased the platination rate, and the impact from Mg^{2+} was higher compared to Na^+, especially for the unmodified construct. Due to its higher charge density that better neutralizes the RNA, Mg^{2+} ion is a stronger electrostatic competitor for Pt^+ than Na^+. Therefore, the rate decrease upon Mg^{2+} addition is greater compared to Na^+. Collectively, these results show an effect from Na^+ and Mg^{2+} in decreasing the platination rates of H69 rRNA hairpins.

The reactions of complex **1** with the two H69 RNAs in the presence of Mg^{2+} showed similar platination rates. In Chapter 4, different platination rates were reported for the two H69 RNAs under low salt conditions. Those results indicated screening of structural differences with added salts, which lead to similar platination rates for the unmodified and modified RNAs. That observation is further supported by the results in this chapter, in which no difference in platination rates was observed under high salt conditions for the two H69 RNAs. Therefore, the impact of Mg^{2+} appears to be larger for unmodified than modified H69 due to the bigger rate differences in the absence of salt.

5.3.2 Determination of Electrostatics of Cisplatin-RNA Interactions in the Presence of Divalent Cations

A number of studies have shown the importance of electrostatics on platinum drug-nucleic acid interactions [163-166,168,173,175,176,179,180]. Using a similar approach, Mg^{2+}-dependent platination kinetic data were analyzed according to the Brønsted-Debye-Hückel and polyelectrolyte theories as described in Chapter 2, Section 2.6.1. These analyses provide information regarding the electrostatic properties of the RNAs. According to the Brønsted-Debye-Hückel theory, the product of reactant charge (Z_AZ_B) and k_0, the limiting platination rate at infinite dilution can be determined (Equation 2, Chapter 2) [244,305]. Evaluation of the platination kinetics according to the polyelectrolyte theory by a logarithmic plot of $k_{2,app}$ versus total cation concentration, $[M^{+/2+}]$ (*i.e.*, the sum of cation concentrations in each addition of Mg^{2+} to corresponding monovalent solutions), allowed determination of the fraction of counterions condensed per phosphate ($n\Psi'$) on the RNA surface (Equation 3, Chapter 2).

The Mg^{2+}-dependent platination kinetics in both monovalent ion conditions can be explained by the two electrostatic theories. The equations after fitting the data to electrostatic models and the corresponding R^2 values are given in Figure 5.4. The Z_AZ_B, log k_0, and $n\Psi'$ values determined by the two electrostatic models are provided in Table 5.2. Figure 5.5 shows a comparison of the electrostatic parameters determined in the presence of Mg^{2+} (buffer B titrated with Mg^{2+} and buffer B + Na^+ titrated with Mg^{2+}) to those obtained and reported in Chapter 4 (absence of Mg^{2+}, in which buffer B was titrated with Na^+) for the two H69 RNA

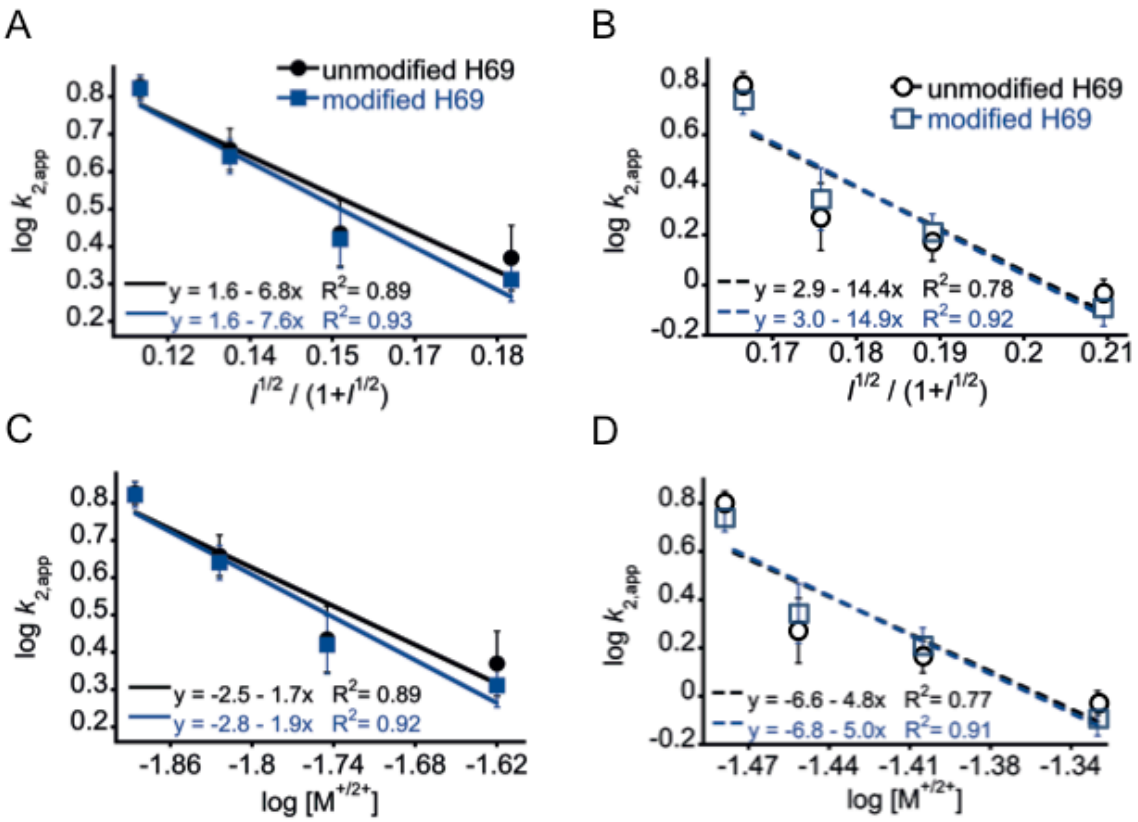

Figure 5.4. Evaluation of salt-dependent platination kinetics of H69 RNAs with two electrostatic models is shown. The Brønsted-Debye-Hückel plots for A) buffer B and B) buffer B + Na^+ (ionic strength is changed by addition of Mg^{2+}) are shown. The graphs using the polyelectrolyte theory in C) buffer B and D) buffer B + Na^+ are shown. The total cation concentration, [$M^{+/2+}$], was varied by adding Mg^{2+}.

Table 5.2. A comparison of electrostatic parameters determined by Brønsted-Debye-Hückel (Z_AZ_B and log k_0) and polyelectrolyte ($n\Psi'$) theories for the H69 hairpin RNAs in different cationic conditions.

Oligonucleotide	Cation Conditions	Z_AZ_B	log k_0	$n\Psi'$
unmodified H69	[a]buffer B + Mg^{2+}	-6.5 ± 0.4	1.6 ± 0.1	1.7 ± 0.1
	buffer B + Na^+ + Mg^{2+}	-13.8 ± 1.0	2.9 ± 0.2	4.8 ± 0.4
	buffer B + Na^+	-9.5 ± 1.5	2.7 ± 0.5	1.5 ± 0.2
modified H69	[a]buffer B + Mg^{2+}	-7.2 ± 0.1	1.6 ± 0.1	1.9 ± 0.1
	buffer B + Na^+ + Mg^{2+}	-14.2 ± 1.8	3.0 ± 0.3	5.0 ± 0.5
	buffer B + Na^+	-8.7 ± 0.5	2.5 ± 0.2	1.4 ± 0.1

[a] buffer B: 10 mM K_2HPO_4/KH_2PO_4, pH 6.2

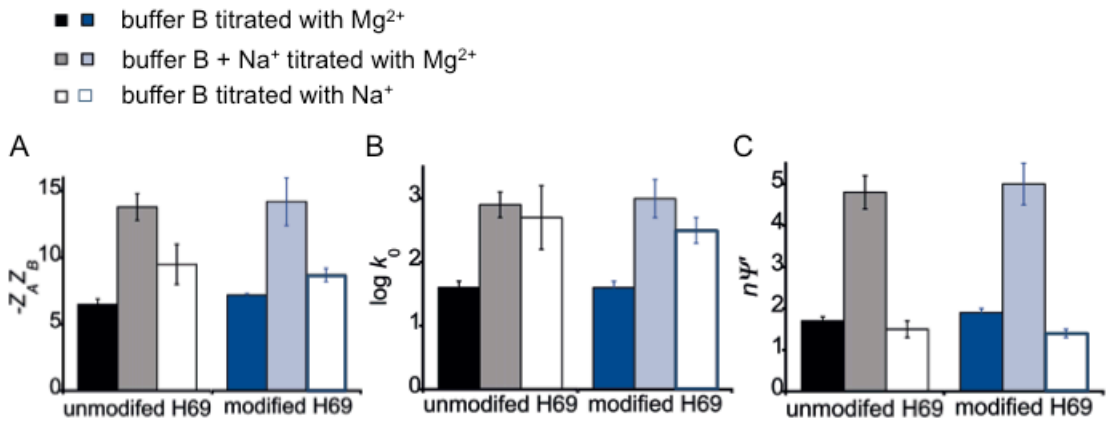

Figure 5.5. Comparisons of electrostatic parameters derived from different salt-dependent kinetic studies are shown. The A) $-Z_AZ_B$ and B) log k_0 values obtained using the Brønsted-Debye-Hückel theory and C) $n\Psi'$ values found employing the polyelectrolyte theory are shown. The data represented by solid (black, blue) and shaded (grey, light blue) bars were obtained in buffer B and buffer B + Na^+ titrated with Mg^{2+}, respectively, in this chapter. The open white bars show the data obtained in Chapter 4, in which buffer B was titrated with Na^+.

models. The electrostatic parameters were similar for the two H69 RNAs (unmodified and modified) for all the conditions studied. The highest Z_AZ_B and $n\Psi'$ values were found when buffer B + Na^+ was titrated with Mg^{2+}. The log k_0 was also about 1.5-fold higher in those same conditions compared to the absence of Na^+, but similar to conditions with buffer B titrated with Na^+ only.

When a reduction in the reaction rate with increasing ionic strength is observed, the Brønsted-Debye-Hückel theory, which is related to the activated-complex-theory (Chapter 2), suggests a reaction between unlike ions that goes through a less-charged state [17]. The increasing ionic strength poorly stabilizes the less-charged state and increases the activation energy, thereby reducing the reaction rate [17]. Therefore, the decreasing platination rate with increasing ionic strength is consistent with a reaction between negatively charged RNA and positively charged complex **1** (Figure 5.4). Such a reaction provides a negative

slope in the Brønsted-Debye-Hückel plot, which gives a negative Z_AZ_B value (Figure 5.4 and Table 5.2). The Z_AZ_B value indicates the charge of the reactants interacting in a chemical reaction. Therefore, in this study the Z_AZ_B values represent the charge of complex **1** and charge density of H69 RNA. The negative Z_AZ_B values are consistent with other studies [173,176] and data from Chapter 4. Since the charge of the platinum complex **1** is +1, the product Z_AZ_B represents the charge density of the reacting H69 RNAs. The highest Z_AZ_B values were observed for buffer B + Na^+ titration with Mg^{2+} (Table 5.2 and Figure 5.5A shaded bars). The Z_AZ_B values were about 1.4–2.1-fold lower for buffer B titrated either with Mg^{2+} or Na^+ (Figure 5.5A solid and open bars, respectively). This result shows that a cation combination that includes K^+, Na^+, and Mg^{2+} has the highest Z_AZ_B value followed by K^+ with Na^+ and K^+ with Mg^{2+}, indicating an increased effect from Na^+ and Mg^{2+} on the charge density of H69 RNA. Table 5.3 lists previously reported Z_AZ_B values for RNA and DNA. For the phosphorothioate oligomers in which Na^+ or Mg^{2+} ions were used as the prominent cations, the Z_AZ_B values were dependent on the choice of counterions in the reaction medium [173]. It should be noted, however, that the platination compounds used in those studies are different from complex **1**. Similar to previous studies, data presented in this chapter shows that cation choice influences the Z_AZ_B value. Extending this knowledge, the current study shows that Na^+ and Mg^{2+} combined increase the Z_AZ_B values, hence the RNA charge density, than when they are present individually.

Table 5.3. Reported Z_AZ_B values for nucleic acids under different cation conditions [173,176].

Nucleic acid	Predominant cation	Pt cmpd	Z_AZ_B
r(CGCGUUGUUCGCG)	Na^+	**2**	-3.7 ± 0.2
		3	3.7 ± 0.1
d(CGCGTTGTTCGCG)	Na^+	**2**	-3.8 ± 0.1
		3	-3.4 ± 0.4
$d(T_8p(S)T_8)$	Na^+	**2**	-4.9 ± 0.5
	Mg^{2+}	**2**	-3.6 ± 0.8
$d(T_8p(S)T_8)$	Na^+	**2**	-5.0 ± 0.8
	Mg^{2+}	**2**	-4.0 ± 0.2

2 = *cis*-$[PtCl(NH_3)(c\text{-}C_6H_{11}NH_2)(OH_2)]^+$; **3** = *trans*-$[PtCl(NH_3)$ (quinoline)$(OH_2)]^+$

The k_o is obtained as the intercept when graphing the data according to the Brønsted-Debye-Hückel theory. This value represents the limiting reaction rate or the platination rate at infinite dilution conditions. Such a condition provides the intrinsic reaction rate in the absence of electrostatic screening by the counterions. The highest log k_0 values observed for buffer B + Na^+ titrated with Mg^{2+} and buffer B titrated with Na^+ conditions (Figure 5.5B, shaded and open bars) indicate that K^+, Na^+, and Mg^{2+}, and K^+ and Na^+ cation combinations have the greatest electrostatic suppression of the platination rates. The 1.8-fold lower log k_0 value of buffer B titration with Mg^{2+} (Figure 5.5B, solid bars) indicates that the electrostatic impact from the K^+ and Mg^{2+} combination is lower compared to the other two conditions.

The $n\Psi'$ value indicates the fraction of counterions condensed on the oligomer surface. In this chapter, highest $n\Psi'$ value was obtained when buffer B + Na^+ was titrated with Mg^{2+} (Figure 5.5C, shaded bars). The $n\Psi'$ values for buffer B titrated with Mg^{2+} and Na^+ separately (Figure 5.5C, solid and open bars, respectively) are similar to each other and 2.6–3.5-fold lower than in buffer B +

Na^+ titrated with Mg^{2+}. As mentioned previously, due to the higher charge to volume ratio compared to monovalent ions, Mg^{2+} more effectively screens the negative charge of RNA. Therefore, twice the amount of K^+ ions are needed to screen RNA charge as Mg^{2+} [93]. However, this is applicable to situations in which mono- and divalent cations are used separately. The behavior of mono- and divalent ions in mixtures are more complex [93]. The current study showed that whereas in mixtures of K^+/Mg^{2+} (buffer B titrated with Na^+) and K^+/Na^+ (buffer B titrated with Na^+) the $n\Psi'$ values are similar, the $n\Psi'$ value is higher in the mixture of $K^+/Na^+/Mg^{2+}$ (buffer B + Na^+ titrated with Mg^{2+}). This result indicates that Na^+ and Mg^{2+} in combination have a higher counterion condensation compared to when they are present individually.

When comparing the platination rates, reactions in buffer B + Na^+ titration with Mg^{2+} were 1.6–2.5-fold slower compared to those in buffer B titrated with Mg^{2+}. The former condition showed a 2.6–3-fold higher $n\Psi'$ value compared to the latter. These data can be interpreted as the Pt^+ center experiencing a greater competition from the higher amount of condensed counterions constituting K^+, Na^+, and Mg^{2+}, resulting in lower platination rates in buffer B + Na^+ titrated with Mg^{2+} compared to buffer B titrated with Mg^{2+} only conditions.

The highest Z_AZ_B and $n\Psi'$ values were found under buffer B + Na^+ titrated with Mg^{2+}. The number of counterions retained by oligomers has been shown to be determined by the packaging of phosphate charges or the charge density of RNA [93,306]. An increase from 0.84 K^+ to 0.94 K^+ per phosphate going from single stranded poly(U) to double-helical RNA has been observed due to the

close charge packing on the latter molecule [93]. This observation indicates a connectivity between RNA structure and counterion condensation. Consistent with these studies, work reported in this chapter shows that condensed counterions in ionic clouds impact RNA structure and affect the charge density [93]. This result further suggests that the association of cations likely "compresses" (or stabilizes) the RNA molecule and increases the effective charge or charge density of the nucleic acid.

Comparison of Z_AZ_B values of RNAs (Table 5.2) studied in this work to other oligomers (Table 5.3) shows that H69 has higher Z_AZ_B values, thus higher charge density under the studied cation conditions. Similarly, a comparison of the $n\Psi'$ values reported for other RNA and DNA oligomers (Chapter 4, Table 4.3) also indicates higher counterion condensation on H69 RNAs under the studied cationic conditions. Together, the higher Z_AZ_B and $n\Psi'$ values observed for H69 RNAs indicate that these RNAs possess higher electrostatic potentials, which may be preferred for cationic drug targeting.

The Z_AZ_B, log k_0, and $n\Psi'$ values determined in the presence of Mg^{2+} are similar in the bulk range for the two H69 RNAs. This indicates a minimal influence from Ψs on H69 electrostatics in the presence of Mg^{2+}. However, the absence of observable electrostatic differences between the two H69 RNAs in the presence of Mg^{2+} is somewhat surprising. In a 2-aminopurine substituted modified H69 titration with Mg^{2+}, an increased exposure of residue 1913 to solvent was reported with the addition of the divalent ion [105]. Electrostatic properties are dependent on the structure and shape of RNA molecules [18].

Therefore, high exposure of residue 1913 in the presence of Mg^{2+} could change the electrostatics of modified H69 RNA. However, the absence of global electrostatic differences between the two H69 RNAs in the presence of Mg^{2+} as determined by platination kinetics indicates that such electrostatic changes resulting from A1913 exposure are probably localized to the loop region. This observation indicates that platination kinetics are valuable to determine whether local structural changes have an impact on global electrostatics of RNA.

5.4 Summary and Conclusions

In summary, the kinetic data showed a decrease in platination rates with the addition of Mg^{2+} indicating electrostatic competition and steric barriers for Pt^{+} association on RNA. Supporting the findings from Chapter 4, the prominent Mg^{2+}-dependent platination rate decrease observed in K^{+} + Na^{+} conditions compared to K^{+}-only conditions showed that Na^{+} decreases the platination rate. Comparison of the platination rate decrease in the presence of Mg^{2+} determined in this chapter to Na^{+} (Chapter 4) showed that the divalent ion has a greater impact, likely due to higher electrostatic competition with the Pt^{+} center. Therefore, in solutions in which both Na^{+} and Mg^{2+} are present, an increased effect from Mg^{2+} and Na^{+} was observed. The $n\Psi'$ values indicated that an ionic atmosphere composed of K^{+}, Na^{+}, and Mg^{2+} greatly decreases the platination rate compared to K^{+} and Mg^{2+} or K^{+} and Na^{+}, again indicating an increased effect from Mg^{2+} and Na^{+}. The electrostatic data revealed that deposition of cations can "compress" the nucleic acid and increase the RNA charge density. The data did

not indicate a major influence from pseudouridine either on platination rate or on the global electrostatic properties of H69 RNA.

Collectively, these data show that the sequence and global folding likely play a bigger role than local structural deviations in charged ligand-RNA interactions. The combined impact of monovalent and divalent metal ions in regulating the electrostatic environment is important to consider when studying cationic ligand interaction with RNA. As the electrostatic models used in this study take the "non-specifically" associated ions into account, data from this chapter support the significant contribution of such ionic interactions on the structure, stability, and drug reactivity of RNA. This study further revealed the application of platination kinetics as a tool to probe the cation-dependent global microenvironment changes in RNA.

CHAPTER 6

pH-DEPENDENT PLATINATION KINETICS OF RIBOSOMAL RNA HAIRPINS

6.1 Abstract

Biochemical interactions are influenced by various factors including pH. The changes in bulk pH levels can cause protonation/deprotonation of large biomolecules as well as small ligands, which affects their biological interactions. In this chapter, the pH-dependence of H69 RNA platination reactions was studied. The platination rate was higher at pH 5.8 compared to pH 6.8. At each pH, salt dependence of the reaction rate was determined by changing the Na^+ concentration. Platination rates decreased with increasing ionic strength at both pH values. Electrostatic analyses carried out using the Brønsted-Debye-Hückel and polyelectrolyte theories showed higher RNA charge density and counterion condensation at pH 5.8 compared to pH 6.8. The pH-dependent platination kinetics and electrostatics were insensitive to pseudouridine modifications in the H69 RNA constructs. Collectively, this study showed that H^+ ions can influence the platination rates and electrostatics of RNA. These findings provide insight into the pH influence on rRNA platinations and support the application of platination kinetics as a probe to monitor RNA microenvironments at different pH levels.

6.2 Introduction

Structure, dynamics, and function of biomolecules are sensitive to their surrounding environments. Factors that influence the structure and activity of RNA include temperature, concentration and identity of salts, cofactors (such as metal ions), and pH. Both bulk and local pH are important for stability,

conformational changes, ligand binding, and catalysis of RNA [307,308]. RNAs that have been studied with respect to varying pH environments include yeast $tRNA^{Phe}$, *E. coli* $tRNA^{Tyr}$, ribozymes, viral RNAs, and rRNA [309-316]. In one temperature-jump experiment, *E. coli* 5S rRNA showed release of H^+ ions during RNA melting [316].

Bulk ionic strength plays a critical role in pH-dependent nucleic acid dynamics. Salt-dependent studies revealed that for every proton released, ~0.3 K^+ ions are taken up by an A^+•C wobble pair in DNA, indicating that both cations and H^+ ions collectively modulate the dynamics of nucleic acids [317]. A number of pH-dependent platination reactions have been reported to date. The platination rates of 1-methylinosine and inosine with certain platinum compounds decrease with pH [318]. Platination of cytosine, CMP, N1- and N7-bound 1:1 inosine-Pt complexes, 7-methylguanosine, and 7-methylinosine show bell-shaped curves for pH-dependent reactions [318-320]. In contrast to results with individual nucleosides, nucleic acids have shown either insensitivity or a decrease in platination rates with increasing pH [158,164,174]. Platination of chicken erythrocyte DNA with cisplatin has shown no difference in reactivity at pH 6.5 and 7.4 [158]. DNA oligomers with 13 to 16 nucleotides have shown decreasing platination rates with increasing pH [164,174].

In this chapter, platination of H69 rRNAs (unmodified and modified H69) at pH 5.8 and 6.8 was studied. The salt-dependent platination reactivity at each pH was determined by changing the Na^+ concentration. Platination reactions were carried out under pseudo-first-order conditions with the use of excess complex **1**. The

reactions were monitored by using gel assays, and rate constants were determined as described in Chapters 2 and 4. The kinetic data at each pH value were analyzed by Brønsted-Debye-Hückel and polyelectrolyte theories. The platination rate was higher at pH 5.8 compared to pH 6.8 for all Na^+ concentrations studied. Furthermore, addition of Na^+ decreased the reaction rates in both pH conditions. A higher RNA charge density, limiting reaction rate and counterion condensation were observed at pH 5.8 compared to pH 6.8. Perhaps not surprising, these results indicated that RNA microenvironments and corresponding platination reactions are sensitive to bulk pH. This study further revealed the possibility of using platination kinetics to monitor RNA microenvironments in response to changes in bulk pH.

6.3 Results and Discussion

Protonation/deprotonation events can impact the structure and function of biomolecules, as well as the pH-dependent properties of small molecules. In previous studies, modified H69 showed pH-dependent structural changes with a pK_a value of 6.3 ± 0.2 [75,76]. The aquated cisplatin complex **1,** *cis*-diammine(aqua)chloridoplatinum(II) exists in aqua/hydroxo equilibrium with a pK_a value of 6.41 [321,322]. Therefore, solution pH would likely impact the H69-complex **1** interaction. In this chapter, pH-dependent platination rates of H69 RNAs were determined at pH 5.8 and 6.8 as described in Chapter 2, Section 2.5 Given the pK_a of 6.3 ± 0.2 and with the assumption that average conformation may not exist, pH 5.8 and 6.8 were selected to represent the two different conformations of modified H69 in high percentage at each pH. In contrast, the

unmodified H69 did not show conformational shifts with changing pH. Therefore, these pH values were chosen to carry out the platination reactions. Platination kinetics were carried out under pseudo-first-order conditions using excess complex **1**, in which [**1**] >> [RNA]. The platination rate constants were obtained by gel assays. The impact of salt on the platination kinetics at each pH value was determined by varying the Na^+ concentration and evaluating by the Brønsted-Debye-Hückel and polyelectrolyte theories.

6.3.1 Determination of Platination Rate Constants at pH 5.8 and 6.8

The rate of complex **1** reacting with H69 RNAs was monitored by gel assays as described in Chapter 2, Section 2.5. Briefly, after refolding the RNA, the platination reaction was initiated by adding freshly prepared, activated cisplatin, or complex **1**. The pseudo-first-order conditions were maintained by using a 1:10 molar ratio of RNA:complex **1**. Under these conditions, a linear dependence between the reaction rate and complex **1** concentration was observed (Chapter 4, Figure 4.3), and also allowed us to monitor experimentally the faster platination kinetics at the lower pH value of 5.8. The unreacted RNA fraction versus time was fit to a single-exponential decay to obtain the pseudo-first-order rate constant (k_{obs}).

Figure 6.1 shows the autoradiograms of H69 platination reactions carried out at pH 5.8 and 6.8. The addition of complex **1** to RNA produced slower migrating platinated product bands on polyacrylamide gels. The unreacted RNA

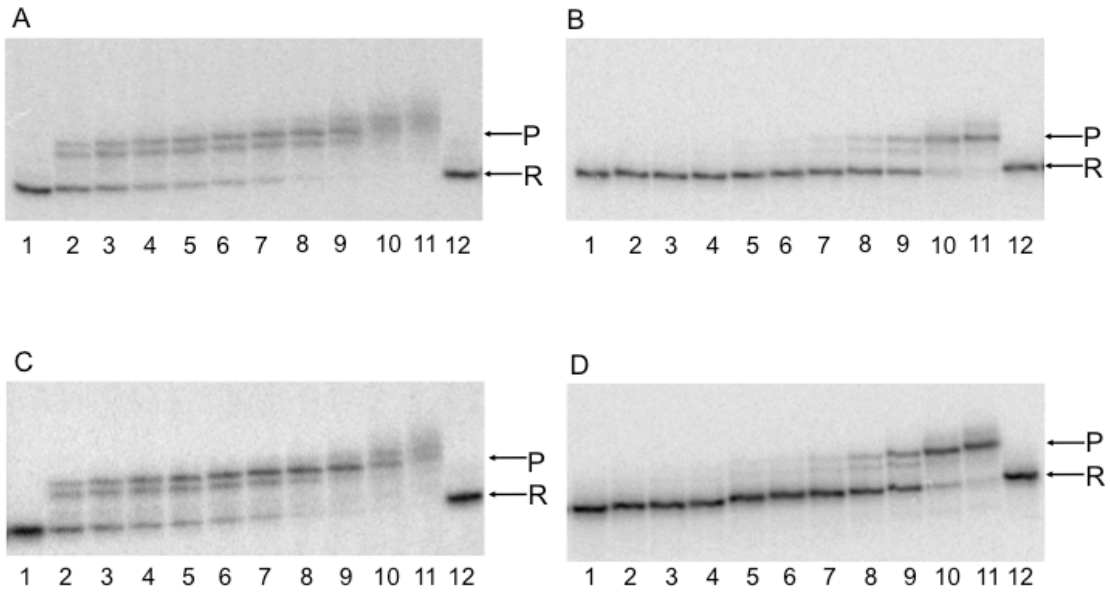

Figure 6.1. The determination of platination rates of H69 RNAs at different pH values is shown. Autoradiograms of unmodified H69 at pH A) 5.8 and B) 6.8, and modified H69 at pH C) 5.8 and D) 6.8 are shown. All gels represent the kinetic experiments carried out in 10 mM K_2HPO_4/KH_2PO_4 and 5 mM $NaClO_4$. R, unreacted RNA, and P, platinated products, in lanes 1-8 (0, 2, 4, 6, 8, 10, 15, 30 min, respectively), lanes 9-11 (1, 3, 6 h, respectively), and lane 12 (6 h con, no Pt) are indicated.

band intensity decreased with time while the intensity of product bands increased. The decrease of unreacted RNA fraction over time was well described by single-exponential decay fits for both H69 RNAs (Figure 6.2). The decrease of unreacted RNA fraction was greater at pH 5.8 compared to pH 6.8 for both H69 RNAs, indicating a faster platination rate at pH 5.8.

The aqua ligand of *cis*-diammine(aqua)chloridoplatinum(II), complex **1,** used in this study has a reported pK_a value of 6.41 for deprotonation (Figure 6.3) [321]. Given this pK_a for complex **1** and assuming that all activated cisplatin species exist between these two forms (without further hydrolyzing to the bis-aquated compound), Henderson-Hasselbalch calculations at pH 5.8 suggest that about

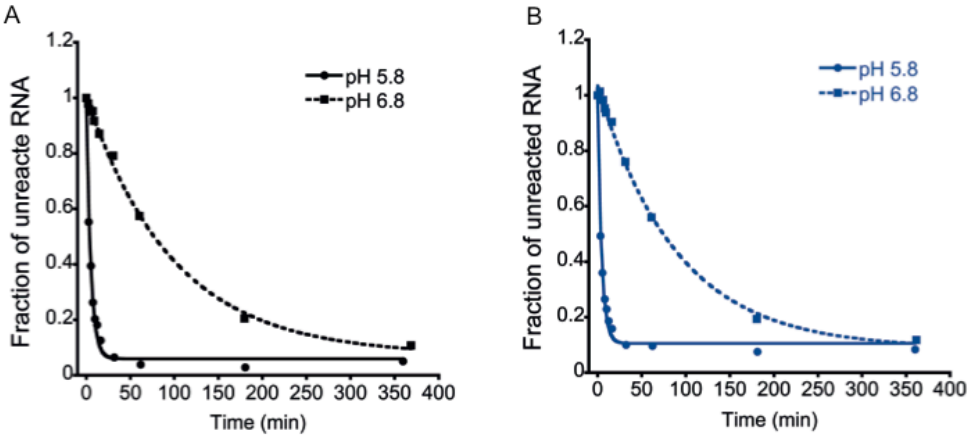

Figure 6.2. Determination of the observed pseudo-first-order rate constant (k_{obs}) for the platination reaction of H69 RNAs at pH 5.8 and 6.8 is shown. The single-exponential decay fits for the unreacted RNA fraction over time for A) unmodified H69 (black) and B) modified H69 (blue) are shown. Both graphs correspond to the kinetic experiments carried out in 10 mM K_2HPO_4/KH_2PO_4 and 5 mM $NaClO_4$. The solid and dashed fits indicate kinetic data obtained at pH 5.8 and 6.8, respectively.

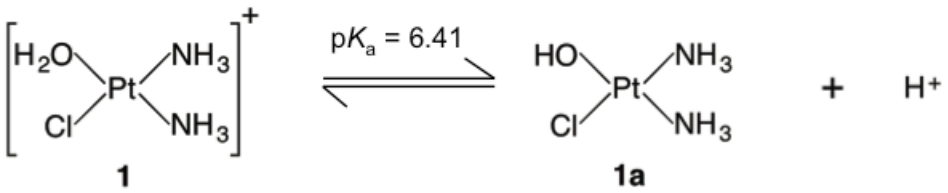

Figure 6.3. The acid-base equilibrium of *cis*-diammine(aqua)chloridoplatinum(II), complex **1**, is illustrated. The aqua ligand of **1** deprotonates to form *cis*-diammine(chlorido)hydroxoplatinum complex, **1a**.

80% of complex **1** exists in the aqua (H_2O) form. At pH 6.8, the percentage of aqua complex drops to about 30%, with formation of the hydroxo complex. The Pt-H_2O bond is kinetically more labile compared to the Pt-OH bond [158,318,323]. Therefore, the aqua complex of cisplatin reacts readily with nucleic acids, whereas the hydroxo complexes are less reactive [151,324]. Hence, the lower platination rates observed at pH 6.8 compared to pH 5.8 likely result from higher amounts of the inactive hydroxo complex at basic pH.

The pH-dependent reactivity profiles for many platinum complexes with different targets are available. In platinations of individual nucleosides 1-methylguanosine, inosine, and 1-methylinosine with $[Pt(dien)(H_2O)]^{2+}$, *cis*-$[Pt(NH_3)_2(H_2O)_2]^{2+}$, and *trans*-$[PtCl(NH_3)_2(H_2O)]^{+}$, the reaction rates decreased with increasing pH [318,320,323,325]. Similarly, several reports showed pH-dependent reactivity of nucleic acid-platinum interactions. For examples, the rate constants for reactions between phosphorothioate-containing poly(T) and *cis*-$[Pt(NH_3)(NH_2C_6H_{11})Cl(OH_2)]^{+}$ decreased with increasing pH [164]. Platination of a small DNA hairpin with *cis*-$[Pt(NH_3)(NH_2C_6H_{11})Cl(OH_2)]^{+}$ showed a lower reaction rate at pH 6.3 compared to pH 4.1 for a range of salt concentrations studied [174]. In all of these cases in which the platination rates declined with pH, the results were interpreted as a consequence of inactivation of the aqua platinum complexes by deprotonation at high pH. Therefore, consistent with previous reports, the lower platination rate observed at pH 6.8 compared to pH 5.8 could originate due to the generation of inactive hydroxo platinum complexes at high pH.

An alternative hypothesis is that high surface H^+ concentrations near platinum targets increase the reaction rates by forming aqua complexes. Mathematical calculations have shown high H^+ concentrations in the major groove near N7 of G of a G–C base pair [111]. The local pH values were found to decrease by 2-3 pH units near the base pair when the bulk pH was 7.5 [111]. The pH maps calculated at pH 5.7 or 7.0 showed that acidity near the surface of B-DNA was higher than the bulk pH [112]. This result indicated that low bulk pH levels could

create even lower pH environments near nucleic acids. The presence of such acidic domains was explained due to increased water pK_a values by extremely negative surface electrostatic potentials of DNA [112]. For RNA, which could have even higher electronegative exteriors due to their higher-order structures [18,88], the pH values within local environments could be further lowered. Therefore, such low pH environments near platinum target sites, especially the N7 of Gs to which complex **1** coordination is observed (Chapter 3), could potentially increase the platination rates.

6.3.2 The Impact of Salts on the Platination Rates at Different pH Conditions

The impact of salts on the platination rate of H69 RNAs at pH 5.8 and 6.8 was determined by changing the Na^+ concentration. The observed pseudo-first-order rate constant (k_{obs}) was obtained by single-exponential decay fits (Figure 6.4)

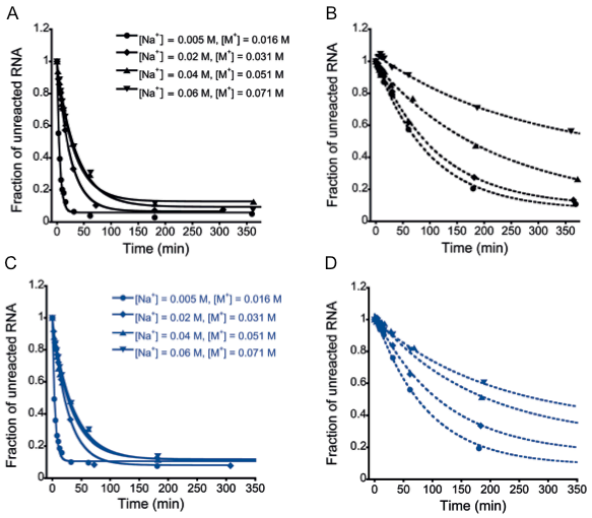

Figure 6.4. The salt-dependent reactivity of H69 RNAs at different pH values is shown. The single-exponential decay fits for the unreacted RNA fraction over time for unmodified H69 (black) at pH A) 5.8 and B) 6.8, and for modified H69 (blue) at pH C) 5.8 and D) 6.8 are shown. The solid and dashed lines represent fittings for pH 5.8 and 6.8, respectively. The pH was maintained by using a 10 mM K_2HPO_4/KH_2PO_4 buffer [233]. The different Na^+ concentrations and total cation concentrations, M^+, are indicated.

as described in Chapter 4. The activated form of cisplatin, *cis*-diammine(aqua) chloridoplatinum(II) or complex **1**, has an acid/base equilibrium with a pK_a value of 6.41 (Figure 6.3) [321]. When determining the apparent second-order rate constant ($k_{2,app}$) under different pH conditions, the acid dissociation of complex **1** was taken into consideration. The acid dissociation equilibrium (Equation 10) and complex **1** binding to RNA (Equation 11) can be written as shown in Scheme 6.1.

$$\mathbf{1} \underset{}{\overset{K_a}{\rightleftharpoons}} \mathbf{1a} + H^+ \qquad (10)$$

$$\mathbf{1} + \text{RNA} \xrightarrow{k_2} \mathbf{1}\text{–RNA} \qquad (11)$$

Scheme 6.1. The acid dissociation equilibrium (K_a) and complex **1** coordination to RNA (k_2).

The acid dissociation constant (K_a) and the rate of platination reaction can be written as;

$$K_a = \frac{[\mathbf{1a}][H^+]}{[\mathbf{1}]} \qquad (12)$$

$$\text{rate} = k_2\,[\mathbf{1}]\,[\text{RNA}]$$

Under pseudo-first-order conditions in which [**1**]>>[RNA], the concentration of complex **1** becomes a constant and the observed rate constant, k_{obs}, is equal to;

$$k_{obs} = k_2\,[\mathbf{1}] \qquad (13)$$

The total platinum concentration [Pt] can be written as;

$$[\text{Pt}]=[\mathbf{1}]+[\mathbf{1a}]$$

$$[\mathbf{1a}] = [\text{Pt}] - [\mathbf{1}] \qquad (14)$$

Substituting Equation 14 into Equation 12 and deriving for [**1**] gives;

$$K_a = \frac{([Pt]-[\mathbf{1}])[H^+]}{[\mathbf{1}]}$$

$$[\mathbf{1}] = \frac{[Pt]\,[H^+]}{K_a + [H^+]} \qquad (15)$$

Substituting Equation 15 into Equation 13, gives a relationship to calculate the experimentally determined apparent second-order rate constant, $k_{2,app}$, by taking the H^+ and thus the pH into consideration (Equation 16) [164].

$$k_{2,app} = \frac{k_{obs}}{[Pt]} \frac{K_a+[H^+]}{[H^+]} \qquad (16)$$

As mentioned previously, the observed pseudo-first-order rate constant, k_{obs}, was determined by fitting the unreacted RNA fraction versus time to a single-exponential decay. Substituting the k_{obs} value into Equation 16 then allows determination of the apparent second-order rate constant ($k_{2,app}$) of platination reactions at different pH levels.

At both pH conditions studied, both RNA constructs showed decreasing reactivity with complex **1** when the total cation concentration, $[M^+]$, was increased in the medium (Figure 6.5). The observed pseudo-first-order and apparent second-order rate constants at different salt conditions for H69 RNAs at pH 5.8 and 6.8 are given in Tables 6.1 and 6.2. A ca. one-order-of-magnitude decrease in platination rate ($k_{2,app}$) was observed for both H69 RNAs between the lowest and highest total cation concentration at pH 5.8. At the same pH, a prominent salt-dependence in the interval of 0.016 to 0.031 M total cation concentration was observed. At pH 6.8, H69 RNAs showed a 2.5–2.3-fold decrease in platination rate ($k_{2,app}$) between the lowest and highest total cation concentration. Therefore,

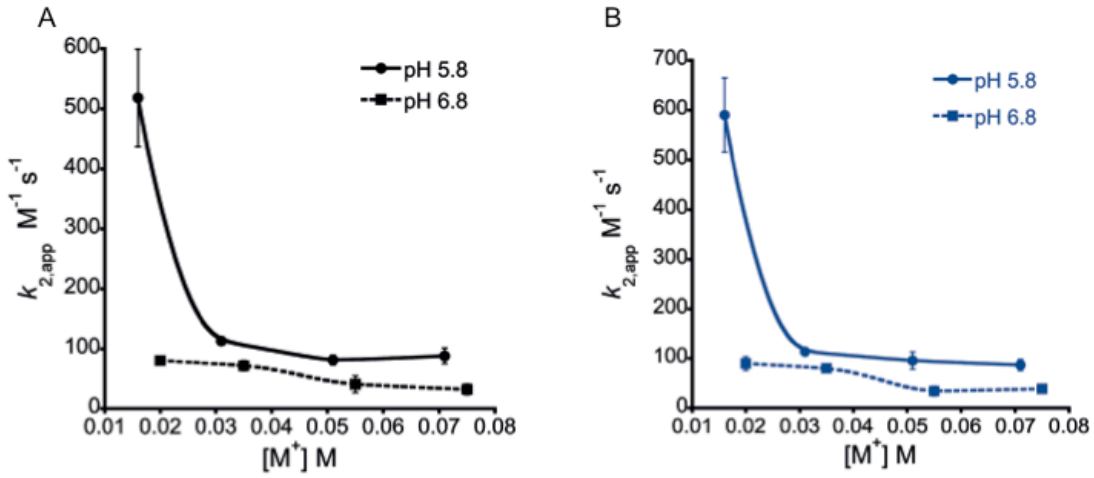

Figure 6.5. The salt-dependent platination rates of H69 RNAs in different pH conditions are shown. The apparent second-order rate constant ($k_{2,app}$) versus the total cation concentration, [M^+], for A) unmodified H69 and B) modified H69 at pH 5.8 and 6.8 is shown. The error bars represent the standard error calculated from two to three independent experiments.

Table 6.1. The observed pseudo-first-order rate constant (k_{obs}) and the apparent second-order rate constant ($k_{2,app}$) of unmodified H69 determined as a function of Na^+ and total cation, M^+, concentrations.

	unmodified H69					
[Na^+][a] (M)	**pH 5.8[b] K^+ = 0.11 M**			**pH 6.8[b] K^+ = 0.015 M**		
	[M^+][c] (M)	**k_{obs} (10^{-4} s^{-1})**	**$k_{2,app}$ (M^{-1} s^{-1})**	**[M^+][c] (M)**	**k_{obs} (10^{-4} s^{-1})**	**$k_{2,app}$ (M^{-1} s^{-1})**
0.005	0.016	27.9 ± 4.3	518.4 ± 80.9	0.020	1.6 ± 0.1	80.4 ± 7.7
0.02	0.031	6.1 ± 0.3	113.2 ± 6.6	0.035	1.4 ± 0.2	72.0 ± 8.5
0.04	0.051	4.3 ± 0.4	81.4 ± 8.3	0.055	0.8 ± 0.3	40.8 ± 14.0
0.06	0.071	4.8 ± 0.7	88.4 ± 13.1	0.075	0.6 ± 0.2	32.2 ± 8.7

[a]Na^+ was added from a $NaClO_4$ solution. [b]The pH was maintained by using a 10 mM K_2HPO_4/KH_2PO_4 solution [233]. [c]Total cation concentration ([M^+]) was calculated by combining Na^+ and K^+ concentrations.

Table 6.2. The observed pseudo-first-order rate constant (k_{obs}) and the apparent second-order rate constant ($k_{2,app}$) of modified H69 determined at different Na^+ and total cation, M^+, concentrations.

	modified H69					
$[Na^+]^a$ (M)	pH 5.8[b] K^+ = 0.11 M			pH 6.8[b] K^+ = 0.015 M		
	$[M^+]^c$ (M)	k_{obs} (10^{-4} s^{-1})	$k_{2,app}$ (M^{-1} s^{-1})	$[M^+]^c$ (M)	k_{obs} (10^{-4} s^{-1})	$k_{2,app}$ (M^{-1} s^{-1})
0.005	0.016	31.7 ± 4.0	590.3 ± 74.4	0.020	1.7 ± 0.2	89.5 ± 13.3
0.02	0.031	6.1 ± 0.3	113.2 ± 5.7	0.035	1.5 ± 0.2	80.0 ± 8.4
0.04	0.051	5.1 ± 0.9	95.5 ± 16.8	0.055	0.7 ± 0.2	34.2 ± 9.6
0.06	0.071	4.7 ± 0.6	86.9 ± 11.0	0.075	0.8 ± 0.1	38.9 ± 3.3

[a]Na^+ was added from a $NaClO_4$ solution. [b]The pH was maintained by using a 10 mM K_2HPO_4/KH_2PO_4 solution [233]. [c]Total cation concentration ($[M^+]$) was calculated by combining Na^+ and K^+ concentrations.

the salt-dependent reactivity at pH 6.8 was not as prominent as pH 5.8. However, a subtle drop in platination rate was observed between 0.035 to 0.055 M total cation concentration. The platination rates and impact of salt on unmodified and modified H69 RNAs were similar at both pH values. Therefore, the presence of pseudouridine did not appear to affect the H69 platination rate or response to salt. For all cation concentrations, the platination rate was higher at pH 5.8 compared to pH 6.8. The largest platination rate ($k_{2,app}$) difference between two pH values was observed at the lowest salt condition (approximately one-order-of-magnitude difference at 0.016 M total cation concentration compared to a 1.4–2.8-fold difference at higher salt concentrations).

Salt-dependent platinations have been rationalized due to the polyelectrolyte properties of nucleic acids [176]. Nucleic acids are highly charged biopolymers

that behave as polyelectrolytes in solution. RNAs acquire high negative charge densities as they fold into compact structures, thus attracting solution cations [188,245,246]. With added salt, the increasing electrostatic competition between the two cations (*e.g.,* Pt^+ and Na^+) to associate with RNA would therefore decrease the platination rate.

The prominent salt dependence of the platination rate observed at pH 5.8 compared to pH 6.8 indicates a sensitivity to H^+ concentration. At low Na^+ concentrations (0.005 M) and low pH (pH 5.8), the platination rate could be high due to the dominant effect from H^+ ions favoring the aqua Pt complexes, and lack of competing cationic species for RNA association. At higher Na^+ concentrations (>0.02 M) and low pH (pH 5.8), the electrostatic competition from Na^+ on Pt^+ would dominate, causing the platination rate to drop. At pH 6.8, in which the H^+ concentration is lowered, the electrostatic competition from Na^+ dominates at all salt conditions, thus lowering the platination rate. The higher platination rate at pH 5.8 compared to pH 6.8 observed in all Na^+ concentrations suggests that H^+ may not be as competitive as Na^+ for Pt^+ to associate on RNA. However, of note is that association of H^+ ions on H69 will also depend on the pK_a values of RNA sites. The lower platination rates at pH 6.8 compared 5.8 could also occur due to reduction of aqua species in the former pH.

The data presented in this chapter showed that platination reactivity at both pH levels is similar between the two H69 RNAs at all salt conditions studied. As shown in Chapter 4, unmodified H69 showed a higher platination rate compared to modified H69 at low salt (<0.052 M total cation concentration). It should be

noted that at pH 6.2, the conditions in which that study was initially carried out, more than one conformation of modified H69 exists (pK_a for the conformational shift was 6.3 ± 0.2 [75]) and both aqua and hydroxo forms of complex **1** (pK_a = 6.41 [321] are present. At low pH, residue A1913 stacks in the helix in a "closed" conformation, whereas at high pH this residue flips out and forms an "open" conformation in modified H69 [75]. Therefore, the lowered platination rate of modified H69 could be a combined effect of about 50% of complex **1** reacting with mixed conformations of modified H69. The pH-dependent conformational study on modified H69 also revealed a slight enhancement (0.5 kcal/mol) in stability at pH 5.5 compared to pH 7.0 [75], which suggests that the closed conformation may not be as reactive towards platination as the open conformation.

At pH 5.8, although a less reactive, closed conformation of modified H69 may dominate, the more reactive and more highly available aqua complex could in turn increase the platination rate of modified H69 comparable to unmodified H69. When the pH is altered to 6.8, the open conformation of modified H69 dominates and may be more reactive towards modifying agents. However, at this pH (6.8), the availability of active complex **1** decreases, thus lowering the platination rate and leading to overall similar rates of platination for the unmodified and modified H69 RNAs. Under high salt conditions, the electrostatic competition from Na^+ towards Pt^+ dominates above all and results in comparable reactivity for the two H69 RNAs. The similar rates observed for the two H69 RNAs in Mg^{2+}-dependent kinetics (Chapter 5) is consistent with such a hypothesis. With the addition of 1

mM Mg^{2+}, which could be an even stronger electrostatic competitor for Pt^{+}, the platination rates between H69 RNAs are similar at pH 6.2. Collectively, these observations indicate that H69 platination reactivity depends on the combined effects from pseudouridylation, presence of cations (Na^{+} and Mg^{2+}), and solution pH, but the individual impacts of these solution conditions are not possible to discern.

6.3.3 Evaluation of Salt-Dependent Platination Rates by Electrostatic Models

Electrostatics are important for the structure and function of biomolecules. Especially for highly charged molecules such as RNA, interactions with charged ligands can be strongly governed by electrostatics. The Brønsted-Debye-Hückel and polyelectrolyte theories can be used to determine the electrostatic properties of charged biopolymers by evaluating their reaction rates at different ionic strengths. Assessment of electrostatics in RNA-ligand interactions can provide valuable information regarding salt-dependent macromolecule dynamics and ligand-binding characteristics.

The analysis of kinetic data according electrostatic models was carried out as described in Chapter 2, Section 2.6.1. Briefly, the logarithm of apparent second-order rate constants (log $k_{2,app}$) determined at different salt conditions was graphed versus $I^{1/2}/(1+I^{1/2})$, in which I is the ionic strength (Chapter 2, Equation 2) to evaluate the kinetics according to the Brønsted-Debye-Hückel theory. A graph of logarithm of apparent second-order rate constants (log $k_{2,app}$) versus logarithm of total cation concentration, $[M^{+}]$ (Chapter 2, Equation 3) was used to analyze kinetic data according to the polyelectrolyte theory. The slope ($Z_A Z_B$) of the

Brønsted-Debye-Hückel plot indicates the charge (Z) of species (A and B) interacting in a reaction, and the intercept (log k_0) denotes the rate constant at infinite dilution conditions. The slope of the polyelectrolyte theory plot gives the $n\Psi'$ value, which reveals the fraction of counterions condensed, or thus displaced by complex **1** binding. Analysis of the salt-dependent platination rates according to the two electrostatic theories is shown in Figure 6.6.

The equations after fitting the data to electrostatic models and their corresponding R^2 values are given in each figure. The quantified electrostatic parameters for the two H69 RNAs at different pH conditions are given in Table 6.3. Figure 6.7 shows a comparison of the electrostatic parameters, Z_AZ_B, log k_0, and $n\Psi'$, for the two H69 RNAs at pH 5.8 and 6.8. All electrostatic parameters were higher at pH 5.8 compared to pH 6.8 for both H69 RNAs. The Z_AZ_B values were 1.6-fold higher at pH 5.8 compared to pH 6.8 for both H69 RNAs. The two H69 RNAs showed 1.3- and 1.7-fold higher log k_0 and $n\Psi'$ values, respectively, at pH 5.8 in comparison to pH 6.8. The electrostatic properties were similar between the two H69 RNAs indicating no effect from pseudouridine on the global H69 electrostatics, which govern the platination reactions.

The Z_AZ_B value given by the Brønsted- Debye-Hückel plot reveals the charge (Z) of species A and B reacting in a chemical reaction. In this thesis work, these values represent the charge of platinum complex **1** and the charge density of H69 RNA. Similar to the results reported in Chapters 4 and 5, the Z_AZ_B values in this pH-dependence study were negative. This observation is consistent for a reaction between oppositely charged ions, the positively charged complex **1** and

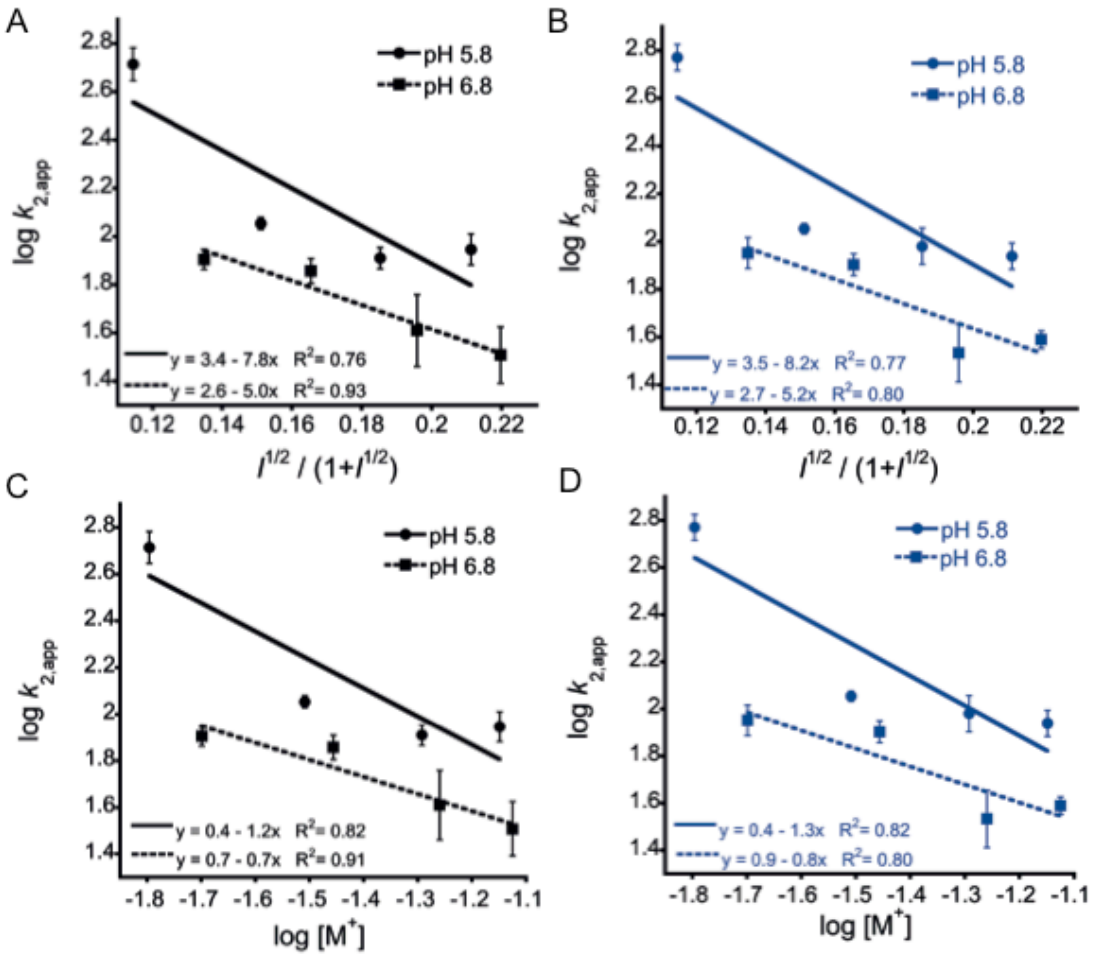

Figure 6.6. Determination of electrostatic properties of H69 RNAs is shown. The plots according to the Brønsted-Debye-Hückel theory for A) unmodified H69 and B) modified H69, and polyelectrolyte theory for C) unmodified H69 and D) modified H69 at different pH conditions are shown.

Table 6.3. The quantified electrostatic properties of H69 RNAs according to the Brønsted-Debye-Hückel and polyelectrolyte theories.

	unmodified H69		**modified H69**	
	pH 5.8	**pH 6.8**	**pH 5.8**	**pH 6.8**
$Z_A Z_B$	-7.5 ± 1.2	-4.8 ± 0.2	-7.8 ± 1.3	-4.9 ± 0.1
log k_0	3.4 ± 0.2	2.6 ± 0.1	3.5 ± 0.3	2.7 ± 0.1
$n\Psi'$	1.2 ± 0.2	0.7 ± 0.1	1.3 ± 0.2	0.8 ± 0.1

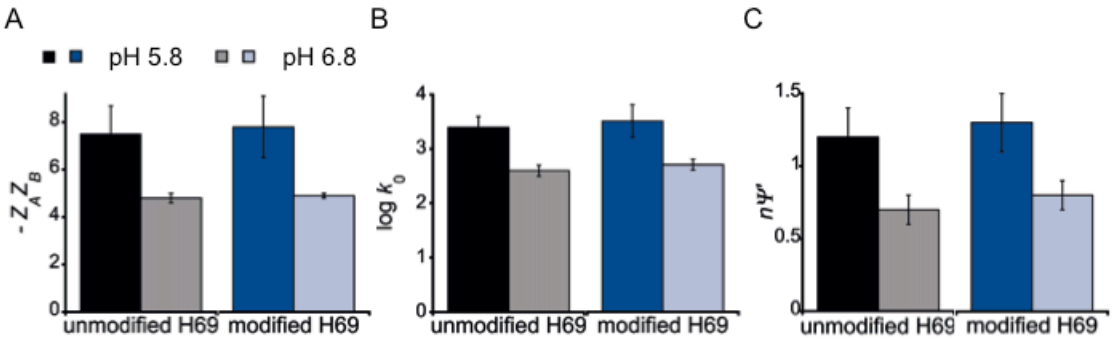

Figure 6.7. Comparisons of the electrostatic parameters at pH 5.8 and 6.8 are shown. The A) $-Z_AZ_B$ and B) log k_0 values obtained from the Brønsted-Debye-Hückel theory and C) $n\Psi'$ values determined from the polyelectrolyte theory are shown. The data represented by solid (black, blue) bars were obtained at pH 5.8 and shaded (grey, light blue) bars were obtained at pH 6.8.

negatively charge RNA. Since, the charge of the reactive platinum complex **1**, *cis*-diammine(aqua)chloridoplatinum(II) is +1, the Z_AZ_B value represents the charge density of H69 RNA.

The more negative Z_AZ_B values for both H69 constructs at pH 5.8 therefore suggests that a higher amount of counterions, including H^+ ions, have deposited and increased the effective charge of RNA. This result further suggests that counterion associations at pH 5.8 may compress or stabilize the RNA molecules and increase the RNA charge density. The higher counterion condensation is supported by the higher $n\Psi'$ values obtained at pH 5.8. The observation of higher Z_AZ_B values at pH 5.8, which contains a higher amount of cationic H^+ ions, compared to pH 6.8 is supported by similar trends reported in Chapter 5. In that chapter, higher Z_AZ_B values were observed at high cationic conditions (buffer B + Na^+ titrated with Mg^{2+}) compared to low cationic conditions (buffer B titrated either with Mg^{2+} or Na^+). Therefore, these comparisons suggest that similar to

metal cations, association of H^+ ions under acidic conditions increases the charge density of RNA.

The limiting rate constant, k_0, obtained as the x-intercept of Brønsted-Debye-Hückel plot, represents the rate constant at infinite dilution. Under such conditions in which electrostatic screening by counterions is absent, log k_0 indicates the intrinsic reactivity of RNA with complex **1**. The log k_0 values determined in this pH-dependence kinetic study are 1.3-fold higher at pH 5.8 compared to pH 6.8 for both H69 RNAs. This result indicates that in the absence of electrostatic influences, counterions, which include H^+ ions, impact the platination rate. This result probably indicates that the higher availability of the aqua complex increases the reaction rate at pH 5.8 in the absence of an electrostatic impact from counterions.

The $n\Psi'$ value determined by the slope of polyelectrolyte plot designates the fraction of counterions condensed on the nucleic acid surface. The current study showed 1.7-fold higher $n\Psi'$ values at pH 5.8 compared pH 6.8. This result indicates that a higher amount of counterions, including H^+ ions, are deposited on the RNA surfaces at pH 5.8. The higher counterion condensation (including H^+ ions) at pH 5.8 observed in this study, is supported by the presence of acidic domains on DNA when the bulk pH is 5.7 [112]. These data indicate that H^+ ions impact the counterion deposition on RNA.

In Chapter 5, the higher counterion condensation observed at higher cationic conditions (buffer B + Na^+ titrated with Mg^{2+}) was partly used to explain the lower platination rate in that medium. Those results indicated that electrostatic

competition between the condensed metal cations such as Na^+ and Mg^{2+}, and Pt^+ lower the platination rate. In contrary, this study shows that under higher acidic levels (pH 5.8), in which higher amount of H^+ ions are condensed, the platination rate is faster compared to low acidic conditions (pH 6.8). This result suggests that condensed H^+ ions may not electrostatically compete with Pt^+ ions to reduce the platination rate. Combined, these results indicate that while metal cations such as Na^+ and Mg^{2+} in condensation layers reduce the platination rates, deposited H^+ ions may not decrease platinum interactions with RNA. As discussed in Section 6.3.2, the higher platination rates observed at pH 5.8 compared to pH 6.8 supports this conclusion.

The higher $n\Psi'$ values observed at pH 5.8, which resemble those at higher counterion condensations, also indicate that a higher fraction of counterions should be displaced during complex **1** binding [176]. The counterion displacements are reported to drive other nucleic acid-ligand interactions by entropic effects [272]. Therefore, faster platination rates observed at pH 5.8 compared to pH 6.8 may originate, at least in part, due to entropic driving forces of counterion displacements. These data provide evidence for the impact of bulk pH levels on the electrostatic properties of RNA, which might modulate the platination binding kinetics. The $n\Psi'$ and Z_AZ_B values of H69 RNAs at pH 5.8 and 6.8 are higher compared to other oligomer systems (Tables 4.3 and 5.3). This observation provides evidence for the higher electrostatic potentials that H69 RNAs carry, which could be useful targets for cationic drugs.

Similar to the results in Chapters 4 and 5, no difference in electrostatic parameters was observed between the two H69 RNAs. However, the modified H69 shows pH-dependent structural conformations, whereas no such dynamics are reported for unmodified H69 [75]. The electrostatics of RNA molecules are dependent on their structures [18]. Hence, pH-dependent structural dynamics of modified H69 RNA could lead to different electrostatic properties compared to unmodified H69. The platination kinetics monitor the global electrostatics of RNA. The absence of electrostatic differences between two H69 RNAs determined by platination kinetics therefore indicates that pH-dependent electrostatic changes in modified H69 may be limited to the loop region. This result indicates that platination kinetics are a valuable tool to monitor the influence of local electrostatic changes on global environments.

6.4 Summary and Conclusions

In summary, this kinetic study showed that bulk pH conditions influence the platination rates of rRNA. The platination kinetics at pH 5.8 were faster compared to pH 6.8. This result was supported by other nucleobase and oligomer platination studies, which reported faster rates at low pH compared to high pH [164,174,318,320,323,325]. This observation was explained due to the formation of inactive hydroxo platinum complexes in which the Pt–OH bond is inert to substitutions compared to the Pt–H_2O bond [318,323]. The existence of acidic domains near nucleic acid surfaces that are 2-3 units lower than bulk pH could also increase the fraction of active cisplatin complexes and increase the reaction rate at pH 5.8 [111,112]. The similar platination rates between the two H69 RNAs

were explained due to combined effects from pH-dependent properties of H69 RNA and cisplatin.

A prominent salt-dependent reactivity was observed at low pH, suggesting that salt-dependence of the platination reaction is also sensitive to H^+ concentration in the medium. However, a more detailed comparison of the salt-dependent platination profiles at pH 5.8 and 6.8 indicated that H^+ ions are not stronger competitors of Pt^+ compared to Na^+. Comparison of Mg^{2+}-dependent (Chapter 5) and pH-dependent platination profiles further supported the idea that H^+ ions are not strong competitors of Pt^+ ions compared to Mg^{2+} and Na^+.

Analysis of salt-dependent kinetics by the Brønsted-Debye-Hückel and polyelectrolyte theories revealed higher RNA charge density and counterion (including H^+ ions) depositions at pH 5.8 compared to pH 6.8. Collectively, these observations suggested that unlike Na^+ and Mg^{2+}, H^+ ions may not decrease the platination rates through electrostatic competitions with Pt^+. However, electrostatic properties of RNA depend on the H^+ ion conditions in the medium. The log k_0 data indicated that in the absence of electrostatic influence by H^+ ions, the greater abundance of aqua platinum complexes could increase the platination rates. The electrostatic properties between the two H69 RNAs were similar. This result indicated that electrostatic changes originating from pH-dependent structural changes in modified H69 may be limited to the loop region.

In conclusion, the current study showed that H^+ ions impact platination reactions via combined effects on platinum compounds and RNA. These findings provided insight into a more detailed mechanism of platinum complex binding to

RNA. Further, this study showed the application of platination kinetics to probe RNA electrostatics under different acidic environments.

CHAPTER 7

THE INVESTIGATION OF AMINOGLYCOSIDE-RNA INTERACTIONS USING PLATINATION KINETICS

7.1 Abstract

Cationic antibiotics such as aminoglycosides target many RNAs. Biochemical and computational studies have revealed that electrostatic interactions play an important role in aminoglycoside mode of action. In this chapter, platination kinetics were applied to probe an aminoglycoside-H69 interaction. Platination rates were monitored on H69 RNAs with or without pseudouridine modification pre-incubated with aminoglycoside. The complex **1** binding rate decreased in the presence of RNA-neomycin interactions. The fold-decrease in platination rate was higher for unmodified H69 compared to modified H69. This study revealed the application of platination kinetics to evaluate the impact of pseudouridine on RNA-aminoglycoside interactions.

7.2 Introduction

Since the early 1960s, aminoglycosides have been used to treat bacterial infections [326]. They are bactericidal antibiotics that bind primarily to rRNA regions in the ribosome [117,327]. Aminoglycosides have been identified to bind to the A site of 30S subunits in bacterial ribosomes [117,327]. Aminoglycoside-A-site interactions interfere with the tRNA anticodon-mRNA codon recognition [328]. This leads to misincorporation of amino acids into the growing polypeptide chain and reduces the accuracy of translation [329]. Neomycin, one of the aminoglycosides that targets the bacterial ribosome, also binds to H69 of the 50S subunit (Figure 1.22) [127]. The neomycin-H69 interaction interferes with subunit

rotation and also impacts the ribosome recycling process [106,127]. Fluorescence studies using 2-aminopurine-containing H69 RNAs have shown conformational changes upon aminoglycoside binding [105]. Beside rRNA, aminoglycosides also bind to introns, ribozymes, and HIV RNAs [131,330-333].

Aminoglycosides are a class of antibiotics that contain 2-deoxystreptamine-containing (2-DOS) amino sugars. The chemical structure of neomycin (aminoglycoside used in this study) is shown in Figure 7.1. Aminoglycosides contain 5 to 6 amino groups. The pK_a values of the amino groups range from 5.7-9.5 [120,121]. Therefore, aminoglycosides exist as oligocations at physiological pH. As highly charged polycations, electrostatics are important for aminoglycoside interactions with RNA. Many experimental and theoretical studies have shown that aminoglycoside binding is strongly governed by electrostatic interactions via charged amino groups [122-126,136,330].

The work reported in this chapter focused on probing neomycin-H69 interactions using platination kinetics. The H69 RNAs (unmodified and modified H69) were incubated with neomycin prior to platination. Platinations were carried out under pseudo-first-order conditions. The platination kinetics were monitored using gel assays. The observed pseudo-first-order rate constant (k_{obs}) and apparent second-order rate constant ($k_{2,app}$) was determined as described in Chapter 2, Section 2.5. Platination rates were lower in the presence of aminoglycoside-RNA complexes compared to RNA alone. The fold-decrease of platination rate was higher in unmodified H69 compared to modified H69.

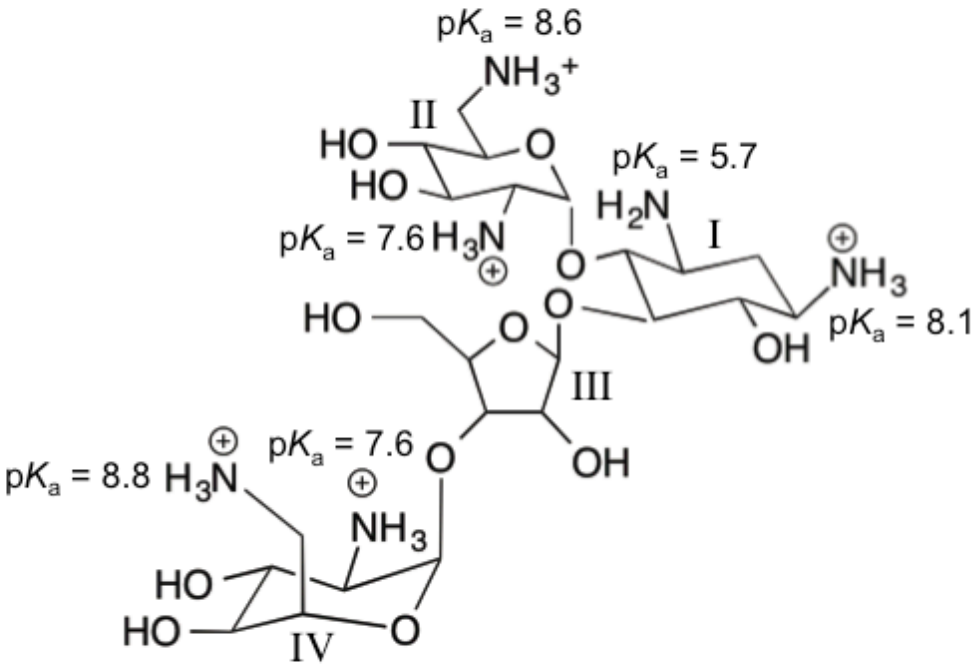

Figure 7.1. The chemical structure of neomycin at pH 7 is shown. The pK_a values of amino groups are indicated [131]. The aromatic ring numbering system is denoted in Arabic numerals. Ring I is the 2-deoxystreptamine moiety (2-DOS).

7.3 Results and Discussion

Many researchers have reported that electrostatic interactions are crucial for RNA-aminoglycoside interactions [122-126,136]. With the aim of testing the application of platination kinetics to probe aminoglycoside-RNA interactions, complex **1** binding rates to antibiotic-bound, modified and unmodified H69 RNAs were determined in this chapter. Experimental details are given in Chapter 2, Section 2.5. Briefly, after incubating H69 RNAs with neomycin at 37 °C for 30 min, complex **1** was added to initiate the platination reaction. The platination kinetics was monitored under pseudo-first-order conditions. The ratio of complex **1** to RNA was 1 to 268, which allowed us to experimentally determine the slower platination rates in the presence of highly cationic neomycin. Aliquoted reaction

mixtures at different time intervals were run on polyacrylamide gels, and unreacted and platinated RNA was quantified. Single-exponential decay fits were used to obtain the observed pseudo-first-order rate constant, k_{obs}. The apparent second-order rate constant ($k_{2,app}$) was determined by using $k_{2,app} = k_{obs}/[\mathbf{1}]_{t=0}$ relationship.

The addition of complex **1** to the neomycin-H69 complex resulted in a decrease of the unreacted RNA band with time (Figures 7.2A and B). The decrease of unreacted RNA with time is well explained by single-exponential decay fits (Figures 7.2C and D), and was used to obtain the observed pseudo-first-order rate constants. The observed pseudo-first-order, k_{obs}, and apparent second-order rate constant, $k_{2,app}$, values are given in Table 7.1. Standard errors were calculated using two or three independent experiments.

In the absence of neomycin, the platination rates between the two H69 RNAs were similar. Due to the slower platination rate in the presence of neomycin, a higher ratio of cisplatin:RNA was used in this work compared to Chapter 4. This change can lead to a higher amount of active complex **1** compared to conditions used in Chapter 4. The platination rate of unmodified H69 is similar to that reported in Chapter 4 under the same cation conditions (Table 4.1, 10 mM K_2HPO_4/KH_2PO_4, pH 6.2 and 20 mM $NaClO_4$). However, under the same salt conditions, the platination rate of modified H69 was 1.7-fold slower than the

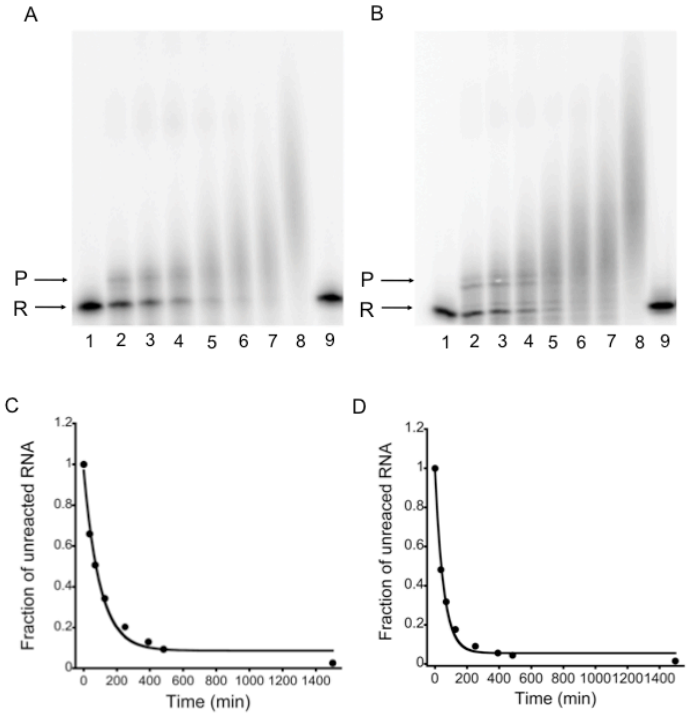

Figure 7.2. Kinetics of cisplatin binding to H69-neomycin complex is shown. Autoradiograms of A) unmodified H69 and B) modified H69 incubated with 1 μM neomycin are shown (R: unreacted RNA; P: slower migrating platinum products; [RNA] = 0.7 μM, [**1**] = 188 μM; 10 mM K_2HPO_4/KH_2PO_4, pH 6.2, and 20 mM $NaClO_4$). Lanes 1-3; 0, 15, and 30 min, respectively; lanes 4-9; 1, 3, 6, 8, 24, and 24 h control, respectively are indicated. The single-exponential decay fits for the disappearance of unreacted RNA for C) unmodified H69 and D) modified H69 versus time are shown.

Table 7.1. The observed pseudo-first-order (k_{obs}) and apparent second-order ($k_{2,app}$) rate constants for the reaction between complex **1** and neomycin-incubated RNA.

Oligonucleotide	[Neomycin] (μM)	k_{obs} (10^{-4} s^{-1})[a]	$k_{2,app}$ ($M^{-1}s^{-1}$)[b]
unmodified H69	0	28.8 ± 2.7	15.3 ± 1.4
	1	1.7 ± 0.3	0.9 ± 0.2
	3	1.1 ± 0.1	0.6 ± 0.1
	6	1.3 ± 0.3	0.7 ± 0.2
modified H69	0	25.1 ± 2.2	13.3 ± 1.2[c]
	1	3.0 ± 0.5	1.5 ± 0.2
	3	1.4 ± 0.1	0.8 ± 0.1
	6	1.3 ± 0.5	0.7 ± 0.3

[a] All rate constants were determined in 10 mM K_2HPO_4/KH_2PO_4, pH 6.2, and 20 mM $NaClO_4$ at 37 °C. [b] $k_{2,app}$ was determined by using $k_{2,app} = k_{obs}/[\mathbf{1}]_{t=0}$ relationship.

unmodified H69. The pH-dependent platination study carried out in Chapter 6 suggested that the availability of active aqua complex could affect the platination rate of modified H69. The pH value used in Chapter 4 and in this chapter was the same (6.2), but the complex **1**:RNA ratio was higher in the latter. Therefore, the higher platination rate observed for the modified H69 in this chapter could be due the presence of a higher amount of aqua complex **1** present in the medium compared to the conditions used in Chapter 4.

Upon addition of neomycin, the platination rate of H69 RNAs decreased (Figure 7.3A). Specifically, a ca. one-order-of-magnitude rate decrease was observed with the addition of 1 μM neomycin to both H69 RNAs (Table 7.1). At 1 μM neomycin, the platination rate ($k_{2,app}$) of modified H69 was 1.7-fold faster compared to unmodified H69. Except 1 μM neomycin, in all other concentrations the platination rates between the two H69 RNAs were similar in the bulk range. In the 2-aminopurine substituted studies, A1913 in modified H69 showed increased fluorescence intensity with neomycin binding [105]. This result suggested that with neomycin binding, A1913 flips out of the H69 loop, which forms a structure similar to the "open" conformation. This conformation is slightly less stable [75] and probably less constrained. Therefore, the higher platination rate observed after neomycin binding to modified H69 could be due to this less constrained structure. With further addition of aminoglycoside, the increasing competition between highly cationic neomycin and Pt^{+} may decrease the platination rates (similar to data observed in the Mg^{2+} dependence kinetic study) resulting in comparable reactivities between the two H69 constructs.

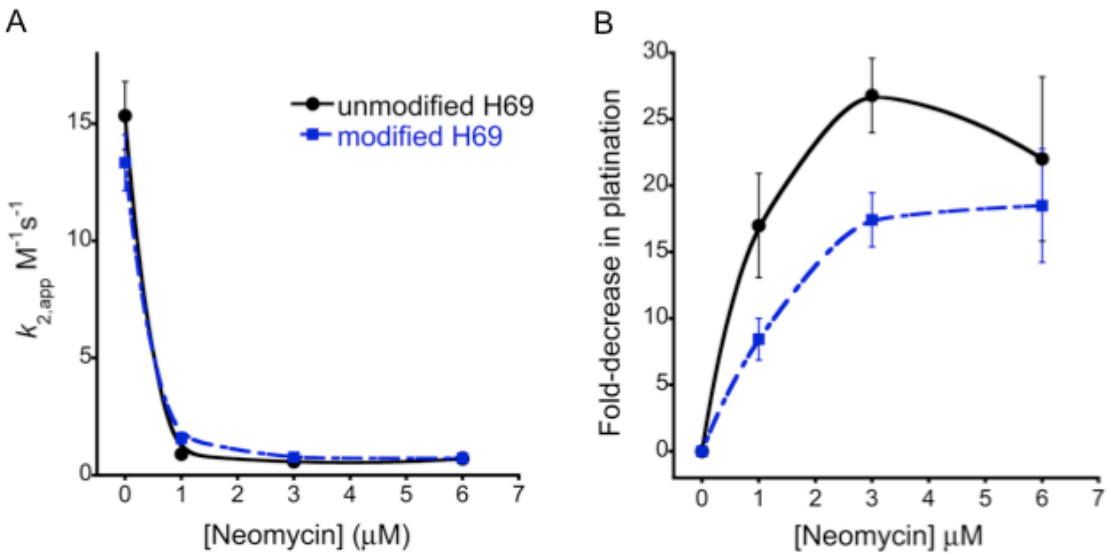

Figure 7.3. The platination of the H69-neomycin complex is shown. A) The decrease of apparent second-order rate constant ($k_{2,app}$) with increasing neomycin concentration is shown. B) The fold-decrease of platination rate ($k_{2,app}$) versus neomycin concentration is shown.

The decrease of platination rate upon addition of neomycin is not surprising. Crystallographic studies have revealed neomycin binding to the H69 stem, with ring II closely interacting with G1906, G1921, and G1922 through the major groove (Figure 1.22) [127]. Complex **1**, as shown in Chapter 3, also binds to these residues of H69. According to studies with DNA, cisplatin accesses the base N7 through the major groove [149]. Therefore, preoccupation of the same target site by neomycin would be expected to decrease the platination rate. Neomycin could carry at least a +5 charge at pH 6.2, the conditions in which this kinetic study was carried out. The active form of cisplatin, complex **1,** carries only a +1 charge (Figure 2.5). Therefore, the higher charge of neomycin could reduce the platination rate by electrostatic competition.

To compare the inhibitory effect of neomycin on platination, the fold-decrease of complex **1** reactivity ($k_{2,app}$) was determined (Figure 7.3B). A ca. 16, 26, and 22-fold decrease in unmodified H69 and 8, 17, and 18-fold decrease in modified H69 was observed by adding 1, 3, and 6 μM neomycin, respectively. Therefore, the fold-decrease of platination rate is lower for modified H69 compared to unmodified H69. As mentioned previously, the binding of neomycin to modified H69 forms an "open" conformation, which is likely less constrained. No such conformational change is reported for unmodified H69. Therefore, the "open" conformation could react faster with complex **1** compared to slightly more stable "closed" conformation. Hence, the fold-decrease of platination rate for modified H69 could be less compared to unmodified H69. The similar fold-decrease at higher neomycin concentrations (6 μM) may indicate a strong electrostatic competition from the aminoglycoside towards Pt^{+}.

7.4 Summary and Conclusions

Aminoglycosides are used to treat many bacterial infections [326]. Their primary mode of action results from binding to rRNA [117,327]. Electrostatic interaction between aminoglycoside amino groups and RNA is crucial for drug binding and inhibition [122-126,136,330]. In this chapter, the neomycin-H69 RNA interaction was probed using platination kinetics. The study revealed slower platination rates in the presence of neomycin. The platination rate of modified H69 at low neomycin concentrations (1 μM) was 1.7-fold higher compared to unmodified H69. This result was explained due to the less-constrained structures that might occur in modified H69 after neomycin binding. The inhibitory effect

from neomycin was determined by using the fold-decrease of platination rate. The unmodified H69 showed higher fold-decrease in platination rate compared to modified H69. This result further supported the hypothesis of a fast-reacting and less-constrained structure of neomycin-bound modified H69, which leads to a lower-fold-decrease in platination due to electrostatic competition. Collectively, this work supports the application of platination kinetics to probe Ψ-dependent drug reactivities of H69 RNAs, although further work is needed to have a better understanding of this system.

CHAPTER 8

OVERALL CONCLUSIONS AND FUTURE DIRECTIONS

8.1 Overall Conclusions

RNA is essential for many biological functions. Therefore, RNA is an effective drug target [334]. Although well known to bind to DNA, many recent studies report that cisplatin can also coordinate to RNA [149,150]. Detailed kinetic studies on RNA-cisplatin interactions are limited. In this thesis work, a broad kinetic study was carried out to investigate the platination of rRNA. The application of this kinetic study is two-fold. The kinetic data are useful to understand the impact of intrinsic RNA characteristics such as modified nucleotides and sequences, as well as bulk conditions such as cations and pH, on platination reactions. The analysis of kinetic data by Brønsted-Debye-Hückel and polyelectrolyte theories was used to illustrate the application of platination kinetics as a probe to interrogate RNA microenvironments.

Three model RNA hairpins were selected representing the *E. coli* ribosome. Helix 69 (H69) of the large ribosomal subunit is essential for protein synthesis and a known drug target [65]. The wild-type H69 carries three pseudouridine (Ψ) modifications in the loop, which are implicated in structural dynamics [74,75]. The impact of pseudouridine on platination kinetics was evaluated by using two H69 models: unmodified H69 (without pseudouridine) and modified H69 (with pseudouridine). The 790 loop in the small subunit is important for translation and also a known antibiotic target [79-82,129]. The size and nucleotide composition of the 790 loop is identical to unmodified H69, but the sequence is different.

Therefore, these models allowed us to evaluate the impact of Ψs and RNA sequence on platination kinetics.

Prior to kinetic studies, the platinum targets on each RNA were identified using RNase T1 mapping with MALDI MS, and dimethyl sulfate (DMS) probing (Chapter 3). Consistent with DNA platination profiles [150], MALDI MS and chemical probing revealed that GpG sites are the likely targets of cisplatin. Chemical probing further revealed a structural impact on rRNA by platination, which was also dependent on pseudouridylation and RNA sequence.

The structure of the ribosome is crucial for protein synthesis [335]. Nucleotide modifications in rRNA are located in the functionally important regions of the ribosome [72]. The sequence determines the higher-order structure of RNA, which ultimately impacts the ribosome function [64,271]. Therefore, rigidity or alterations to rRNA structure after platinum coordination can impact translation. Initial studies by Rosenberg have shown inhibitory effects of cisplatin on protein synthesis [253]. Structural effects from platinum complex binding to DNA have been implicated in the drug mode of action [151]. Sharp bends induced by cisplatin coordination in DNA were shown to recruit HMG-domain proteins, which prevents them from their normal cellular functions and sequesters platinum adducts from repair proteins [151,336,337]. HMG proteins are also reported to bind to RNA [338]. Therefore, cisplatin-induced structural changes in rRNA may recruit similar proteins that could ultimately contribute to drug cytotoxicity.

The kinetic study was carried out with two objectives. First, a broad kinetic study was designed to gain insight on RNA platination reactions, for which only

limited reports are available. The kinetic study reported in Chapter 4 showed that changes in rRNA structures due to Ψs can lead to subtle differences in platination rates, under low salt concentrations. The impact from RNA sequence was prominent compared to nucleotide modifications. The intracellular cation concentration varies, depending on the cell stage, type, and external conditions [339-341]. In Chapter 5, platination rates of H69 RNAs were determined under different salt conditions. The electrostatic competition between Mg^{2+}/Na^{+} and Pt^{+} was shown to decrease the platination rate.

The pH is important for normal cell growth, development, and proliferation, as well as for tumor survival [342,343]. Therefore, interactions between pH-sensitive larger biomolecules and smaller ligands can depend on bulk acidity levels. The higher platination rate at pH 5.8 was interpreted as greater formation of reactive aqua species of complex **1** in the bulk as well as local acidic environments on RNA (Chapter 6). The comparable reactivities of H69 RNAs were explained due to the combined effect from pseudouridylation, availability of reactive aqua cisplatin species, and electrostatic competitions between Na^{+} and Pt^{+} ions. Lastly, in this thesis work platination kinetics were applied to probe neomycin-RNA interactions (Chapter 7). The kinetic data indicated that altered conformations of modified H69 upon neomycin binding could lead to higher platination rates compared to unmodified H69, although, under higher neomycin concentrations electrostatic competitions may lead to comparable reactivities. The fold-decrease in platination rate was determined to evaluate the inhibitory effect of neomycin on platination. The fold-decrease data also suggested that

H69 structure and electrostatic competitions impact the inhibitory effects by neomycin.

Second, the application of platination kinetics as a probe for the RNA microenvironment was explored. This was accomplished by analyzing the salt-dependent kinetic data using different electrostatic models. To date, computational-based approaches are primarily used to evaluate the electrostatic properties of RNA [18,88]. These methods may not reflect the true environment of biomolecules. Although some solution-based methods such as small-angle x-ray scattering and spectroscopic techniques are available, they provide limited electrostatic information [192-195]. Chapter 4 showed a prominent impact from nucleotide sequence on electrostatic properties over pseudouridylation. Analysis of Mg^{2+}-dependent platination data by electrostatic models revealed effects from Na^{+} and Mg^{2+} that increase the RNA charge density and the counterion condensation (Chapter 5).

The higher RNA charge density and counterion condensation at pH 5.8 compared to 6.8 indicated that H^{+} ions impact the electrostatic microenvironment of RNA (Chapter 6). Throughout the thesis work, the global electrostatic parameters between unmodified and modified H69 RNAs were found to be similar. This result indicated that electrostatic changes originating from altered structures of modified H69 could be limited to the loop region. Electrostatic data further revealed that platination rates in the absence of electrostatics depend on target characteristics, cation combinations, and active Pt complex availability. Collectively, this thesis work showed RNA platination kinetics are dependent on

the intrinsic nucleic acid characteristics and surrounding bulk environment, and also supported for its application to determine the dynamic electrostatic properties of RNA.

This thesis work showed the capability of using platination kinetics to study microenvironment properties of RNA. Cisplatin is a relatively small ligand. Therefore, it can be used to determine the microenvironment properties in large RNA molecules. For comparison, *lac* repressor binding to DNA showed involvement of 12 ± 2 phosphate groups, whereas cisplatin very likely interacts with 1-2 phosphate groups as shown by crystal structures [149,264]. The possibility of finding a target site for cisplatin in a studied RNA can be relatively easy, as cisplatin shows many targets such as GpG, ApG, and stretches of Gs on nucleic acids [150]. As kinetic studies are carried out under pseudo-first-order conditions and data are fitted to single-exponential decays, complications arising from the presence of many platination sites may also be avoided. Overall, this thesis work showed that cisplatin kinetics could be a valuable method to study electrostatic microenvironments of various RNA architectures.

8.2 Future Directions

Although model rRNA constructs were used to monitor platination kinetics and electrostatic properties, rRNA is much larger and structurally complex. The microenvironments of rRNA therefore can be drastically different from model systems. As RNA microenvironments are dependent on the structure and sequence shown by this thesis work and other studies, and they are important for ligand interactions, it is necessary to probe these local environments in

ribosomes [18]. Sequencing-based approaches are the primary methods used to interrogate larger RNAs [214]. However, determination of platination kinetics in large rRNA by primer extension could be challenging. For example, use of multiple primers (thus multiple gels pictures) to generate cDNA can produce unreliable quantitative data during normalization. Thus, generating a cDNA read-through across the whole rRNA is necessary. A simultaneous determination of adduct site is also required. A recent report shows measurement of adduct-induced misincorporation rates during cDNA synthesis using massively parallel sequencing [344]. This method seems to be a good approach to find platination rates in ribosomes. The study used Moloney murine leukemia virus reverse transcriptase with Mn^{2+}, which made the enzyme read through and misincorporate nucleotides at SHAPE adducts. The authors optimized conditions to have a complete readthrough across the complete rRNA. The misincorporation rates were then used to predict the secondary structures of large RNA molecules. Similar experimental design which determines misincorporation rate/frequency at a platinated adduct using next-generation sequencing technique can therefore be applied to determine platination rates and electrostatics in complete ribosomes.

There are many other methods that have been applied to monitor platination kinetics of larger nucleic acids. Bancroft *et al.* reported determination of platination rates of chicken erythrocyte DNA by cisplatin using ^{195}Pt NMR [158]. Platination kinetics of salmon sperm DNA have been determined by using atomic absorption spectroscopy on acid hydrolyzed DNA [345]. Other techniques have been employed to monitor platination kinetics of salmon testis DNA include DNA

polymerase standard assay, circular dichroism, ethidium bromide fluorescence, and endonuclease digestion combined with HPLC analysis [239,346]. Although complex data fittings and kinetic model derivations were necessary, important information regarding the pathways of platinum adduct formation and differences between different platinum compound coordinations have been shown by these kinetic studies. Therefore, application of these techniques to determine platination kinetics of rRNA in ribosomes is also feasible.

Many electrostatic studies of nucleic acids are based on computational modeling methods [18,88,125,189,241,347,348]. Although very limited reports exist investigating the counterionic atmospheres and electrostatic properties of nucleic acids by non-computational approaches such as x-ray scattering, spectroscopic techniques, and small molecule probes, experimental determination of these environments are reported to be challenging [192-195,224]. Now that electrostatic parameters are available for H69 RNA from platination kinetic studies, these results can be used as a benchmark to compare computational calculations and results from other methods such as small-angle x-ray scattering. Comparison of experimental and theoretical work may provide clues for differences between the two approaches and may help to improve computational predictions.

Electrostatic interactions between cationic amine groups in aminoglycosides and RNA are important for drug binding [124,125,136,137]. Aminoglycoside derivatives generated by deoxygenation of amine-adjacent hydroxyls, which increases the basicity of amines, are strong inhibitors of hammerhead ribozyme

compared to the parent compounds [124]. Similarly, substitution of hydroxyl groups in aminoglycosides with amino groups has shown to convert poor binders to stronger inhibitors [349]. For self-cleaving catalytic RNAs, the impact from aminoglycosides on the chemical reaction can be directly determined. However, for other non-catalytic RNAs such as H69, which also show aminoglycoside interactions, such straightforward determinations are not possible due to the absence of a chemical reaction. Therefore, with the application of platination kinetics as a tool, the impact of electrostatics on RNA binding can be determined. Similar to previous reports, compounds with different numbers and combinations of hydroxyl and amino groups on aminoglycosides can be used to probe the strength of electrostatic interactions in drug-rRNA complexes. Further, performing salt-dependent platination kinetics can provide details on the impact of RNA charge density and counterion displacements on aminoglycoside-rRNA bounding. These data can be compared to the work reported in this thesis work to determine the microenvironment effects by polycationic drug binding.

This thesis work showed that aminoglycoside binding reduces the platination rate. Comparing the previously published crystallographic structures and probing results from this thesis work indicate that both compounds target the same region of H69 [127]. These residues include G1906, G1921, and G1922. Therefore, it is likely that neomycin preincubation competitively inhibits complex **1** binding. To test this hypothesis, an inhibition assay, as been carried out on Group I intron, can be performed [350,351]. In those experiments, the Lineweaver-Burk graphs obtained by plotting the rate of splicing reactions in the presence of different

competitor amounts at varying guanosine concentrations allowed determination of the type of competition between the two molecules. Similarly, for the system studied in this thesis work, pseudo-first-order rate constants can be determined at different complex **1** concentrations for H69 RNA incubated with varying aminoglycoside concentrations. In relation to Lineweaver-Burk plots, a graph of $1/k_{obs}$ versus 1/[**1**] for H69 RNAs should be able to indicate the type of competition between aminoglycoside and complex **1**.

APPENDIX

This appendix shows the determination of K^+ concentration under different pH levels. A 10 mM KH_2PO_4/K_2HPO_4 buffer was used to maintain the pH in the kinetic studies of this thesis work. The pK_a of potassium phosphate buffer is 6.86 [233]. In Chapters 4 and 5 the pH was 6.2 and in Chapter 6 two pH conditions, 5.8 and 6.8 were used. The pH of each buffer was maintained by mixing different volumes of 1 M solutions of KH_2PO_4 and K_2HPO_4 [233]. The 10 mM KH_2PO_4/K_2HPO_4 buffer was made by diluting this mixture. The following table shows the volume of each species mixed, their final concentrations in 10 mM buffer, and the total concentration of K^+ ions. This K^+ concentration was used when calculating the ionic strength in the medium at each pH.

Table. Determination of K^+ concentrations under different pH.

pH	**1 M K_2HPO_4 (mL)**	**1 M KH_2PO_4 (mL)**	**Concentration of species in 10 mM buffer**		**[K^+] mM**
			[K_2HPO_4] (mM)	**[KH_2PO_4] (mM)**	
5.8	8.5	91.5	0.85	9.15	11
6.2	19.2	80.8	1.92	8.08	12
6.8	49.7	50.3	4.97	5.03	15

REFERENCES

1. Blackburn, G. M. (2006) *Nucleic acids in chemistry and biology*, 3rd ed., The Royal Society of Chemistry.
2. http://www.nobelprize.org/nobel_prizes/medicine/laureates/1965/. access date; 9 Apr 2015.
3. Jacob, F., and Monod, J. (1961) Genetic regulatory mechanisms in the synthesis of proteins. *J. Mol. Biol.* **3**, 318-356.
4. Lwoff, A. (1953) Lysogeny. *Bacteriol. Rev.* **17**, 269-337.
5. Holley, R. W., Apgar, J., Everett, G. A., Madison, J. T., Marquisee, M., Merrill, S. H., Penswick, J. R., and Zamir, A. (1965) Structure of a ribonucleic acid. *Science* **147**, 1462-1465.
6. Nirenberg, M. W., and Matthaei, J. H. (1961) The dependence of cell-free protein synthesis in *E. coli* upon naturally occurring or synthetic polyribonucleotides *Proc. Natl. Acad. Sci. U. S. A.* **47**, 1588-1602.
7. Khorana, H. G., Büchi, H., Ghosh, H., Gupta, N., Jacob, T. M., Kössel, H., Morgan, R., Narang, S. A., Ohtsuka, E., and Wells, R. D. (1966) Polynucleotide synthesis and the genetic code. *Cold Spring Harb. Symp. Quant. Biol.* **31**, 39-49.
8. Gilbert, W. (1986) Origin of life: the RNA world. *Nature* **319**, 618-618.
9. Carr, K. (1993) Nobel goes to discoverers of "split genes". *Nature* **365**, 597-597.
10. Kruger, K., Grabowski, P. J., Zaug, A. J., Sands, J., Gottschling, D. E., and Cech, T. R. (1982) Self-splicing RNA: autoexcision and

autocyclization of the ribosomal RNA intervening sequence of *Tetrahymena*. *Cell* **31**, 147-157.

11. Guerrier-Takada, C., Gardiner, K., Marsh, T., Pace, N., and Altman, S. (1983) The RNA moiety of ribonuclease P is the catalytic subunit of the enzyme. *Cell* **35**, 849-857.
12. Fire, A., Xu, S., Montgomery, M. K., Kostas, S. A., Driver, S. E., and Mello, C. C. (1998) Potent and specific genetic interference by double-stranded RNA in *Caenorhabditis elegans*. *Nature* **391**, 806-811.
13. Selmer, M., Dunham, C. M., Murphy, F. V., Weixlbaumer, A., Petry, S., Kelley, A. C., Weir, J. R., and Ramakrishnan, V. (2006) Structure of the 70S ribosome complexed with mRNA and tRNA. *Science* **313**, 1935-1942.
14. Ban, N., Nissen, P., Hansen, J., Moore, P. B., and Steitz, T. A. (2000) The complete atomic structure of the large ribosomal subunit at 2.4 Å resolution. *Science* **289**, 905-920.
15. Tocilj, A., Schlünzen, F., Janell, D., Glühmann, M., Hansen, H. A. S., Harms, J., Bashan, A., Bartels, H., Agmon, I., Franceschi, F., and Yonath, A. (1999) The small ribosomal subunit from *Thermus thermophilus* at 4.5 Å resolution: pattern fittings and the identification of a functional site. *Proc. Natl. Acad. Sci. U. S. A.* **96**, 14252-14257.
16. Saenger, W. (1984) *Principles of Nucleic Acid Structure*, Springer-Verlag, New York.

17. Bloomfield, V. A., Crothers, D. M., and Tinoco, I. J. (1999) *Nucleic acids: Structures, Properties, and Function*, University Science Books, Sausalito, California.

18. Chin, K., Sharp, K. A., Honig, B., and Pyle, A. M. (1999) Calculating the electrostatic properties of RNA provides new insights into molecular interactions and function. *Nat. Struct. Mol. Biol.* **6**, 1055-1061.

19. Kieft, J. S., and Tinoco, I., Jr. Solution structure of a metal-binding site in the major groove of RNA complexed with cobalt (III) hexammine. *Structure* **5**, 713-721.

20. Cate, J. H., and Doudna, J. A. Metal-binding sites in the major groove of a large ribozyme domain. *Structure* **4**, 1221-1229.

21. Shen, L. X., Cai, Z., and Tinoco, I. (1995) RNA structure at high resolution. *FASEB J.* **9**, 1023-1033.

22. Brion, P., and Westhof, E. (1997) Hierarchy and dynamics of RNA folding. *Annu. Rev. Biophys. Biomol. Struct.* **26**, 113-137.

23. Tian, B., Bevilacqua, P. C., Diegelman-Parente, A., and Mathews, M. B. (2004) The double-stranded-RNA-binding motif: interference and much more. *Nat. Rev. Mol. Cell Biol.* **5**, 1013-1023.

24. Lilley, D. M. J., Clegg, R. M., Diekmann, S., Seeman, N. C., Von Kitzing, E., and Hagerman, P. J. (1995) A nomenclature of junctions and branchpoints in nucleic acids. *Nucleic Acids Res.* **23**, 3363-3364.

25. Noller, H. F. (2005) RNA structure: reading the ribosome. *Science* **309**, 1508-1514.

26. Batey, R. T., Gilbert, S. D., and Montange, R. K. (2004) Structure of a natural guanine-responsive riboswitch complexed with the metabolite hypoxanthine. *Nature* **432**, 411-415.

27. Chang, K. Y., and Tinoco, I. (1994) Characterization of a "kissing" hairpin complex derived from the human immunodeficiency virus genome. *Proc. Natl. Acad. Sci. U. S. A.* **91**, 8705-8709.

28. Staple, D. W., and Butcher, S. E. (2005) Pseudoknots: RNA structures with diverse functions. *PLoS Biol.* **3**, e213.

29. Alexander, R. P., Fang, G., Rozowsky, J., Snyder, M., and Gerstein, M. B. (2010) Annotating non-coding regions of the genome. *Nat. Rev. Genet.* **11**, 559-571.

30. Esteller, M. (2011) Non-coding RNAs in human disease. *Nat. Rev. Genet.* **12**, 861-874.

31. Brennecke, J., Aravin, A. A., Stark, A., Dus, M., Kellis, M., Sachidanandam, R., and Hannon, G. J. (2007) Discrete small RNA-generating loci as master regulators of transposon activity in *Drosophila*. *Cell* **128**, 1089-1103.

32. Mercer, T. R., Dinger, M. E., and Mattick, J. S. (2009) Long non-coding RNAs: insights into functions. *Nat. Rev. Genet.* **10**, 155-159.

33. Barrick, J. E., and Breaker, R. R. (2007) The distributions, mechanisms, and structures of metabolite-binding riboswitches. *Genome Biol.* **8**, R239-R239.

34. Crick, F. (1970) Central dogma of molecular biology. *Nature* **227**, 561-563.

35. Tropp, B. E. (2008) Protein synthesis: The ribosome. in *Molecular biology: Genes to proteins*, John and Bartlett Publishers, Sudbury, MA. pp 916.

36. Poehlsgaard, J., and Douthwaite, S. (2005) The bacterial ribosome as a target for antibiotics. *Nat. Rev. Micro.* **3**, 870-881.

37. Steitz, T. A. (2008) A structural understanding of the dynamic ribosome machine. *Nat. Rev. Mol. Cell Biol.* **9**, 242-253.

38. Korostelev, A., Ermolenko, D. N., and Noller, H. F. (2008) Structural dynamics of the ribosome. *Curr. Opin. Chem. Biol.* **12**, 674-683.

39. Wimberly, B. T., Brodersen, D. E., Clemons, W. M., Morgan-Warren, R. J., Carter, A. P., Vonrhein, C., Hartsch, T., and Ramakrishnan, V. (2000) Structure of the 30S ribosomal subunit. *Nature* **407**, 327-339.

40. Schuwirth, B. S., Borovinskaya, M. A., Hau, C. W., Zhang, W., Vila-Sanjurjo, A., Holton, J. M., and Cate, J. H. D. (2005) Structures of the bacterial ribosome at 3.5 Å resolution. *Science* **310**, 827–834.

41. Cannone, J. J., Subramanian, S., Schnare, M. N., Collett, J. R., D'Souza, L. M., Du, Y., Feng, B., Lin, N., Madabusi, L. V., Müller, K. M., Pande, N., Shang, Z., Yu, N., and Gutell, R. R. (2002) The comparative RNA web (CRW) site: an online database of comparative sequence and structure information for ribosomal, intron, and other RNAs. *BMC Bioinf.* **3**, 2.

42. Ramakrishnan, V., and Moore, P. B. (2001) Atomic structures at last: the ribosome in 2000. *Curr. Opin. Struct. Biol.* **11**, 144-154.

43. Yusupov, M. M., Yusupova, G. Z., Baucom, A., Lieberman, K., Earnest, T. N., Cate, J. H. D., and Noller, H. F. (2001) Crystal structure of the ribosome at 5.5 Å resolution. *Science* **292**, 883–896.

44. Gutell, R. R., Larsen, N., and Woese, C. R. (1994) Lessons from an evolving rRNA: 16S and 23S rRNA structures from a comparative perspective. *Microbiol. Rev.* **58**, 10-26.

45. Frank, J., Verschoor, A., Li, Y., Zhu, J., Lata, R. K., Radermacher, M., Penczek, P., Grassucci, R., Agrawal, R. K., and Srivastava, S. (1995) A model of the translational apparatus based on a three-dimensional reconstruction of the *Escherichia coli* ribosome. *Biochem. Cell Biol.* **73**, 757-765.

46. Ban, N., Nissen, P., Hansen, J., Capel, M., Moore, P. B., and Steitz, T. A. (1999) Placement of protein and RNA structures into a 5 Å-resolution map of the 50S ribosomal subunit. *Nature* **400**, 841-847.

47. Schmeing, T. M., and Ramakrishnan, V. (2009) What recent ribosome structures have revealed about the mechanism of translation. *Nature* **461**, 1234-1242.

48. Jenner, L. B., Demeshkina, N., Yusupova, G., and Yusupov, M. (2010) Structural aspects of messenger RNA reading frame maintenance by the ribosome. *Nat. Struct. Mol. Biol.* **17**, 555-560.

49. Antoun, A., Pavlov, M. Y., Lovmar, M., and Ehrenberg, M. (2006) How initiation factors maximize the accuracy of tRNA selection in initiation of bacterial protein synthesis. *Mol. Cell* **23**, 183-193.

50. Grigoriadou, C., Marzi, S., Pan, D., Gualerzi, C. O., and Cooperman, B. S. (2007) The translational fidelity function of IF3 during transition from the 30 S initiation complex to the 70 S initiation complex. *J. Mol. Biol.* **373**, 551-561.

51. Milon, P., Konevega, A. L., Gualerzi, C. O., and Rodnina, M. V. (2008) Kinetic checkpoint at a late step in translation initiation. *Mol. Cell* **30**, 712-720.

52. Ogle, J. M., Brodersen, D. E., Clemons, W. M., Tarry, M. J., Carter, A. P., and Ramakrishnan, V. (2001) Recognition of cognate transfer RNA by the 30S ribosomal subunit. *Science* **292**, 897-902.

53. Nissen, P., Ippolito, J. A., Ban, N., Moore, P. B., and Steitz, T. A. (2001) RNA tertiary interactions in the large ribosomal subunit: the A-minor motif. *Proc. Natl. Acad. Sci. U. S. A.* **98**, 4899-4903.

54. Valle, M., Sengupta, J., Swami, N. K., Grassucci, R. A., Burkhardt, N., Nierhaus, K. H., Agrawal, R. K., and Frank, J. (2002) Cryo‐EM reveals an active role for aminoacyl‐tRNA in the accommodation process. *EMBO J* **21**, 3557-3567.

55. Berk, V., Zhang, W., Pai, R. D., and Cate, J. H. D. (2006) Structural basis for mRNA and tRNA positioning on the ribosome. *Proc. Natl. Acad. Sci. USA* **103**, 15830-15834.

56. Johansson, M., Bouakaz, E., Lovmar, M., and Ehrenberg, M. The kinetics of ribosomal peptidyl transfer revisited. *Mol. Cell* **30**, 589-598.

57. Moazed, D., and Noller, H. F. (1989) Intermediate states in the movement of transfer RNA in the ribosome. *Nature* **342**, 142-148.

58. Frank, J., and Agrawal, R. K. (2000) A ratchet-like inter-subunit reorganization of the ribosome during translocation. *Nature* **406**, 318-322.

59. Gilbert, R. J. C., Fucini, P., Connell, S., Fuller, S. D., Nierhaus, K. H., Robinson, C. V., Dobson, C. M., and Stuart, D. I. (2004) Three-dimensional structures of translating ribosomes by Cryo-EM. *Mol. Cell* **14**, 57-66.

60. Hirashima, A., and Kaji, A. (1973) Role of elongation factor G and a protein factor on the release of ribosomes from messenger ribonucleic acid. *J. Biol. Chem.* **248**, 7580-7587.

61. Raychaudhuri, S., Conrad, J., Hall, B. G., and Ofengand, J. (1998) A pseudouridine synthase required for the formation of two universally conserved pseudouridines in ribosomal RNA is essential for normal growth of *Escherichia coli*. *RNA* **4**, 1407-1417.

62. Gu, X., Liu, Y., and Santi, D. V. (1999) The mechanism of pseudouridine synthase I as deduced from its interaction with 5-fluorouracil-tRNA. *Proc. Natl. Acad. Sci. U. S. A.* **96**, 14270-14275.

63. Varani, G., and McClain, W. H. (2000) The G·U wobble base pair. *EMBO Rep.* **1**, 18-23.

64. Noller, H. F., Kop, J., Wheaton, V., Brosius, J., Gutell, R. R., Kopylov, A. M., Dohme, F., Herr, W., Stahl, D. A., Gupta, R., and Woese, C. R. (1981)

Secondary structure model for 23S ribosomal RNA. *Nucleic Acids Res.* **9**, 6167-6189.

65. Jiang, J., Sakakibara, Y., and Chow, C. S. (2013) Helix 69: a multitasking RNA motif as a novel drug target. *Isr. J. Chem.* **53**, 379-390.

66. Ali, I. K., Lancaster, L., Feinberg, J., Joseph, S., and Noller, H. F. Deletion of a conserved, central ribosomal intersubunit RNA bridge. *Mol. Cell* **23**, 865-874.

67. Weixlbaumer, A., Jin, H., Neubauer, C., Voorhees, R. M., Petry, S., Kelley, A. C., and Ramakrishnan, V. (2008) Insights into translational termination from the structure of RF2 bound to the ribosome. *Science* **322**, 953-956.

68. Laurberg, M., Asahara, H., Korostelev, A., Zhu, J., Trakhanov, S., and Noller, H. F. (2008) Structural basis for translation termination on the 70S ribosome. *Nature* **454**, 852-857.

69. Agrawal, R. K., Sharma, M. R., Kiel, M. C., Hirokawa, G., Booth, T. M., Spahn, C. M. T., Grassucci, R. A., Kaji, A., and Frank, J. (2004) Visualization of ribosome-recycling factor on the *Escherichia coli* 70S ribosome: functional implications. *Proc. Nat. Acad. Sci. U.S.A.* **101**, 8900–8905.

70. Kipper, K., Hetényi, C., Sild, S., Remme, J., and Liiv, A. (2009) Ribosomal intersubunit bridge B2a is involved in factor-dependent translation initiation and translational processivity. *J. Mol. Biol.* **385**, 405–422.

71. O'Connor, M., and Dahlberg, A. E. (1995) The involvement of two distinct regions of 23 S ribosomal RNA in tRNA selection. *J. Mol. Biol.* **254**, 838-847.

72. Decatur, W. A., and Fournier, M. J. rRNA modifications and ribosome function. *Trends Biochem. Sci.* **27**, 344-351.

73. Ofengand, J., and Bakin, A. (1997) Mapping to nucleotide resolution of pseudouridine residues in large subunit ribosomal RNAs from representative eukaryotes, prokaryotes, archaebacteria, mitochondria and chloroplasts. *J. Mol. Biol.* **266**, 246-268.

74. Jiang, J., Aduri, R., Chow, C. S., and SantaLucia, J. (2013) Structure modulation of helix 69 from *Escherichia coli* 23S ribosomal RNA by pseudouridylations. *Nucleic Acids Res.* **42**, 3971-3981.

75. Abeysirigunawardena, S. C., and Chow, C. S. (2008) pH-Dependent structural changes of helix 69 from *Escherichia coli* 23S ribosomal RNA. *RNA* **14**, 782–792.

76. Sakakibara, Y., and Chow, C. S. (2011) Probing conformational states of modified helix 69 in 50S ribosomes. *J. Am. Chem. Soc.* **133**, 8396–8399.

77. Sakakibara, Y., and Chow, C. S. (2012) Role of pseudouridine in structural rearrangements of helix 69 during bacterial ribosome assembly. *ACS Chem. Biol.* **7**, 871–878.

78. Gutell, R. R., Weiser, B., Woese, R. C., and Noller, F. H. (1985) Comparative anatomy of 16-S-like ribosomal RNA. in *Progress in Nucleic*

Acid Research and Molecular Biology (Waldo, E. C., and Kivie, M. eds.), Academic Press, Orlando, Florida pp 155-216.

79. Muralikrishna, P., and Wickstrom, E. (1989) *Escherichia coli* initiation factor 3 protein binding to 30S ribosomal subunits alters the accessibility of nucleotides within the conserved central region of 16S rRNA. *Biochemistry* **28**, 7505–7510.

80. Tapprich, W. E., and Hill, W. E. (1986) Involvement of bases 787-795 of *Escherichia coli* 16S ribosomal RNA in ribosomal subunit association. *Proc. Natl. Acad. Sci. U.S.A.* **83**, 556–560.

81. Herr, W., Chapman, N. M., and Noller, H. F. (1979) Mechanism of ribosomal subunit association: discrimination of specific sites in 16 S RNA essential for association activity. *J. Mol. Biol.* **130**, 433-449.

82. Moazed, D., and Noller, H. F. Transfer RNA shields specific nucleotides in 16S ribosomal RNA from attack by chemical probes. *Cell* **47**, 985-994.

83. Tapprich, W. E., Goss, D. J., and Dahlberg, A. E. (1989) Mutation at position 791 in *Escherichia coli* 16S ribosomal RNA affects processes involved in the initiation of protein synthesis. *Proc. Natl. Acad. Sci. U.S.A.* **86**, 4927–4931.

84. Lee, K., Varma, S., SantaLucia Jr, J., and Cunningham, P. R. (1997) *In vivo* determination of RNA structure-function relationships: analysis of the 790 loop in ribosomal RNA. *J. Mol. Biol.* **269**, 732–743.

85. Banatao, D. R., Altman, R. B., and Klein, T. E. (2003) Microenvironment analysis and identification of magnesium binding sites in RNA. *Nucleic Acids Res.* **31**, 4450-4460.

86. Sharp, K. A., Honig, B., and Harvey, S. C. (1990) Electrical potential of transfer RNAs: codon-anticodon recognition. *Biochemistry* **29**, 340-346.

87. Correll, C. C., Freeborn, B., Moore, P. B., and Steitz, T. A. (1997) Metals, motifs, and recognition in the crystal structure of a 5S rRNA domain. *Cell* **91**, 705-712.

88. Baker, N. A., Sept, D., Joseph, S., Holst, M. J., and McCammon, J. A. (2001) Electrostatics of nanosystems: application to microtubules and the ribosome. *Proc. Natl. Acad. Sci. U. S. A.* **98**, 10037-10041.

89. Battiste, J. L., Mao, H., Rao, N. S., Tan, R., Muhandiram, D. R., Kay, L. E., Frankel, A. D., and Williamson, J. R. (1996) α Helix-RNA major groove recognition in an HIV-1 Rev peptide-RRE RNA complex. *Science* **273**, 1547-1551.

90. Tao, J., and Frankel, A. D. (1993) Electrostatic interactions modulate the RNA-binding and transactivation specificities of the human immunodeficiency virus and simian immunodeficiency virus Tat proteins. *Proc. Natl. Acad. Sci. U. S. A.* **90**, 1571-1575.

91. Eargle, J., Black, A. A., Sethi, A., Trabuco, L. G., and Luthey-Schulten, Z. (2008) Dynamics of recognition between tRNA and elongation factor Tu. *J. Mol. Biol.* **377**, 1382-1405.

92. Castle, A. M., Macnab, R. M., and Shulman, R. G. (1986) Measurement of intracellular sodium concentration and sodium transport in *Escherichia coli* by ^{23}Na nuclear magnetic resonance. *J. Biol. Chem.* **261**, 3288-3294.

93. Draper, D. E. (2004) A guide to ions and RNA structure. *RNA* **10**, 335-343.

94. Pyle, A. (2002) Metal ions in the structure and function of RNA. *J. Biol. Inorg. Chem.* **7**, 679-690.

95. Feig, A. L., and Uhlenbeck, O. C. (1999) The role of metal ions in RNA biochemistry. in *The RNA World*, 2nd Ed., Cold Spring Harbor Laboratory Press. pp 287-319.

96. Bloomfield, V. A., Crothers, D. M., and Tinoco, I. J. (1999) Interaction of nucleic acids with water and ions. in *Nucleic Acids: Structures, Properties, and Function*, University Science Books, Sausalito, California. pp 488.

97. Auffinger, P., Grover, N., and Westhof, E. (2011) Metal ion binding to RNA. in *Met. Ions Life Sci.* (Sigel, A., Sigel, H., and Sigel, R. K. O. eds.), Royal Society of Chemistry. pp 1-35.

98. Manning, G. S. (1978) The molecular theory of polyelectrolyte solutions with applications to the electrostatic properties of polynucleotides. *Q. Rev. Biophys.* **2**, 179-246.

99. Record, M. T., Anderson, C. F., and Lohman, T. M. (1978) Thermodynamic analysis of ion effects on the binding and conformational equilibria of proteins and nucleic acids: the roles of ion association or release, screening, and ion effects on water activity. *Q. Rev. Biophys.* **11**, 103-178.

100. Misra, V. K., and Draper, D. E. (2000) Mg^{2+} binding to tRNA revisited: the nonlinear poisson-boltzmann model. *J. Mol. Biol.* **299**, 813-825.

101. Misra, V. K., and Draper, D. E. (2002) The linkage between magnesium binding and RNA folding. *J. Mol. Biol.* **317**, 507-521.

102. Tinoco Jr, I., and Kieft, J. S. (1997) The ion core in RNA folding. *Nat. Struct. Biol.* **4**, 509-512.

103. Cate, J. H., Gooding, A. R., Podell, E., Zhou, K., Golden, B. L., Kundrot, C. E., Cech, T. R., and Doudna, J. A. (1996) Crystal structure of a group I ribozyme domain: principles of RNA packing. *Science* **273**, 1678-1685.

104. Blaha, G., Stanley, R. E., and Steitz, T. A. (2009) Formation of the first peptide bond: the structure of EF-P bound to the 70S ribosome. *Science* **325**, 966-970.

105. Sakakibara, Y., Abeysirigunawardena, S. C., Duc, A.-C. E., Dremann, D. N., and Chow, C. S. (2012) Ligand- and pH-induced conformational changes of RNA domain helix 69 revealed by 2-aminopurine fluorescence. *Angew. Chem., Int. Ed. Engl.* **51**, 12095–12098.

106. Borovinskaya, M. A., Pai, R. D., Zhang, W., Schuwirth, B. S., Holton, J. M., Hirokawa, G., Kaji, H., Kaji, A., and Cate, J. H. D. (2007) Structural basis for aminoglycoside inhibition of bacterial ribosome recycling. *Nat. Struct. Mol. Biol.* **14**, 727-732.

107. Spitnik-Elson, P., and Atsmon, A. (1969) Detachment of ribosomal proteins by salt: I. Effect of conditions on the amount of protein detached. *J. Mol. Biol.* **45**, 113-124.

108. Kennard, O., and Hunter, W. N. (1989) Oligonucleotide structure: a decade of results from single crystal X-ray diffraction studies. *Q. Rev. Biophys.* **22**, 327-379.

109. Izatt, R. M., Christensen, J. J., and Rytting, J. H. (1971) Sites and thermodynamic quantities associated with proton and metal ion interaction with ribonucleic acid, deoxyribonucleic acid, and their constituent bases, nucleosides, and nucleotides. *Chem. Rev.* **71**, 439-481.

110. Lippert, B. (2005) Alteration of nucleobases pK_a values upon metal coordination: origins and consequences. in *Prog. Inorg. Chem.* (Karlin, K. D. ed.), John Wiley & Sons, Inc. pp 385-447.

111. Lamm, G., and Pack, G. R. (1990) Acidic domains around nucleic acids. *Proc. Natl. Acad. Sci. U. S. A.* **87**, 9033-9036.

112. Pack, G. R., and Wong, L. (1996) Electrostatic effects on the rates of DNA-catalyzed reactions. *Chem. Phys.* **204**, 279-288.

113. Böttger, E. C. (2006) The ribosome as a drug target. *Trends Biotechnol.* **24**, 145-147.

114. Franceschi, F. (2007) Back to the future: the ribosome as an antibiotic target. *Future Microbiol.* **2**, 571-574.

115. Aas, P. A., Otterlei, M., Falnes, P. O., Vagbo, C. B., Skorpen, F., Akbari, M., Sundheim, O., Bjoras, M., Slupphaug, G., Seeberg, E., and Krokan, H. E. (2003) Human and bacterial oxidative demethylases repair alkylation damage in both RNA and DNA. *Nature* **421**, 859-863.

116. Auerbach T., B. A., Harms J., Schluenzen F., Zarivach R., Bartels H., Agman I., Kessler M., Pioletti M., Franceschi F., Yonath A. (2002) Antibiotics targeting ribosomes: crystallographic studies. *Curr. Drug Targets: Infect. Disord.* **2**, 169-186.

117. Moazed, D., and Noller, H. F. (1987) Interaction of antibiotics with functional sites in 16S ribosomal RNA. *Nature* **327**, 389-394.

118. Vicens, Q., and Westhof, E. (2001) Crystal structure of paromomycin docked into the eubacterial ribosomal decoding A Site. *Structure* **9**, 647-658.

119. Feldman, M. B., Terry, D. S., Altman, R. B., and Blanchard, S. C. (2010) Aminoglycoside activity observed on single pre-translocation ribosome complexes. *Nat. Chem. Biol.* **6**, 54-62.

120. Dorman, D. E., Paschal, J. W., and Merkel, K. E. (1976) ^{15}Nnuclear magnetic resonance spectroscopy. The nebramycin aminoglycosides. *J. Am. Chem. Soc.* **98**, 6885-6888.

121. Kaul, M., Barbieri, C. M., Kerrigan, J. E., and Pilch, D. S. (2003) Coupling of drug protonation to the specific binding of aminoglycosides to the A Site of 16 S rRNA: elucidation of the number of drug amino groups involved and their identities. *J. Mol. Biol.* **326**, 1373-1387.

122. Hermann, T., and Westhof, E. (1999) Docking of cationic antibiotics to negatively charged pockets in RNA folds. *J. Med. Chem.* **42**, 1250-1261.

123. Smith, A. L., Kassman, J., Srour, K. J., and Soto, A. M. (2011) Effect of salt concentration on the conformation of TAR RNA and its association with aminoglycoside antibiotics. *Biochemistry* **50**, 9434-9445.

124. Wang, H., and Tor, Y. (1997) Electrostatic interactions in RNA aminoglycosides binding. *J. Am. Chem. Soc.* **119**, 8734-8735.

125. Ma, C., Baker, N. A., Joseph, S., and McCammon, J. A. (2002) Binding of aminoglycoside antibiotics to the small ribosomal subunit: a continuum electrostatics investigation. *J. Am. Chem. Soc.* **124**, 1438-1442.

126. Tor, Y., Hermann, T., and Westhof, E. (1998) Deciphering RNA recognition: aminoglycoside binding to the hammerhead ribozyme. *Chem. Biol.* **5**, R277-R283.

127. Wang, L., Pulk, A., Wasserman, M. R., Feldman, M. B., Altman, R. B., Cate, J. H. D., and Blanchard, S. C. (2012) Allosteric control of the ribosome by small-molecule antibiotics. *Nat. Struct. Mol. Biol.* **19**, 957-963.

128. Wirmer, J., and Westhof, E. (2006) Molecular contacts between antibiotics and the 30S ribosomal particle. in *Methods in Enzymology* (Minoru, F. ed.), Academic Press. pp 180-202.

129. Pioletti, M., Schlünzen, F., Harms, J., Zarivach, R., Glühmann, M., Avila, H., Bashan, A., Bartels, H., Auerbach, T., Jacobi, C., Hartsch, T., Yonath, A., and Franceschi, F. (2001) Crystal structures of complexes of the small ribosomal subunit with tetracycline, edeine and IF3. *EMBO J.* **20**, 1829-1839.

130. McCoy, L. S., Xie, Y., and Tor, Y. (2011) Antibiotics that target protein synthesis. *Wiley Interdiscip. Rev.: RNA* **2**, 209-232.

131. Walter, F., Vicens, Q., and Westhof, E. (1999) Aminoglycoside–RNA interactions. *Curr. Opin. Chem. Biol.* **3**, 694-704.

132. Hansen, J. L., Moore, P. B., and Steitz, T. A. (2003) Structures of five antibiotics bound at the peptidyl transferase center of the large ribosomal subunit. *J Mol. Biol.* **330**, 1061-1075.

133. Allen, D. W., and Zamecnik, P. C. (1962) The effect of puromycin on rabbit reticulocyte ribosomes. *Biochim. Biophys. Acta* **55**, 865-874.

134. Sakakibara, Y. (2012) *Exploring conformational variability of an RNA domain in the ribosome: from structure and function to potential antibiotic targeting.* PhD, Wayne State University.

135. Odon, O. W., Kramer, G., Henderson, A. B., Pinphanichakarn, P., and Hardesty, B. (1978) GTP hydrolysis during methionyl-$tRNA_f$ binding to 40 S ribosomal subunits and the site of edeine inhibition. *J. Biol. Chem.* **253**, 1807-1816.

136. Hermann, T., and Westhof, E. (1998) Aminoglycoside binding to the hammerhead ribozyme: a general model for the interaction of cationic antibiotics with RNA. *J. Mol. Biol.* **276**, 903-912.

137. Jin, E., Katritch, V., Olson, W. K., Kharatisvili, M., Abagyan, R., and Pilch, D. S. (2000) Aminoglycoside binding in the major groove of duplex RNA: the thermodynamic and electrostatic forces that govern recognition. *J. Mol. Biol.* **298**, 95-110.

138. Davis, B., Afshar, M., Varani, G., Murchie, A. I. H., Karn, J., Lentzen, G., Drysdale, M., Bower, J., Potter, A. J., Starkey, I. D., Swarbrick, T., and Aboul-ela, F. (2004) Rational design of inhibitors of HIV-1 TAR RNA through the stabilisation of electrostatic “hot spots”. *J. Mol. Biol.* **336**, 343-356.

139. Kauffman, G. B. (2010) Michele Peyrone (1813-1883), discoverer of cisplatin. *Platinum Metals Rev.* **54**, 250-256.

140. Kauffman, G. B. (1997) Alfred Werner's research on the platinum metals; a centennial retrospect. *Platinum Metals Rev.* **41**, 34-40.

141. Rosenberg, B., Van Camp, L., and Krigas, T. (1965) Inhibition of cell division in *Escherichia coli* by electrolysis products from a platinum electrode. *Nature* **205**, 698–699.

142. Rosenberg, B., Van Camp, L., Grimley, E. B., and Thomson, A. J. (1967) The inhibition of growth or cell division in *Escherichia coli* by different ionic species of platinum(IV) complexes. *J. Biol. Chem.* **242**, 1347-1352

143. (2000) *Platinum-Based Drugs in Cancer Therapy (Cancer Drug Discovery and Development)*, Humana Press.

144. Ali, I., Wani, W. A., Saleem, K., and Haque, A. (2013) Platinum compounds: a hope for future cancer chemotherapy. *Anti-Cancer Agents Med. Chem.* **13**, 296–306.

145. Pinto, A. L., and Lippard, S. J. (1985) Binding of the antitumor drug *cis*-diamminedichloroplatinum(II) (cisplatin) to DNA. *Biochim. Biophys. Acta* **780**, 167-180.

146. Dhar, S., and Lippard, S. J. (2009) Structural and mechanistic studies of anticancer platinum drugs: uptake, activation, and the cellular response to DNA binding. in *Platinum and Other Heavy Metal Compounds in Cancer Chemotherapy*, Humana Press. pp 135-147.

147. Gately, D. P., and Howell, S. B. (1993) Cellular accumulation of the anticancer agent cisplatin: a review. *Br. J. Cancer* **67**, 1171-1176.

148. Wang, D., and Lippard, S. J. (2005) Cellular processing of platinum anticancer drugs. *Nat. Rev. Drug Discovery* **4**, 307-320.

149. Sherman, S., Gibson, D., Wang, A., and Lippard, S. (1985) X-ray structure of the major adduct of the anticancer drug cisplatin with DNA: *cis*-[$Pt(NH_3)_2$(d(pGpG))]. *Science* **230**, 412-417.

150. Fichtinger-Schepman, A. M. J., Van der Veer, J. L., Den Hartog, J. H. J., Lohman, P. H. M., and Reedijk, J. (1985) Adducts of the antitumor drug *cis*-diamminedichloroplatinum(II) with DNA: formation, identification, and quantitation. *Biochemistry* **24**, 707–713.

151. Jamieson, E. R., and Lippard, S. J. (1999) Structure, recognition, and processing of cisplatin−DNA adducts. *Chem. Rev.* **99**, 2467–2498.

152. Takahara, P. M., Rosenzweig, A. C., Frederick, C. A., and Lippard, S. J. (1995) Crystal structure of double-stranded DNA containing the major adduct of the anticancer drug cisplatin. *Nature* **377**, 649-652.

153. Cohen, G., Bauer, W., Barton, J., and Lippard, S. (1979) Binding of *cis*- and *trans*-dichlorodiammineplatinum(II) to DNA: evidence for unwinding and shortening of the double helix. *Science* **203**, 1014-1016.

154. Van Garderen, C. J., and Van Houte, L. P. A. (1994) The solution structure of a DNA duplex containing the *cis*-Pt(NH_3)$_2$[d(-GTG-)-N7(G), N7(G)] adduct, as determined with high-field NMR and molecular mechanics/dynamics. *Eur. J. Biochem.* **225**, 1169-1179

155. Nunomura, K., Maeda, Y., and Ohtsubo, E. (1991) The interaction of platinum complxes with DNA studied by differential scanning calorimetry. *J. Gen. Appl. Microbiol.* **37**, 207-214.

156. Poklar, N., Pilch, D. S., Lippard, S. J., Redding, E. A., Dunham, S. U., and Breslauer, K. J. (1996) Influence of cisplatin intrastrand crosslinking on the conformation, thermal stability, and energetics of a 20-mer DNA duplex. *Proc. Natl. Acad. Sci. U. S. A.* **93**, 7606-7611

157. Carbtree, R. H. *The Organometallic Chemistry of the Transition Metals*, A John Wiley & Sons, Inc, Hoboken, New Jersey.

158. Bancroft, D. P., Lepre, C. A., and Lippard, S. J. (1990) ^{195}Pt NMR kinetic and mechanistic studies of *cis*- and *trans*-diamminedichloroplatinum(II) binding to DNA. *J. Am. Chem. Soc.* **112**, 6860–6871.

159. Reedijk, J. (2003) New clues for platinum antitumor chemistry: kinetically controlled metal binding to DNA. *Proc. Natl. Acad. Sci. U. S. A.* **100**, 3611-3616.

160. Segal, E., and Le Pecq, J.-B. (1985) Role of ligand exchange processes in the reaction kinetics of the antitumor drug *cis*-diamminedichloroplatinum(II) with its targets. *Cancer Res.* **45**, 492-498.

161. Johnson, N. P., Hoeschele, J. D., and Rahn, R. O. (1980) Kinetic analysis of the in vitro binding of radioactive *cis*- and *trans*-dichlorodiammineplatinum(II) to DNA. *Chem.-Biol. Interact.* **30**, 151-169.

162. Kozelka, J., Legendre, F., Reeder, F., and Chottard, J.-C. (1999) Kinetic aspects of interactions between DNA and platinum complexes. *Coord. Chem. Rev.* **190–192.**, 61-82.

163. Elmroth, S. K. C., and Lippard, S. J. (1994) Platinum binding to d(GpG) target sequences and phosphorothioate linkages in DNA occurs more rapidly with increasing oligonucleotide length. *J. Am. Chem. Soc.* **116**, 3633-3634.

164. Elmroth, S. K. C., and Lippard, S. J. (1995) Surface and electrostatic contributions to DNA-promoted reactions of platinum(II) complexes with short oligonucleotides: a kinetic study. *Inorg. Chem.* **34**, 5234–5243.

165. Kjellstrom, J., and K. C. Elmroth, S. (1997) Large variation of rates for platination of phosphorothioate-containing oligonucleotides: end effects and counter ion influence. *Chem. Commun.*, 1701-1702.

166. Snygg, A. S., Brindell, M., Stochel, G., and Elmroth, S. K. C. (2005) A combination of access to preassociation sites and local accumulation tendency in the direct vicinity of G-N7 controls the rate of platination of single-stranded DNA. *Dalton Trans.*, 1221–1227.

167. Monjardet-Bas, V., Elizondo-Riojas, M.-A., Chottard, J.-C., and Kozelka, J. (2002) A combined effect of molecular electrostatic potential and N7 accessibility explains sequence-dependent binding of *cis*-

$[Pt(NH_3)_2(H_2O)_2]^{2+}$ to DNA duplexes. *Angew. Chem., Int. Ed.* **41**, 2998-3001.

168. Gonnet, F., Reeder, F., Kozelka, J., and Chottard, J.-C. (1996) Kinetic analysis of the reactions between GG-containing oligonucleotides and platinum complexes. 1. Reactions of single-stranded oligonucleotides with *cis*-$[Pt(NH_3)_2(H_2O)_2]^{2+}$ and $[Pt(NH_3)_3(H_2O)]^{2+}$. *Inorg. Chem.* **35**, 1653-1658.

169. Kozelka, J. (2009) Molecular origin of the sequence-dependent kinetics of reactions between cisplatin derivatives and DNA. *Inorg. Chim. Acta* **362**, 651-668.

170. Reeder, F., Gonnet, F., Kozelka, J., and Chottard, J.-C. (1996) Reactions of the double-stranded oligonucleotide $d(TTGGCCAA)_2$ with *cis*-$[Pt(NH_3)_2(H_2O)_2]^{2+}$ and $[Pt(NH_3)_3(H_2O)]^{2+}$. *Chem. Eur. J.* **2**, 1068-1076.

171. Davies, M. S., Berners-Price, S. J., and Hambley, T. W. (1998) Rates of platination of AG and GA containing double-stranded oligonucleotides: insights into why cisplatin binds to GG and AG but not GA sequences in DNA. *J. Am. Chem. Soc.* **120**, 11380-11390.

172. Sadler, P. J., Barnham, K. J., Berners-Price, S. J., and Frey, U. (1996) Kinetic analysis of the stepwise platination of single- and double-stranded GG oligonucleotides with cisplatin and *cis*-$[PtCl(H_2O)(NH_3)_2]^{+}$. *Chem. - Eur. J.* **2**, 1283-1291.

173. Kjellström, J., and Elmroth, S. K. C. (1999) Medium effects on reactivity profiles for platination of phosphorothioate-containing oligonucleotide. *Inorg. Chem.* **38**, 6193–6199.

174. Meroueh, M., Kjellström, J., Mårtensson, K. S. M., Elmroth, S. K. C., and Chow, C. S. (2000) Reactions of platinum(II) complexes with a DNA hairpin, d(CGCGTTGTTCGCG): structural characterization and kinetic studies. *Inorg. Chim. Acta* **297**, 145–155.

175. Kjellström, J., and Elmroth, S. (2003) Kinetics and mechanism for platination of thione-containing nucleotides and oligonucleotides: evaluation of the salt dependence. *J. Biol. Inorg. Chem.* **8**, 38–44.

176. Hägerlöf, M., Papsai, P., Chow, C., and Elmroth, S. (2006) More pronounced salt dependence and higher reactivity for platination of the hairpin r(CGCGUUGUUCGCG) compared with d(CGCGTTGTTCGCG). *J. Biol. Inorg. Chem.* **11**, 974–990.

177. Papsai, P., Aldag, J., Persson, T., and Elmroth, S. K. C. (2006) Kinetic preference for interaction of cisplatin with the G-C-rich wobble basepair region in both $tRNA^{Ala}$ and Mh^{Ala}. *Dalton Trans.*, 3515-3517.

178. Baik, M.-H., Friesner, R. A., and Lippard, S. J. (2003) Theoretical study of cisplatin binding to purine bases: why does cisplatin prefer guanine over adenine? *J Am. Chem. Soc.* **125**, 14082-14092.

179. Wang, Y., Farrell, N., and Burgess, J. D. (2001) Direct evidence for preassociation preceding covalent binding in the reaction of *cis*-$[Pt(NH_3)_2(H_2O)_2]^{2+}$ with surface immobilized oligonucleotides. *J. Am. Chem. Soc.* **123**, 5576-5577.

180. Sykfont, A., Ericson, A., and Elmroth, S. K. C. (2001) Non-uniform rate for platination of guanine-N7 located in short DNA oligomers. *Chem. Commun.*, 1190–1191.

181. Rijal, K., and Chow, C. S. (2009) A new role for cisplatin: probing ribosomal RNA structure. *Chem. Commun.*, 107–109.

182. Rijal, K., Bao, X., and Chow, C. S. (2014) Amino acid-linked platinum(II) analogues have altered specificity for RNA compared to cisplatin. *Chem. Commun.*, 3918-3920.

183. Hostetter, A. A., Osborn, M. F., and DeRose, V. J. (2011) RNA-Pt adducts following cisplatin treatment of *Saccharomyces cerevisiae*. *ACS Chem. Biol.* **7**, 218–225.

184. Hostetter, A. A., Chapman, E. G., and DeRose, V. J. (2009) Rapid cross-linking of an RNA internal loop by the anticancer drug cisplatin. *J. Am. Chem. Soc.* **131**, 9250–9257.

185. Chapman, E. G., and DeRose, V. J. (2011) Site-specific platinum(II) cross-linking in a ribozyme active site. *J. Am. Chem. Soc.* **134**, 256-262.

186. Chapman, E. G., and DeRose, V. J. (2010) Enzymatic processing of platinated RNAs. *J. Am. Chem. Soc.* **132**, 1946–1952.

187. Hägerlöf, M., Papsai, P., Hedman, H., Jungwirth, U., Jenei, V., and Elmroth, S. (2008) Cisplatin and siRNA interference with structure and function of Wnt-5a mRNA: design and in vitro evaluation of targeting AU-rich elements in the 3′ UTR. *J. Biol. Inorg. Chem.* **13**, 385-399.

188. Manning, G. S. (1969) Limiting laws and counterion condensation in polyelectrolyte solutions I. colligative properties. *J. Chem. Phys.* **51**, 924-933.

189. Sharp, K. A., and Honig, B. (1995) Salt effects on nucleic acids. *Curr. Opin. Struct. Biol.* **5**, 323-328.

190. Pabit, S. A., Qiu, X., Lamb, J. S., Li, L., Meisburger, S. P., and Pollack, L. (2009) Both helix topology and counterion distribution contribute to the more effective charge screening in dsRNA compared with dsDNA. *Nucleic Acids Res.* **37**, 3887-3896.

191. Kirmizialtin, S., Silalahi, Alexander R. J., Elber, R., and Fenley, Marcia O. (2012) The ionic atmosphere around A-RNA: Poisson-Boltzmann and molecular dynamics simulations. *Biophys. J.* **102**, 829-838.

192. Das, R., Mills, T. T., Kwok, L. W., Maskel, G. S., Millett, I. S., Doniach, S., Finkelstein, K. D., Herschlag, D., and Pollack, L. (2003) Counterion distribution around DNA probed by solution x-ray scattering. *Phys. Rev. Lett.* **90**, 188103-188101–188104.

193. Hecht, J. L., Honig, B., Shin, Y.-K., and Hubbell, W. L. (1995) Electrostatic potentials near the surface of DNA: comparing theory and experiment. *J. Phys. Chem.* **99**, 7782-7786.

194. Kirmizialtin, S., Pabit, Suzette A., Meisburger, Steve P., Pollack, L., and Elber, R. (2012) RNA and its ionic cloud: solution scattering experiments and atomically detailed simulations. *Biophys. J.* **102**, 819-828.

195. Bai, Y., Greenfeld, M., Travers, K. J., Chu, V. B., Lipfert, J., Doniach, S., and Herschlag, D. (2007) Quantitative and comprehensive decomposition of the ion atmosphere around nucleic acids. *J. Am. Chem. Soc.* **129**, 14981-14988.

196. Owens, D. R., Bothner, B., Phung, Q., Harris, K., and Siuzdak, G. (1998) Aspects of oligonucleotide and peptide sequencing with MALDI and electrospray mass spectrometry. *Bioorg. Med. Chem.* **6**, 1547-1554.

197. Compton, B. J., and Siuzdak, G. (2003) Mass spectrometry in nucleic acid, carbohydrate and steroid analysis. *Journal of Spectroscopy* **17**, 699-713.

198. Zenobi, R., and Knochenmuss, R. (1998) Ion formation in MALDI mass spectrometry. *Mass Spectrom. Rev.* **17**, 337-366.

199. El-Aneed, A., Cohen, A., and Banoub, J. (2009) Mass spectrometry, review of the basics: electrospray, MALDI, and commonly used mass analyzers. *Appl. Spectrosc. Rev.* **44**, 210-230.

200. Fitzgerald, M. C., and Smith, L. M. (1995) Mass spectrometry of nucleic acids: the promise of matrix-assisted laser desorption-ionization (MALDI) mass spectrometry. *Annu. Rev. Biophys. Biomol. Struct.* **24**, 117-140.

201. Nordhoff, E., Kirpekar, F., and Roepstorff, P. (1996) Mass spectrometry of nucleic acids. *Mass Spectrom. Rev.* **15**, 67-138.

202. Wu, K. J., Steding, A., and Becker, C. H. (1993) Matrix-assisted laser desorption time-of-flight mass spectrometry of oligonucleotides using 3-

hydroxypicolinic acid as an ultraviolet-sensitive matrix. *Rapid Commun. Mass Spectrom.* **7**, 142-146.

203. Dass, C. (2007) *Fundamentals of contemporary mass spectrometry*, John Wiley & Sons, Inc, Hoboken, New Jersey.

204. Glish, G. L., and Vachet, R. W. (2003) The basics of mass spectrometry in the twenty-first century. *Nat. Rev. Drug Discov.* **2**, 140-150.

205. Lewis, J. K., Wei, J., and Siuzdak, G. (2006) Matrix-assisted laser desorption/ionization mass spectrometry in peptide and protein analysis. in *Encyclopedia of Analytical Chemistry*, John Wiley & Sons, Ltd. pp 5880-5894.

206. Spengler, B., Pan, Y., Cotter, R. J., and Kan, L.-S. (1990) Molecular weight determination of underivatized oligodeoxyribonucleotides by positive-ion matrix-assisted ultraviolet laser-desorption mass spectrometry. *Rapid Commun. Mass Spectrom.* **4**, 99-102.

207. Kirpekar, F., Nordhoff, E., Kristiansen, K., Roepstorff, P., Lezius, A., Hahner, S., Karas, M., and Hillenkamp, F. (1994) Matrix assisted laser desorption/ionization mass spectrometry of enzymatically synthesized RNA up to 150 kDa. *Nucleic Acids Res.* **22**, 3866-3870.

208. Nordhoff, E., Ingendoh, A., Cramer, R., Overberg, A., Stahl, B., Karas, M., Hillenkamp, F., Crain, P. F., and Chait, B. (1992) Matrix-assisted laser desorption/ionization mass spectrometry of nucleic acids with wavelengths in the ultraviolet and infrared. *Rapid Commun. Mass Spectrom.* **6**, 771-776.

209. Meng, Z., and Limbach, P. A. (2005) Quantitation of ribonucleic acids using ^{18}O labeling and mass spectrometry. *Anal. Chem.* **77**, 1891-1895.

210. Hossain, M., and Limbach, P. A. (2007) Mass spectrometry-based detection of transfer RNAs by their signature endonuclease digestion products. *RNA* **13**, 295-303.

211. Durairaj, A., and Limbach, P. A. (2008) Matrix-assisted laser desorption/ionization mass spectrometry screening for pseudouridine in mixtures of small RNAs by chemical derivatization, RNase digestion and signature products. *Rapid Commun. Mass Spectrom.* **22**, 3727-3734.

212. Guittard, J., Pacifico, C., Blais, J. C., Bolbach, G., Chottard, J. C., and Spassky, A. (1995) Matrix-assisted laser desorption ionization time-of-flight mass spectrometry of DNA–Pt(II) complexes. *Rapid Commun. Mass Spectrom.* **9**, 33-36.

213. Brunel, C., and Romby, P. (2000) Probing RNA structure and RNA-ligand complexes with chemical probes. in *Methods Enzymol.*, Academic Press. pp 3-21.

214. Ehresmann, C., Baudin, F., Mougel, M., Romby, P., Ebel, J. P., and Ehresmann, B. (1987) Probing the structure of RNAs in solution. *Nucleic Acids Res.* **15**, 9109-9128.

215. Helfer, A.-C., Romilly, C., Chevalier, C., Lioliou, E., Marzi, S., and Romby, P. (2014) Probing RNA structure *In Vitro* with enzymes and chemicals. in *Handbook of RNA Biochemistry*, Wiley-VCH Verlag GmbH & Co. KGaA. pp 205-230.

216. Richardson, C. C. (1965) Phosphorylation of nucleic acid by an enzyme from T4 bacteriophage-infected *Escherichia coli*. *Proc. Natl. Acad. Sci. U. S. A.* **54**, 158-165.

217. Bruce, A. G., and Uhlenbeck, O. C. (1978) Reactions at the termini of tRNA with T4 RNA ligase. *Nucleic Acids Res.* **5**, 3665-3678.

218. Fabbretti, A., Milon, P., Giuliodori, A. M., Gualerzi, C. O., and Pon, C. L. (2007) Real-time dynamics of ribosome-ligand interaction by time-resolved chemical probing methods. in *Methods Enzymol.* (Jon, L. ed.), Academic Press. pp 45-58.

219. Ralston, C. Y., Sclavi, B., Sullivan, M., Deras, M. L., Woodson, S. A., Chance, M. R., and Brenowitz, M. (2000) Time-resolved synchrotron x-ray footprinting and its application to RNA folding. in *Methods Enzymol.*, Academic Press. pp 353-368.

220. Liebeg, A., and Waldsich, C. (2009) Probing RNA structure within living cells. in *Methods in Enzymology* (Daniel, H. ed.), Academic Press. pp 219-238.

221. Maxam, A. M., and Gilbert, W. (1977) A new method for sequencing DNA. *Proc. Natl. Acad. Sci. U. S. A.* **74**, 560-564.

222. Peattie, D. A. (1979) Direct chemical method for sequencing RNA. *Proc. Natl. Acad. Sci. U.S.A.* **76**, 1760–1764.

223. Huntzinger, E., Possedko, M., Winter, F., Moine, H., Ehresmann, C., and Romby, P. (2008) Probing RNA structures with enzymes and chemicals *In*

Vitro and *In Vivo*. in *Handbook of RNA Biochemistry*, Wiley-VCH Verlag GmbH. pp 151-171.

224. Shan, S.-o., Narlikar, G. J., and Herschlag, D. (1999) Protonated 2‘-aminoguanosine as a probe of the electrostatic environment of the active site of the *Tetrahymena* group I ribozyme. *Biochemistry* **38**, 10976-10988.

225. Lindell, M., Romby, P., and Wagner, E. G. H. (2002) Lead(II) as a probe for investigating RNA structure *in vivo*. *RNA* **8**, 534-541.

226. Szewczak, L. W. (2008) *In vivo* analysis of ribonucleoprotein complexes using nucleotide analog interference mapping. in *RNA-Protein Interaction Protocols* (Lin, R.-J. ed.), Humana Press. pp 153-166.

227. Pace, C. N., Heinemann, U., Hahn, U., and Saenger, W. (1991) Ribonuclease T1: structure, function, and stability. *Angew. Chem., Int. Ed. Engl.* **30**, 343-360.

228. Heinemann, U., and Saenger, W. (1983) Crystallographic study of mechanism of ribonuclease T1-catalysed specific RNA hydrolysis. *J. Biomol. Struct. Dyn.* **1**, 523–538.

229. Walz Jr, F. G., Osterman, H. L., and Libertin, C. (1979) Base-group specificity at the primary recognition site of ribonuclease T1 for minimal RNA substrates. *Arch. Biochem. Biophys.* **195**, 95-102.

230. Ding, J., Koellner, G., Grunert, H. P., and Saenger, W. (1991) Crystal structure of ribonuclease T1 complexed with adenosine 2'-monophosphate at 1.8-Å resolution. *J. Biol. Chem.* **266**, 15128-15134.

231. Raines, R. T. (1998) Ribonuclease A. *Chem. Rev.* **98**, 1045-1066.

232. delCardayre, S. B., and Raines, R. T. (1994) Structural determinants of enzymic processivity. *Biochemistry* **33**, 6031-6037.

233. Russell, D. W., and Sambrook, J. (2001). in *Molecular cloning A laboratory manual*, third Ed., Cold spring harbor laboratory press, New York. pp A5.1.

234. Murakami, S., Saito, K., Muromatsu, A., Moriyasu, M., Kato, A., and Hashimoto, Y. (1988) Studies on the reactions of $PtCl_2$en, *cis*-$Pt(NH_3)_2Cl_2$ and their aqua species with adenosine, deoxyadenosine and adenine using ion-pair HPLC. *Inorg. Chim. Acta* **152**, 91-99.

235. Djuran, M. I., Lempers, E. L. M., and Reedijk, J. (1991) Reactivity of chloro- and aqua(diethylenetriamine)platinum(II) ions with glutathione, S-methylglutathione, and guanosine 5'-monophosphate in relation to the antitumor activity and toxicity of platinum complexes. *Inorg. Chem.* **30**, 2648-2652.

236. Struik, A. F., Zuiderwijk, C. T. M., van Boom, J. H., Reedijk, J., and Elding, L. I. (1991) Guanine-06 methylation reduces the reactivity of d(GpG) towards platinum complexes. *J. Inorg. Biochem.* **44**, 249-260.

237. Polonyi, C., Alshiekh, A., Sarsam, L. A., Clausen, M., and Elmroth, S. K. C. (2014) Cisplatin-induced duplex dissociation of complementary and destabilized short GG-containing duplex RNAs. *Dalton Trans.* **43**, 11941-11949.

238. Brabec, V., Kleinwächter, V., Butour, J.-L., and Johnson, N. P. (1990) Biophysical studies of the modification of DNA by antitumour platinum coordination complexes. *Biophys. Chem.* **35**, 129-141.

239. Schaller, W., Reisner, H., and Holler, E. (1987) Kinetic investigation of the DNA platination reaction: evidence for a transient adduct between deoxyribonucleic acid and *cis*-platinum(II). *Biochemistry* **26**, 943-950.

240. Molloy, P. (2000) Electrophoretic mobility shift assays. in *Transcription Factor Protocols* (Tymms, M. ed.), Humana Press. pp 235-246.

241. Greenbaum, N. (2005) Role of a conserved pseudouridine in U2 snRNA on the structural and electrostatic features of the spliceosomal pre-mRNA branch site. in *Fine-Tuning of RNA Functions by Modification and Editing* (Grosjean, H. ed.), Springer Berlin Heidelberg. pp 205-221.

242. Crow, D. R. (1994) Determination and investigation of physical parameters. in *Principles and Applications of Electrochemistry*, Fourth Ed., Blackie Academic and Professional, an imprint of Chapman & Hall. pp 157.

243. Ma, J. K. H., and Hadzija, B. Molecular expressions and electrolyte properties of drug molecules. in *Basic physical pharmacy*, Jones & Bartlett Learning, Burlington, MA. pp 13.

244. Houston, P. L. (2001) Reactions in liquid solutions. in *Chemical Kinetics and Reaction Dynamics*, 1st Ed., McGraw-Hill, Dubuque, Iowa. pp 154.

245. Manning, G. S. (1979) Counterion binding in polyelectrolyte theory. *Acc. Chem. Res.* **12**, 443-449.

246. Olmsted, M. C., Anderson, C. F., and Record, M. T. (1989) Monte Carlo description of oligoelectrolyte properties of DNA oligomers: range of the

end effect and the approach of molecular and thermodynamic properties to the polyelectrolyte limits. *Proc. Natl. Acad. Sci. U.S.A.* **86**, 7766-7770.

247. Fenley, M. O., Manning, G. S., and Olson, W. K. (1990) Approach to the limit of counterion condensation. *Biopolymers* **30**, 1191-1203.

248. Espenson, J. H. (1995) *Chemical Kinetics and Reaction Mechanisms*, 2 nd edition ed., McGraw-Hill, Inc., New York.

249. Miller, S. E., and House, D. A. (1989) The hydrolysis products of *cis*-diamminedichloroplatinum(II). I. The kinetics of formation and anation of the *cis*-diammine(aqua)chloroplatinum(II) cation in acidic aqueous solution. *Inorg. Chim. Acta* **161**, 131–137.

250. Van Hemelryck, B., Girault, J. P., Chottard, G., Valadon, P., Laoui, A., and Chottard, J. C. (1987) Sequence-dependent platinum chelation by adenylyl(3'-5')guanosine and guanylyl(3'-5')adenosine reacting with *cis*-diamminedichloroplatinum(II) and its diaqua derivative. *Inorg. Chem.* **26**, 787–795.

251. Dewan, J. C. (1984) Binding of the antitumor drug *cis*-diamminedichloroplatinum to crystalline $tRNA^{Phe}$ at 6-Å resolution. *J. Am. Chem. Soc.* **106**, 7239–7244.

252. Gelasco, A., and Lippard, S. J. (1998) NMR solution structure of a DNA dodecamer duplex containing a *cis*-diammineplatinum(II) d(GpG) intrastrand cross-link, the major adduct of the anticancer drug cisplatin. *Biochemistry* **37**, 9230–9239.

253. Herder, H. C., and Rosenberg, B. (1970) Inhibitory effects of anti-tumor platinum compounds on DNA, RNA and protein syntheses in mammalian cells *in vitro*. *Int. J. Cancer* **6**, 207–216.

254. Rosenberg, J., and Sato, P. (1988) Messenger RNA loses the ability to direct *in vitro* peptide synthesis following incubation with cisplatin. *Mol. Pharmacol.* **33**, 611–616.

255. Heminger, K. A., Hartson, S. D., Rogers, J., and Matts, R. L. (1997) Cisplatin inhibits protein synthesis in rabbit reticulocyte lysate by causing an arrest in elongation. *Arch. Biochem. Biophys.* **344**, 200–207.

256. Danenberg, P. V., Shea, L. C. C., Danenberg, K. D., and Horikoshi, T. (1991) Inactivation of *Tetrahymena* rRNA self-splicing by *cis*-platin proceeds through dissociable complexes. *Nucleic Acids Res.* **19**, 3123–3128.

257. Rosenberg, J. M., and Sato, P. H. (1993) Cisplatin inhibits *in vitro* translation by preventing the formation of complete initiation complex. *Mol. Pharmacol.* **43**, 491–497.

258. Polonyi, C., Albertsson, I., Damian, M. S., and Elmroth, S. K. C. (2013) Comparison of *cis*- and oxaliplatin-induced destabilization of 15-mer DNA- and RNA duplexes by binding to centrally located GG- and GNG sequences. *Z. Anorg. Allg. Chem.* **639**, 1655–1660.

259. Bakin, A., and Ofengand, J. (1993) Four newly located pseudouridylate residues in *Escherichia coli* 23S ribosomal RNA are all at the

peptidyltransferase center: analysis by the application of a new sequencing technique. *Biochemistry* **32**, 9754-9762.

260. Iannitti-Tito, P., Weimann, A., Wickham, G., and Sheil, M. M. (2000) Structural analysis of drug-DNA adducts by tandem mass spectrometry. *Analyst* **125**, 627–634.

261. Costello, C. E., Nordhoff, E., and Hillenkamp, F. (1994) Matrix-assisted UV and IR laser desorption—ionization time-of-flight mass spectrometry of diamminoplatinum(II) oligodeoxyribonucleotide adducts and their unplatinated analogs. *Int. J. Mass Spectrom. Ion Processes* **132**, 239-249.

262. Rijal, K. (2011) *Exploring potential drug target sites in the ribosome using cisplatin and its analogues.* Doctor of Philosophy, Wayne State University.

263. Anderson, C. F., and Record, M. T. (1995) Salt-nucleic acid interactions. *Annu. Rev. Phys. Chem.* **46**, 657-700.

264. DeHaseth, P. L., Lohman, T. M., and Record, M. T. (1977) Nonspecific interaction of *lac* repressor with DNA: an association reaction driven by counterion release. *Biochemistry* **16**, 4783-4790.

265. Zhang, W., Bond, J. P., Anderson, C. F., Lohman, T. M., and Record, M. T. (1996) Large electrostatic differences in the binding thermodynamics of a cationic peptide to oligomeric and polymeric DNA. *Proc. Natl. Acad. Sci. U.S.A.* **93**, 2511-2516.

266. Misra, V. K., Sharp, K. A., Friedman, R. A., and Honig, B. (1994) Salt effects on ligand-DNA binding: minor groove binding antibiotics. *J. Mol. Biol.* **238**, 245-263.

267. Mohanty, U., Spasic, A., Kim, H. D., and Chu, S. (2005) Ion atmosphere of three-way junction nucleic acid. *J. Phys. Chem. B* **109**, 21369-21374.

268. Woodson, S. A. (2005) Metal ions and RNA folding: a highly charged topic with a dynamic future. *Curr. Opin. Chem. Biol.* **9**, 104-109.

269. García-García, C., and Draper, D. E. (2003) Electrostatic interactions in a peptide–RNA complex. *J. Mol. Biol.* **331**, 75-88.

270. Gutell, R. R., Gray, M. W., and Schnare, M. N. (1993) A compilation of large subunit (23S and 23S-like) ribosomal RNA structures: 1993. *Nucleic Acids Res.* **21**, 3055–3074.

271. Woese, C. R., Magrum, L. J., Gupta, R., Siegel, R. B., Stahl, D. A., Kop, J., Crawford, N., Brosius, R., Gutell, R., Hogan, J. J., and Noller, H. F. (1980) Secondary structure model for bacterial 16S ribosomal RNA: phylogenetic, enzymatic and chemical evidence. *Nucleic Acids Res.* **8**, 2275–2294.

272. Record Jr, M. T., Lohman, T. M., and Haseth, P. d. (1976) Ion effects on ligand-nucleic acid interactions. *J. Mol. Biol.* **107**, 145-158.

273. Record, M. T., DeHaseth, P. L., and Lohman, T. M. (1977) Interpretation of monovalent and divalent cation effects on the *lac* repressor-operator interaction. *Biochemistry* **16**, 4791-4796.

274. Pullman, A., and Pullman, B. (1981) Molecular electrostatic potential of the nucleic acids. *Q. Rev. Biophys.* **14**, 289-380.

275. Olmsted, M. C., Bond, J. P., Anderson, C. F., and Record Jr, M. T. (1995) Grand canonical Monte Carlo molecular and thermodynamic predictions of

ion effects on binding of an oligocation (L^{8+}) to the center of DNA oligomers. *Biophys. J.* **68**, 634-647.

276. Stein, V. M., Bond, J. P., Capp, M. W., Anderson, C. F., and Record Jr, M. T. (1995) Importance of coulombic end effects on cation accumulation near oligoelectrolyte B-DNA: a demonstration using ^{23}Na NMR. *Biophys. J.* **68**, 1063-1072.

277. Fedor, M. J. (2002) The role of metal ions in RNA catalysis. *Curr. Opin. Struct. Biol.* **12**, 289-295.

278. Bowman, J. C., Lenz, T. K., Hud, N. V., and Williams, L. D. (2012) Cations in charge: magnesium ions in RNA folding and catalysis. *Curr. Opin. Struct. Biol.* **22**, 262-272.

279. Basu, S., P. Rambo, R., Strauss-Soukup, J., H.Cate, J., R. Ferre-Damare, A., Strobel, S. A., and Doudna, J. A. (1998) A specific monovalent metal ion integral to the AA platform of the RNA tetraloop receptor. *Nat. Struct. Mol. Biol.* **5**, 986-992.

280. Kim, J., Cheong, C., and Moore, P. B. (1991) Tetramerization of an RNA oligonucleotide containing a GGGG sequence. *Nature* **351**, 331-332.

281. Conn, G. L., Gittis, A. G., Lattman, E. E., Misra, V. K., and Draper, D. E. (2002) A compact RNA tertiary structure contains a buried backbone–K^+ complex. *J. Mol. Biol.* **318**, 963-973.

282. Ennifar, E., Walter, P., and Dumas, P. (2003) A crystallographic study of the binding of 13 metal ions to two related RNA duplexes. *Nucleic Acids Res.* **31**, 2671-2682.

283. Williamson, J. R., Raghuraman, M. K., and Cech, T. R. (1989) Monovalent cation-induced structure of telomeric DNA: The G-quartet model. *Cell* **59**, 871-880.

284. Klein, D. J., Moore, P. B., and Steitz, T. A. (2004) The contribution of metal ions to the structural stability of the large ribosomal subunit. *RNA* **10**, 1366-1379.

285. Auffinger, P., and Hashem, Y. (2007) SwS: a solvation web service for nucleic acids. *Bioinformatics* **23**, 1035-1037.

286. Quigley, G. J., Teeter, M. M., and Rich, A. (1978) Structural analysis of spermine and magnesium ion binding to yeast phenylalanine transfer RNA. *Proc. Natl. Acad. Sci. U. S. A.* **75**, 64-68.

287. Westhof, E., and Sundaralingam, M. (1986) Restrained refinement of the monoclinic form of yeast phenylalanine transfer RNA. Temperature factors and dynamics, coordinated waters, and base-pair propeller twist angles. *Biochemistry* **25**, 4868-4878.

288. Laing, L. G., Gluick, T. C., and Draper, D. E. (1994) Stabilization of RNA structure by Mg ions: specific and non-specific effects. *J. Mol. Biol.* **237**, 577-587.

289. Reid, S. S., and Cowan, J. A. (1991) Metallobiochemistry of a ribosomal RNA. A possible role for Na^+ and K^+ in the regulation of Mg^{2+} binding sites on *Escherichia coli* 5S rRNA: implications for activity. *J. Am. Chem. Soc.* **113**, 673-675

290. Cowan, J. A. (1991) Coordination chemistry of magnesium ions and 5S rRNA (*Escherichia coli*): binding parameters, ligand symmetry, and implications for activity. *J. Am. Chem. Soc.* **113**, 675-676.

291. Celander, D. W., and Cech, T. R. (1991) Visualizing the higher order folding of a catalytic RNA molecule. *Science* **251**, 401-407.

292. Bassi, G. S., Mollegaard, N.-E., Murchie, A. I. H., Kitzing, E. v., and Lilley, D. M. J. (1995) Ionic interactions and the global conformations of the hammerhead ribozyme. *Nat. Struct. Mol. Biol.* **2**, 45-55.

293. Misra, V. K., Hecht, J. L., Sharp, K. A., Friedman, R. A., and Honig, B. (1994) Salt effects on protein-DNA interactions: the λcI repressor and EcoRI endonuclease. *J. Mol. Biol.* **238**, 264-280.

294. Soto, A. M., Misra, V., and Draper, D. E. (2007) Tertiary structure of an RNA pseudoknot is stabilized by "diffuse" Mg^{2+} Ions. *Biochemistry* **46**, 2973-2983.

295. Misra, V. K., and Draper, D. E. (1998) On the role of magnesium ions in RNA stability. *Biopolymers* **48**, 113-135.

296. Draper, D. E., Grilley, D., and Soto, A. M. (2005) Ions and RNA folding. *Annu. Rev. Biophys. Biomol. Struct.* **34**, 221-243.

297. Cowan, J. A., Huang, H. W., and Hsu, L. Y. (1993) Sequence selective coordination of $Mg^{2+}_{(aq)}$ to DNA. *J. Inorg. Biochem.* **52**, 121-129.

298. Buckin, V., Tran, H., Morozov, V., and Marky, L. A. (1996) Hydration effects accompanying the substitution of counterions in the ionic

atmosphere of Poly(rA)·Poly(rU) and Poly(rA)·2Poly(rU) helices. *J. Am. Chem. Soc.* **118**, 7033-7039.

299. Gagnon, M. G., Seetharaman, S. V., Bulkley, D., and Steitz, T. A. (2012) Structural basis for the rescue of stalled ribosomes: structure of YaeJ bound to the ribosome. *Science* **335**, 1370-1372.

300. Stanley, R. E., Blaha, G., Grodzicki, R. L., Strickler, M. D., and Steitz, T. A. (2010) The structures of the anti-tuberculosis antibiotics viomycin and capreomycin bound to the 70S ribosome. *Nat Struct Mol Biol* **17**, 289-293.

301. Sumita, M., Desaulniers, J.-P., Chang, Y.-C., Chui, H. M.-P., Clos, L., and Chow, C. S. (2005) Effects of nucleotide substitution and modification on the stability and structure of helix 69 from 28S rRNA. *RNA* **11**, 1420-1429.

302. Robinson, H., Gao, Y.-G., Sanishvili, R., Joachimiak, A., and Wang, A. H.-J. (2000) Hexahydrated magnesium ions bind in the deep major groove and at the outer mouth of A-form nucleic acid duplexes. *Nucleic Acids Res.* **28**, 1760-1766.

303. Huppler, A., Nikstad, L. J., Allmann, A. M., Brow, D. A., and Butcher, S. E. (2002) Metal binding and base ionization in the U6 RNA intramolecular stem-loop structure. *Nat. Struct. Mol. Biol.* **9**, 431-435.

304. Sherman, S. E., Gibson, D., Wang, A. H. J., and Lippard, S. J. (1988) Crystal and molecular structure of *cis*-[$Pt(NH_3)_2$[d(pGpG)]], the principal adduct formed by *cis*-diamminedichloroplatinum(II) with DNA. *J. Am. Chem. Soc.* **110**, 7368-7381.

305. Hill Jr., C. G. (1977). in *An Intorduction to Chemical Engineering Kinetics & Reactor Design*, John Wiley & Sons. pp 217-219.

306. Record Jr., M. T., and Richey, B. (1988) Physical chemical analysis of biopolymer self-assembly interactions. in *ACS sourcebook for physical chemistry instructors* (Lippincott, E. T. ed.), American Chemical Society, Washington, DC. pp 145-159.

307. Tang, C. L., Alexov, E., Pyle, A. M., and Honig, B. (2007) Calculation of pK_as in RNA: on the structural origins and functional roles of protonated nucleotides. *J. Mol. Biol.* **366**, 1475-1496.

308. Wilcox, J. L., Ahluwalia, A. K., and Bevilacqua, P. C. (2011) Charged nucleobases and their potential for RNA catalysis. *Acc. Chem. Res.* **44**, 1270-1279.

309. Vary, C. P. H., and Vournakis, J. N. (1984) RNA structure analysis using T2 ribonuclease: detection of pH and metal ion induced conformational changes in yeast $tRNA^{Phe}$. *Nucleic Acids Res.* **12**, 6763-6778.

310. Bina-Stein, M., and Crother, D. M. (1974) Conformational changes of transfer ribonucleic acid. pH phase diagram under acidic conditions. *Biochemistry* **13**, 2771-2775.

311. Legault, P., and Pardi, A. (1997) Unusual dynamics and pK_a shift at the active site of a lead-dependent ribozyme. *J. Am. Chem. Soc.* **119**, 6621-6628.

312. Nakano, S.-i., Chadalavada, D. M., and Bevilacqua, P. C. (2000) General acid-base catalysis in the mechanism of a hepatitis delta virus ribozyme. *Science* **287**, 1493-1497.

313. Nixon, P. L., and Giedroc, D. P. (2000) Energetics of a strongly pH dependent RNA tertiary structure in a frameshifting pseudoknot. *J. Mol. Biol.* **296**, 659-671.

314. Muth, G. W., Chen, L., Kosek, A. B., and Strobel, S. A. (2001) pH-dependent conformational flexibility within the ribosomal peptidyl transferase center. *RNA* **7**, 1403-1415.

315. Xiong, L., Polacek, N., Sander, P., Böttger, E. C., and Mankin, A. (2001) pK_a of adenine 2451 in the ribosomal peptidyl transferase center remains elusive. *RNA* **7**, 1365-1369.

316. Kao, T. H., and Crothers, D. M. (1980) A proton-coupled conformational switch of *Escherichia coli* 5S ribosomal RNA. *Proc. Natl. Acad. Sci. U. S. A.* **77**, 3360-3364.

317. Siegfried, N. A., O'Hare, B., and Bevilacqua, P. C. (2010) Driving forces for nucleic acid pK_a shifting in an A^+·C wobble: effects of helix position, temperature, and ionic strength. *Biochemistry* **49**, 3225-3236.

318. Arpalahti, J., and Lehikoinen, P. (1990) Kinetics of complexation of aquated (diethylenetriamine)platinum(II) with inosine and 1-methylinosine as a function of pH. *Inorg. Chem.* **29**, 2564-2567.

319. Jacobs, R., Prinsloo, F., and Breet, E. (1992) Kinetics of binding of DNA nucleotides to antitumour type complexes. *J. Chem. Soc., Chem. Commun.*, 212-213.

320. Ritala, M., and Arpalahti, J. (1991) Platinum(II) binding to the N1 and N7 ring nitrogens of guanosine. Kinetics of complexation of aquated (diethylenetriamine)platinum(II) with 1- and 7-methylguanosines. *Inorg. Chem.* **30**, 2826-2828.

321. Berners-Price, S. J., Frenkiel, T. A., Frey, U., Ranford, J. D., and Sadler, P. J. (1992) Hydrolysis products of cisplatin: pK_a determinations via [^{1}H, ^{15}N] NMR spectroscopy. *J. Chem. Soc., Chem. Commun.*, 789-791.

322. Arpalahti, J. (1996) Platinum (II)-nucleobase interactions. A kinetic approach. in *Interactions of metal Ions with Nucleotides, Nucleic acids, and their Constituents* (Sigel, A., and Sigel, H. eds.), Taylor & Francis, New York. pp 379-395.

323. Arpalahti, J. (1990) Kinetics for pH-dependent complexation of aquated *cis*-diammineplatinum(II) with inosine and 1-methylinosine. *Inorg. Chem.* **29**, 4598-4602.

324. Berners-Price, S., and Appleton, T. (2000) The chemistry of cisplatin in aqueous solution. in *Platinum-Based Drugs in Cancer Therapy* (Kelland, L., and Farrell, N. eds.), Humana Press. pp 3-35.

325. Mikola, M., Oksman, P., and Arpalahti, J. (1996) Kinetics and mechanism of complexation of *trans*-$[PtCl(NH_3)_2(H_2O)]^+$ with inosine and 1-

methylinosine in aqueous solution at different pH values. *J. Chem. Soc., Dalton Trans.*, 3101-3104.

326. Avent, M. L., Rogers, B. A., Cheng, A. C., and Paterson, D. L. (2011) Current use of aminoglycosides: indications, pharmacokinetics and monitoring for toxicity. *Intern. Med. J.* **41**, 441-449.

327. Fourmy, D., Recht, M. I., Blanchard, S. C., and Puglisi, J. D. (1996) Structure of the A site of *Escherichia coli* 16S ribosomal RNA complexed with an aminoglycoside antibiotic. *Science* **274**, 1367-1371.

328. Carter, A. P., Clemons, W. M., Brodersen, D. E., Morgan-Warren, R. J., Wimberly, B. T., and Ramakrishnan, V. (2000) Functional insights from the structure of the 30S ribosomal subunit and its interactions with antibiotics. *Nature* **407**, 340-348.

329. Davies, J., Gorini, L., and Davis, B. D. (1965) Misreading of RNA codewords induced by aminoglycoside antibiotics. *Mol. Pharmacol.* **1**, 93-106.

330. von Ahsen, U., Davies, J., and Schroeder, R. (1991) Antibiotic inhibition of group I ribozyme function. *Nature* **353**, 368-370.

331. Stage, T. K., Hertel, K. J., and Uhlenbeck, O. C. (1995) Inhibition of the hammerhead ribozyme by neomycin. *RNA* **1**, 95-101.

332. Mei, H.-Y., Galan, A. A., Halim, N. S., Mack, D. P., Moreland, D. W., Sanders, K. B., Hoa, N. T., and Czarnik, A. W. (1995) Inhibition of an HIV-1 Tat-derived peptide binding to TAR RNA by aminoglycoside antibiotics. *Bioorg. Med. Chem. Lett.* **5**, 2755-2760.

333. Zapp, M. L., Stern, S., and Green, M. R. (1993) Small molecules that selectively block RNA binding of HIV-1 rev protein inhibit rev function and viral production. *Cell* **74**, 969-978.

334. Hermann, T., and Westhof, E. (1998) RNA as a drug target: chemical, modelling, and evolutionary tools. *Curr. Opin. Biotechnol.* **9**, 66-73.

335. Ramakrishnan, V. (2002) Ribosome structure and the mechanism of translation. *Cell* **108**, 557-572.

336. Bellon, S. F., and Lippard, S. J. (1990) Bending studies of DNA site-specifically modified by cisplatin, *trans*-diamminedichloroplatinum(II) and *cis*-[$Pt(NH_3)_2$ (N3-cytosine) $Cl]^+$. *Biophys. Chem.* **35**, 179-188.

337. Chow, C. S., Whitehead, J. P., and Lippard, S. J. (1994) HMG domain proteins induce sharp bends in cisplatin-modified DNA. *Biochemistry* **33**, 15124-15130.

338. Arimondo, P. B., Gelus, N., Hamy, F., Payet, D., Travers, A., and Bailly, C. (2000) The chromosomal protein HMG-D binds to the TAR and RBE RNA of HIV-1. *FEBS Lett.* **485**, 47-52.

339. Schultz, S. G., and Solomon, A. K. (1961) Cation transport in *Escherichia coli* : I. intracellular Na and K concentrations and net cation movement. *J gen. physiol.* **45**, 355-369.

340. Epstein, W., and Schultz, S. G. (1965) Cation transport in *Escherichia coli* : V. regulation of cation content. *J gen. physiol.* **49**, 221-234.

341. Cameron, I. L., Smith, N. K. R., Pool, T. B., and Sparks, R. L. (1980) Intracellular concentration of sodium and other elements as related to mitogenesis and oncogenesis *in vivo*. *Cancer Res.* **40**, 1493-1500.

342. Moolenaar, W. H. (1986) Effects of growth factors on intracellular pH regulation. *Annu. Rev. Physiol.* **48**, 363-376.

343. Gerweck, L. E., and Seetharaman, K. (1996) Cellular pH gradient in tumor versus normal tissue: potential exploitation for the treatment of cancer. *Cancer Res.* **56**, 1194-1198.

344. Siegfried, N. A., Busan, S., Rice, G. M., Nelson, J. A. E., and Weeks, K. M. (2014) RNA motif discovery by SHAPE and mutational profiling (SHAPE-MaP). *Nat. Meth.* **11**, 959-965

345. Jestin, J. L., Lambert, B., and Chottard, J. C. (1998) Kinetic study of DNA binding of cisplatin and of a bicycloalkyl-substituted (ethylenediamine)dichloroplatinum(II) complex. *J. Biol. Inorg. Chem.* **3**, 515-519.

346. Bernges, F., and Holler, E. (1991) The reaction of platinum(II) complexes with DNA. Kinetics of intrastrand crosslink formation *in vitro*. *Nucleic Acids Res.* **19**, 1483-1489.

347. Khandogin, J., and York, D. M. (2002) Quantum mechanical characterization of nucleic acids in solution: a linear-scaling study of charge fluctuations in DNA and RNA. *J. Phys. Chem. B* **106**, 7693-7703.

348. Sharp, K. A. (1994) Electrostatic interactions in macromolecules. *Curr. Opin. Struct. Biol.* **4**, 234-239.

349. Wang, H., and Tor, Y. (1998) RNA–aminoglycoside interactions: design, synthesis, and binding of “aminoaminoglycosides” to RNA. *Angew. Chem., Int. Ed.* **37**, 109-111.

350. Bass, B. L., and Cech, T. R. (1986) Ribozyme inhibitors. Deoxyguanosine and dideoxyguanosine are competitive inhibitors of self-splicing of the *Tetrahymena* ribosomal ribonucleic acid precursor. *Biochemistry* **25**, 4473-4478.

351. von Ahsen, U., Davies, J., and Schroeder, R. (1992) Non-competitive inhibition of group I intron RNA self-splicing by aminoglycoside antibiotics. *J. Mol. Biol.* **226**, 935-941.

ABSTRACT

PLATINATION KINETICS: INSIGHT INTO RNA-CISPLATIN INTERACTIONS AS A PROBE FOR RNA MICROENVIRONMENTS

by

GAYANI N P DEDDUWA-MUDALIGE

August 2015

Advisor: Prof. Christine S Chow

Major: Chemistry (Biochemistry)

Degree: Doctor of Philosophy

RNAs are crucial for many cellular functions. Thus, studying ligand-RNA interactions and their dynamics in response to changes in the surrounding environment is important. In spite of the well-known DNA coordination, current research also indicates cisplatin binding to RNA. Kinetic studies of rRNA platination reactions are largely unexplored. This research was conducted to achieve two objectives. First, a broad kinetic study was carried out to investigate the cisplatin-rRNA interactions. The structure, function, and ligand interactions depend on RNA microenvironments. Second, the application of platination kinetics as a tool to interrogate RNA electrostatic environments was explored.

Three model rRNA hairpins from *E. coli* ribosome were selected. Two helix 69 (H69) constructs, modified H69 (with pseudouridine) and unmodified H69 (without pseudouridine), and the 790 loop, which has an identical size and nucleotide composition to unmodified H69, were used. Prior to kinetic studies, cisplatin targets on each RNA were determined using RNase T1 mapping combined with MALDI MS, and dimethyl sulfate (DMS) probing. The kinetic

studies were carried out under pseudo-first-order conditions and electrostatic properties were evaluated using Brønsted-Debye-Hückel and polyelectrolyte theories.

RNase T1 mapping with MALDI MS and dimethyl sulfate (DMS) probing revealed GpG sites as cisplatin targets on RNA. The DMS probing further revealed platination-induced structural changes in RNA. Both the RNA sequence and modified nucleotides showed an impact on platination rates. Kinetic data showed that the platination rate is dependent on cations and the abundance of active cisplatin complexes. Structure, pseudouridylation, availability of active cisplatin species, and cation/Pt^{+} electrostatic competitions all impact platination of the two H69 RNAs. Probing neomycin-H69 interactions by platination kinetics indicated that structural changes in modified H69 upon aminoglycoside binding could also impact the platination kinetics. Electrostatic models revealed that nucleotide sequence, cations, and H^{+} ions impact the global RNA electrostatics. The similar global electrostatic properties between the two H69 RNAs indicated that structure-dependent electrostatic changes in modified H69 could be limited to the loop region.

In conclusion, this thesis work showed that both intrinsic RNA characteristics such as structure, sequence, and dynamics, as well as bulk solution conditions (*e.g.* cations and pH), impact cisplatin-RNA interactions. The RNA electrostatic parameters determined in this thesis work illustrated platination kinetics can be used as an informatory tool for probing dynamic RNA microenvironments.

AUTOBIOGRAPHICAL STATEMENT

GAYANI N P DEDDUWA-MUDALIGE

ADVISOR: Prof. Christine S Chow

THESIS TITLE: PLATINATION KINETICS: INSIGHT INTO RNA-CISPLATIN INTERACTIONS AS A PROBE FOR RNA MICROENVIRONMENTS

EDUCATION

- **Ph.D.; Biological Chemistry**, 2015, Wayne State University, MI, USA
- **B.S. (Honors); Chemistry,** 2007, University of Kelaniya, Sri Lanka

PUBLICATION:

1. **Gayani N P Dedduwa-Mudalige**, Sofi K C Elmroth, and Christine S Chow; Electrostatic microenvironments of ribosomal RNA hairpins with modified nucleotides determined by platination reactions. Manuscript in preparation
2. **Gayani N P Dedduwa-Mudalige**, Sofi K C Elmroth, and Christine S Chow; Identification, comparison, and implications of cisplatin coordination to *Escherichia coli* ribosomal RNA hairpins. Manuscript in preparation
3. **Gayani N P Dedduwa-Mudalige**, Sofi K C Elmroth, and Christine S Chow; The impact of cations on kinetics and electrostatics of RNA-platinum drug interactions. Manuscript in preparation
4. **Gayani N P Dedduwa-Mudalige**, Sofi K C Elmroth, and Christine S Chow; The impact of pH on kinetics and electrostatics of cisplatin-RNA interactions. Manuscript in preparation